

PhD dissertation

ENERGY AND SUSTAINABILITY IN CHILE: SIMULATION MODELLING OF LOW-CARBON TECHNOLOGIES AND ENERGY IN BUILDINGS

A thesis submitted in partial fulfilment of the requirements for the degree of
Doctor of the Universidad de Granada.

Escuela Internacional de Posgrado

Departamento de Ingeniería de la Construcción y Proyectos de Ingeniería

Universidad de Granada

by **François SIMON**

Supervisors:

Javier ORDOÑEZ GARCÍA / Aymeric GIRARD

June 2017



**UNIVERSIDAD
DE GRANADA**

Editor: Universidad de Granada. Tesis Doctorales
Autor: François Simon
ISBN: 978-84-9163-695-3
URI: <http://hdl.handle.net/10481/48835>

This page was intentionally left blank.

Declaration

I, François Simon, confirm that the work presented in this thesis is my own, and that it has been done under the direction of the thesis supervisors Javier Ordoñez García and Aymeric Girard.

We confirm that as far as our knowledge reaches, in the performance of the work, the rights of other authors to be cited (when their results or publications have been used) have been respected.

Granada, June 7th, 2017

Thesis supervisors

Javier Ordoñez García

Aymeric Girard

Thesis author

François Simon

Abstract

Fossil fuels reserves are diminishing rapidly across the world, intensifying the stress on existing reserves due to increased demand. Moreover, the production of greenhouse gas (GHG) emissions driven by human activities, in particular the combustion of fossil fuels, presently contributing to 81% of the world primary energy, inflict disastrous impacts on human health, economics and environment of the planet. Increase in GHG concentrations is directly responsible for the rise in the earth average temperature and its associated climate change implications.

The Chilean economy grew at a rate of 4% between 2003 and 2015 and is forecast to continue to grow over the coming years. As for most developing countries, pressures from economic and population growth have traditionally forced governments to look at cost-effective options, mainly those exploiting fossil fuel sources, to cope with the increased demand for electricity from households and industry. However, besides the serious concerns on whether the actual strategy is environmentally sustainable, the lack of fossil fuel sources in Chile makes also the country vulnerable to supply disruptions of foreign fossil fuel and energy price volatility, and thus raises concerns over satisfying the country energy demand. Therefore, there is an urgent need to look at sustainable options for energy production and energy saving in Chile, especially since the Chilean government pledged to reduce the country GHG emissions by 30% below 2007 levels by 2030 at the latest Paris climate negotiations in December 2015. The present work is aimed to demonstrate that sustainability in the field of energy can be achieved in a cost effective manner in Chile, through clean energy generation from renewable sources and efficient use of energy in buildings.

The energy sector has a key role in the production of environmentally harmful substances. It has thus become crucial for the sustainability of modern societies to switch over of energy systems from conventional to renewables. Solar energy represents an attractive alternative to conventional fossil energy, as it is freely available in abundant and inexhaustible quantity and can make an important contribution towards a sustainable future. The study explores the economic viability of large scale solar technologies for clean electricity generation, in terms of levelised cost of electricity (LCOE) on the Atacama Solar Platform (PSDA) for a solar-solar hybrid energy mix with the objective of evaluating new options for continuous solar electricity delivery.

For this purpose, a simulation model was built to predict LCOE evolutions until 2050 of three different types of 50 MW solar power plants, a photovoltaic (PV), a concentrating solar power (CSP) plant with 15 hours thermal energy storage (TES), and a hybrid PV-CSP plant with 15 hours TES. Calculations present two scenario projections (Blue Map and Roadmap) until 2050 for each type of plant. Due to the huge solar resource available in northern Chile, the PV-CSP hybrid plant results to be a feasible option for electricity generation, as well as being effectively able to meet electricity demand profile of the mining industry present in the area. This type of energy could mitigate long-term energy costs for the heavy mining activity, as well as the country CO₂ emissions. Findings point out that PV-CSP plants are a feasible option able to contribute to the continuous delivery of sustainable electricity in northern Chile. Moreover, this option can also contribute towards electricity price stabilization, thus benefiting the mining industry, as well as reducing Chile's carbon footprint.

The building sector contributes to approximately 40% of the global energy consumption and more than a third of the global GHG emissions. Therefore, there is a need to seek adequate solutions to minimize energy consumption and deploy the renewable energy technologies, with the objective of “low-energy building”. In order to achieve this objective, buildings must combine two main requirements: (1) being energy efficient as to have a low energy demand, and (2) being able to generate electricity, or other energy carriers, from renewable sources in order to compensate for its energy demand.

Ground source heat-pump (GSHP) is one of the energy saving technologies available for building applications. With high efficiency characteristics, such technology has a great potential in reducing energy use and consequently carbon emissions from buildings. The performance of GSHP, often expressed as Power drawn and/or the COP, depends on several operating parameters. Manufacturers usually publish such data in tables for certain discrete values of the operating fluid temperatures and flow rates conditions. In actual applications, such as in dynamic simulations of heat pump system integrated to buildings, there is a need to determine equipment performance under operating conditions other than those listed.

The investigation describes a simplified methodology for predicting the performance of GSHPs using multiple regression (MR) models as applicable to manufacturer data. It is found that fitting second-order MR models with eight statistically significant x-variables from 36 observations appropriately selected in the manufacturer catalogue can predict the system global behaviour with good accuracy. For the three studied GSHPs, the external prediction error of the MR models identified following the methodology are 0.2%, 0.9% and 1% for heating capacity (HC) predictions and 2.6%, 4.9% and 3.2% for COP predictions. No correlation is found between residuals and the response, thus validating the models. The operational approach appears to be a reliable tool to be integrated in dynamic simulation codes, as the method is applicable to any GSHP catalogue data.

Energy efficiency in buildings, by means of energy saving design is the most economically viable short-term solution to rapidly reduce energy usage and mitigate the repercussions of carbon emissions in buildings. In order to reduce the energy consumption in homes, there is a demand for tools that identify significant parameters of building energy performance. The work presents such a methodology, based on a simulation model and graphical figures, for the interactive investigation of energy performance in different climatic regions in Chile. The simulation tool (called MEEDI) is based on the ISO 13790 monthly calculation method of building heating and cooling energy use with two additional procedures for the calculation of the heat transfer through the floor and the solar heat gains. The graphical figures are illustrating the effects of the climate conditions, the different envelope components and the size and the orientation of windows on the energy consumption. The MEEDI program can contribute to find

Abstract

the best solution to increase energy efficiency in residential buildings. It can be adapted for various parameters, making it useful for future projects.

The economic viability of different specific measures for building envelope materials are analysed as a function of their payback periods. Payback periods range from 6 to 31 years depending on location and the source of primary energy scenario. The study illustrates how decisions in the early stages of building design can have a significant impact on final energy performance. With simple building envelope components modification, valuable energy gains and carbon emission reductions can be achieved in a cost effective manner in Chile.

“Sustainable development is development that meets the needs of the present without compromising the ability of future generations to meet their own needs.”

Our Common Future, Report of the Brundtland Commission, 1987

Resumen

Las reservas de combustibles fósiles están disminuyendo rápidamente en todo el mundo, provocando un aumento del estrés sobre las reservas existentes debido al incremento de la demanda. Por otra parte, la producción de emisiones de gases de efecto invernadero (GEI) impulsadas por las actividades humanas, en particular la combustión de combustibles fósiles, que actualmente contribuyen al 81% de la energía primaria mundial, causan impactos desastrosos sobre la salud humana, la economía y el medio ambiente del planeta. El aumento de las concentraciones de GEI es directamente responsable del aumento de la temperatura media de la Tierra y sus implicaciones relacionadas con el cambio climático.

La economía chilena creció a una tasa del 4% entre 2003 y 2015 y se prevé que seguirá creciendo en los próximos años. En cuanto a la mayoría de los países en desarrollo, las presiones del crecimiento económico y demográfico han obligado tradicionalmente a los gobiernos a considerar como opción, desde el punto de vista económico aquellas que se basan en el uso de fuentes de combustibles fósiles, para hacer frente al aumento de la demanda de electricidad de los hogares y las industrias. Sin embargo, además de las serias preocupaciones sobre si la estrategia actual es ambientalmente sostenible, la falta de fuentes de combustibles fósiles en Chile también hace que el país sea muy vulnerable a las interrupciones del suministro de combustibles fósiles importados y a la volatilidad de los precios de la energía. Por lo tanto, existe una necesidad urgente de considerar opciones sostenibles para la producción de energía y el ahorro energético en Chile, especialmente desde que el gobierno chileno se comprometió a reducir las emisiones de GEI en un 30% por debajo de los niveles de 2007 para el año 2030 en las últimas negociaciones

climáticas de París en diciembre de 2015. El presente trabajo tiene como objetivo demostrar que la sostenibilidad en el ámbito de la energía puede lograrse de una manera rentable en Chile, a través de la generación de energía limpia a partir de fuentes renovables y el uso eficiente de la energía en los edificios.

El sector de la energía tiene un papel clave en la producción de sustancias nocivas para el medio ambiente. Por lo tanto, es crucial para la sostenibilidad de las sociedades modernas el cambio de los sistemas energéticos de los convencionales a los renovables. La energía solar representa una alternativa atractiva a la energía fósil convencional, ya que está disponible gratuitamente en cantidad abundante e inagotable y puede hacer una importante contribución a un futuro sostenible. El estudio explora la viabilidad económica de las tecnologías solares a gran escala para la generación de electricidad limpia, en términos de costo nivelado de electricidad (LCOE) en la Plataforma Solar de Atacama (PSDA) para una mezcla híbrida solar-solar con el objetivo de evaluar nuevas opciones de generación de electricidad, procedente de la energía solar, en producción continua.

Para este propósito se desarrolló un modelo de simulación que permitiera predecir las evoluciones del coste de la electricidad generada en la planta (LCOE), hasta 2050, de tres tipos diferentes de plantas solares de 50 MW: instalación fotovoltaica (PV), planta de energía solar concentrada (CSP) con 15 horas de almacenamiento de energía térmica (TES) y una planta híbrida PV-CSP con 15 horas de TES. Los cálculos presentan dos proyecciones de escenarios (Blue Map y Roadmap) hasta 2050 para cada tipo de planta. Debido al enorme recurso solar disponible en el norte de Chile, la planta híbrida PV-CSP resulta ser una opción factible para la generación de electricidad, además de ser capaz de satisfacer el perfil de demanda de electricidad de la industria minera presente en la zona. Este tipo de energía podría mitigar los costes de energía a largo plazo para la intensiva actividad minera, así como las emisiones de CO₂ del país. Los resultados señalan que la planta híbrida PV-CSP es una opción viable que puede contribuir al suministro continuo de electricidad sostenible en el norte de Chile. Asimismo, esta opción también puede contribuir a la estabilización de los precios de la electricidad, beneficiando así a la industria minera, además de reducir la huella de carbono de Chile.

El sector de la edificación consume, aproximadamente, el 40% del consumo mundial de energía y genera más de un tercio de las emisiones mundiales de GEI. Por lo tanto, es necesario buscar soluciones adecuadas para minimizar el consumo de energía y desplegar las tecnologías de energía renovable, con el objetivo de diseñar y construir "edificios de bajo consumo energético". Para alcanzar este objetivo, los edificios deben combinar dos requisitos principales: (1) ser eficientes energéticamente para tener una demanda de energía baja y (2) ser capaces de generar energía a partir de fuentes renovables para compensar su demanda energética.

La bomba de calor geotérmica (GSHP) es una de las tecnologías de ahorro de energía disponibles para edificios. Con características de alta eficiencia, esta tecnología tiene un gran potencial para reducir el consumo de energía y, en consecuencia, las emisiones de carbono de los edificios. El rendimiento de GSHP, generalmente expresado como el COP, depende de varios parámetros operativos. Los fabricantes suelen publicar estos datos en tablas para ciertos valores de temperaturas y caudales de los fluidos de funcionamiento. En aplicaciones reales, así como en las simulaciones dinámicas del sistema de bomba de calor integrado a los edificios, es necesario determinar el rendimiento del equipo en condiciones de funcionamiento distintas de las enumeradas.

La investigación describe una metodología simplificada para predecir el desempeño de GSHPs usando modelos de regresión múltiple (MR) a partir de los datos del fabricante. Se encontró que la adaptación de modelos MR de segundo orden con ocho x -variables significativas estadísticamente y 36 observaciones apropiadamente seleccionadas del catálogo del fabricante puede predecir el comportamiento global del sistema con buena precisión. Para los tres GSHP estudiados, el error de predicción externa de los modelos de MR identificados siguiendo la metodología es 0,2%, 0,9% y 1% para las predicciones de capacidad de calentamiento (HC) y 2,6%, 4,9% y 3,2% para las predicciones de COP. No se encuentra correlación entre los residuos y la respuesta, validándose así los modelos. El enfoque operacional parece ser una herramienta viable para ser integrada en códigos de simulación dinámica, ya que el método es aplicable a cualquier sistema de GHSP usando el correspondiente catálogo de datos.

La eficiencia energética en los edificios, mediante el diseño de ahorro de energía es la solución a corto plazo más económicamente viable para reducir rápidamente el consumo de energía y mitigar las repercusiones de las emisiones de carbono en los edificios. Con el fin de reducir el consumo de energía en los hogares, existe una demanda de herramientas que identifiquen los parámetros significativos del rendimiento energético del edificio. El trabajo presenta esta metodología, basada en un modelo de simulación y figuras gráficas, que permiten obtener el rendimiento energético para diferentes regiones climáticas de Chile. La herramienta de simulación (denominada MEEDI) se basa en el método de cálculo mensual ISO 13790 del consumo de energía de calefacción y refrigeración con dos procedimientos adicionales para el cálculo de la transferencia de calor a través del suelo y las ganancias de calor solar. Las figuras gráficas ilustran los efectos de las condiciones climáticas, los diferentes componentes de la envoltura del edificio y el tamaño y la orientación de las ventanas sobre el consumo de energía. El programa MEEDI puede contribuir a encontrar la mejor solución para aumentar la eficiencia energética en edificios residenciales, ya que puede adaptarse para diversos parámetros, lo que lo hace útil para futuros proyectos.

La viabilidad económica de diferentes medidas específicas para materiales de envoltura del edificio se analiza en función de sus períodos de retorno. Los períodos de retorno varían de 6 a 31 años dependiendo de la ubicación y el escenario de energía primaria. El estudio ilustra cómo las decisiones, en las primeras etapas del diseño del edificio, pueden tener un impacto significativo en el uso eficiente de la energía en el edificio. Con simples modificaciones de los componentes de la envoltura del edificio, se pueden lograr valiosas ganancias de energía y reducciones de emisiones de carbono de manera rentable en Chile.

“El desarrollo sostenible es un desarrollo que satisface las necesidades del presente sin comprometer la capacidad de las generaciones futuras para satisfacer sus propias necesidades.”

Our Common Future, Report of the Brundtland Commission, 1987

Acknowledgments

I would like to thank all those who helped and support me during the course of the PhD. First, I owe gratitude to my principal supervisors Professor Javier Ordoñez García and Dr. Aymeric Girard, for their insightful guidance, encouragement, understanding and patience from the inception of the research. I am also grateful to Dr. Eulalia Jadraque Gago for her advice and support.

I am also thankful to Professor Agami Reddy at the Arizona State University, Professor Tariq Muneer at the Edinburgh Napier University, and Cristobal Parado at the University of Antofagasta for their support, advice and encouragement.

This thesis would not have been possible without the support of my close friends and family. I am very grateful for their support and understanding during these last three years, especially to Juliana, Francesco, and Pierre. This thesis is dedicated to my parents, Cécile and Éric, and my grandmother Suzette, who have given me their unequivocal support.

Acknowledgments

Contents

| | |
|---|-----------|
| Abstract..... | 5 |
| Acknowledgments..... | 13 |
| List of figures..... | 19 |
| List of tables..... | 23 |
| Chapter 1 – Introduction..... | 25 |
| 1.1 Context..... | 25 |
| 1.1.1 <i>The global energy panorama.....</i> | 25 |
| 1.1.2 <i>The global environmental scene.....</i> | 26 |
| 1.1.3 <i>The global energy problem.....</i> | 28 |
| 1.2 The Chilean energy scenario..... | 31 |
| 1.2.1 <i>Background information.....</i> | 31 |
| 1.2.2 <i>Energy demand and supply.....</i> | 32 |
| 1.2.3 <i>Energy and environmental challenges.....</i> | 34 |
| 1.2.4 <i>Electricity generation.....</i> | 38 |
| 1.2.5 <i>The renewable energy sector.....</i> | 43 |
| 1.2.6 <i>Support mechanisms for renewable energy.....</i> | 49 |
| 1.2.7 <i>Energy in the built environment.....</i> | 55 |
| 1.3 Outline of the thesis..... | 62 |

| | |
|---|------------|
| Chapter 2 – Aims and objectives..... | 63 |
| Chapter 3 – Literature review | 67 |
| 3.1 Solar energy..... | 67 |
| 3.1.1 The solar radiation..... | 67 |
| 3.1.2 Photovoltaic technology (PV)..... | 76 |
| 3.1.3 Concentrating solar thermal power (CSP)..... | 80 |
| 3.1.4 Proof of concept and economics of solar electricity production..... | 83 |
| 3.2 Low-grade geothermal energy | 90 |
| 3.2.1 Ground-source heat pump (GSHP) principles | 90 |
| 3.2.2 Theoretical background..... | 95 |
| 3.2.3 Performance prediction | 100 |
| 3.3 Energy efficiency in buildings | 108 |
| 3.3.1 Energy modelling..... | 108 |
| 3.3.2 Fundamentals for energy use calculation..... | 111 |
| 3.3.3 Policy tools for enhancing building energy efficiency..... | 122 |
| Chapter 4 – Methodology | 125 |
| 4.1 LCOE modelling for solar power in the PSDA | 126 |
| 4.1.1 Configurations of the studied solar power plants | 127 |
| 4.1.2 LCOE model..... | 129 |
| 4.1.3 Simulation | 130 |
| 4.2 Developing MR models from GSHP catalogue data..... | 135 |
| 4.2.1 Description of studied manufacturer’s data tables | 136 |
| 4.2.2 MR model identification..... | 140 |
| 4.2.3 Statistical evaluation..... | 140 |
| 4.3 Modelling energy use in residential buildings | 142 |
| 4.3.1 Input data gathering..... | 145 |
| 4.3.2 Data processing: energy use modelling..... | 149 |

| | |
|--|------------|
| Chapter 5 – Results | 157 |
| 5.1 2050 LCOE projection for solar power in the PSDA | 157 |
| 5.2 Regression analysis..... | 161 |
| 5.2.1 Statistical evaluation for HPI..... | 161 |
| 5.2.2 Modelling approach validation | 164 |
| 5.2.3 Discussion..... | 169 |
| 5.3 Analysis of input parameter influence on residential energy use | 171 |
| 5.3.1 Simulated energy use and model validation | 171 |
| 5.3.2 Influence of envelope factors on energy use..... | 173 |
| 5.3.3 Influence of building orientation on energy use..... | 177 |
| 5.3.4 Financial analysis | 180 |
| Chapter 6 – Conclusions..... | 183 |
| References | 191 |

Content

List of figures

| | |
|--|----|
| Figure 1.1. Trends in CO ₂ emissions from fossil fuel combustion..... | 27 |
| Figure 1.2. World primary energy supply..... | 28 |
| Figure 1.3. Total primary energy consumption in Chile..... | 32 |
| Figure 1.4. Primary energy sources in Chile in 2014..... | 33 |
| Figure 1.5. Energy consumption per sector in 2014..... | 34 |
| Figure 1.6. Temperatures anomalies in central area of Chile, 1961 to 2010..... | 35 |
| Figure 1.7. CO ₂ emissions trend in Chile..... | 36 |
| Figure 1.8. Electricity generation in Chile in 2016..... | 39 |
| Figure 1.9. Electricity generation in Chile 1996-2016..... | 40 |
| Figure 1.10. Geographic division of electricity production..... | 42 |
| Figure 1.11. Total electricity generation from the SING grid during 2016..... | 43 |
| Figure 1.12. Total electricity generation from the SIC grid during 2016..... | 43 |
| Figure 1.13. Global Horizontal Irradiation (GHI) in Chile..... | 44 |
| Figure 1.14. State of RE projects in Chile in 2016 (GW) | 47 |
| Figure 1.15. RE installed capacity evolution..... | 47 |
| Figure 1.16. Payment exemption of transmission charges to NCRE..... | 50 |
| Figure 1.17. Obligations of NCRE integration according to Law 20.257..... | 51 |
| Figure 1.18. Energy capacity projection and NCRE participation in Chile..... | 55 |
| Figure 1.19. Residential fuel consumption in Chile..... | 56 |
| Figure 1.20. Electricity use by sector in 2014..... | 57 |
| Figure 1.21. Construction year of buildings in Chile..... | 58 |

List of figures

| | |
|---|-----|
| Figure 2.1. The Three E's of sustainability..... | 64 |
| Figure 3.1. Solar radiation components..... | 68 |
| Figure 3.2. Solar geometry of a sloped surface..... | 69 |
| Figure 3.3. Global PV market by type in 2015..... | 76 |
| Figure 3.4. Solar cell efficiency evolution by type..... | 77 |
| Figure 3.5. Evolution of global PV cumulative installed capacity (GW)..... | 78 |
| Figure 3.6. Renewable energy potential for 2050 in EJ/year by energy source..... | 78 |
| Figure 3.7. The decreasing cost of c-Si PV module (1977-2016)..... | 79 |
| Figure 3.8. The decreasing cost of c-Si PV module (2011-2016) | 79 |
| Figure 3.9. CSP system technologies..... | 80 |
| Figure 3.10. PV module and CSP system prices as a function of global cumulative installed capacity..... | 87 |
| Figure 3.11. PV grid parity in Europe 2016 (shaded area). A 2010 forecast..... | 88 |
| Figure 3.12. PV and CSP LCOE evolution for the BLUE and ROADMAP Scenarios and grid parities for coal-fired thermal power plants with a carbon emission price of 0, 25 and 50 \$/ton CO ₂ | 89 |
| Figure 3.13. GSHP schematic in the heating mode..... | 90 |
| Figure 3.14. GSHP types..... | 91 |
| Figure 3.15. Air and ground temperatures, Falmouth, England..... | 93 |
| Figure 3.16. Evolution of global GSHP installed capacity 1995 – 2015..... | 94 |
| Figure 3.17. Pressure-enthalpy chart for the heat pump cycle using the refrigerant R134a..... | 95 |
| Figure 3.18. Evolution of temperatures through GSHP heat exchangers (from left to right: ground coil (GC), evaporator, and condenser) | 96 |
| Figure 3.19. Three dimensional interpolations..... | 104 |
| Figure 3.20. Energy balance of a building during winter..... | 111 |
| Figure 3.21. Conduction and convection heat transfer..... | 113 |
| Figure 3.22. Characteristic dimension of solid ground floor..... | 114 |
| Figure 3.23. Solid ground floor with horizontal (A) and vertical (B) edge insulation..... | 116 |
| Figure 3.24. Cooling utilization factor vs. loss/gain ratio for different time constants, as in Equation (3.82) | 122 |

List of figures

| | |
|--|-----|
| Figure 4.1. Daily average GHI on monthly mean at selected locations, representative of northern Chile..... | 126 |
| Figure 4.2. Global CSP cumulative installed capacity and annual CSP electricity production...130 | |
| Figure 4.3. Global PV cumulative installed capacity and annual PV electricity production.....131 | |
| Figure 4.4. Projection of cumulative installed capacity for Blue Map and Roadmap scenario to PV and CSP technologies.....132 | |
| Figure 4.5. Heat capacity against inlet source temperature for $t_{il} = 15.6^{\circ}\text{C}$ and $v_l = 1.45\text{L/s}$138 | |
| Figure 4.6. Heat capacity against inlet load temperature for $v_s = 1.45\text{L/s}$ and $v_l = 1.45\text{L/s}$138 | |
| Figure 4.7. COP against inlet source temperature for $t_{il} = 15.6^{\circ}\text{C}$ and $v_l = 1.45\text{L/s}$139 | |
| Figure 4.8. COP against inlet load temperature for $v_s = 1.45\text{L/s}$ and $v_l = 1.45\text{L/s}$139 | |
| Figure 4.9. Structure of the MEEDI simulation tool.....144 | |
| | |
| Figure. 5.1. 2050 LCOE projection to PSDA between 2014 and 2050 for PV, CSP and PV-CSP in Blue Map scenario (1)..... | 158 |
| Figure 5.2. 2050 LCOE projection to PSDA between 2014 and 2050 for PV, CSP and PV-CSP in Roadmap scenario (2)..... | 159 |
| Figure 5.3. Plot of HC_1 (kW) and COP_1 observed versus predicted..... | 167 |
| Figure 5.4. Plot of residuals versus predicted HC_1 (kW) and COP_1 | 168 |
| Figure 5.5. Plot of residuals versus predicted HC_2 (kW) and COP_2 | 168 |
| Figure 5.6. Plot of residuals versus predicted HC_3 (kW) and COP_3 | 168 |
| Figure 5.7. BCH annual energy use for scenario 1 and 2 (S1 and S2)..... | 172 |
| Figure 5.8. Influence of wall (a), ceiling (b) additional insulation thickness, windows (c), doors (d) U-values, and air infiltration rate (e) to the annual energy use E..... | 174 |
| Figure 5.9. Influence comparison of wall/ceiling insulation thickness on annual energy use in Santiago..... | 176 |
| Figure 5.10. Influence comparison of window/door U-value on energy use in Santiago..... | 176 |
| Figure 5.11. Annual solar gain through side 1 windows..... | 177 |
| Figure 5.12. Influence of BCH orientation on annual energy use..... | 178 |
| Figure 5.13. Influence of window area and building orientation on energy use in Santiago..... | 179 |

List of figures

List of tables

| | |
|---|-----|
| Table 1.1. The patterns of the Strategy for climate change..... | 38 |
| Table 1.2. Solar PV industry evolution 2013 -2016 in Chile..... | 45 |
| Table 1.3. Chilean RE potential..... | 48 |
| Table 1.4. Minimum requirements for building elements per climatic zone..... | 59 |
| Table 1.5. Maximum window glazing percentage area per climatic zone..... | 60 |
| Table 1.6. Balanced U-values, alternative method to comply with regulation..... | 60 |
| | |
| Table 3.1. Costs comparison between solar PV, CSP and conventional power plants..... | 85 |
| Table 3.2. Global GSHP installations in year 2015 (change from 2010 to 2015) | 94 |
| Table 3.3. Heating Capacity Data NDW100 WaterFurnace GSHP..... | 102 |
| Table 3.4. GSHP heating capacity (kW) data from manufacturer’s performance table..... | 103 |
| | |
| Table 4.1. Values for the projection of LCOE for PV and CSP..... | 134 |
| Table 4.2. Technical features of the considered GSHP..... | 137 |
| Table 4.3. Parameter variation in data tables in heating mode and operating limits..... | 137 |
| Table 4.4. Climate conditions of 7 Chilean locations..... | 145 |
| Table 4.5. Heating and cooling seasons by location..... | 146 |
| Table 4.6. Reference house dimensions..... | 147 |
| Table 4.7. Reference house orientation and window distribution..... | 147 |
| Table 4.8. Physical characteristics of the BCH envelope materials..... | 148 |
| Table 4.9. Heating and cooling systems overall efficiencies..... | 148 |
| Table 4.10. Fuel costs and carbon emission factors..... | 149 |

List of tables

| | |
|--|-----|
| Table 5.1. Test results of MR models for HP1..... | 163 |
| Table 5.2. Model coefficients and statistics (Model for HC1)..... | 165 |
| Table 5.3. Model coefficients and statistics (Model for COP1)..... | 165 |
| Table 5.4. Summary of statistical evaluation of MR models for HP1, HP2, and HP3..... | 166 |
| Table 5.5. BCH envelope component U-values..... | 171 |
| Table 5.6. Physical characteristics of the LEH..... | 180 |
| Table 5.7. Annual energy savings from BCH to LEH and payback periods..... | 181 |

Chapter 1 – Introduction

1.1 Context

1.1.1 The global energy panorama

The energy in the modern society has become a major challenge for users, suppliers and political actors. This challenge is to provide accessible, sufficient and secure supply of energy. The demand for energy worldwide is rising and will not slow down as emerging countries are developing rapidly and developed countries are maintaining their energy level needs. Between 1973 and 2014, world global final energy consumption increased by 125% [1] and the General global trends of the International Energy Agency predicts world energy consumption to annually increase by 1.5% through 2030 compared to 2007 levels [2].

Sources of energy present in the world are of three main categories. The most used source is fossil fuels [1, 3]. Nuclear power, with relative dangerousness and unknown effects of waste disposal on the environment and health, is used mostly in developed countries [1, 3]. Renewable energy (RE) sources are used worldwide as possible as they represent a solution, which is not only environmentally friendly but also non-dependent to energy suppliers. Renewable energy source is abundant and available in a wide range (solar, wind, biomass, hydraulic).

In the actual energy situation, the use of fossil fuel is not seen sustainable as earth reserves are diminishing rapidly due to increasing demand. Also the great concern about burning fossil fuels

is the resulting impact on the natural environment, like increase of greenhouse gases (GHG) concentration causing global warming, as well as the increase of poisonous substances in air, water and lands affecting living health. Nuclear power is not seen to be the energy which will replace fossil fuels. Following the March 2011 Fukushima nuclear disaster, Germany permanently shut down eight of its reactors and pledged to shutter the rest by 2022. Shortly thereafter, the Italians voted overwhelmingly to keep their country non-nuclear. Switzerland and Spain followed suit, banning the construction of any new reactors [4]. The reasons mentioned bring to consider renewable energy as an adequate alternative to fossil fuels.

1.1.2 The global environmental scene

Energy has a considerable role to play in the environmental scene as its production, distribution and consumption is directly linked with GHG emissions. Since the Industrial Revolution, annual CO₂ emissions from burning fossil fuels dramatically increased from near zero to about 9 gigatons (Gt) of carbon in 2010, which represent about 33 Gt of CO₂-gas, as shown in Figure 1.1 [5]. Carbon dioxide (CO₂) is the most emitted GHG, but other gases such as methane (CH₄), nitrous oxide (NO) emitted from agricultural activities and other sources also have effects on global warming.

The increase of GHG in the atmosphere results in the global warming of the earth temperatures. The concentration of atmospheric GHG could reach double its pre-industrial level within the next 30 years, leading to a temperature rise of at least 2°C [6]. As global temperatures rise, sea levels will also go up. Coasts will become more vulnerable to flooding and erosion, with significant consequences for the people, infrastructure, businesses and nature in these areas. The latest study from the International Panel on Climate Change (IPCC) predicts that sea levels will rise by 18-59 cm by the end of the century [7], and even these estimates are conservative.

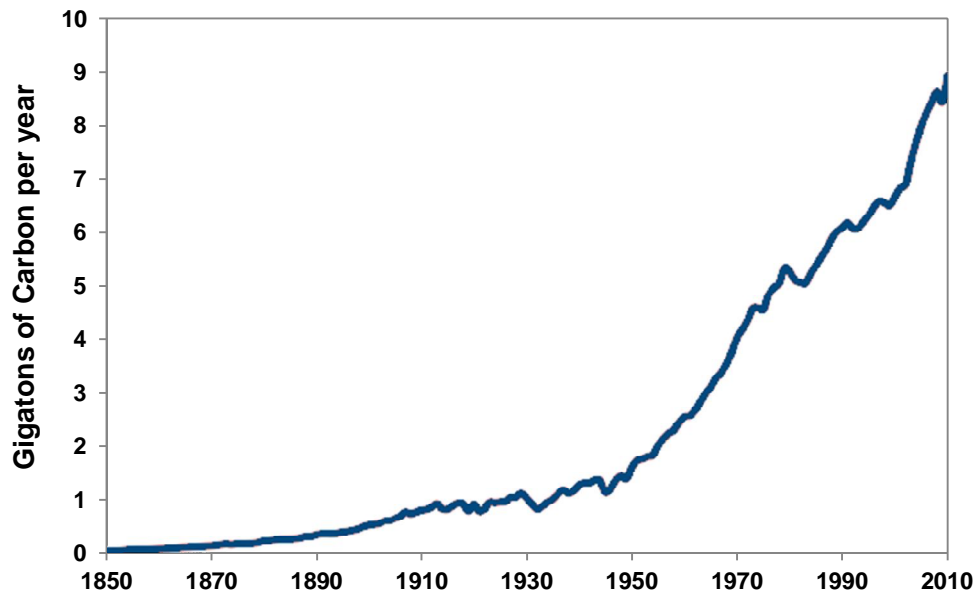


Figure 1.Error! Use the Home tab to apply 0 to the text that you want to appear here.**1. Trends in CO₂ emissions from fossil fuel combustion [5]**

Global warming is also directly linked with the increase number of natural catastrophes resulting from extreme weather such as intense storms. Heavy rains and floods can affect millions of people, drive them from their homes, and create important losses, not only taking people lives but also destroying buildings, infrastructures, materials, and crops in a very sudden manner. In 2011, the human and economic impacts of the disasters were massive. Natural disasters killed a total of 30,773 people and caused 244.7 million victims worldwide [8]. The economical losses from natural catastrophes between 1954 and 1959 were US\$ 35 billion, while between 1995 and 1999 these losses were around US\$ 340 billion [9]. In 2011, economic damages from natural disasters were the highest ever registered, with an estimated US\$ 366.1 billion [8].

In order to avoid greater damage on ecology, more frequent and intense natural catastrophes in the future, there is a need to take control on GHG emissions. It can be done in two ways: firstly, existing energy resources must become more efficient, and secondly produce energy in a sustainable manner replacing energy systems that use conventional fossil fuel sources by renewable energy driven systems.

1.1.3 The global energy problem

1.1.3.1 Status and trends

Fossil fuels have always been the main sources of primary energy supply worldwide (see Figure 1.2). The demand for fossil fuels has been continuously rising since 1973, and as a consequence, their reserves are diminishing rapidly around the world. In 2014 fossil fuels (oil, coal and gas) still represent 81% of the global primary energy supply [1].

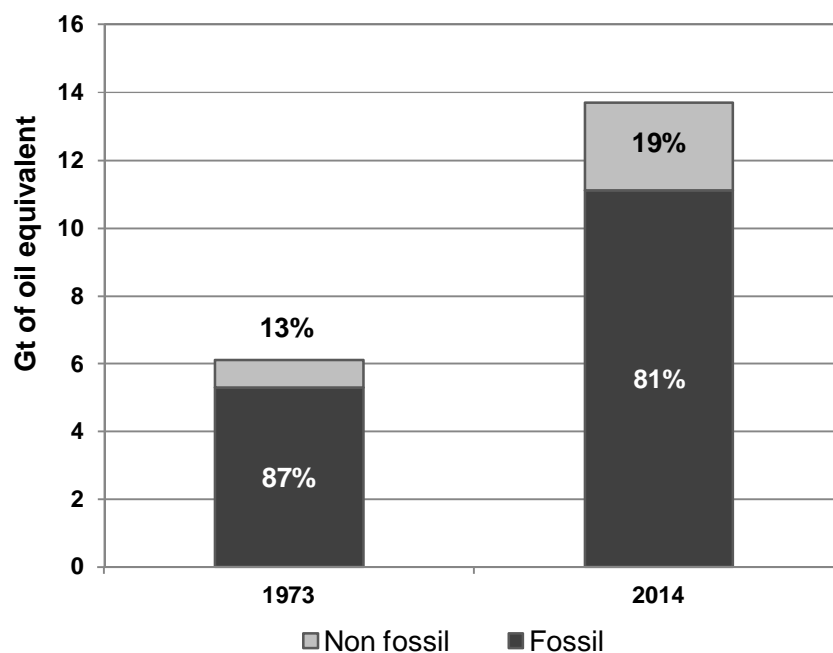


Figure 1.2. World primary energy supply [1]

Nuclear gained an increased market share after the oil crises in the 1970s. In 2014, nuclear supplied 4.8% of the world primary energy which generated 2,535 terawatt hours (TWh) (10.7% of the world total electricity) [1]. Nuclear power continues to play a role in lowering GHG emissions, along with renewable energy. However the risks of handling the uranium fuel, as well as the toxicity of the nuclear waste are real issues. Also hazardous consequences remain concerning radiation that can be rejected to the environment in case of accident.

The renewable energy share in 2014 represents 14.1% of the global primary energy supply [1]. The share is expected to become more important in the future. The sector is growing fast,

investors are seeing business opportunities, the market is offering more affordable solutions, while consumers concerns toward clean and environment friendly energy are rising. With new technologies developments and appropriate policies, the share of renewables in the energy market could reach a high share in the future.

The world gross domestic product (GDP) is a key driver of energy demand in all regions. It is assumed to grow by an average of 3.2% per year over the period 2008-2035 [10]. The 2015 World Energy Outlook (WEO) New Policies Scenario projects an increase of nearly 33% of primary energy consumption between 2013 and 2040, with a share of fossil fuels in the global energy mix falling from 86% to 79% during that period, nuclear growing to a 16% share, and renewables growing in the generation mix from 14% in 2013 to 19% in 2040 [11].

1.1.3.2 Future challenges and prospects

The access to energy sources is crucial for the social and economic development of countries. The key strategic challenges presented by the World Energy Outlook (WEO) are security of supplies, investment in energy infrastructure, threat of environmental damage caused by energy use, and uneven access of the world's population to modern energy. In 2010, the WEO estimated at US\$ 33 trillion the global investment on energy supply infrastructure to meet energy demand in 2035 [10]. From this estimation, the electricity sector investment accounts for US\$16.6 trillion in view of the increase of the electric demand, the replacement of many old plants that will be retired, and the shift to higher unit cost renewables [10]. In 2011, global investment in renewable power and fuels increased 17% from 2010 to \$257 billion. It is 6 times the investments of 2004 and 93% higher than in 2007 [12]. Renewable energy sources can also provide commercially attractive options to meet consumers' needs and create employment opportunities as shown by Burgos-Payán et al. for Spain [13]. Fossil fuels are diminishing rapidly around the world as the demand is rising since the industrial revolution. At the end of 2015, the reserves to production ratio were estimated to 50.7 years for oil, 52.8 years for natural gas, and 114 years for coal [14]. This situation highlights on the need to switch to sustainable energy source, which at the same time should be environment friendly avoiding stress on ecology.

The potential of renewable energy is huge. The abundant and inexhaustible resource of sustainable energy can be easily sufficient to provide the global energy demand [15, 16].

Renewable energy sources such as solar, bioenergy, wind, wave, tidal and hydro, can potentially meet several times the global energy demand, and thus present all the characteristics to be a viable solution to overcome future energy challenges. Electrification is a key issue to channel demand into electricity for which a multitude of renewable source options exist. The IEA WEO 2012 predicts in the New Policies Scenario an increase of 70% of electricity demand between 2010 and 2035 to almost 32 000 TWh with a share of renewables in the generation mix to grow from 20% in 2010 to 31% in 2035 giving the assumption that subsidies to renewable-based electricity would amount to a total of \$3.5 trillion over 2012-2035 [17].

Solar energy is the most promising renewable source, mainly because it is the most abundant and inexhaustible of all and thus presents a great potential [18]. Solar energy is everywhere. It can provide security of supply even to remote places where grids not yet come or is too costly to install. For instance, it can be a more economical solution to provide power to the nearly 1.3 billion people who remain without access to electricity and 2.6 billion that do not have access to clean cooking facilities [17]. Solar power is not yet completely seen as a viable solution for large scale commercial applications, because it is still costly and the governmental policy does not offer the support that would be expected by the market. However, new technology developments such as Concentrated Solar thermal Power (CSP) are emerging in the clean electricity market, presenting the ability to store heat energy in order to produce electricity after sunset, thus providing 24 hour per day electricity [19].

1.2 The Chilean energy scenario

1.2.1 Background information

Chile is part of the South American continent occupying a long, narrow strip of land between the Andean mountains to the east and the Pacific Ocean to the west. The main land of Chile lies between 13.7 and 55.59 south latitude and 66.3 and 75.38 west longitude. It has a total area of 748,800 km², which is slightly more than the size of Spain and Portugal combined. Chile measures 4,270 km from north to south and is 356 km wide at its broadest point (just north of Antofagasta), with an average width of 175 km from east to west. It has a land frontier of 6,339 km and a coastline of 6,435 km. Chile shares borders with Peru to the north, Bolivia to the northeast, Argentina to the east.

The nation is divided into five natural regions: the desert region in the north; the fertile, densely populated central valley; the great mountain zone (the Andes) along the east border, the dense rain forest in the south-central region; and the cold, wet and windswept landscape in the southern region. The coastline of the southern region includes thousands of islands, extending down to Cape Horn. Climate varies considerably because of the wide range of latitudes covered by the country. Temperatures steadily cool as the country extends southward, away from the equator and toward Antarctica. The mean temperature at Arica (in the far north) is 18°C, while that of Santiago (in the centre) is 14°, and Punta Arenas (in the extreme south) averages 6°C. Winter temperatures are moderated by winds off the Pacific Ocean, and sea winds also temper the heat in summer. Central Chile, where most of the country's population is concentrated, has a Mediterranean type of climate, with mild winters and warm and dry summers [20].

Chile has a population of 16.3 million (2012 figures) with an annual growth rate of 0.99% (2002-2012) [21]. The electricity consumption per capita of 3.9 megawatt hours (MWh) remains below that of the Spanish (5.4 MWh), Germans (7.0 MWh), or the North Americans (13.0 MWh), but it is the highest of the South American countries, such as Brazil (2.6 MWh), Argentina (3.1 MWh), Peru (1.3 MWh), Bolivia (0.8 MWh), and above the world average (3.0 MWh) [1]. With net imports of fossil fuels (oil, coal and gas) of 24.3 million tonnes of oil equivalent (Mtoe) mainly used in power generation and a net energy production of 12.9 Mtoe (2014 figures) [22, 23], Chile has currently an energy dependency equivalent to 65%. As a

1.2 Chilean energy scenario

comparison, Argentina has an energy dependency of 15%, Brazil has 14% dependency on energy imports, and Peru and Bolivia produce more energy than they consume. Unlike its South American neighbours, the high dependency on foreign fossil fuel imports makes Chile vulnerable to supply disruptions and energy price volatility. At the same time, the use of these fuels increases levels of air pollution, being the sectors of energy and transport that contribute the most to harmful gas emissions with 47% and 30% respectively of the national emissions of CO₂ equivalent [24].

In the year 2015, GDP per capita was reported to be US\$ 15,653 with an annual growth of 2.3% and an annual inflation of 3.0% [25]. Chile's GDP is composed of agriculture (4%), industry (32%) and services (64%) [26]. Main industries include copper and other minerals mining, iron and steel, wood and wood products, food and beverage processing, transportation equipment, cement, textiles, chemicals, petroleum and machinery.

1.2.2 Energy demand and supply

The evolution and patterns of energy use has a great importance for understanding the energy situation of Chile. It allows knowing the limits and the context of the energy production of the country. The total energy consumption in Chile in 2014 was 34.7 Mtoe [27]. The evolution of total primary energy consumption in Chile is shown in Figure 1.3.

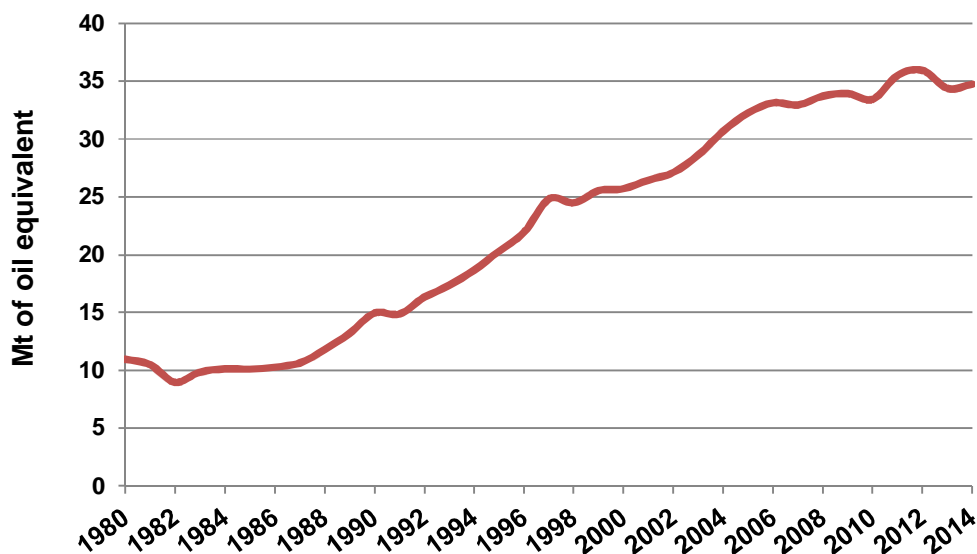


Figure 1.3. Total primary energy consumption in Chile [27]

In modern history, fossil fuels have always been the main sources of primary energy supply worldwide [1, 14, 24]. There are no exceptions in Chile, as for most developing countries, pressures from economic and population growth have traditionally forced governments to look at cost-effective options, mainly those exploiting fossil fuel sources, to cope with the increased demand for electricity from households and industry [28]. Figure 1.4 presents the sources of primary energy in 2014.

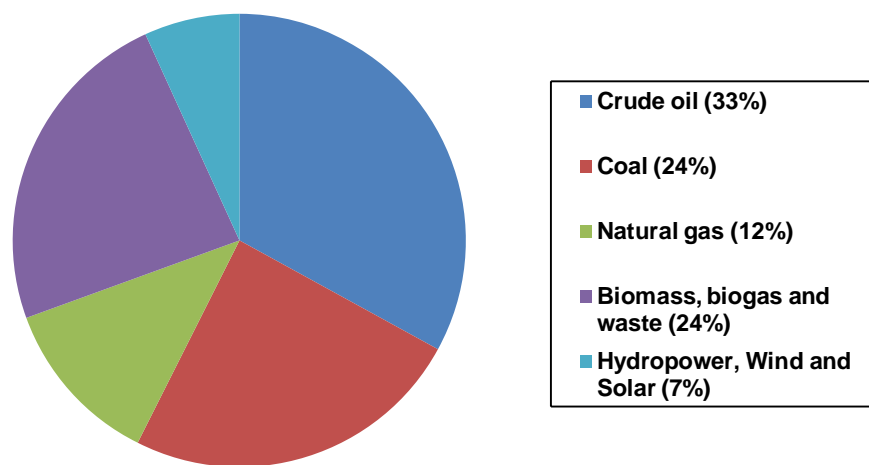


Figure 1.Error! Use the Home tab to apply 0 to the text that you want to appear here.**4. Primary energy sources in Chile in 2014 [29]**

While economic growth is often linked to increased energy demand, in competitive markets all producers are interested in lowering the energy consumption per unit of production while different signs of climate change created an urgent need to reduce emissions from burning fossil fuels. Indeed, burning fossil fuels (oil, gas, and coal) has been identified as the predominant cause of the increase of greenhouse gas (GHG) concentrations in the atmosphere. In Chile, the most common source of energy is petroleum, which represents 54% of the final secondary consumption. Virtually all derivatives are products of the refining of crude oil, which accounted for 96.5% of imports in 2014 [29].

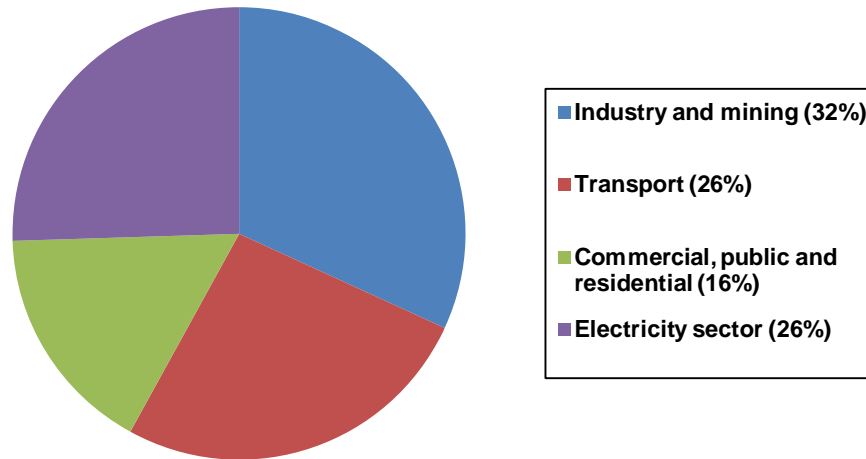


Figure 1.Error! Use the Home tab to apply 0 to the text that you want to appear here.**5. Energy consumption per sector in 2014 [29]**

In Chile, a country experiencing rapid industrialization and development but still with a medium income per capita, economic growth and increased energy consumption are directly related. As shown in Figure 1.5, industry and mining and transport are the sectors with the highest energy demand. These are also the ones which rely mostly on fossil fuels.

Statistics say that there is a link between the GHG growth and the final energy consumed by the population. One of the tasks for the future is to achieve a decoupling between both variables, which would increase competitiveness in a context where economical energy sources will become increasingly scarce.

1.2.3 Energy and environmental challenges

Traditionally, the pressure for economic growth coupled with burgeoning populations has forced governments to pursue the most cost-effective energy solutions (the exploitation of fossil fuels), to cope with the increased demand for electricity from households and industry [30]. Studies have shown that cost-benefit analyses and project evaluations rarely consider environmental and social costs associated with electricity generated from fossil fuels [31, 32]. Burning fossil fuels is responsible for the dramatic increase in greenhouse gases (GHG)

concentrations in the atmosphere resulting in a global warming with severe consequences for the planet's environment and populations. Moreover fossil fuels reserves are diminishing rapidly. Thus, renewable energy is considered as an adequate and sustainable alternative.

According to research, the country has experienced a warming trend ranging from 0.2 to 1.1 °C in the interior regions of the north, centre and southern, while there has been a cooling of -0.2 to -0.5 °C in the southern regions of the country, during the period 1901-2005. There has also been a chill in the northern coastal area and south-central Chile of -0.2°C per decade [33]. Figure 1.6 shows the anomalies or differences between normal and extreme temperatures averaged each year over the period 1961-2010 for the central regions: Valparaíso, the archipelago Juan Fernández, Santiago, Curicó, Chillán and Concepción. These locations show an increase in the minimum temperatures up to the late seventies, but later it doesn't present a significant increase. In cities of the inner core area, like Santiago, increases in extreme temperatures are recorded in both the minimum and maximum.

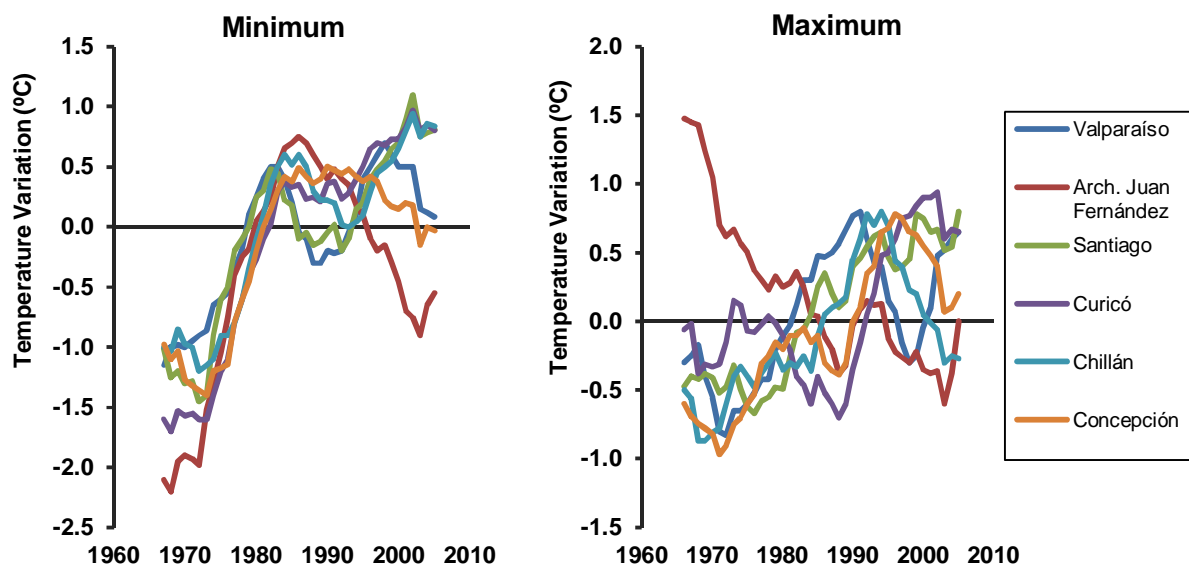


Figure 1. Error! Use the Home tab to apply 0 to the text that you want to appear here. **6. Temperatures anomalies in central area of Chile, 1961 to 2010 [34]**

Temperature anomalies affect, among other factors, the future availability of water resources, which are essential for human development. Chile has one of the largest and most varied glacial reserves in the world, representing 3.8% of the total world area, excluding Antarctica and

1.2 Chilean energy scenario

Greenland. It also has the largest coverage in South America, with 76% of the glacier area of the continent, estimated at 28,286 km². The vast majority of the country's glaciers are experiencing a general trend of mass loss, with rates of linear regression which vary from a few meters annually (especially in the north zone), up to hundreds of meters per year in southern Chile.

One of the main reasons of climate change is airborne emissions of GHG, where the most damaging gases are: carbon dioxide (CO₂), methane (CH₄), nitrous oxide (N₂O), hydro fluorocarbon gases (HFCs), perfluorocarbons (PFCs) and sulphur hexafluoride (SF₆). While CO₂ has the largest share with 65%, CH₄ and N₂O represent 21% and 14% of the GHG emissions respectively, and HFCs, PFCs and SF₆ emissions are insignificant. CO₂ emissions are attributed mainly to fossil fuel burning, cement production and mining activities. Net emissions from Chile for 2014 were 76 million tonnes (Mt) of CO₂ equivalent approximately (4.7 tonnes per capita and per year) [27, 24]; the following Figure 1.7 shows the trend of total net emissions of CO₂ equivalent for the period between 1980 and 2014. CO₂ emissions in Chile have doubled in 2014 compared to 1995 level. At sector level, the energy industry sector makes a major contribution and increasingly shapes the values of national emissions, reaching a value of over 35 million tonnes of CO₂ equivalent in 2014 (46% of the total Chilean emissions) [24]. The second highest CO₂ emitter is the transport sector with 24.5 Mt of CO₂ equivalent emitted (over 32% of the national emissions) [24].

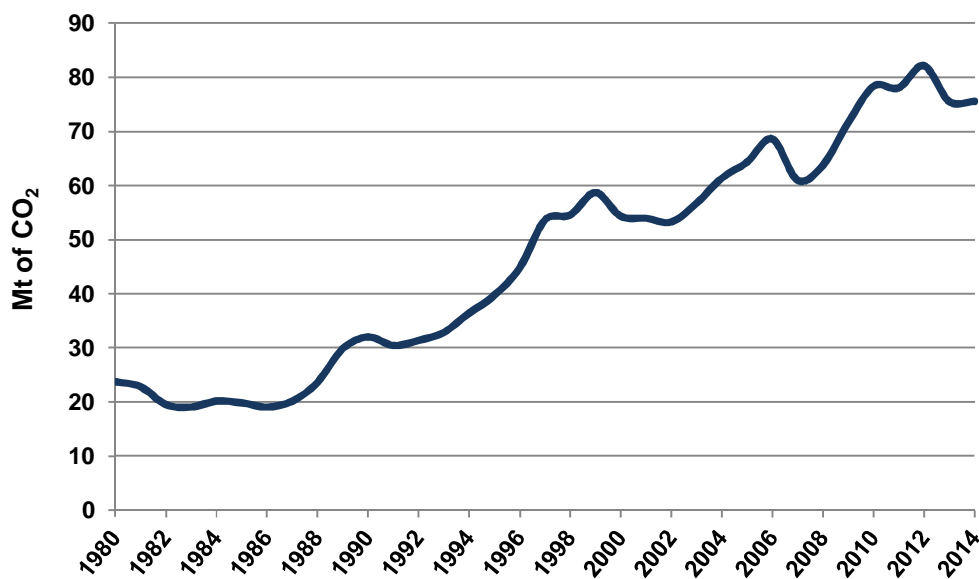


Figure 1.Error! Use the Home tab to apply 0 to the text that you want to appear here.**7. CO₂ emissions trend in Chile** [24, 27]

Globally, the Kyoto Protocol, signed the year 1997, is the only treaty that has set binding obligations on almost all industrialized countries in the purpose of reducing the emissions of their GHG. Although Chile participates in the Clean Development Mechanism (CDM) set in the Kyoto Protocol in order to assist developing countries in achieving sustainable development by promoting environmentally friendly investment from industrialized country governments and businesses, Chile has currently no legally binding emission limit under the Kyoto Protocol ratified in 2002. The Environment National Committee (*Comisión Nacional del Medio Ambiente, CONAMA*) is the organism dedicated to the protocol. At the 2009 United Nations Climate Change Conference (Copenhagen Climate Summit 2009), Chile however announced its commitment to reduce by 20% its GHG emissions by the year 2020 [35].

In Chile, The National Advisory Committee on Global Change (*Comité Nacional Asesor Sobre Cambio Global, CNACG*) was created in 1996 by the Supreme Decree N°466 to discuss and elaborate the government strategy on climate change [36]. This committee is formed by different national institutions, the CONAMA as president, the Ministry of external relations as vice-president, the Ministry of Agriculture, the National Energy Commission (*Comisión Nacional de Energía, CNE*), the Meteorological Office of Chile (*Dirección Meteorológica de Chile*), the Scientific and Technological Investigation National Committee (*Comisión Nacional de Investigación Científica y Tecnológica*), the Science Chilean Academy (*Academia Chilena de Ciencias*), the General Office of Maritime Territory and Merchant Marine (*Dirección General del Territorio Marítimo y de Marina Mercante*) and the Hydrographic and Oceanographic Army of Chile (*Servicio Hidrográfico y Oceanográfico de la Armada de Chile*). The CNACG has developed the National Strategy Plan for Climate Change in 2006, which includes three principal action programs in order to tackle climate change over the period 2008-2012, as shown in Table 1.1 [37]. The three programs entail the willingness of Chile to involve relevant sectors and Chilean experts to participate in the discussion on economical mechanism established by the Kyoto protocol, to utilize the CDM, the basic orientation design that respect new ways of limitations and/or reductions of GHG for developing countries. The National Strategy Plan for Climate Change also implied the creation of a special fund for technical and scientific investigation.

Table 1.1. The patterns of the Strategy for climate change [37]

| Program | Objectives |
|---|--|
| Adaptation to climate change impacts | <ol style="list-style-type: none"> 1. Evaluation of environmental, social and economical impacts of climate change. 2. Definition of adaptation measures. 3. Realization and monitoring of adaptation measures. |
| Mitigation of GHG emissions | <ol style="list-style-type: none"> 1. Options analysis of GHG emissions mitigation in Chile. 2. Definition of mitigation measures. 3. Realization and monitoring of mitigation measures. |
| Creation and promote capacities in climate change | <ol style="list-style-type: none"> 1. Spread the word and raise public awareness on climate change. 2. Develop education and research on climate change. 3. Improve systematic climate observation. 4. Generate accessible and high quality information for decision making. 5. Develop institutional capacities for mitigation and adaptation. 6. Develop and transfer technologies for mitigation and adaptation. 7. Review and update regularly GHG inventory. 8. Actively participate in climate change international agenda. 9. Reinforce international cooperation in climate change 10. Establish synergies with implementation of others global conventions. |

1.2.4 Electricity generation

The total electricity consumption of Chile over one year period from 1st January 2016 to 31st December 2016 was 73.364 terawatt hours (TWh) [38]. Over that period of time, 63% of Chile's electricity was generated using thermoelectric sources (fossil fuels), specifically coal, gas and oil, as shown in Figure 1.8. However, Chile is not a fossil energy producer; the country satisfies its internal consumption based mainly on imported fuels, which makes Chile dependent on international energy markets in order to secure its needs [39]. The remaining 37% of electricity comes mainly from hydropower (27%), including small and large dams, but their production of electricity varies significantly from one year to another. This dependence on the hydrology of a

particular period can lead to electricity rationing in dry years. Over that period, 6% of the electricity generated in the country comes from wind (3%), biomass (4%) and solar (3%) sources.

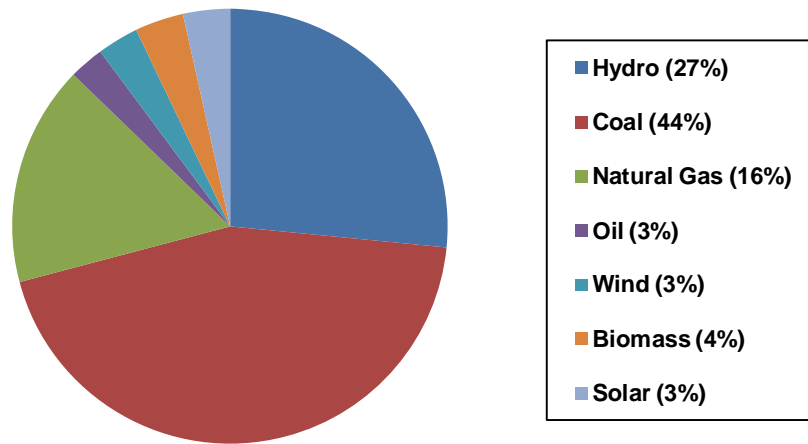


Figure 1.8. Electricity generation in Chile in 2016 [38]

In order to secure energy supply, Chile is not only staying dependent on imported energy, but is also going directly against the definition of sustainable development, especially since the electricity sector has begun to rely heavily on coal-fired power plants. Up to 3 gigawatt (GW) of capacity are being planned to enter the system in the next three to five years [39], including for example the 470 megawatt (MW) Angamos Power Plant, which has adopted battery storage and seawater cooling tower technologies [40]. However, environmental concerns and local opposition have resulted in delays, cancellations, and court rejections for other coal-fired power projects [41], and the country is shifting its focus to the expansion of natural gas supplies [42]. Approval has recently been granted to expand regasification capacity at the liquefied natural gas (LNG) plant in Quintero Bay by 50%, from 10 million cubic meters per day (m^3/day) to 15 million m^3/day [43]. As another solution to meet its future electricity needs, Chile has announced that it intends to pursue nuclear power, although it currently has no nuclear power plants [44]. Nuclear energy presents the advantage of not producing carbon emissions when generating electricity, but environmental concerns remain regarding the handling of the wastes it produces. Patterns of the energy sector evolution in Chile can be seen on Figure 1.9 [45], such as the rapid growth of electricity production since the start of natural gas imports from Argentina in 1998, the variations of hydro power plants production during the years, the recent growth of coal power, the gas

1.2 Chilean energy scenario

shortage in 2008 replaced by diesel power production, as well as the uptake of RE particularly since 2012.

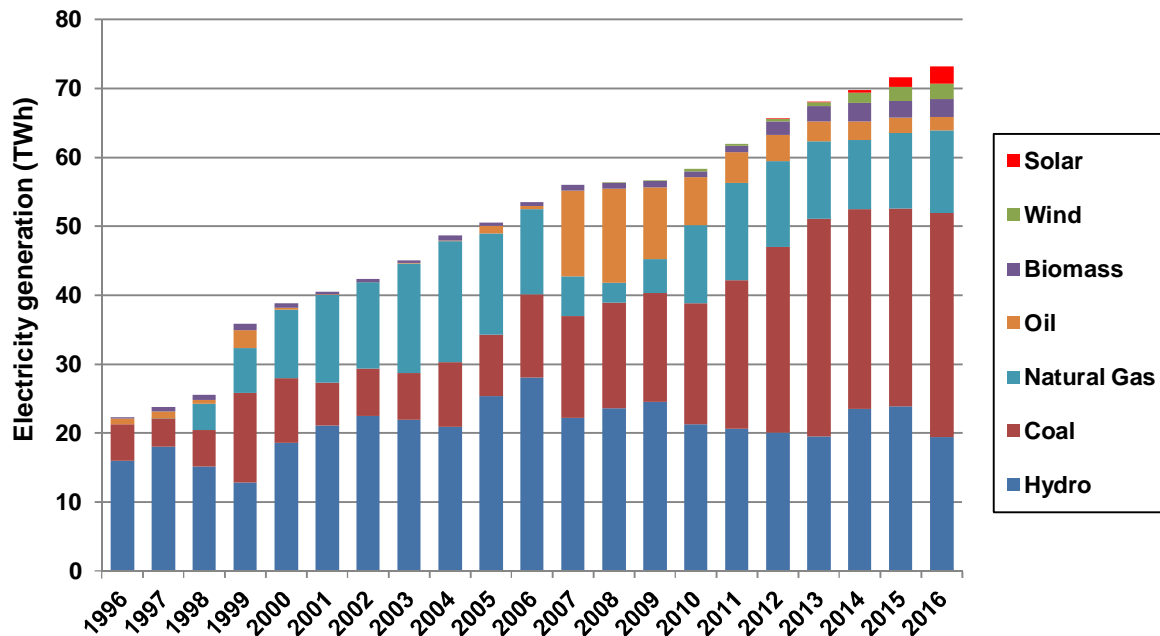


Figure 1.Error! Use the Home tab to apply 0 to the text that you want to appear here.9. Electricity generation in Chile 1996-2016 [45]

RE sources for electricity generation in use is mostly hydroelectricity, while wood based biomass and wind account for only 3% for the generation of grid electricity. The construction of five hydroelectric plants with large dams and reservoirs was approved in 2011 on two rivers in the Aysén Region (Chilean Patagonia): the Baker and the Pascua, both of which have river basins with the richest biodiversity in the country [46]. These hydropower plants are supposed to generate approximately 2.75 GW to be incorporated into the central national grid. It is expected to flood about 5,000 ha of land, currently used for agriculture, recreation, tourism, and biodiversity conservation zones. For instance, it is here that some endangered species such as the huemul, a typical Chilean deer, would be affected. Other environmental concerns include the impacts on rivers, water activities and ecological processes and functions. The installation of a network of pylons crossing the Patagonian landscape is also part of the project, thus spoiling the scenic view to tourists visiting the area. There are doubts concerning the environmental sustainability of such project; however it has the potential to help Chile in matching its demand

for electricity, as well as making it more energy independent and contributing to reduce CO₂ emissions from electricity generation.

Periodic hydroelectricity shortages (due to low precipitation), past Argentine natural gas cutoffs, or the rise of fossil fuel costs and investment costs of new energy projects are all factors that have a direct impact on the inflation of the electricity cost in the country. According to Andrés Santa Cruz, president of the Production and Trade Confederation (*Confederación de la Producción y del Comercio*, CPC) [47], the marginal cost of electricity of 200 US\$/MWh in 2013 would have been only 90 US\$/MWh if hydrology was normal. If hydropower presents an important potential in Chile, periodic shortages have motivated the government to seek greater diversity in the fuel mix for its electric power generation and spurred the government to study the extent to which non-hydropower renewable energy (also referred as “non-conventional renewable”) could contribute to the electricity fuel mix [48].

It has become crucial for the country to be able to provide adequate energy supplies in order to continue its economic growth. Therefore, Hanel et al. [39] have noted that it is of critical importance to ensure the development of indigenous energy sources at a sufficient rate such as needed for the substitution of imported energy resources in order to rapidly achieve energy security and a degree of energy independence.

The Chilean electricity market is composed of three independent and private sectors: generation, transmission and distribution. The government plays a role of regulator in the National Energy Commission (*Comisión Nacional de Energía* - CNE). The CNE is a public organism responsible for analyzing prices, tariffs and technical standards of energy, and is responsible to make the corresponding analysis in order to coordinate plans and standards for this sector. The Chilean electricity system is divided into 4 subsystems (Figure 1.10):

1.2 Chilean energy scenario



Figure 1. Error! Use the Home tab to apply 0 to the text that you want to appear here. **10. Geographic division of electricity production**

- Northern Interconnected System (*Sistema Interconectado del Norte Grande - SING*): it represents 28% of total electricity generation. Supplies energy from Arica to the south of Antofagasta and uses mainly thermoelectric, coal and diesel to generate power. Figure 1.11 illustrates the total electricity generation in SING in 2016.
- Central Interconnected System (*Sistema Interconectado Central - SIC*): represents 71% of the total energy generated and it is responsible for supplying from the second region to Chile. Its main sources of power generation are thermoelectric, hydroelectric, wind and solar energy. Figure 1.12 illustrates the total electricity generation in SIC in 2016.
- Aysén System: represents 0.3% of the total energy generation, serves the Aysén energy consumption. The electric generation sources for this system are thermoelectric, hydroelectric and wind power.

- Magallanes System: supplies energy for Magallanes and Chilean Arctic and it represents 0.7% of the country’s total energy generation, and it does not use renewable sources.

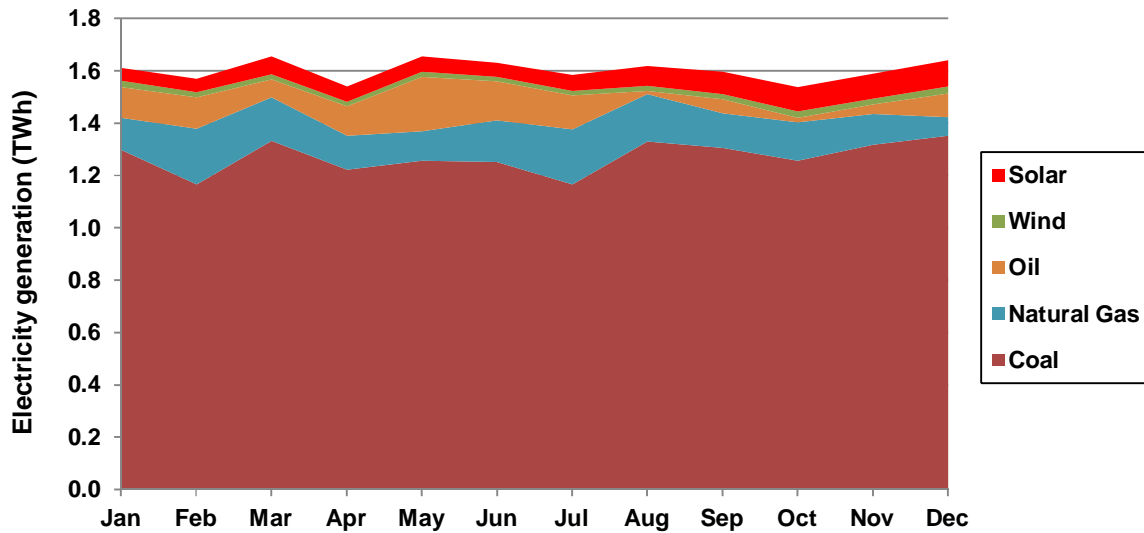


Figure 1.11. Total electricity generation from the SING grid during 2016

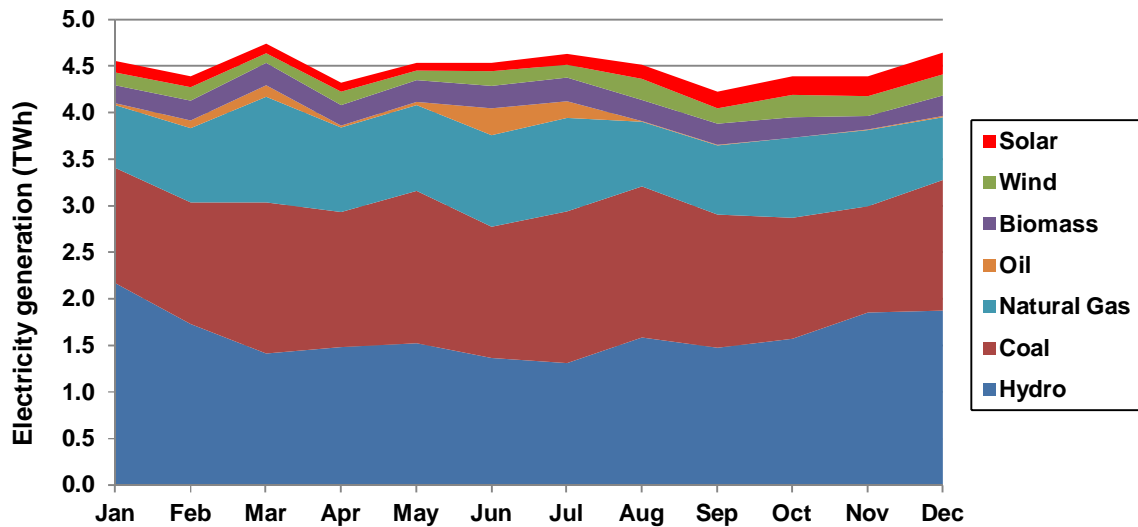


Figure 1.12. Total electricity generation from the SIC grid during 2016

1.2.5 The renewable energy sector

The urgent need for more electricity generation coupled with energy crises in recent years have increased the Chile’s reluctance to rely on volatile import conditions and have strengthened

1.2 Chilean energy scenario

national energy debates and investments into the country's energy security. Although RE systems are generally more expensive than traditional fossil fuels, they are recognized for reducing environmental and social impacts [49, 50]. Relying more on RE sources, aims also at taking more control in the future over the increasing cost of electricity, because by definition, RE sources are free. Therefore politicians seriously started to take into consideration RE as a genuine sustainable solution.

With some of the highest solar direct normal irradiance (DNI) rates in the world, up to 3,300 kilowatt hours per square meter (kWh/m²), when only 2,000 kWh/m² is generally required by a solar power plant to achieve economical performance [16, 19, 51, 52], Chile presents a great potential for solar power. Figure 1.13 presents the distribution of annual global horizontal irradiation (GHI) in Chile [53]. The GHI (kWh/m²/year) is represented as the yearly sum of direct normal and diffuse horizontal irradiations (DNI and DIF) incident per unit area on a surface horizontal to the ground.

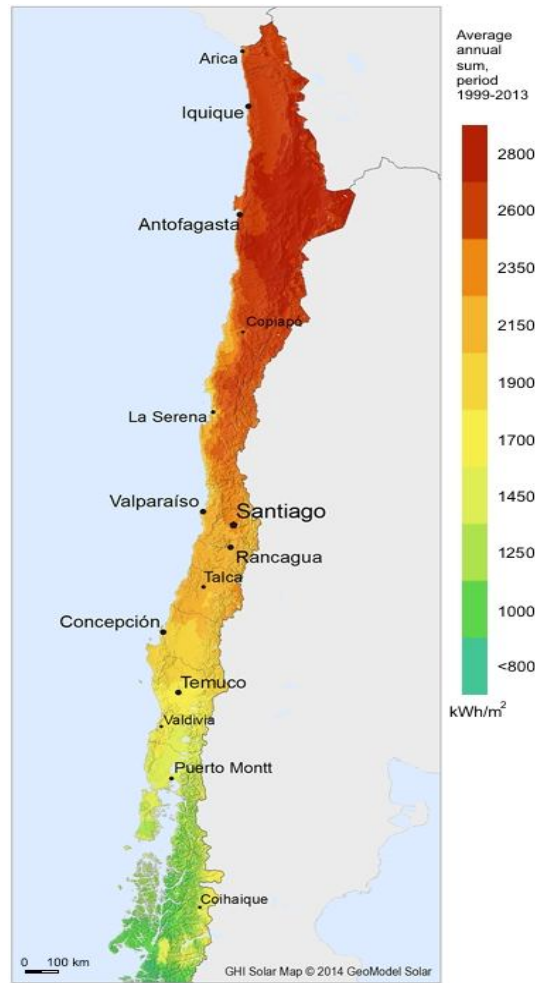


Figure 1.13. Global Horizontal Irradiation (GHI) in Chile [53]

In the last four years, the solar photovoltaic (PV) industry in Chile has experienced a boom without precedent. The change was particularly considerable when the installed capacity of plants in operation was multiplied by over 60 during 2015, and was again almost tripled as of June 2016 to reach 1,217 MWp installed capacity (see Table 1.2). According to the Sustainable Energy Development and Innovation Centre (*Centro para la Innovación y Fomento de las Energías Sustentables*, CIFES), the capacity of solar PV projects under construction and which were granted permission has also significantly grown during the period 2013-2016.

Table 1.2. Solar PV industry evolution 2013 -2016 in Chile [54, 55, 56]

| | | 2013 | 2014 | 2015 | 2016 |
|-----------------------------|--------------|------|------|------|-------|
| Total Capacity (MWp) | Operation | 3.7 | 7.5 | 452 | 1,217 |
| | Construction | 68.3 | 244 | 748 | 1,897 |

1.2 Chilean energy scenario

| | | | | |
|------------------|-------|-------|-------|--------|
| Permits approved | 3,032 | 4,632 | 8,173 | 11,621 |
| Permitting | 1,902 | 2,940 | 4,792 | 6,493 |

For example, the Italian company Enel Green Power SpA has completed construction in 2016 of a 160 MW solar PV farm in the Antofagasta region. The company invested approximately US\$ 270 million and signed a long-term Power Purchase Agreement (PPA) with a local utility supply company [57]. The same year, SunPower Corp. has secured a PPA for the supply of 300 GWh per year of solar energy to the subway of Santiago, provided by the company's 100 MW El Pelicano project located in the regions of Coquimbo and Atacama. The plant is scheduled to become operational by the end of 2017 [57]. Another example is the inauguration of the 146 MW Boléro PV solar plant in the Atacama Desert in northern Chile. The plant comprises of 475,000 photovoltaic modules fitted with solar trackers, and covers an area of more than 500 hectares. It is capable of supplying 191,000 Chilean households with electricity and is expected to cut down CO₂ emissions by 380,000 tons [58].

The solar thermal power technology (i.e. concentrated solar power, CSP) presents also a great potential, although it is not quite established yet in Chile. The advantage of CSP lies in higher capacity factors compared to PV technology. Indeed, CSP plants are able to produce electricity during the night and on cloudy days with the use of thermal storage systems. More details about the CSP technology is introduced in section 3.1.3. The construction of the first Chilean CSP plant has started in 2014 [59], and it is expected to be fully operating in 2019 [60]. As of June 2016, there are several new CSP projects which obtained a favourable environmental rating from the Chilean Environmental Service authorities, representing a total capacity of 1,085 MW, and a growth of 25% in one year. Moreover, the capacity of CSP projects which are still under environmental evaluation have more than quadrupled within a year, from 260 MW in June 2015 to 1,120 MW in June 2016, according to CIFES reports [56, 61].

The promulgation of the new Electricity Transmission Law passed in July 2016 is an important step towards the expansion of solar energy. The Law key measure is the inter-connection between the two main national grids, which will directly benefit the solar industry in Chile. The objective is to eliminate the bottleneck that is preventing the full penetration of solar energy in the Chilean market, alleviating the intermittent overcapacity on one grid and allowing the distribution of clean solar electricity to the other grid, or vice-versa, depending on the

available solar resource and the local electricity demand [62]. For instance, the grid inter-connection will allow solar industry to produce electricity in large solar plants in the northern region where the radiation is more powerful and supply it where the demand is the strongest in the central region. The 3,000 km grid inter-connection is expected to be operational by the beginning of 2018.

Chile’s wind resource is also very attractive; with many global wind companies currently active in the country. A number of new projects has recently been announced, including San Juan’s 185 MW wind farm in the coastal area of Chañaral de Aceituno, Atacama Region [63]; Acciona’s 183 MW San Gabriel wind project [64]; WPD MallecoSpA’s 273 MW project situated in La Araucanía, which the company says will become Chile’s largest wind farm when it becomes operational in 2022 [65].

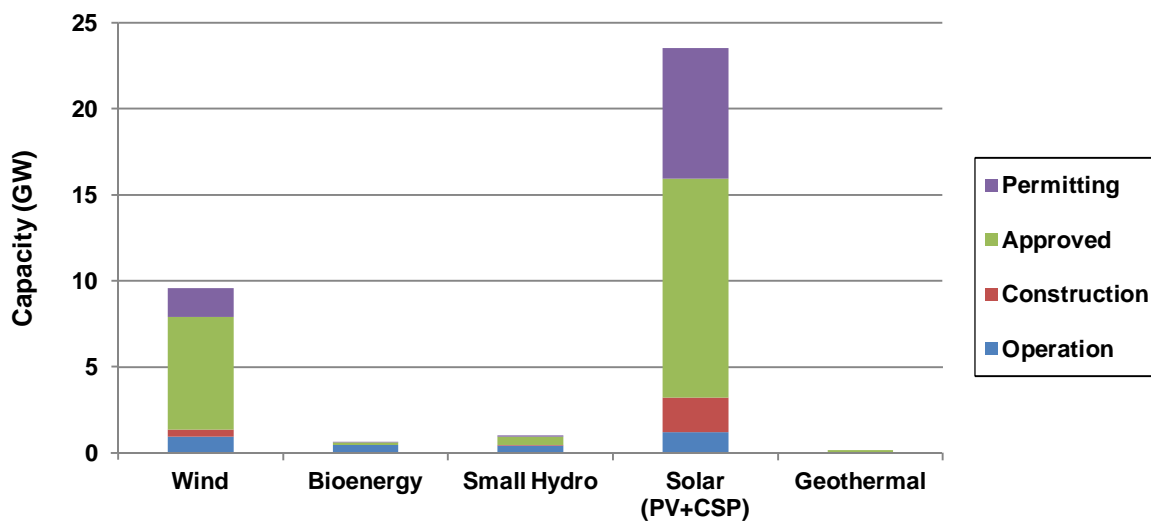


Figure 1.14. State of RE projects in Chile in 2016 (GW) [56]

According to CIFES [56], over 19.9 GW of renewable energy projects (small hydro, wind, biomass, biogas, solar, and geothermal) were approved in 2016 in Chile and another 9.5 GW were awaiting approval (Figure 1.14). Chile's renewable energy capacity has almost tripled compared to 2013. It soared 20% in 2016 alone to over 3 GW (bioenergy 459 MW; small hydropower 446 MW; wind 1,029 MW; solar 1,041 MW), with approximately 14% of total capacity in the country grids, according to figures from the CIFES and CNE (Figure 1.15) [66,

1.2 Chilean energy scenario

67, 68]. RE generation were 7.65 TWh in 2016, a 39% increase from 2015 and representing 10.4% of overall electricity generation [38].

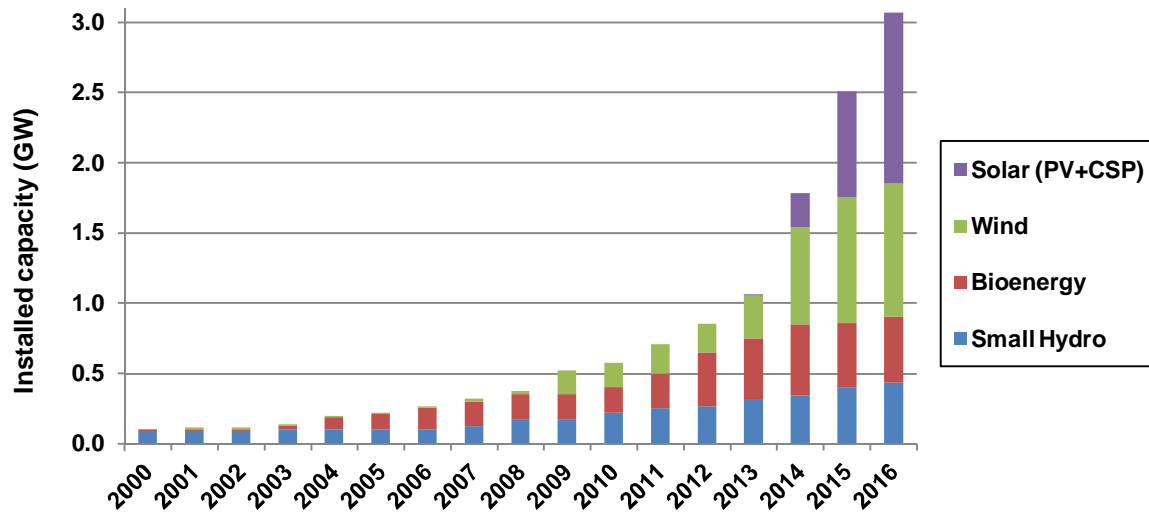


Figure 1. Error! Use the Home tab to apply 0 to the text that you want to appear here. **15. RE installed capacity evolution. Own elaboration using data from [30, 55, 56, 67, 69]**

With almost 30 GW in projects in the pipeline approved but not yet built or in qualification, the CIFES has launched new funding programs to help get more of them grid-connected. Among these plans: US\$ 2.3 million in funding to develop and finance grid-connected projects in the coming year, plus another US\$ 4.1 million for self-supplying renewable energy systems [70]. CIFES and the German Development Bank KfW have also launched a US\$ 600,000 program to help implement more of the projects within that vast pipeline [70]. Moreover, in March 2014, CIFES has pledged US\$ 1.8 million to back engineering studies for projects in the pre-investment stage, and allocating US\$ 4.3 million to back smaller projects to develop renewable energy systems for self-consumption; an example is the nation's dairy sector, which seeks to develop more biogas options [71].

Several studies have demonstrated the enormous potential in Chile for renewable energy generation, and their technical feasibility to implement projects by the year 2025 [72]. The results of these studies can be seen in the following Table 1.3. With such a potential, Chile is adopting large scale renewable energy implementation plans, in order to rapidly achieve energy security and a degree of energy independence. These plans include strategies for integrating renewable energy systems in a coherent manner designing appropriate energy systems that may be

influenced by energy efficiency measures and energy savings, as advised in the scientific literature [73, 74].

Table 1.3. Chilean RE potential [72]

| Technology | Potential (MW) | |
|-----------------|----------------|---------------|
| | Theoretical | Technical |
| Solar PV | 1,000 | 680 |
| CSP | 100,000 | 2,200 |
| Geothermal | 16,000 | 2,200 |
| Small hydraulic | 20,400 | 4,000 |
| Wind | 40,000 | 1,900 |
| Biomass | 13,600 | 3,300 |
| Total | 191,000 | 14,280 |

Besides addressing the issues of energy dependence and security of energy supply, the adoption of renewable energy for electricity generation has also environmental benefits. According to the CNE [75], considering the actual source of primary energy used for electricity generation in Chile (i.e. shown in the previous section 1.2.4), the emissions factors of the two main national grids can be assumed as 0.77 and 0.38 kilograms of CO₂-equivalents per kilowatt-hour of electricity generated (kgCO_{2eq}/kWh) for the SING and SIC networks respectively. The difference between the two networks is due to the difference primary energy sources used in the actual electricity generation mix (Figure 1.11 and 1.12). It is worth mentioning that the progressive integration of RE electricity into national grids tends to lower the CO₂ emissions factors for electricity generation.

1.2.6 Support mechanisms for renewable energy

1.2.6.1 Public policies

Due to the depletion of resources, dependence on imports and increased admissions prices, fossil fuels are no longer an attractive source for energy generation, even without taking into account the environmental impact associated to their use. Moreover, due to the high potential resources for renewable energy generation, Chile has taken notice of the situation and is setting

1.2 Chilean energy scenario

up institutional legislation that forces the electricity generation companies to develop different innovation projects for the diversification of the power grid by Non-Conventional Renewable Energy (NCRE)¹, as defined by Chilean law [76]. Apart from being a sustainable alternative to fossil fuels, NCREs can also contribute to develop the local economy and provide the country with independence in power generation.

The National Energy Commission (CNE), body responsible for regulating, preparing and implementing energy policy, has prepared favourable conditions for electricity generation from non-conventional renewable energy sources, as part of the National Energy Strategy 2012-2030 [77]. This includes regulation of grid access, integration into the electricity market, and development of expansion strategies and promotional instruments for renewable energies. The public policies which have been developed and implemented in the last decade are presented in the following.

A second priority area of the National Energy Strategy for the deployment of NCRE is the removal of structural market constraints hindering their expansion in Chile. These include, besides lack of knowledge about energy resources and their geographical distribution, lack of experience with planning and approval procedures and with grid connection. Therefore, the Chilean Government with the assistance of the German Technical Cooperation (GTZ) is financing measurement campaigns to investigate the technical and economic energy potential in NCRE sectors and to provide the CNE with advisory services for project planning, approval procedures, and environmental impact studies [78].

Law I (“Short Law I”)

The Ministry of Economy, Development and Reconstruction, in the year 2004, enacted Law 19.940. Nationally known as the “Short Law I”, the Law was implemented to provide consumers with a greater degree of security and quality of supply at a reasonable price. It also provides a modern and more efficient regulatory framework. The Law enables small power generation (from

¹ Non-conventional renewable energy (NCRE) sources include wind power, geothermal energy, solar energy (thermal and photovoltaic), biomass (solid, liquid and biogas), marine (tides and waves) and small hydraulic energy (< 20 MW installed capacity).

50 kW to 2 MW) to participate in the electricity market. In addition, it includes the partial or total toll exemption for the transmission systems of NCRE with installed capacity smaller than 20 MW (factor of exception), as shown in the Figure 1.16 [78].

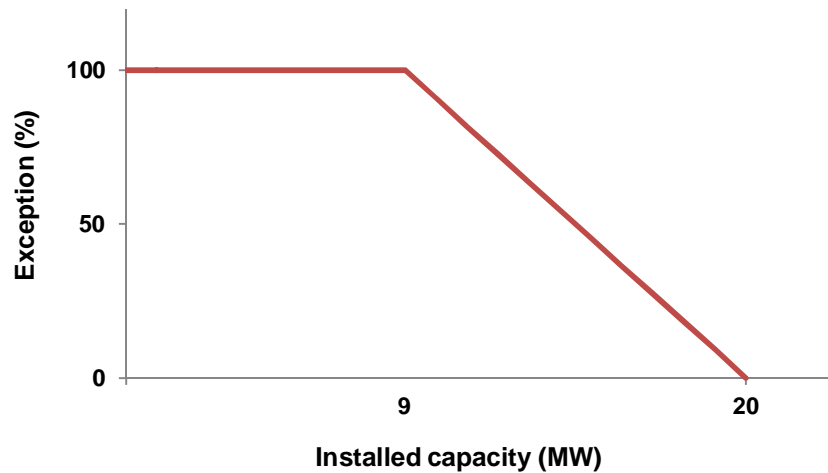


Figure 1.16. Payment exemption of transmission charges to NCRE [78]

Law II (“Short Law II”)

Law 20.018 was enacted in 2005 by the Ministry of Economy, Development and Reconstruction, mainly because of the uncertainty associated with the availability of natural gas from Argentina. Among the main aspects the law considers is the permission of bidding for long-term contracts by distributing companies, and the existence of prices higher than the generation-transportation rate (not subject to its variation). The law also widens the price adjustment band regulated with respect to free prices, creates a market that allows generating companies to give incentives for clients that consume less than 2 MW, and stipulates that the lack of supply of Argentinean gas does not constitute a case of force majeure [79].

NCRE Law

Law 20.257 of 2008, also known as “NCRE Law” modifies the General Law on Electrical Services (Ley General de Servicios Eléctricos) introducing an NCRE quota system. The law requires electricity providing companies, withdrawing electricity to supply their contract commitments, to demonstrate that a certain percentage of their total energy committed was injected in the system by NCRE sources. The energy can be produced by their own plants, or by

1.2 Chilean energy scenario

contracting from third-parties. This quota came into force at the start of 2010, and until 2014 will require 5% of electricity to come from non-conventional renewable energy sources. Starting from 2015, the obligation will be increased by 0.5% annually, reaching 10% in 2024. The obligation shown in Figure 1.17 will last for 25 years (2010-2034).

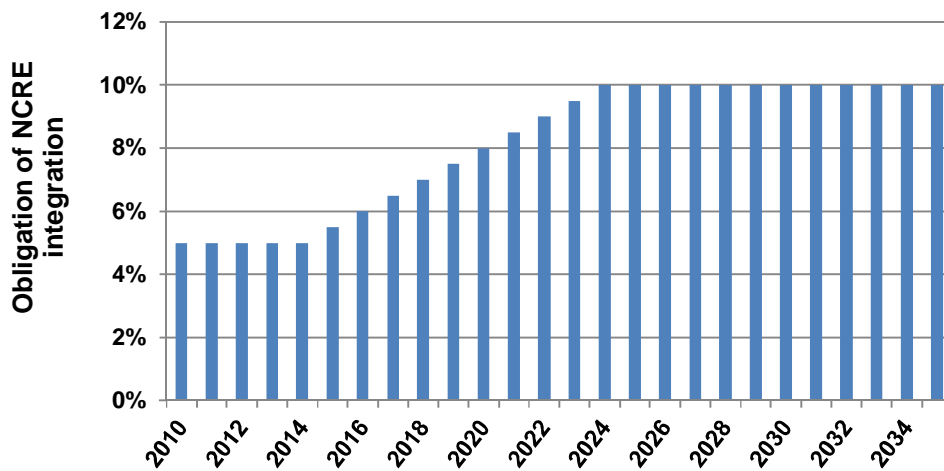


Figure 1.17. Obligations of NCRE integration according to Law 20.257

The law will apply to all agreements executed as of 31 May 2007 (new agreements, renewals, extensions, or similar arrangements). Non-compliance with the law will result in fines per MW not obtained from NCRE sources per year [77]. On 14 October 2013, the law was reformed and mandates that electric utilities with more than 200MW operational capacity should generate 20% of electricity from renewable sources by 2025.

Renewable Energy Centre

In August 2009 the Renewable Energy Centre (Centro de Energías Renovables, CER), institution that consolidates the country's efforts for the development of NCRE was created. The CER acts as a central point of information and support for the promotion of investment and technology transfer.

The key functions of the CER are [80]:

- Study the evolution and development of NCRE technologies and their applicability in Chile, in order to facilitate the elimination of barriers in the materialization of projects.

- Promote and develop an agreement network with centres and institutions, both nationally and internationally, that are promoting innovation in NCRE.
- Serve as a centre of information and orientation for government entities, investors, project developers and academic researchers.
- Generate natural resources registries for the development of NCRE.
- Watch over the existence of accreditation for the competence of human resources, as well as the certifying of products and services connected to NCRE projects.

1.2.6.2 Financial and tax incentives for NCRE integration

There are several financial and tax incentives existing in Chile designed to boost the development of renewable energy. In general, financial incentives are channelled through CORFO, a government agency in charge of supporting entrepreneurship, innovation and competitiveness in the country, which have not necessarily been developed to promote RE, but there are characteristics that coincide with what the instruments require. The mechanisms that can be seized by NCRE technologies are described next.

Initiatives of Integrated Development

These subsidies were created to materialize investment in fixed assets, preferably in parks or technological condominiums, originated by the investment projects. This instrument subsidizes the purchase of critical and/or technological assets; in high technology investment projects that extensively promote the development and/or use in the ICTs fields, biotechnology, new materials, electronics and engineering processes fields. Indeed, projects that apply new production techniques and added value to the natural resources industry in the country, such as renewable generation power plants, are eligible. The subsidy amount could not be higher than 30% of the investment in critical and/or technological assets with a maximum of US\$ 5,000,000. It is addressed to investment projects of US\$ 2,000,000 minimum [81].

Technological Contracts for Innovation

This subsidy supports projects destined to generate innovation in goods, services, commercialization or organizational methods that have a considerable associated risk. This

1.2 Chilean energy scenario

subsidy is aimed at innovative projects that have the potential to successfully introduce in the market innovations in goods and services and that, at the same time, have the potential to significantly improve the company's performance. Some of the activities that it subsidizes are: research for the development of new goods or services; design and construction of prototypes or pilot plants; payment of royalties and patents; pre-investment studies, among others. The subsidy can amount up to 50% of the total project with a maximum of US\$ 280,000 [82].

Tax Exemption for Extreme Zones

There are specific laws in Chile for extreme regions in the country that look to strengthen the development of productive activities in order to stimulate economic growth. These contemplate exceptional tax benefits, and subsidies for the installation of services required by the citizens [83]. The zones that benefit from these tax exemptions are:

- Regions: Tarapacá, Arica y Parinacota, Aysén and Magallanes.
- Provinces of Chiloé and Palena.
- Communes of Tocopilla and Isla de Pascua.

Within the described benefits, the country's Northern and Southern extremes stand out as beneficiaries. Through the tax exemption, the amount of necessary investment to develop renewable energy projects is reduced. This is relevant considering the abundance of solar resources in the North, and of water and wind resources in the South.

1.2.6.3 Prospects for RE development

In 2005, the *Invest Chile Program* was launched by the Ministry of Energy and CORFO to support renewable energy projects and finance renewable energy generation nationwide. In the period 2005-2009, the program consisted of a subsidy with a maximum of 50% for studies with a maximum of US\$ 60,000 and 50% of investment with a maximum of US\$ 160,000 [84]. In this way the Program supported projects that were trying to generate power based on NCRE with power surplus equal or lower than 20 MW. All kinds of pre-investment studies were financed: pre-feasibility and feasibility studies, specialized consultancies necessary to realize the project (prospective studies of energy source, technical and economic, basic engineering, detailed engineering, environmental impact among others), studies necessary to evaluate and incorporate

projects to the Clean Development Mechanism, among others. In the period 2008-2010, the Ministry of Energy transferred US\$ 2 million to CORFO to continue the program. After 2010 the applications were received directly without contest. In 2011, CORFO has launched two programs to subsidize pre-investment studies of NCRE projects, the *Support for NCRE Development Program* and the *TodoChile Program*. These consisted in a subsidy with a maximum of 50% for studies and 2% of investment with a maximum of US\$ 60,000 [83]. Since 2012, CORFO has also developed two new contests to finance NCRE projects, the *Innovation in Renewable Energies* which has US\$ 5 million for subsidies and the *Concentrated Solar Power plants contest*, which has US\$ 20 million [85].

Other past CORFO funding programs such as the *Pre-investment Program in NCRE*, the *Technological Packaging for new Businesses*, the *Individual Business Innovation* and the *Innovation Projects of fast implementation* in 2011 [83] also helped to develop NCRE projects in Chile. All the presented funding programs resulted in a rapid growth of NCRE installed capacity in the recent years (Figure 1.15). Considering the governmental efforts towards cleaner energy development, the projections of installed capacity and NCRE participation are shown in the following Figure 1.18.

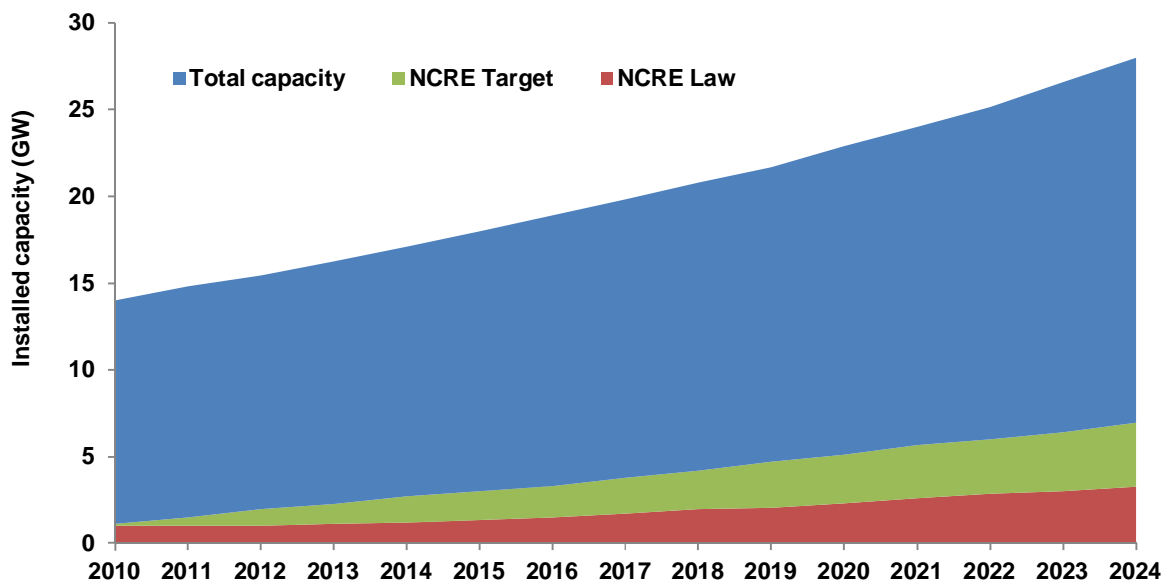


Figure 1.18. Energy capacity projection and NCRE participation in Chile [72]

1.2.7 Energy in the built environment

1.2.7.1 Energy use

The residential sector plays an important role in energy consumption all over the world. Globally, buildings are responsible for approximately 40% of total world energy consumption [73, 86, 87, 88, 89, 90], with space heating/cooling accounting for a majority with a share of between 61% and 70% of home energy use [91]. In Chile, because of the large and high energy consuming industry sector, buildings account for only 21% of the country total energy consumption [29], with space heating representing 52% of the energy used in dwellings [92]. The energy use by fuel in Chilean buildings is presented in Figure 1.19 [93]. Fossil fuels and electricity, which are both great emitters of CO₂, account for 35% and 18% respectively of the energy consumption in Chilean buildings. Wood burning, which represents 47% of the energy consumption in buildings (principally for space heating), is also responsible for abundant CO₂ emissions, although it can be considered as a renewable source when trees used as fuel are replanted after being cut off. In this case, the quantity of CO₂ turned into wood is assumed to be equivalent as the one produced when burning that wood.

It is important to note that values of Figure 1.19 may be biased by the fact that wood is principally used in southern regions, where the space heating demand is particularly high. The space heating demand per square meters of buildings in the south of Chile can easily be triple the demand of a building in central Chile. This is why the proportion of wood consumption represents such a great share of the total fuel use in the residential sector.

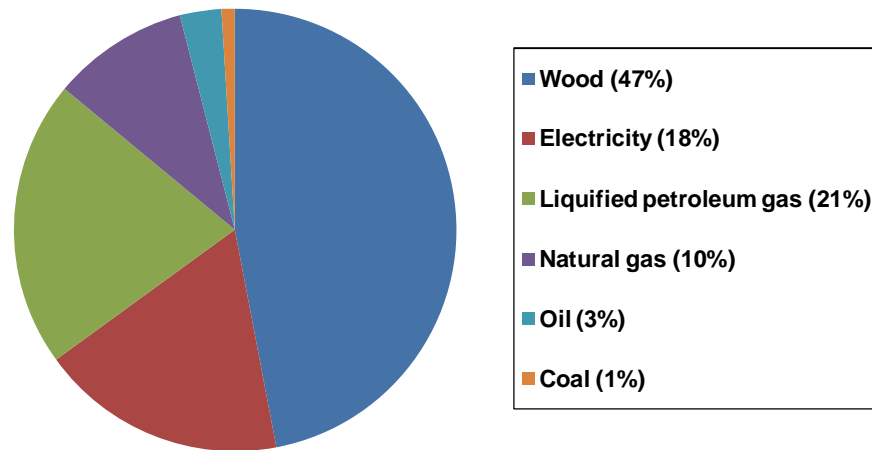


Figure 1.19. Residential fuel consumption in Chile [93]

According to the World Bank [94], the electricity sector is responsible of 47% of the Chilean CO₂ emissions from fuel combustion in 2013. The electricity demand of residential, commercial and public buildings is about one third of the total country electricity use [29], as shown in Figure 1.20. Therefore, it can be deduced that buildings in Chile are responsible for about 13% of the country total CO₂ emissions from electricity use. It is estimated that buildings also account for 8% of Chile CO₂ emissions from fossil fuel combustion [94]. To resume, Buildings in Chile were responsible for 21% of the country CO₂ emissions in 2013, summing emissions from electricity use and from direct fuel combustion, thus making them the third most important sector of emissions after business activities and transport [94]. It is estimated that in Chile residential carbon emissions are dominated by space and water heating (about 73%), and that lighting, cooking, and other homes appliances are responsible for the remaining 27% [76, 92].

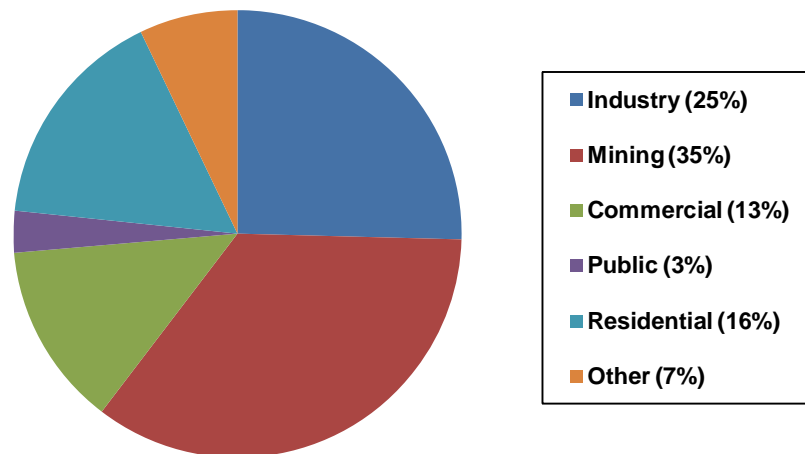


Figure 1.20. Electricity use by sector in 2014 [29]

Achieving a more efficient use of energy in buildings (i.e. minimizing energy waste) is the strategy presenting the greatest potential towards reducing energy usage and GHG emissions from the building sector in a fast and cost effective manner. Factors such as high energy prices, concerns for the environment and security of supply in Chile have all contributed to a growing awareness of the need for further developing energy efficiency. Yet, this must translate into immediate actions and energy efficiency must become a normal habit for all actors throughout the building sector.

It is only recently that energy efficiency and carbon emissions have started to have significant influence on the evolution of the construction industry in Chile, most particularly since 2005 with the introduction of the National Program for Energy Efficiency (*Programa País de Eficiencia Energética*, PPEE), and in 2012 with the creation of the Chilean Agency for Energy Efficiency (*Agencia Chilena de Eficiencia Energética*, AChEE). A specific goal for energy efficiency was set and different action programs were created in 2012 with the Energy Efficiency Action Plan 2012-2020 (PAEE20) [77]. In the construction sector, the Action Plan aims to improve thermal insulation for buildings, to design buildings with high energy efficiency standards and to offer construction products and services with energy efficiency criteria. Modern appliances with low energy consumption are also promoted through the establishment of efficiency standards and incentives.

1.2.7.2 Building thermal regulations

According to the Technological Development Board (*Corporación de Desarrollo Tecnológico, CDT*) [93], almost 80% of the Chilean building stock was built before the year 2000 (Figure 1.21). The principal concern is that few of these older buildings include thermal insulation unless they have been refurbished or restored. Besides, newer buildings are usually poorly insulated, as most of them were built without thermal regulation constraints, which were firstly introduced in 2007 [95, 96]. Although the actual situation of the Chilean residential sector in terms of energy efficiency is not satisfying, the potential for reducing residential energy usage through improvement measures remains significant.

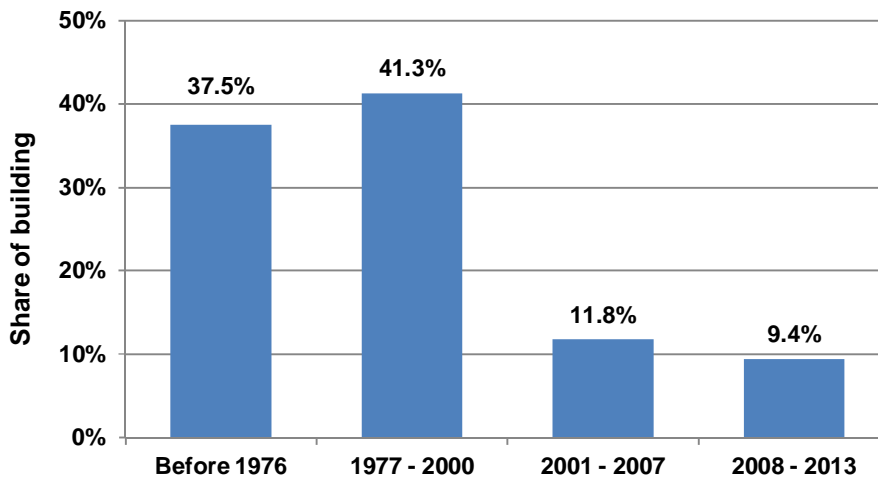


Figure 1.21. Construction year of buildings in Chile [93, 97]

Driven by the introduction of the PPEE and PAEE20 programs and the need to reduce carbon dioxide emissions, the construction industry is experiencing a strong push towards the improvement of the energy performance of new and refurbished buildings [98, 99, 100, 101]. Much work has been carried out in this area, including the approved building thermal regulations in Chile [77, 102, 103], through which it is intended that all new dwellings lower their energy consumption. Inspired by the regulatory frameworks adopted by countries of the European Union and particularly the United Kingdom, Germany and Spain, the Chilean Thermal Regulation Procedure has been designed by the Ministry of Housing (*Ministerio de Vivienda y Urbanismo, MINVU*) in association with the PPEE since 2009 [104]. This Procedure has come into force in

1.2 Chilean energy scenario

2012 and it aims to implement energy rating labels to all new residential buildings. The Procedure also includes the implementation of its own Simplified Calculation Method, as well as its own alternative Dynamic Energy Design Tool (*Certificación del Comportamiento Térmico para Edificios en Chile*, CCTE_CL 2.0) [105]. Such procedures are an important step to increase the interest of people in energy efficiency of buildings in Chile, and to encourage designers and builders to add the energy efficiency aspect in their services.

The current baseline for benchmarking the energy performance of residential buildings in the Thermal Regulation Procedure is based on the current building requirements given by the existing General Law of Urban Planning and Construction (*Ordenanza General de Urbanismo y Construcción*, OGUC) as implemented in 2007 [102]. According to the Article N° 4.1.10, all new houses would have to comply with requirements of thermal conditioning, according to the heating degree days from the classified seven climatic zones across the country. These requirements for thermal conditioning are given by maximum U-values allowed for the different envelope components, according to climatic zones. The following Table 1.4 shows U-values for opaque components (wall, floor and roof) whereas Table 1.5 presents the maximum window to wall ratios allowed by climatic zone.

Table 1.4. Minimum requirements for building elements per climatic zone - Chile thermal regulation [102]

| Climatic zone | Roof | | Wall | | Floor | |
|---------------|------------------------------|---------------------------------|------------------------------|---------------------------------|------------------------------|---------------------------------|
| | U-value (W/m ² K) | Resistance (m ² K/W) | U-value (W/m ² K) | Resistance (m ² K/W) | U-value (W/m ² K) | Resistance (m ² K/W) |
| 1 | 0.84 | 1.19 | 4.0 | 0.25 | 3.60 | 0.28 |
| 2 | 0.60 | 1.67 | 3.0 | 0.33 | 0.87 | 1.15 |
| 3 | 0.47 | 2.13 | 1.9 | 0.53 | 0.70 | 1.43 |
| 4 | 0.38 | 2.63 | 1.7 | 0.59 | 0.60 | 1.67 |
| 5 | 0.33 | 3.03 | 1.6 | 0.63 | 0.50 | 2.00 |
| 6 | 0.28 | 3.57 | 1.1 | 0.91 | 0.39 | 2.56 |
| 7 | 0.25 | 4.00 | 0.6 | 1.67 | 0.32 | 3.13 |

Table 1.5. Maximum window glazing percentage area per climatic zone [102]

| Climatic zone | Single glazing | Double glazing with gas cavity | |
|---------------|----------------|--|--------------------------------------|
| | | $3.6 \geq U \text{ (W/m}^2\text{K)} > 2.4$ | $U \text{ (W/m}^2\text{K)} \leq 2.4$ |
| 1 | 50% | 60% | 80% |
| 2 | 40% | 60% | 80% |
| 3 | 25% | 60% | 80% |
| 4 | 21% | 60% | 75% |
| 5 | 18% | 51% | 70% |
| 6 | 14% | 37% | 50% |
| 7 | 12% | 28% | 37% |

Regarding the maximum window-to-wall ratios stated in Table 1.5, it is important to observe that the OGUC Article N° 4.1.10 describes also an alternative method to comply with the requirements in climatic zones 3 to 7 (coldest zones). In order to account for the possibility of exceeding the maximum allowed window areas, professionals must certify a “Balanced U-value” through the following Equation (1.1).

$$\text{Balanced } U - \text{value} = \frac{(S_{W1} \times U_1) + (S_{W2} \times U_2) + (S_{W3} \times U_3) + (S_G \times U_G)}{\text{Total Surface Area of external facade}} \quad (1.1)$$

Where S_{W1} , S_{W2} and S_{W3} are the surface areas of each facade walls, U the corresponding wall thermal transmittance U -value, S_G the surface areas of the glazing window, U_G the thermal transmittance U -value of the windows. Values of this balanced U -value must comply with the ones stated in Table 1.6 according to the specific climatic zone.

Table 1.6. Balanced U -values, alternative method to comply with regulation [102]

| Climatic zone | Balanced U -value (W/m ² K) |
|---------------|--|
| 3 | 2.88 |
| 4 | 2.56 |
| 5 | 2.36 |
| 6 | 1.76 |
| 7 | 1.22 |

Although these requirements were a significant technical improvement in building regulations when they were initially released in 2007, they may not be sufficiently challenging today to ensure further energy savings in current residential buildings [92]. Fissore et al. [104] states that in general terms, the average primary energy consumption from a house in Chile complying with the regulatory standards reach 192 kWh/m^2 per year, whereas an optimal energy consumption could be approximately from 88 kWh/m^2 per year (assuming generally affordable measures to improve thermal performance) to 40 kWh/m^2 per year (assuming currently unaffordable measures for thermal improvements). For example, the Chilean Thermal Regulation has not set target values for thermal bridging or air permeability and it hasn't considered the efficiency of the heating systems. Neither is considered the passive gains such as solar or internal gains or an external base temperature to set the artificial heating. Regulations consider thermal resistance values in walls that are quite distant compared to the ones in roof and floor producing heat losses in the areas with less resistance. This increases the risk of cold spots [106]. No recommended ventilation rates or target humidity levels have been set, such as the ones stated by the UK's CIBSE, which recommends a minimum of 0.4 air changes per hour (n) for dwellings and humidity levels between 40% and 70% in order to avoid mould growth [107]. Also, carbon dioxide emissions are still not considered when applying for a building license in Chile.

1.3 Outline of the thesis

Chapter 1 gives the introduction to the thesis, which covers the field of energy, environment and economy. The chapter begins with the global context and the problem identification of the environmental issues related to the use of energy before introducing and discussing energy sources such as fossil fuels, nuclear and renewable energy. Also, the chapter broadly reviews the energy panorama in Chile.

Chapter 2 describes the aims and specific objectives of the thesis, the main objective being to demonstrate that sustainability in the field of energy can be achieved in a cost effective way in Chile, through clean energy generation and efficient use of energy in buildings.

Chapter 3, the literature review, covers the following areas of interest: the solar energy (solar radiation, solar power technologies and economical concepts of solar electricity generation); the low-grade geothermal energy (ground-source heat pump technology and performance); and the energy efficiency in buildings (energy balance modelling and policy instruments).

Chapter 4 introduces the methodologies adopted for the development of the various simulation models proposed in the investigation. In order to reach each of the thesis specific objectives, these include a mathematical model for the prediction of the levelised cost of electricity (LCOE) for solar electricity generation technologies, a method for multiple regression (MR) model identification for ground-source heat pump (GSHP) performance prediction based on manufacturer's catalogue data, and a building energy simulation tool for energy use and parametric sensitivity analysis.

Chapter 5 presents and discusses the results obtained from each particular study.

Chapter 6 draws important conclusions from each aspect of the presented work.

Chapter 2 – Aims and objectives



The global energy context is the need to secure an adequate and equitable access to clean and safe energy for all individuals, while minimizing greenhouse gas emissions. As discussed previously in Chapter 1, energy use and/or generation from direct combustion of fossil fuels gives rise to serious concerns on whether the actual strategy is environmentally and economically sustainable.

The notion of sustainability is defined as the “*development that meets the needs of the present without compromising the ability of future generations to meet their needs*” [108]. Sustainable development requires the reconciliation of environmental, social equity and economic demands referred to as the three Es of sustainability. In the diagram shown in Figure 2.1 [109], the “environment” region of the diagram refers to the conservation of natural resources and the reduction of impacts on eco-systems, “social equity” refers to the protection of the communities’ health and the education and empowerment of populations to participate in the process, and the “economic” region relates to cost. Economic feasibility is required if sustainability is to remain viable in the long term. For example, the generation of incentives for sustainable practices (such as tax credits for solar panels or GSHP equipments and feed-in tariffs for electricity generation from renewable sources) is one means of making important sustainability issues economically viable and accessible. The concept of sustainable development has become a dominant policy paradigm in recent years. It calls for policy action regarding our current lifestyle with its high resource depletion, decay of environmental quality, and increasing socio-economic disparities.

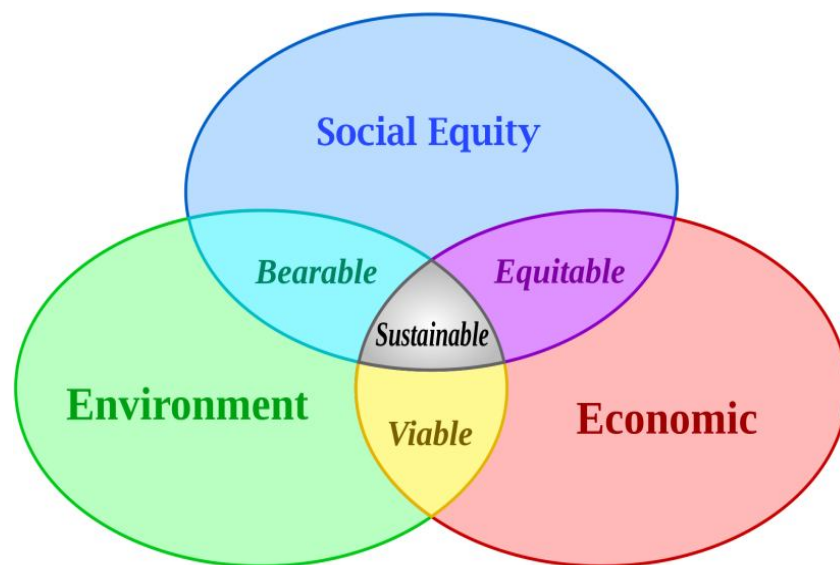


Figure 2.1Error! Use the Home tab to apply 0 to the text that you want to appear here.. **The Three E's of sustainability** [109]

As shown previously in chapter 1, the important responsibility of buildings in Chile energy consumption combined with the great share of fossil fuel sources used to satisfy the building energy demand, including the use of fossil fuels for electricity generation, as well as Chile's high dependence on foreign fossil fuel energy imports, justify the objective of reaching greater levels of sustainability in both the energy and building sectors.

In this context, solar energy represents an attractive alternative to conventional fossil energy, as it is abundantly available and can make an important contribution towards a sustainable future [110]. What is more, the cost of solar electricity from large scale solar power plants has already dropped below the price of conventional electricity in locations with high solar radiation availability, achieving the conceptual understanding of grid parity. Given the facts that, (1) solar technology costs tend to lower with growing market and improving efficiency, and (2) fossil fuels prices tend to increase due to reserves depletion, all trends indicate that solar energy will reach grid parity in more locations in the future, even where solar radiation levels are lower. In the mean time, regulatory bodies, through appropriate legislation and measured tax credit and incentives, have the capacity to build the foundations of a strong economic market for the solar

technologies, which can help shifting more rapidly from conventional power plants to more efficient and cleaner solar ones.

The building sector is seeking adequate solutions to minimize energy consumption and deploy the renewable energy technologies, with the objective of “low-energy building”. Actually, there is a broad spectrum of energy saving technologies and design approaches that are currently available to meet this objective. At one extreme, a building could generate sufficient energy to reduce its fossil fuel consumption. At the other end, the building could be of a radically different type of construction (energy efficient) requiring low energy to provide comfort [111, 112]. Chesné and al. [113] have pointed out a method for designing low-carbon emissions buildings, which consists of assessing both the capacity of the available energy resources to cover the building needs, and the ability of the building to exploit these energy resources. In other words, a low-energy building must combine two main requirements: (1) it needs to be energy efficient as to have a low energy demand, and (2) it needs to be able to generate electricity, or other energy carriers, from renewable sources in order to compensate for its energy demand [114, 115, 116].

Low-grade geothermal energy is one source of renewable energy, which can be exploited by buildings. Indeed, this energy source in the form of low-temperature heat from the earth is present everywhere below the ground and can be harvested by highly efficient ground-source heat pump systems. With overall efficiencies generally in the range of 300 to 400% (3 to 4 units of useful heat output for 1 unit of electrical energy input to drive the system), heat pumps are one of the most promising energy saving technologies available for building applications. Moreover, because heat pump systems run on electricity, their operation could result in near-zero GHG emissions in the case of being powered by solar electricity.

Energy efficiency in buildings, by means of energy saving design is the most economically viable short-term solution to rapidly reduce energy usage and mitigate the repercussions of carbon emissions in buildings. In order to identify the significant parameters of energy consumption in buildings, there is a need for simulation tool capable of predicting energy usage and comparing the cost effectiveness of energy conservation measures. The use of such a tool is essential during the preliminary design phase of new constructions or in building retrofits in order

to evaluate the relative influence of various input parameters, and influence design decision making towards improved energy efficiency in buildings.

The main objective of this work is to demonstrate that sustainability in the field of energy can be achieved in a cost effective way in Chile, through clean energy generation and efficient use of energy in buildings. The specific objectives of the investigation are:

1) Develop a mathematical model for the prediction of the levelised cost of electricity (LCOE) evolution from large scale solar energy technologies, including PV, CSP, and hybrid PV-CSP with thermal storage. The purpose is to analyse the cost effectiveness of such technologies for sustainable electricity generation and evaluate their potential to contribute to the continuous delivery of electricity in northern Chile, where the demand is high.

2) Develop a simplified methodology for multiple regression (MR) model identification from GSHP manufacturer performance data catalogues. Validate the operational modelling approach analysing model prediction errors from observed data. The hypothesis is that the proposed method can help in the selection of the most appropriate GSHP evaluating with precision its performance, and thus increase the potential of GSHP implementation in buildings.

3) Develop a building energy simulation tool which can be used to estimate energy use and resulting carbon emissions in buildings, as well as for sensitivity investigations on the effect of design parameters, such as climate conditions, envelope component characteristics and window size and orientation on the building energy consumption. Analyze the economic viability in term of payback periods of different improvement measures of envelope materials. The intent is to propose a tool which can facilitate decision making in the early stages of construction design or in building retrofits, in order to improve energy efficiency and reduce carbon emission in a cost effective manner in Chilean buildings.



Chapter 3 – Literature review

3.1 Solar energy

3.1.1 The solar radiation

The solar energy or solar radiation is defined as the energy that comes from the sun. The sun is situated at the centre of the solar system, at an average distance of 1.5×10^8 km from the earth. The sun is a sphere of almost 7×10^5 km radius (109 times that of earth), with a surface temperature of approximately 5504°C [117]. It is composed of intensely hot gaseous matter, principally hydrogen ($\approx 73\%$) and helium ($\approx 25\%$). The constant nuclear fusion reactions occurring in its core fuse hydrogen into helium, releasing large amounts of energy. The total energy generated by the sun, which is emitted into space in the form of electromagnetic radiation in all directions, is about 3.8×10^{20} MW. The average annual solar radiation, also called the solar constant, arriving at the top of the earth's atmosphere is estimated to be roughly 1361 W/m^2 [118]. Absorption occurs whilst the solar radiation passes through the earth's atmosphere, which on clear days results in solar energy available at the earth's surface in the direction of the sun to be in the region of 1000 W/m^2 . Although the earth receives only a small fraction of the total radiation emitted from the sun, it is estimated that 84 minutes of solar radiation incident on earth equals to the global energy demand for one year [119].

3.1 Solar energy

The solar radiation incident on the surface of the earth is a physical variable of high interest in many areas, as it is by far the most important source of energy for life on earth. The solar radiation that affects the terrestrial surface consists of three different components: direct, diffuse and reflected, as shown in Figure 3.1. The direct beam solar radiation (H_b) is the direct part of solar radiation that reaches the earth's surface without being scattered or absorbed by the atmosphere. The diffuse radiation (H_d) is the scattered radiation assumed to reach the earth's surface from all directions. The diffuse radiation varies from 10% of the total radiation on a clear day to nearly 100% on a totally cloudy day. Additional to the direct and diffuse component, there is a reflected radiation (H_r) from the ground and surrounding. The direct part and the diffuse part compose the global radiation, H , which is defined as [120]:

$$H = H_b + H_d \quad (3.1)$$

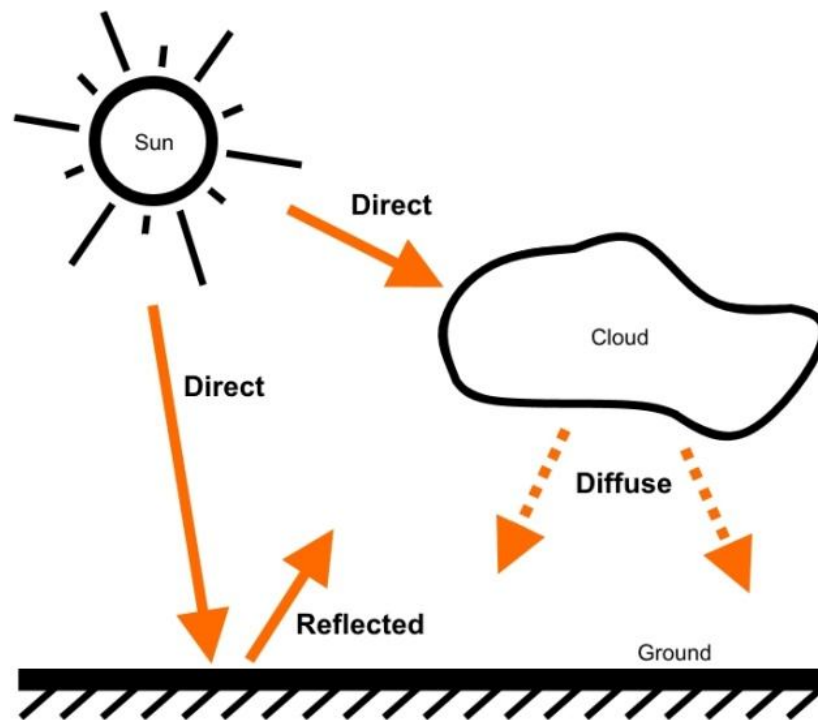


Figure 3.1. Solar radiation components

From an energetic point of view, any system of utilization of solar energy requires, in the first instance, to determine precisely the amount of radiant energy that is received at a specific point. For instance, the accurate modelling of the solar energy received on a tilted surface such as a

solar collector or a building window is essential to determine the performance of the solar energy system at a particular location or to evaluate the solar heat gains in a given building. Hourly solar radiation availability on a tilted surface can be calculated using measurements or estimates of solar direct and diffuse horizontal radiation data (I_b and I_d) by means of mathematical models available in the literature [121, 122, 123, 124]. The hourly global radiation received on an inclined surface (I_β) is the sum of the slope hourly direct, diffuse and reflected radiation parts received by that tilted surface ($I_{b,\beta}$, $I_{d,\beta}$ and $I_{r,\beta}$), expressed as in Equation (3.2). In the following, the symbol β represents the surface tilt angle.

$$I_\beta = I_{b,\beta} + I_{d,\beta} + I_{r,\beta} \quad (3.2)$$

The terms of Equation (3.2) depend on several geometric relationships between a surface of any particular orientation relative to the earth at any time and the incoming beam solar radiation (i.e. the position of the sun relative to that surface), which can be described in terms of several angles. Some of the angles are shown in Figure 3.2.

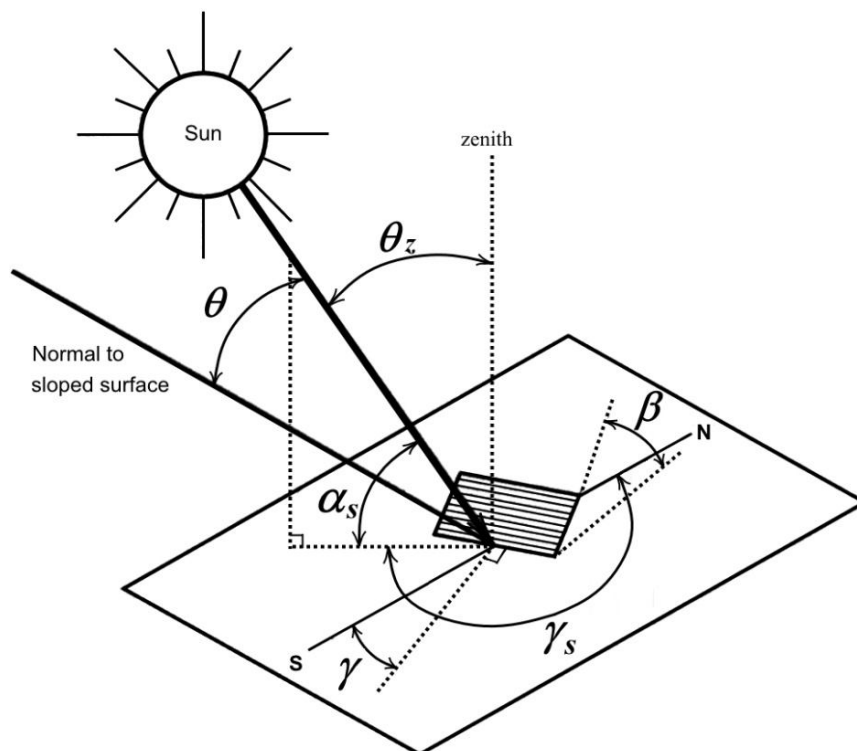


Figure 3.2. Solar geometry of a sloped surface. Elaborated from [120, 123]

3.1 Solar energy

The sun's position in the sky can be described in terms of two angles: the elevation angle above the horizon (α_s) and the azimuth from north (γ_s) of the sun's beam projection on the horizontal plane (clockwise = positive). These two angles are dependent on the hour angle (ω), the location latitude (ϕ), and the declination angle (δ). The solar elevation and azimuth angles can be obtained from the following equations:

$$\sin \alpha_s = \cos \theta_z = \sin \phi \sin \delta - \cos \phi \cos \delta \cos \omega \quad (3.3)$$

$$\cos \gamma_s = [\cos \delta (\cos \phi \tan \delta + \sin \phi \cos \omega)] / \cos \alpha_s \quad (3.4)$$

Where the zenith angle (θ_z) is the angle between the vertical and the line to the sun; the hour angle (ω) is the angular displacement of the sun east or west of the local meridian due to rotation of the earth on its axis, given at 15° per hour (negative before solar noon; positive after solar noon); the declination angle (δ) is the angle of the earth-sun vector calculated by using Equation (3.5) of Muneer [123], where the day number (DN) equals one for January the first and is the total number of days gone by so far in any selected year.

$$\delta = \sin^{-1} \{0.39795 \cos [0.98563 (DN - 173)]\} \quad (3.5)$$

The general relationship among the parameters of declination (δ), latitude (ϕ), slope (β), surface azimuth angle (γ), hour angle (ω) and the angle of incidence of beam radiation (θ) (i.e. the angle between the normal to the surface and the line to the sun) is defined as in Equation (3.6) below [120]. It is worth to note that this relationship includes some limitations: the angle of incidence of beam radiation is $0^\circ \leq \theta < 90^\circ$ (i.e. any angle $\theta \geq 90^\circ$ means the beam radiation does not reach the frontal part of the receiving surface); The hour angle ω is between sunrise and sunset only; the slope $\beta > 90^\circ$ indicates that the surface is facing downward.

$$\begin{aligned} \cos \theta = & \sin \delta \sin \phi \cos \beta - \sin \delta \cos \phi \sin \beta \cos \gamma \\ & + \cos \delta \cos \phi \cos \beta \cos \omega + \cos \delta \sin \phi \sin \beta \cos \gamma \cos \omega \\ & + \cos \delta \sin \beta \sin \gamma \sin \omega \end{aligned} \quad (3.6)$$

The sunset hour angle ω_s , when the zenith angle $\theta_z = 90^\circ$, can be determined using the following Equation (3.7). The sunrise hour angle is termed as $-\omega_s$. The $\pm\omega_s$ is the boundary of hour angle at a location.

$$\cos \omega_s = - \frac{\sin \varphi \sin \delta}{\cos \varphi \cos \delta} = - \tan \varphi \tan \delta \quad (3.7)$$

The co-ordinates that depict the sun's position in the sky are dependent upon the latitude, the solar declination, but also the apparent solar time (*AST*) of the location. Apparent solar time (*AST*) determined from Equation (3.8), is required for solar geometry equations to correct the difference between the time for a specified locality at a certain longitude (*L*) and the standard time meridian (*LSM*). For locations east of *LSM*, the longitudinal correction term in the square brackets is positive.

$$AST = \text{standard time (local civil time)} + EOT \pm [(LSM - L) / 15] \quad (3.8)$$

The equation of time (*EOT*) relates to the difference between the standard time recorded by clocks running at normal speed and the solar time. *EOT* can be calculated as follows [125].

$$EOT = 0.1236 \sin x - 0.0043 \cos x + 0.1538 \sin 2x + 0.0608 \cos 2x \quad (3.9)$$

Where $x = 360 (DN - 1) / 365.242$.

3.1.1.1 Hourly solar radiation on sloped surfaces

For hourly period calculations, solar angles are determined at the hour midpoint. The hourly beam radiation on a tilted surface ($I_{b,\beta}$), the first term of Equation (3.2) can be expressed as:

$$I_{b,\beta} = I_b \times r_b \quad (3.10)$$

Where the hourly horizontal beam radiation I_b equals to the difference between the global and diffuse radiation (i.e. $I_b = I - I_d$), and the geometric factor r_b equals to $\cos \theta / \sin \alpha_s$.

3.1 Solar energy

The second term of Equation (3.2), the diffuse radiation on a sloped surface is more difficult to determine, and there are various calculation models available in the literature. The simplest of all models is the isotropic model, which assumes that the diffuse radiation is uniform over the sky dome and approximates overcast sky conditions. However, since the diffuse radiation is not isotropic in nature and is an angular function of the solar altitude and azimuth [126], Muneer [123] developed a more accurate model, which treats the sky-diffuse component as anisotropic, and distinguishes between overcast and non-overcast conditions. This model can also be applied to vertical surfaces such as windows, as demonstrated by Li et al. [127]. According to Muneer [123], the slope diffuse irradiation ($I_{d,\beta}$), for inclined surfaces under overcast and non-overcast sky can be expressed as in Equation (3.11) and (3.12) respectively.

$$I_{d,\beta} = I_d \left[\cos(\beta/2)^2 + \frac{2b}{\pi(3+2b)} \times (\sin\beta - \beta \cos\beta - \pi \sin(\beta/2)^2) \right] \quad (3.11)$$

$$I_{d,\beta} = I_d [T (1 - F) + F r_b] \quad (3.12)$$

Where T is the function contained within the square brackets in Equation (3.11); b is the radiance distribution index to model the luminance distribution of an overcast sky. On a world basis, Muneer [123] suggested an average value of $b = 2.5$ for surfaces under an overcast sky. For non-overcast skies, based on data obtained from 14 worldwide locations, Muneer [123] recommended the following Equation (3.13), where F is the sky clearness index.

$$\frac{2b}{\pi(3+2b)} = 0.04 - 0.82 F - 2.026 F^2 \quad (3.13)$$

$$F = \frac{I_b}{I_e} = \frac{(I - I_d)}{I_e} \quad (3.14)$$

Where the horizontal extraterrestrial radiation (I_e) can be calculated as follows:

$$I_e = 1361 \times [1 + 0.033 \times \cos(0.0172024 \times \text{DN})] \times \sin(\alpha_s) \quad (3.15)$$

Finally, the reflected radiation received on a tilted surface ($I_{r,\beta}$) can be found using the Equation (3.16), where ρ is the ground reflectance value, also called albedo. This is the most commonly used expression for the radiation reflected from the ground. In this case, the reflection is considered isotropic and the reflectances of beam and diffuse radiation identical.

$$I_{r,\beta} = \rho \times I \times \sin(\beta / 2)^2 \quad (3.16)$$

3.1.1.2 Average solar radiation on sloped surfaces

For use in solar system design procedures, such as long term periods estimations, there is also a need of the monthly average daily radiation on the tilted surface (\bar{H}_β). The procedure for calculating \bar{H}_β is parallel to that for I_β , which is, by summing the monthly average contributions of the beam radiation, the diffuse radiation, and the reflected radiation. The monthly mean daily radiation on a tilted surface can be expressed as in Equation (3.17), where \bar{H} is the monthly mean global horizontal radiation and \bar{R} is the monthly mean global radiation geometric factor.

$$\bar{H}_\beta = \bar{H} \times \bar{R} \quad (3.17)$$

The first method is that of Liu and Jordan [128], then extended by Klein [129], which has been widely used. They assumed the diffuse and ground-reflected radiation to be isotropic. They also suggested that the monthly average direct radiation geometric factor (\bar{R}_b) is a function of transmittance of the atmosphere, but could be estimated by assuming that it has the value which would be obtained if there were no atmosphere.

An alternative approach to calculation of average radiation on sloped surfaces has been developed by Klein and Theilacker [130]. It is a bit more cumbersome to use than the method given by Klein [129] but shows improved results on the isotropic method when compared with integrated hourly calculations for many years of radiation data. The method is for surfaces of any orientation in general. If $\gamma \neq 0^\circ$ (or 180°), the times of sunrise and sunset on the tilted surface will not be symmetrical about solar noon. This method of calculating the tilt factor works for all surface orientations and all latitudes (including negative latitudes, for the southern hemisphere). In this method, the equation for \bar{R} is given as in the following Equation (3.18).

$$\bar{R} = D + \frac{\bar{H}_d}{\bar{H}} \left(\frac{1+\cos\beta}{2} \right) + \rho \left(\frac{1-\cos\beta}{2} \right) \quad (3.18)$$

$$\text{Where } D = \begin{cases} \max(0, G(\omega_{ss}, \omega_{sr})) & \text{if } \omega_{ss} \geq \omega_{sr} \\ \max(0, [G(\omega_{ss}, -\omega_s) + G(\omega_s, \omega_{sr})]) & \text{if } \omega_{sr} > \omega_{ss} \end{cases} \quad (3.19)$$

For a day period, solar radiation is received by an inclined surface between sunrise and sunset. The sunset and sunrise hour angles, ω_{ss} and ω_{sr} , for beam radiation on the inclined surface are determined by letting $\theta = 90^\circ$ in Equation (3.6). This leads to a quadratic equation, giving two values of ω (which must be within $\pm\omega_s$). Depending on the surface orientation and solar geometry, the signs of ω_{ss} and ω_{sr} might be affected as described in the equations below:

$$|\omega_{sr}| = \min \left[\omega_s, \cos^{-1} \left(\frac{AB + C\sqrt{A^2 - B^2 + C^2}}{A^2 + C^2} \right) \right] \quad (3.20)$$

$$\omega_{sr} = \begin{cases} -|\omega_{sr}| & \text{if } (A > 0 \text{ and } B > 0) \text{ or } (A \geq B) \\ +|\omega_{sr}| & \text{otherwise} \end{cases} \quad (3.21)$$

$$\text{And } |\omega_{ss}| = \min \left[\omega_s, \cos^{-1} \left(\frac{AB - C\sqrt{A^2 - B^2 + C^2}}{A^2 + C^2} \right) \right] \quad (3.22)$$

$$\omega_{ss} = \begin{cases} +|\omega_{ss}| & \text{if } (A > 0 \text{ and } B > 0) \text{ or } (A \geq B) \\ -|\omega_{ss}| & \text{otherwise} \end{cases} \quad (3.23)$$

$$\text{With } A = \cos\beta + \tan\phi \cos\gamma \sin\beta \quad (3.24)$$

$$B = \cos\omega_s \cos\beta + \tan\delta \cos\gamma \sin\beta \quad (3.25)$$

$$C = (\sin\beta \sin\gamma) / \cos\phi \quad (3.26)$$

In Equation (3.20) and (3.22), the value within the square root can be negative under certain specific orientation corresponding to the sun path. It is caused by the position of the surface orientation that the solar incidence angle is $<90^\circ$ of sunrise or $>90^\circ$ of sunset. In order to deal

with this limitation, a boundary of solar hour angle was set, in which ω_{ss} and ω_{sr} are set to $-\omega_s$ and $+\omega_s$, respectively. The terms “max” and “min” mean the larger and smaller of the two items in the brackets, correspondingly. The empirical function G is expressed as:

$$\begin{aligned}
 G(\omega_1, \omega_2) = & \frac{1}{2d} \left[\left(\frac{bA}{2} - a'B \right) (\omega_1 - \omega_2) \frac{\pi}{180} \right. \\
 & + (a'A - bB) (\sin \omega_1 - \sin \omega_2) - a'C (\cos \omega_1 - \cos \omega_2) \\
 & + \left(\frac{bA}{2} \right) (\sin \omega_1 - \cos \omega_1 - \sin \omega_2 - \cos \omega_2) \\
 & \left. + \left(\frac{bC}{2} \right) (\sin^2 \omega_1 - \sin^2 \omega_2) \right] \quad (3.27)
 \end{aligned}$$

The ω_1 and ω_2 correspond to ω_{ss} , ω_{sr} or ω_s accordingly as presented in Equation (3.19). Meanwhile, the empirical coefficients a' , b and d are as follows:

$$a = 0.409 + 0.5016 \sin(\omega_s - 60) - \bar{H}_d / \bar{H} \quad (3.28)$$

$$b = 0.6609 - 0.4767 \sin(\omega_s - 60) \quad (3.29)$$

$$d = \sin \omega_s - [(\pi \omega_s) / 180] \cos \omega_s \quad (3.30)$$

If only the monthly mean daily horizontal values of global (\bar{H}) and extraterrestrial (\bar{H}_e) radiation are known, in order to solve the diffuse component (\bar{H}_d), Erbs et al. [131] developed monthly average diffuse fraction correlations from daily diffuse correlations. As with the daily correlations, there is a seasonal dependence; there is a lower fraction of diffuse radiation in winter due to lower moisture and dust in the winter sky. The dependence of \bar{H}_d / \bar{H} on the day clearness index \bar{K}_T is shown for winter and for the other seasons in Equation 3.31 and 3.32, where $\bar{K}_T = \bar{H} / \bar{H}_e$. For $\omega_s \leq 81.4^\circ$ and $0.3 \leq \bar{K}_T \leq 0.8$:

$$\bar{H}_d / \bar{H} = 1.391 - 3.56 \bar{K}_T + 4.189 \bar{K}_T^2 - 2.137 \bar{K}_T^3 \quad (3.31)$$

For $\omega_s > 81.4^\circ$ and $0.3 \leq \bar{K}_T \leq 0.8$:

$$\bar{H}_d / \bar{H} = 1.311 - 3.022 \bar{K}_T + 3.427 \bar{K}_T^2 - 1.821 \bar{K}_T^3 \quad (3.32)$$

3.1.2 Photovoltaic technology (PV)

Solar PV systems convert sunlight into electrical energy through solar cells, which are semi-conductors devices. PV panels are made of multiple interconnected solar cells. PV systems include PV modules, DC to AC current inverters, generation meters, cables, batteries and sun-tracking system in some cases [132]. The first practical applications of PV energy were to power satellites and spacecrafts. Due to its reliable and autonomous characteristics, it then became an economical solution to give power to remote locations that are not connected to the grid. Actually the PV industry is seeing an important growth, driven by technological innovations that have rapidly decreased PV module manufacturing costs by 100, and accelerated by supported schemes and incentives for producers and consumers, such as PV electricity feed-in-tariffs [52, 133, 134, 135, 136, 137, 138]. Large-scale photovoltaic plants have the advantages of bringing down capital expenditure, operation and maintenance costs [18, 139], avoiding large amount of GHG emissions. Muneer et al. [9] explored the long term prospects of large scale PV generation in arid/semi-arid locations, around the globe and its transmission using hydrogen as the energy vector. Several demonstration projects in Japan addressed grid stabilization with large-scale photovoltaic systems by controlling PV generation and local demand [140].

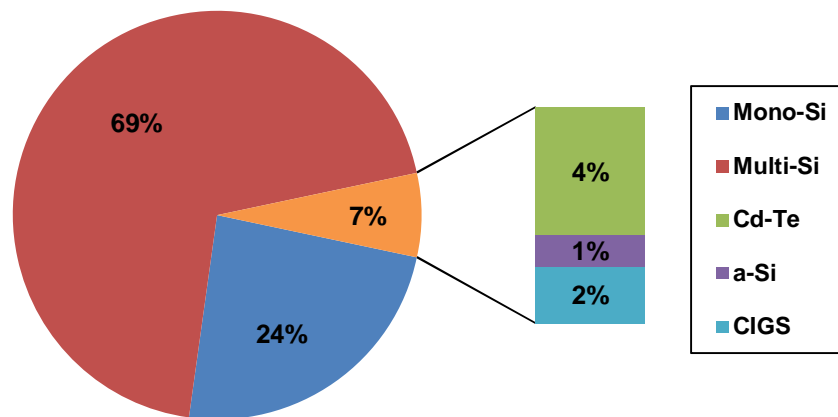


Figure 3.3. Global PV market by type in 2015 [141]

PV modules are composed of a multitude of solar cells assembled in series. A solar cell is an electrical device that converts the light energy (photons) from the sun into electricity. There are two main categories of solar cells: the crystalline silicon (c-Si) and the thin-film. The crystalline silicon cells can be made of monocrystalline or multicrystalline silicon, which represent 93% of

the PV market in 2015. The thin-film PV cells are commercially used in several technologies, including cadmium telluride (CdTe), copper indium gallium diselenide (CIGS), and amorphous silicon (a-Si), which represent the remaining 7% of the PV market. Figure 3.3 displays the global PV market by type in 2015 [141].

In the chase for higher module efficiency, an emerging technology is the multi-junction (MJ) cell made of expensive gallium arsenide (GaAs) and other different semiconductor materials. The MJ solar cells are commonly used for solar panels on space craft, but they are also generally used in concentrator photovoltaics (CPV), an emerging technology in which light is focused by lenses or mirrors onto the cells. This enables the use of cells with a high cost per unit area (such as GaAs) in a more cost-effective way, but CPV are still limited to locations with high solar radiation, and represent only 0.1% of the PV market [142]. Figure 3.4 shows the efficiency evolution of the main solar cells types.

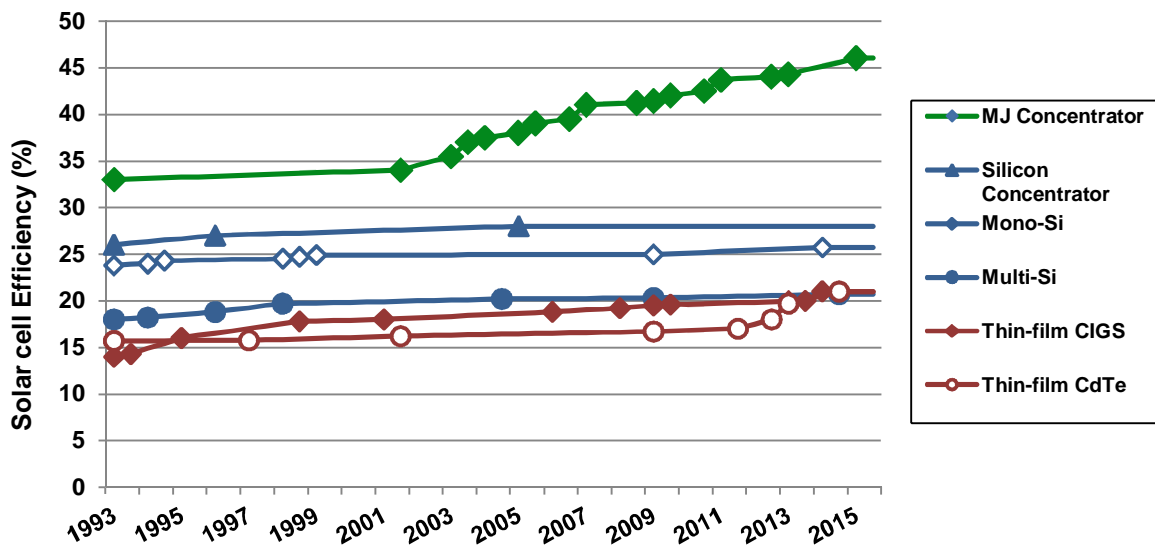


Figure 3.4. Solar cell efficiency evolution by type [141]

Globally, capacity additions in the photovoltaic market have grown from 0.28 gigawatts (GW) in 2000 to 16.6 GW in 2010 [143, 144], corresponding to an average annual growth rate of 50%. In 2015, PV capacity additions were 50 GW [145], and the total global installed capacity amounted to around 229 GW (see Figure 3.5), producing some 280 TWh of electrical power every year, with 35% from the European Union (almost 80 GW installed in 2015), 20% from China, 16% from Japan and 12% from the United [145]. The progress is particularly significant

3.1 Solar energy

in the last 5 years with about 190 GW of new installations over the period 2010 to 2016. Figure 3.6 shows the expected raise in renewable energy in world by 2050, out of which solar energy will be the most [146].

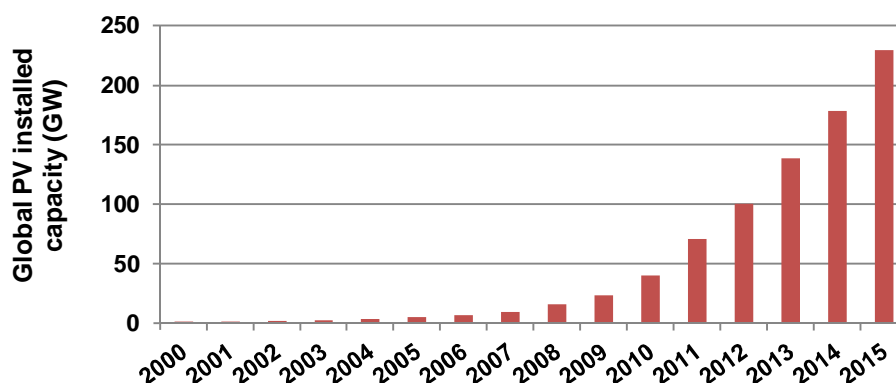


Figure 3.5. Evolution of global PV cumulative installed capacity (GW) [143, 144, 145]

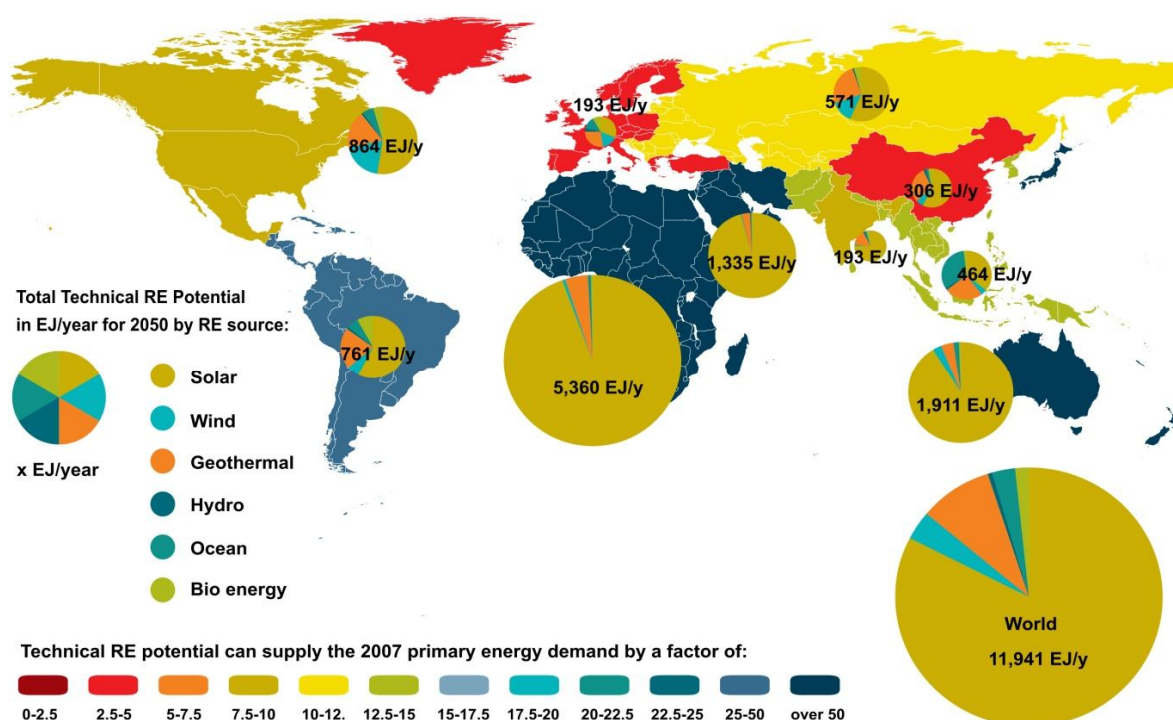


Figure 3.6. Renewable energy potential for 2050 in EJ/year by energy source [146]

The development of solar PV technology is enhanced by more affordable costs. The cost of PV technology is reducing with time, experience and mass production [147]. Figure 3.7 shows the historical downward trend of PV module costs in Germany [148, 149]. The cost in year 2016

has dropped by more than 99% from 1977 price. Within the past five years alone, more than 65% reduction in the average price of crystalline silicon PV module in Germany is indeed impressive (Figure 3.8) [149].

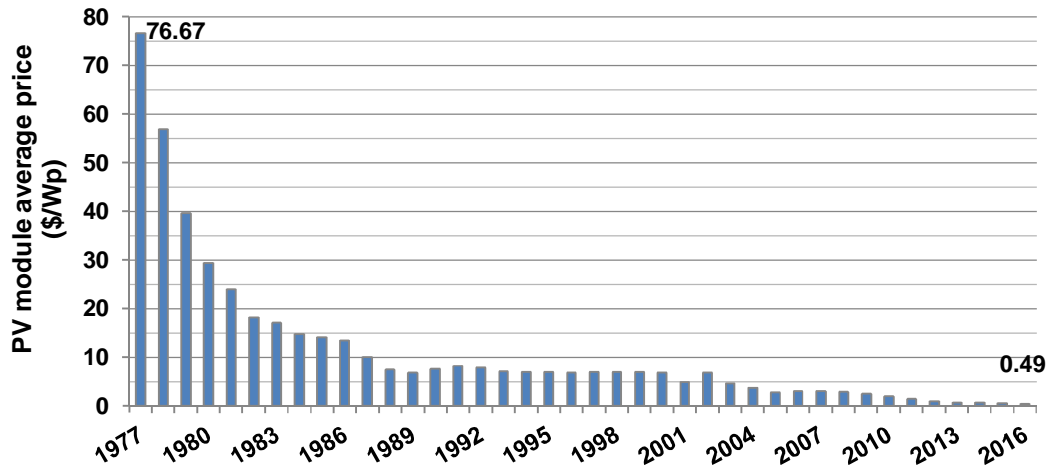


Figure 3.7. The decreasing cost of c-Si PV module (1977-2016) [148, 149]

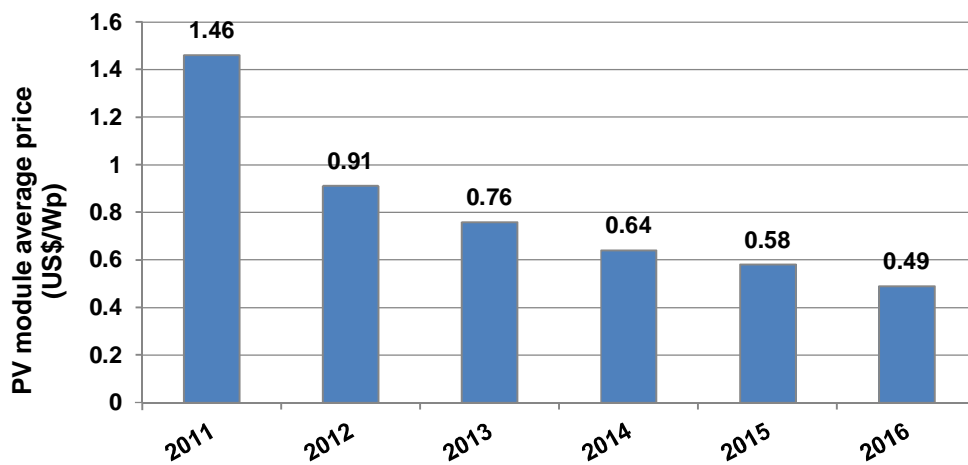


Figure 3.8. The decreasing cost of c-Si PV module (2011-2016) [149]

It is worth to consider that the use of solar energy for electricity generation has much lower impact on the environment than the combustion of fossil fuels in conventional power plants. According to the latest life cycle analyses [150, 151], which measure the environmental impact of solar PV panels from production to decommission, GHG emissions have come down to around 0.03 kgCO_{2eq}/kWh, compared to 0.04-0.05 kgCO_{2eq}/kWh ten years ago. This current estimated value is more than 12 and 25 times lower as compared to the 2017 emission factors for electricity

generation in the SIC and SING national grids, which are estimated at 0.38 and 0.77 kgCO_{2eq}/kWh respectively [75], and which take into account only the environmental impact of fuel combustion and plant operation and maintenance (i.e. excluding fuel mining, extraction, preparation, transport, or plant construction and decommissioning).

3.1.3 Concentrating solar thermal power (CSP)

Concentrating solar thermal power turns sunlight into electricity. CSP technologies use mirrors to reflect and concentrate sunlight onto receivers that collect solar energy and convert it to heat. This thermal energy can be used to produce electricity via a steam turbine or heat engine that drives a generator. The several varieties of CSP systems include Dish/Stirling (DS) systems, Linear Concentrating (LC) and Power Tower (PT) systems (see Figure 3.9). CSP plants represent solutions for generating electricity on a large scale that can supply several hundred thousand households [152, 153, 154].

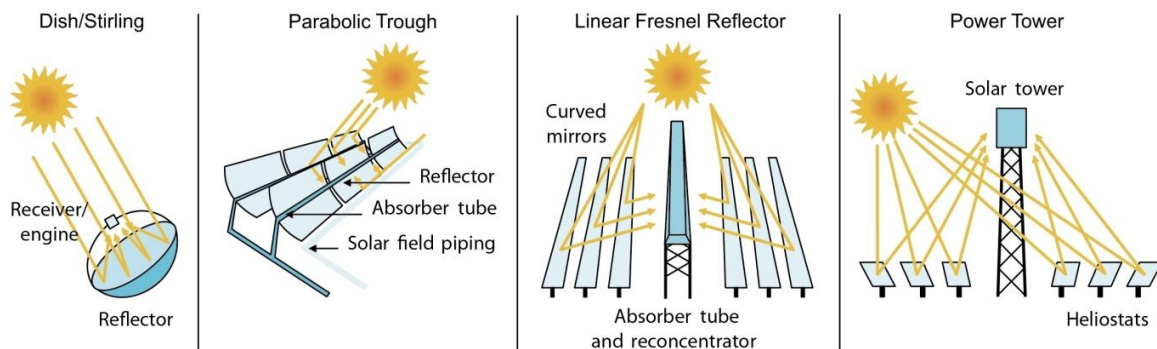


Figure 3.9. CSP system technologies

The Dish/Stirling systems use a parabolic dish of mirrors to direct and concentrate sunlight on a central Stirling engine, which uses the heated fluid to move pistons and create mechanical power. The mechanical work, in the form of the rotation of the engine's crankshaft, drives the generator and produces electrical power. Dish/Stirling CSP technology produces relatively small amounts of electricity compared to other CSP technologies, typically in the range of 3 to 25 kilowatts [155].

Linear Concentrating systems capture the sun's energy with large mirrors that reflect and focus the sunlight onto a linear receiver tube. The heat transfer fluid, when heated by the sunlight then

creates pressurised steam, which runs a turbine that drives a generator to produce electricity. Linear concentrating collectors are typically aligned in parallel rows, in a north-south orientation to maximize annual and summer energy collection. They include a single-axis sun-tracking system to enable mirrors to track the sun from east to west during the day. Linear concentrating systems include Parabolic Trough (PT) systems and Linear Fresnel Reflector (LFR) systems. Parabolic Trough systems consist of a receiver tube fixed to the mirror structure and positioned along the focal line of each parabola-shaped reflector. Fresnel Reflector systems are characterised by flat or slightly curved mirrors mounted on trackers on the ground that are set to reflect sunlight on a receiver tube fixed in space above the mirrors. The typical range of linear concentrating systems goes from 10 MW to 200 MW [155].

In Power Tower CSP systems, large and flat sun-tracking heliostats focus sunlight on a receiver at the top of a tower. A heat-transfer fluid is heated in the receiver to generate steam, which is then used in a conventional turbine generator to produce electricity. The capacity of commercial installation of power tower systems usually ranges from 10MW to 200MW [155].

CSP is a very promising technology as thermal energy can be stored to produce electricity after sunset and thus plant capacity factors are increased. CSP technologies usually use molten salts as the heat transfer fluid in order to store thermal energy into tanks [152, 156, 157, 158, 159]. Tamme et al. have used concrete as thermal storage medium for sensible heat [160], Watanabe et al., phase change materials for latent heat [161], and Gil et al.; Lovegrove et al.; Medrano et al., reversible reactions for thermochemical storage [162, 163, 164]. Thermal energy storage can utilise chemical energy (the heat of reaction), sensible heat, latent heat or a combination of these methods [165, 166]. Zanganeh G et al. have also presented promising results on a thermal energy storage system, consisting of a packed bed of rocks as storing material and air as high-temperature heat transfer fluid, with 95% overall thermal efficiency [167].

Fuel back-up or hybridisation is another way to cope with reduced or curtailed energy production when the sun sets or the sky cloudy, which is the major challenge of solar energy. One type of hybridisation system for CSP plant consists of including one or several auxiliary furnace able to operate with natural gas or oil, and in the future with biofuels or ammonia made from hydrogen produced from solar energy [168]. Instead of using burners, a gas turbine can be combined to the system. This hybridisation concept has the advantages of the combined cycles,

like high efficiency, and additional power production by the gas turbine [169, 170, 171, 172, 173]. The use of fossil fuel back-up results in GHG emissions but the gas turbine or boiler would be utilised only to maintain the required load of the CSP plant at nights or on cloudy days. On an annual basis, GHG emissions for a hybrid CSP plant would be much lower than for a fossil fuel only fired plant. In a hybrid solar power plant, the use of a storage unit is optional, as the hybrid components can cover the operation of the plant during periods of reduced solar input [169].

CSP requires clear skies and strong sunlight. Concentrated solar thermal power provides firm, peak, intermediate or base load capacities with adequate combinations between the turbine size, thermal storage size and/or the use of fuel back-up. The current world annual electricity consumption of 18000TWh could be met through CSP, which has a technical potential of 3,000,000TWh [174].

In 2015, global operating CSP capacity increased by 420 MW to reach nearly 4.8 GW at year's end, with Spain and the United States accounting for almost 90% of installed CSP capacity. The CSP market continued to advance in 2015, with 420 MW of capacity additions reaching a total global capacity of about 4.8 GW. The market is led by Spain and United States with 90% of the global installed capacity [145]. By the end of 2015, several countries launched their first CSP plants and industry activity expanded its attention from Spain and the United States to new regions. For example, new CSP plants facilities were under construction in Australia, Chile, China, India, Israel, Mexico, Saudi Arabia and South Africa. Morocco and South Africa surpassed the United States in capacity added, with Morocco becoming the first developing country to top the global CSP market [145]. Parabolic trough plants continued to dominate the market, but central receiver and Fresnel plants are becoming more common since 2011 [175, 176].

Generally, investment costs for CSP implementation range from US\$ 4.2 to 8.4 per watt, depending on labour and land costs, technologies, the solar resource, and above all the size of the solar field and the amount of thermal storage [19]. Levelised electricity costs range from US\$ 0.2 to 0.3 per kilowatt hours (kWh), depending on quality of the solar resource, technology employed, year, plant specifications, lifetime, loan and incentives, and location [19, 138]. Aabakken predicts levelised electricity costs decreasing from 0.15 in 2005 to 0.06 US\$/kWh in 2020 for DS systems, from 0.06-0.11 in 2005 to 0.04 US\$/kWh in 2020 for PT, and from 0.10 in 2005 to 0.07 US\$/kWh in 2020 for LC [177, 178].

3.1.4 Proof of concept and economics of solar electricity production

3.1.4.1 Levelised cost of electricity (LCOE)

A clear understanding of the relative cost effectiveness of different energy technology is determinant to assess the economic viability of such technology. The actual price of electricity depends on the cost of electricity generated by a given power plant and market policy measures [179]. The LCOE is used as a benchmarking tool to assess the cost-effectiveness or comparing grid parity for different energy generation technologies [134, 137, 52, 180, 181, 182]. The LCOE represents a life cycle cost per unit of electricity output (kWh or MWh) and is to be interpreted as the break-even value (minimum price per kWh or MWh, or TWh) that a power generating plant would have to obtain as sales revenue over the life cycle of the plant in order to justify the investment in such power generation facility [183]. To calculate the LCOE it is necessary to take into consideration the cost of the electricity generating system (in €, US\$ or other value) and the electricity generated over the system lifetime (in kWh or MWh). According to many sources in the literature [138, 155, 179, 184, 185, 186, 187, 188, 189], the LCOE calculations for different electricity generating technologies can be defined as:

$$LCOE = \frac{\text{Lifetime Cost}}{\text{Lifetime Electricity generated}} \quad (3.33)$$

The most general formula for calculating the LCOE of renewable energy technologies is [138, 155, 180, 186, 187, 190]:

$$LCOE = \frac{\sum_{t=1}^n \frac{I_t + M_t + F_t}{(1+r)^t}}{\sum_{t=1}^n \frac{E_t}{(1+r)^t}} \quad (3.34)$$

Where in Equation (3.34), I_t represents the investment expenditures in the year t ; O_t is the operations expenditures in the year t ; M_t the maintenance expenditures in the year t ; F_t representing the fuel expenditures in the year t ; E_t stands for the electricity generation in the year t ; r is the discount rate (%); and n is the life time of the system in years. The discount rate takes the time value of money as well as the risk of the investment. It is a crucial factor in the

3.1 Solar energy

calculation of the cost of electricity [180]. Classic discount rates for PV and CSP can be assumed between 10% and 15% [16, 184], although discount rates of 5% are also reported for PV [52, 144, 191, 192] and for CSP systems [19, 193]. The LCOE seeks to take into account all physical material and resources that is necessary to produce one unit of electricity output. The MIT study [194] gives an interpretation of the LCOE definition: “*the levelised cost of electricity is the constant dollar electricity price that would be required over the life of the plant to cover all operating expenses, payment of debt and accrued interest on initial project expenses, and the payment of an acceptable return to investors*”.

In the case of renewables energy power plants such as solar photovoltaic, or concentrating thermal solar, that require zero fuel cost and low maintenance costs, the cost for generating electricity is mainly the cost of financing the initial investment. The LCOE generated by solar energy can be affected by the method of returning the loan and its interest rate. Singh et al. have pointed out the particular care that should be taken towards that factor [182]. Results have shown that equated payment loans ensures artificially high LCOE for PV in base year as compared to the prevailing price of grid electricity at that time. It was proposed that to arrive at realistic LCOE of solar PV, graduated payment loan with escalation in loan instalments equal to the estimated long-term rate of inflation in price of grid electricity should be chosen. Reichelstein et al. have also shown the influence of the investment credit and depreciation rate on the LCOE calculations [183]. The International Renewable Energy Agency (IRENA) [155] and Dinica [195] have presented the most important parameters that should be included in the calculation to obtain the most precise, reasonable and realistic LCOE for solar power plant implementation. The LCOE should take into account the initial investment cost, including site development, components and system costs, assembly, energy conversion efficiencies, grid connection and financing costs; the plant’s capacity factor and efficiency; the local DNI at the plant site; the operation and maintenance costs; the insurance costs; the cost of capital and the project economic lifetime. If one or more of these factors are misjudged, under or over estimated the resulting value of LCOE for the particular plant will be untrue. Branker et al. [138] have pointed out that reporting the wrong LCOE values for technologies can result in not optimal decisions for a specific project, but can also misguide policy initiatives at the local and global scale.

Table 3.1 gives a broad review on construction costs, LCOE and environmental costs for coal, gas, CSP and PV electricity generating plants. Cost range values shown here are produced

compiling figures from the large literature – some of it is presented here. Not all authors recognise exact same costs, and ranges presented here reflect differences in local conditions and financial assumptions (country incentives, technology retail prices, choice of sub-technology). According to IRENA report [196], in 2015, global weighted average LCOE at utility scale is 0.15 US\$/kWh for CSP technology and 0.13 US\$/kWh for PV, while LCOE is around 0.08 US\$/kWh for new coal power plants, and around 0.10 US\$/kWh for new gas (combined cycle gas turbine) plants, according to IEA [197].

Table 3.1 shows current values of construction costs, LCOEs and environmental costs for different electricity generating plants. The table compares two types of conventional power plant (coal and gas) to the solar PV and CSP power plants. LCOE for coal and gas plants take account of the cost of transporting their fuel from the supplier to the power station. Typical cost breakdown values for 5000 km transport are 2\$/MWh for coal and 10\$/MWh for gas [198].

Table 3.1. Costs comparison between solar PV, CSP and conventional power plants

| | CSP plant | PV plant | Coal power plant | Gas power plant |
|-------------------------------------|--|---|--|----------------------------------|
| Construction cost (\$/W) | 4.2 - 7.1 (without storage) 6.3 - 10.5 (with storage) [19, 155, 196, 199, 200] | 1.8 - 4.0 [186, 196, 201, 202] | 1.0 - 1.5 [179] | 0.4 - 0.8 [179] |
| LCOE (\$/kWh) | 0.14 - 0.36 [10, 19, 155, 186, 196] | 0.09 - 0.40 [134, 138, 186, 196, 202] | 0.05 - 0.12 [155, 179, 195, 197] | 0.08 - 0.12 [155, 179] |
| Environmental cost (USc/kWh) | 0 | 0 | 0.16 [203] | 3.2 [203] |

The lower end of LCOE range for both solar technologies is achievable in locations that benefit from important solar resource, considering equivalent market, financial and technology factors. LCOE of solar technologies is strongly affected by the plant capacity factor and thus the solar resource, while construction costs are directly depending on plant size, plant features (storage, back-up systems for CSP; tracking system, type of mounting hardware for PV), labour and land costs, permitting and commissioning costs, the type of technology used and components retail prices.

The difference of costs between the two solar and the conventional plants highlights clearly the disadvantage of solar energy over coal and gas. However, the figures for coal and gas power plants tend to increase due to the increase of fossil fuel prices and the rise of environmental concern (carbon taxation, compensation measures for global warming) [204]. In the mean time, figures of construction cost and LCOE for PV and CSP tend to decrease when technology is still subject to market growth and high learning rates that will bring it more affordable. Aside from market, financial and technology factors, the lower range of LCOE for solar power plant is achievable in locations where the solar resource is important.

3.1.4.2 Grid parity

Factors like technology capital cost and available resource are fundamental when determining the LCOE of a particular plant, in a particular location. Low capital costs combined with high available sunlight can sometimes result in system LCOE as low or lower than the market price of the utility grid electricity. In such cases, we can say that the system achieves grid parity.

Figure 3.10 shows the evolution in PV module and CSP system prices along with global cumulative installed capacity [186, 205]. The increase of PV module cost in 2005 is due to silicon shortage. In 2013, studies have yet shown effort brought to reduce PV module prices, as well as offering more efficient modules [206, 207, 208]. The new solar module is an ingenious combination of the high quality and efficiency of monocrystalline modules, with the lower cost of multicrystalline modules. Innovative technology improves the uniformity of the grain size and preferred orientation, resulting in higher minor-carrier lifetime and lower dislocation density. The outcome is significantly increased cell efficiency.

There is still a common biased opinion that believe that solar PV technology has a short life and then remain in the long term very expensive [209, 210]. However, in location with high solar resource, the cost of solar PV has already dropped below the cost of conventional fuels achieving grid parity [143, 181, 190, 205, 211, 212]. For example, Girard et al. [213] have shown that a 100 MW solar PV plant in the south of Spain could achieve grid parity without financial subsidies assuming an internal rate of return of 7.3%.

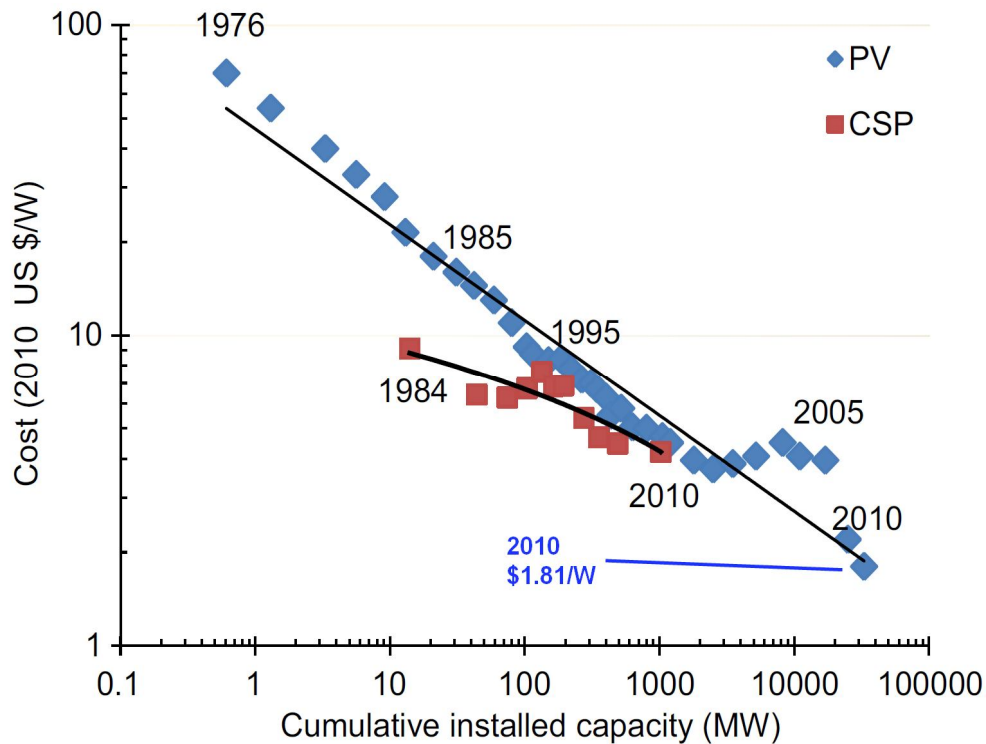


Figure 3.10. PV module and CSP system prices as a function of global cumulative installed capacity [186]

PV and CSP technologies do not make the same use of the solar resource. CSP technology uses only the direct radiation of the sun to concentrate it, while PV uses both direct and diffuse irradiation. Therefore, while projects of PV power plants will look at the global irradiation value, CSP developers tend to consider the value of Direct Normal Irradiance (DNI), since sun tracking systems allow concentrators to always be normally orientated towards the sun. For CSP plants, the low limit value of DNI to achieve economical performance is set between 1900 kWh/m²/yr and 2000 kWh/m²/yr [19, 214]. Currently, most of the CSP power plants are installed in the southwest of the United States and in the south of Spain, where DNI values range from 2000 to 2850 kWh/m²/yr [155, 186, 215, 216]. In the case of fixed optimally-inclined south-oriented PV systems, investors have set the boundary conditions for global irradiation values from 1300 to 2300 kWh/m²/yr and that include many locations with lower direct radiation [52, 51, 217].

Achieving grid parity means that levelised cost of electricity for solar technology has reached the electricity market price or at least the cost of electricity generated from fossil fuel sources.

3.1 Solar energy

Schleicher-Tappeser [212] has presented a forecast from 2010 for the grid parity situation of PV technology in Europe in 2016, as shown in Figure 3.11 [205, 211, 218]. The different circles represents the current average price of electricity of all European countries in commercial (blue) and residential (orange) sectors. The red line is the estimation of LCOE from a PV power plant in 2016 as a function of the irradiation. As the LCOE from PV technology tends to decrease (the red line shifting to the left), more countries would be in the grid parity area, bringing PV plant more competitive compared to traditional power plant for most countries in EU.

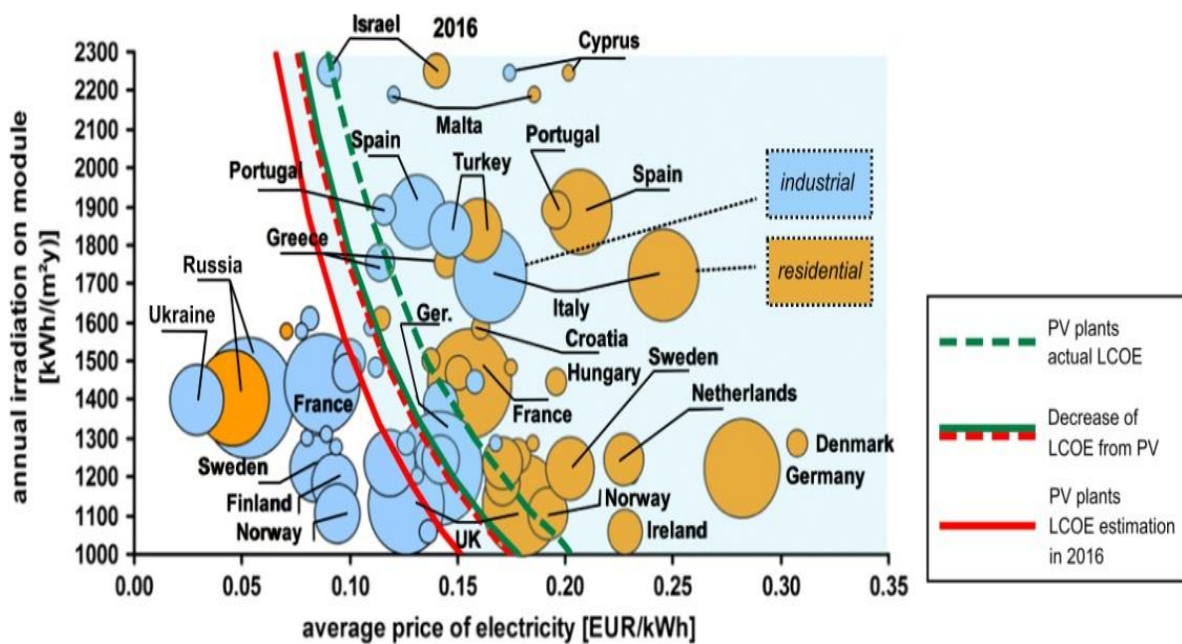


Figure 3.11. PV grid parity in Europe 2016 (shaded area). A 2010 forecast [212]

Another forecast of grid parity for PV and CSP was studied by Hernández-Moro et al. [186]. Results are presented in the Figure 3.12. The BLUE line represents an estimated reasonable scenario of LCOE reduction along time, the ROADMAP line representing a more favourable scenario. Grid parities are presented for LCOE of coal-fired thermal power plants taking into account different carbon emission prices of 0, 25 and 50\$/ton CO₂. These studies show that grid parity for solar technology is eventually to occur with the combination of two factors: solar technology costs reduction and conventional electricity generation costs increase. However Branker et al. have warned policy makers that grid parity for solar power could be more difficult to achieve if fossil fuels and nuclear power still continue to receive larger subsidies than

renewable energy technologies [138, 219, 220]. The European economic crisis also plays an important role restraining governments' efforts towards renewable energy because of limited financing availability [220, 221, 222].

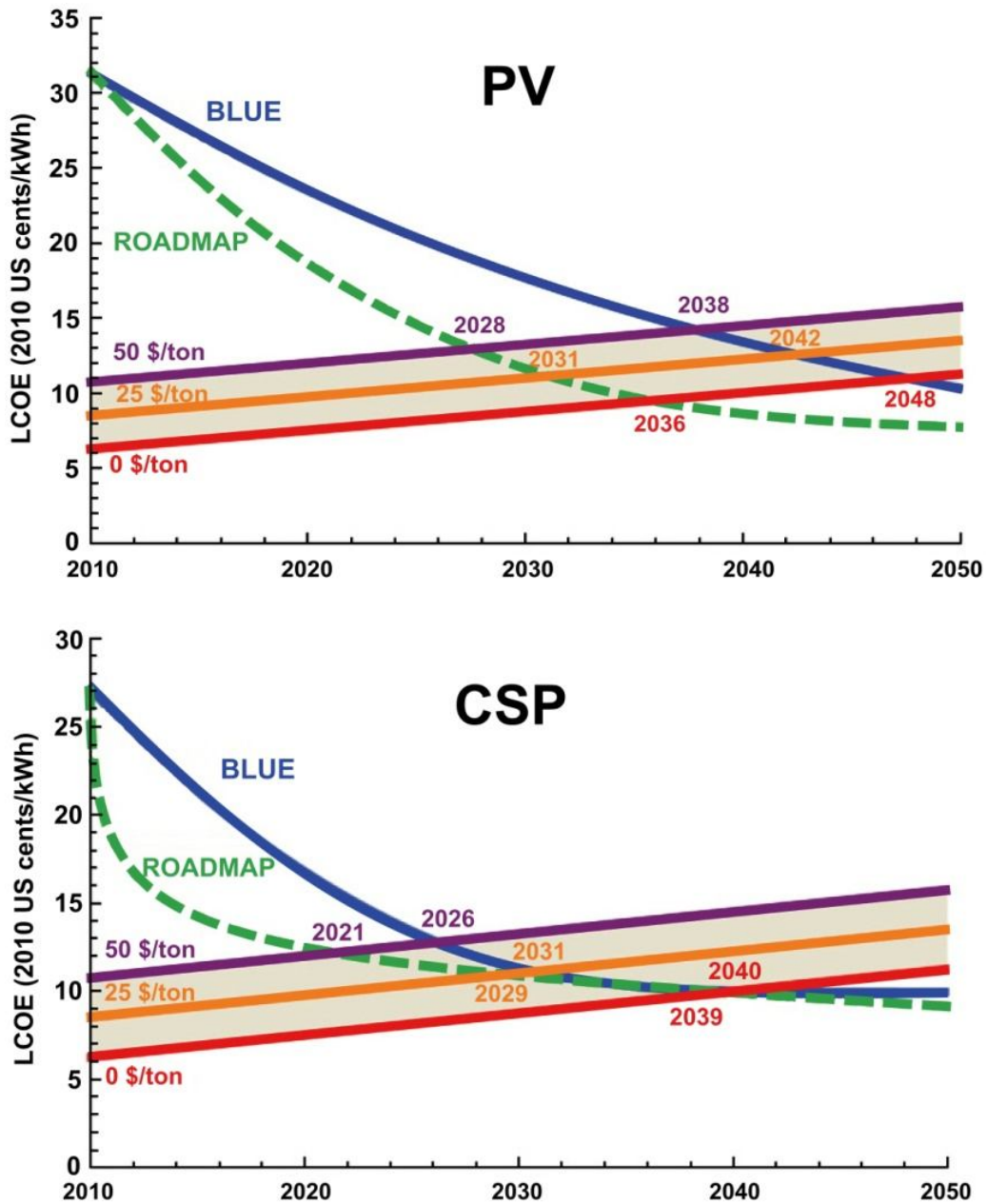


Figure 3.12. PV and CSP LCOE evolution for the BLUE and ROADMAP Scenarios and grid parities for coal-fired thermal power plants with a carbon emission price of 0, 25 and 50 \$/ton CO₂ [186]

3.2 Low-grade geothermal energy

3.2.1 Ground-source heat pump (GSHP) principles

Low-grade geothermal energy or the warmth of the earth that can be found several meters below the ground is free and inexhaustible. Unlike high-grade geothermal energy, which is of higher temperature (i.e. above 30°C) and available in particular locations, low-grade geothermal energy is present everywhere in the world and can be harvested by ground-source heat pumps (GSHP). Such technology is recognized as a sustainable and energy efficient option for residential use in the space heating/cooling market [223, 224, 225, 226, 227], as it can have high energy performance characteristics. Moreover, it has demonstrated economic advantages over conventional heating methods such as liquid petrol gas heating, coal fired heating and diesel oil heating in studies by Esen et al. [228], Pulat et al. [229] both in Turkey and by Healy and Ugursal [230] in Canada. GSHP systems, which can be used for both heating and cooling purposes, consist of three subsystems: the heat pump, the earth connection and the interior distribution system (Figure 3.13).

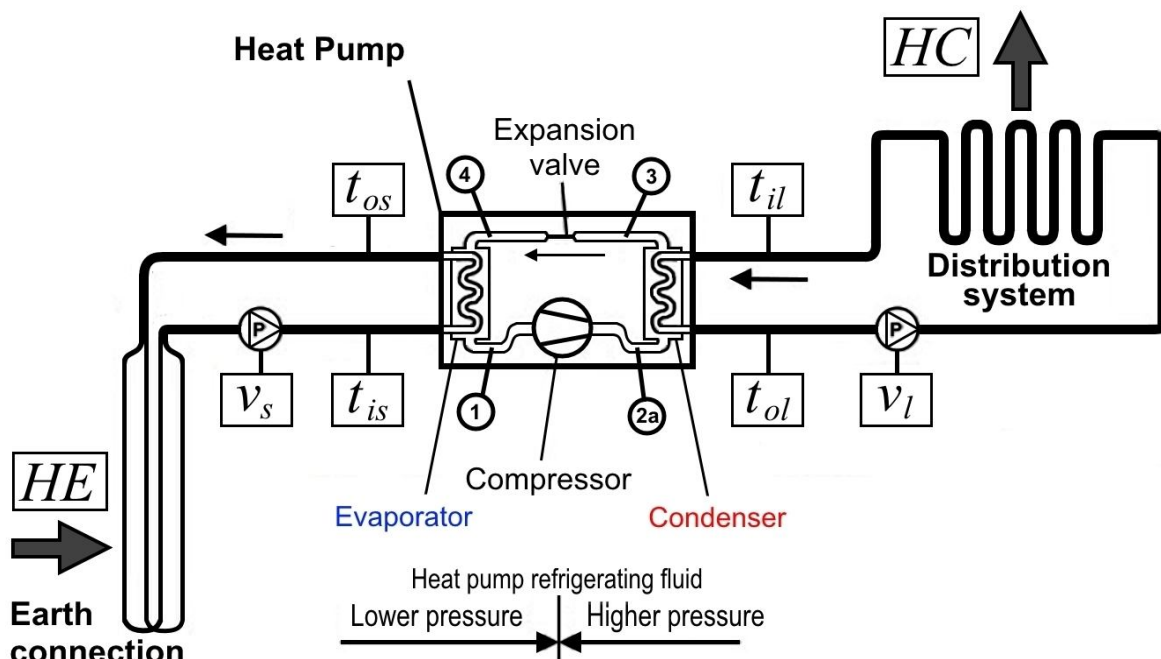


Figure 3.13. GSHP schematic in the heating mode

Heating or cooling absorbed from the ground can be distributed to the building by means of hydronic radiation systems (baseboard radiators, cast iron radiators or radiant floor heating), or through fan coil units or air handling systems. Before designing the GSHP system, one needs to consider that radiant hydronic systems cannot be cooled lower than the dew point temperature in order to avoid condensation to form on the radiators or the floor.

The second subsystem is the earth connection system exchanging heat with the ground. It consists of an open or closed loop system, through which thermal energy is extracted (or dissipated in summer cooling mode) with the use of ground water, surface water or a ground heat exchanger (GHE). Three main categories of GSHP can be identified (Figure 3.14) [231]:

- Ground Water Heat Pump systems (GWHP)
- Surface Water Heat Pump systems (SWHP)
- Ground Coupled Heat Pump (GCHP)

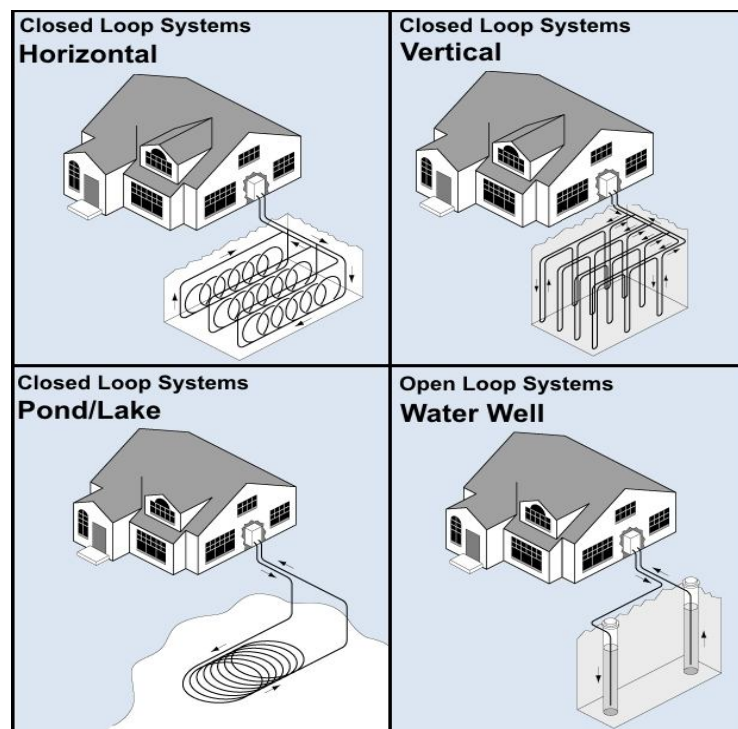


Figure 3.14. GSHP types [232]

GWHP systems also called open-loop systems are the origin of GSHP. The majority of open loop systems rely on one or more wells. Water well and well pumps are used to supply ground water to a heat pump directly. Water is withdrawn from the well or other sources and disposed of

through the use of injection wells. The main advantage of GWHP is their low cost, simplicity and small amount of ground area relative to GSHP. However, the problems are inadequate flow in the production well, plugging that causes pressure build-up in the injection well and failure of the pump.

SWHP systems can either be a closed or an open loop. In the closed loop, heat is being rejected or extracted by circulating a heat exchange fluid through a heat exchanger sized adequately and positioned at the right depth within a lake, pond reservoir or any open channel. In the open loops, water is pumped from the source and discharged to a suitable receptor. SWHP uses the heat transfer mechanisms and the thermal characteristics of surface water bodies which are different from those of soils and rocks. The closed loop design involves a selection of the right depth, coil length, pipe diameter and number of loops to have an adequate thermal capacity.

GCHP systems are connected to a GHE in a closed loop. The GCHP can be either in vertical or horizontal mode. The vertical mode of the GCHP has a heat exchanger that consists of vertically buried pipes or vertical heat exchanger coil typically installed in 45 m to 150 m deep vertical boreholes [231]. A borehole heat exchanger can contain a U-shaped pipe or a spiral shaped vertical coil heat exchanger. Such vertical collectors are used where land area is limited and for larger installations. The horizontal mode of the GCHP has a heat exchanger that consists of using a series of parallel pipe arrangements laid out in 1 m to 2 m deep horizontal trenches. Horizontal collectors require relatively large areas free from hard rock or large boulders and a minimum soil depth. Multiple pipes (up to six, placed either side by side or in an over/under configuration) can be laid in a single trench. The amount of trench required can also be reduced if the pipe is distributed as a series of overlapping coils, placed vertically in a narrow trench or horizontally at the bottom of a wider trench. Trench lengths are likely to be 20% to 30% of those for a single pipe configuration but pipe lengths may be double for the same thermal performance.

GCHP has been used extensively as it eliminates the problems associated with ground water quality and availability [233]. Moreover, they require less pumping energy than the water well systems. The fluid that is circulating in the closed loop GHE and used to transfer the thermal energy is usually a propylene glycol solution (water-based liquid mixture) to prevent from the risk of freezing when the heat pump is turned off. The length of trenches and boreholes greatly depends on soil conditions including temperature, thermal conductivity, moisture content and particle size [234, 235].

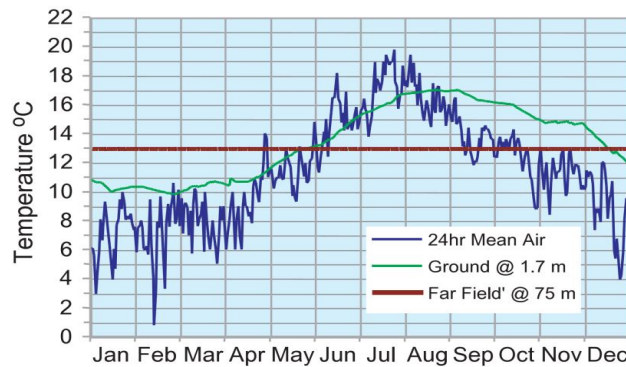


Figure 3.15. Air and ground temperatures, Falmouth, England [236]

The principle of GSHP relies on the fact that temperatures below the ground surface do not fluctuate significantly through the day or the year as do ambient air temperatures. Ground temperatures a few meters below the surface stay relatively constant throughout the year. For a GSHP connected to a vertical borehole source deeper than 10 m, it is accepted that the ground temperature is largely the same as the average annual air temperature [237, 238, 239]. For a GSHP with a horizontal ground loop as a source, a more complex relationship exists, since soil temperature above 10 m depth is still subject to the influence of air temperature, but with a lag dependent on depth and soil type [240, 241]. Figure 3.15 shows the annual variation in ground temperatures at depths of 1.7m and 75m, as compared to the daily average air temperature measured at Falmouth, England. For this reason, GSHPs remain extremely efficient throughout the year in virtually any climate.

GSHP efficiencies are much greater than that of air-source heat pumps (ASHP), which are using ambient air as a heat source. In ASHP, a fan is generally used to create a forced convection and increase the heat transfer capacity of the condenser or evaporator, but higher coefficient of performance (COP) can be achieved by GSHP because the ground temperature is relatively constant throughout the year, and generally of a higher grade than that of the ambient air. Additionally, water based fluid is a better heat transfer medium due to its higher heat capacity.

GSHP for space heating have been used for over 50 years. Despite this fact, the market penetration is still in its infancy, with electrical heaters, gas-boilers or air-source heat pumps largely dominating the space heating market. In 2015, the global installed capacity of GSHPs account for 50,258 megawatts of thermal capacity (MWth), and the annual energy use is 90,791 gigawatt hours per year (GWh/yr) [242]. The size of individual GSHP units generally ranges from 5.5 kW for residential use to over 150 kW for commercial and institutional installations.

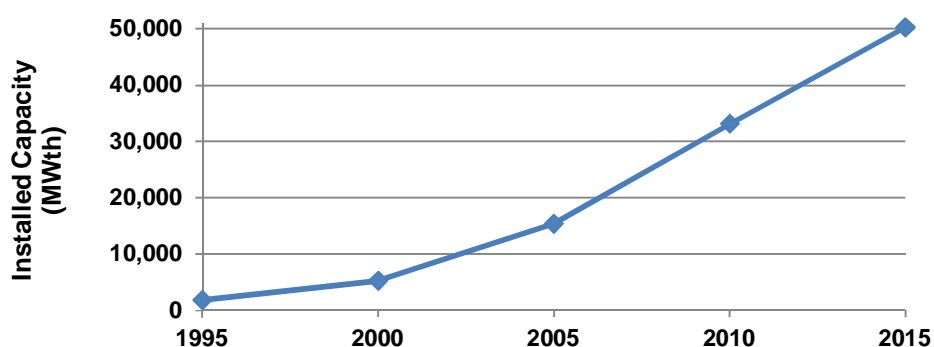


Figure 3.16. Evolution of global GSHP installed capacity 1995 – 2015 [242]

Although the leaders in installed GSHP units in 2015 are the United States, China, Sweden, Germany and France (Table 3.2), the number of countries with installations increased from 26 in 2000, to 33 in 2005, to 43 in 2010, and to 48 in 2015. The number of installed GSHP units is approximately 4.19 million in 2015. This is a 52% increase over the number of installed units reported in 2010, and over three times the number of units reported in 2005 [242]. Table 3.2 shows the GSHP market size in different countries in 2015 and the change from 2010 to 2015, and Figure 3.16 the global market evolution over the period 1995-2015 [242]. In Chile, approximately 83% of the GSHP units are installed in commercial, industrial and institutional buildings, with only 17% in houses and apartments. In 2014, the total installed capacity of GSHP in Chile is 8.61 MWth and the annual energy use is 9.44 GWh/year [243].

Table 3.2. Global GSHP installations in year 2015 (change from 2010 to 2015) [242, 244]

| Country | Installed capacity (MWth) | Installed capacity change (2010-2015) | Annual energy use (GWh/yr) | Annual energy use change (2010-2015) |
|-------------------|---------------------------|---------------------------------------|----------------------------|--------------------------------------|
| USA | 16,800 | +40% | 18,519 | +131% |
| China | 11,781 | +126% | 27,864 | +34% |
| Sweden | 5,600 | +26% | 14,423 | +15% |
| Germany | 2,590 | +16% | 4,500 | +24% |
| France | 2,010 | +101% | 3,028 | +53% |
| Rest of the World | 11,477 | +39% | 22,457 | +8% |
| Total | 50,258 | +52% | 90,791 | +40% |

3.2.2 Theoretical background

The main components of the heat pump are a scroll compressor, two heat exchangers (evaporator and condenser) and a thermostatic expansion valve in a closed circuit through which a refrigerant fluid flows (see Figure 3.13). The heat is transferred by circulating the phase changing refrigerant fluid through a cycle of evaporation and condensation [87, 245]. An example of the refrigerant flow cycle is shown on the pressure-enthalpy (P-h) chart in Figure 3.17, where points 1 to 4 indicate the different states of the refrigerant fluid throughout the refrigerating cycle (points 1 to 4 are also shown in Figure 3.13 after each component of the heat pump).

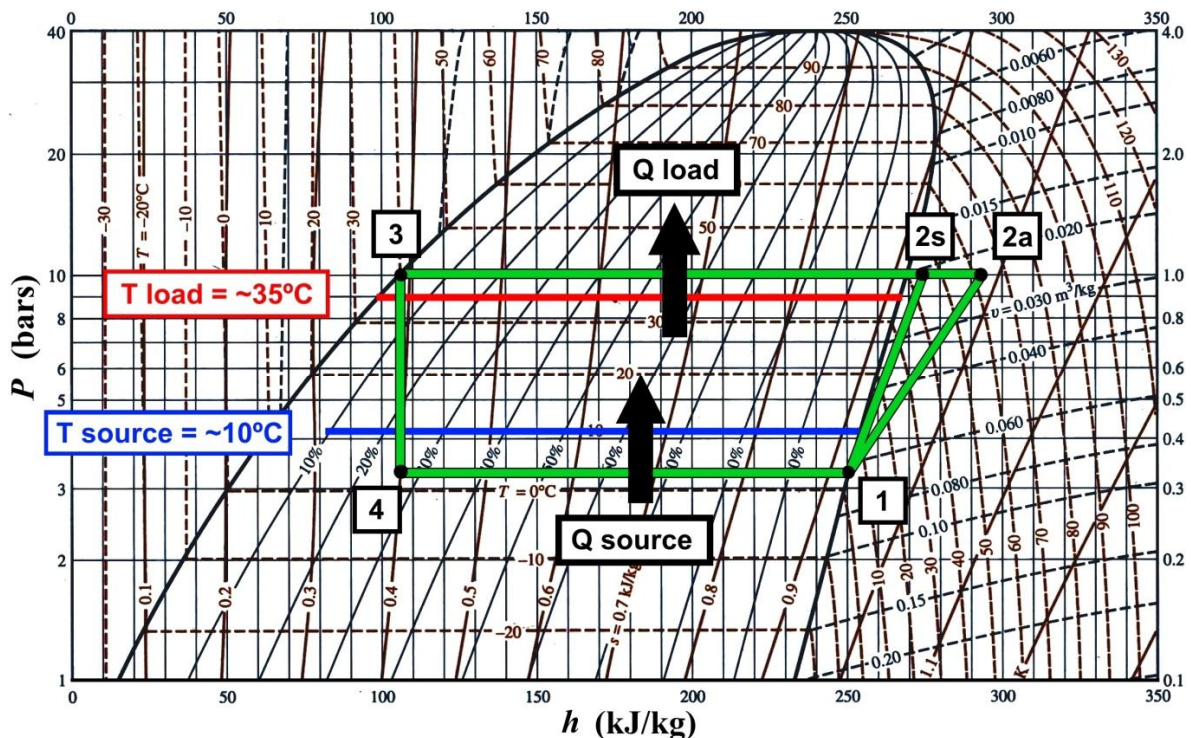


Figure 3.17. Pressure-enthalpy chart for the heat pump cycle using the refrigerant R134a

The compressor maintains a low pressure in the evaporator and, absorbing heat from the heat source, the refrigerant boils at a constant pressure and temperature (point 1). The cold low-pressure vapour formed in the evaporator is then drawn into the compressor where its pressure increases and its temperature rises (Point 2a). Point 2s indicates the state of the refrigerating fluid for an ideal gas compression process (i.e. isentropic compression). Since the compression process

is never isentropic in practice, the real state of the fluid after compression is at point 2a. After being compressed, the warm high-pressure vaporized refrigerant enters the other heat exchanger, where it condenses at a constant pressure and temperature (point 3). At this moment, the refrigerant releases the heat it absorbed earlier in the cycle to the heat sink. Then, the warm high-pressure liquid refrigerant in point 3 is discharged back to the evaporator through the expansion valve at the same rate as it is formed. As it passes through the valve, its pressure decreases to that of the evaporator and its temperature falls to the saturation temperature at the lower pressure (point 4). Finally, the cycle is repeated.

As part of their components, heat pumps can also include a 4-way valve between the compressor inlet and outlet so that the system can be reversed, allowing to switch between heating and cooling mode. In cooling mode, such valve allows the refrigerant to flow in the opposite direction than in heating mode, thus converting the plate heat exchanger shown as the evaporator in Figure 3.13 into the condenser, and the condenser into the evaporator. Thus, the ground is the heat source in heating mode, and the heat sink in cooling mode [246].

A heat pump works in the heating mode by extracting some of the low-grade heat energy in the ground and turning it into a higher grade of energy, perhaps at 35°C, to heat the water for under-floor heating. Having done its work, colder fluid, at perhaps 10°C, is then sent back out to run through the ground again, picking up more low-level heat to use. Figure 3.18 shows the temperature evolutions in the three different GSHP heat exchangers, the ground coil (GC), the heat pump evaporator and condenser, where t is temperature, v is flow rate, subscripts i , l and s are short for the heat pump inlet conditions, load and source, respectively.

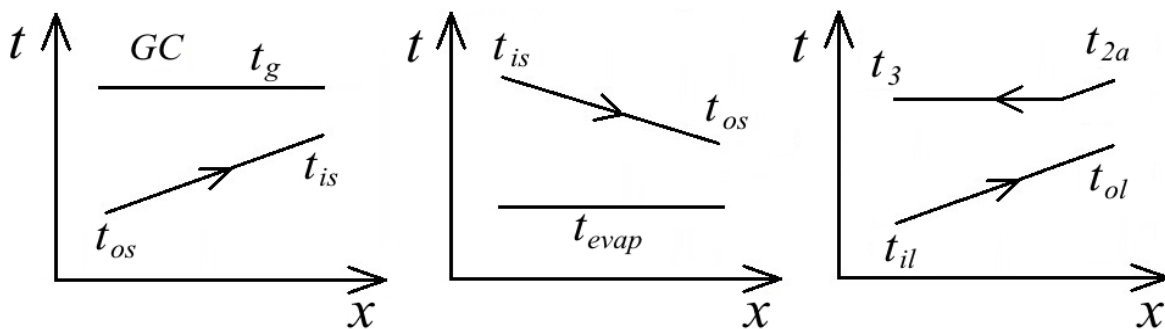


Figure 3.18. Evolution of temperatures through GSHP heat exchangers (From left to right: ground coil (GC), evaporator, and condenser)

Heat pumps remain extremely efficient systems because the energy used to compress the refrigerant is smaller than the useful thermal energy extracted. The efficiency of heat pumps is defined by the coefficient of performance (COP), which can be calculated by the fraction of the output thermal energy available at the heat pump condenser (Q_{cond}) over the input electrical energy of the compressor (W_{comp}), using the enthalpies h of the corresponding points in the P-h chart, as shown in the following Equation (3.35) [247]. Energy in the form of heat is noted Q , while energy in the form of mechanical work is noted W , but both are measured in Watt (W).

$$COP = \frac{\text{heat output}}{\text{electricity input}} = \frac{Q_{cond}}{W_{comp}} = \frac{(h_{2a} - h_3)}{(h_{2a} - h_1)} \quad (3.35)$$

The heat absorbed at the heat pump evaporator, Q_{evap} , is equal to the difference between the energy available at the condenser and the input energy of the compressor. Therefore, Q_{evap} , can be written as a function of the COP value as shown in Equation (3.36).

$$Q_{evap} = Q_{cond} - W_{comp} = Q_{cond} (COP - 1) / COP \quad (3.36)$$

The thermal energy distributed to the load side Q_{load} (the house distribution system in heating mode) is equal to the thermal energy available at the condenser Q_{cond} , written as follows:

$$Q_{cond} = \dot{m}_r (h_{2a} - h_3) = Q_{load} = v_l \rho_l C_{p_l} (t_{il} - t_{ol}) \quad (3.37)$$

Where \dot{m}_r represents the mass flow rate of the refrigerating fluid in the heat pump, h_{2a} and h_3 are the enthalpies of the refrigerating fluid at points 2a and 3 respectively, v_l is the volumetric flow rate of the fluid in the load circuit (m^3/s), ρ_l is the load side fluid density (kg/m^3), C_{p_l} is the specific heat of the load circuit fluid ($\text{J}/\text{kg}^\circ\text{C}$), t_{il} and t_{ol} are the temperatures of the load circuit fluid at the inlet and outlet of the heat pump condenser ($^\circ\text{C}$).

The thermal energy harvested from the heat source Q_{source} (the ground in the heating mode) is equal to the thermal energy collected by the heat pump evaporator Q_{evap} , written as:

$$Q_{evap} = \dot{m}_r (h_1 - h_4) = Q_{source} = v_s \rho_s C_{p_s} (t_{is} - t_{os}) \quad (3.38)$$

3.2 Low-grade geothermal energy

Where v_s is the volumetric flow rate of the fluid in the source circuit (m^3/s), ρ_s is the fluid density (kg/m^3), C_{p_s} is the fluid specific heat ($\text{J}/\text{kg}^\circ\text{C}$), t_{is} and t_{os} are the temperatures of the source circuit fluid at the inlet and outlet of the heat pump evaporator ($^\circ\text{C}$).

The thermal energy transferred from the ground (Q_g) can be written as in Equation (3.39).

$$Q_g = U_c \cdot A_c \cdot \Delta T_{LM} \quad (3.39)$$

Where U_c and A_c are respectively the overall heat transfer coefficient ($\text{W}/\text{m}^2^\circ\text{C}$) and the surface area (m^2) of the ground coil and ΔT_{LM} the log mean temperature difference ($^\circ\text{C}$), which can be calculated using the ground temperature (t_g) as in the following Equation (3.40).

$$\Delta T_{LM} = \frac{(t_{is} - t_{os})}{\text{Ln} \frac{(t_{os} - t_g)}{(t_{is} - t_g)}} \quad (3.40)$$

The overall heat transfer coefficient of the ground coil U_g can be determined as:

$$U_{ground} = \frac{1}{R_c + R_p + R_s} \quad (3.41)$$

Where R_c is thermal resistance due to convection heat transfer between the antifreeze liquid in the ground pipe and the pipe inner surface ($\text{m}^2^\circ\text{C}/\text{W}$), R_p the thermal resistance due to conduction heat transfer between the pipe inner and outer surface ($\text{m}^2^\circ\text{C}/\text{W}$) and R_s is the thermal resistance due to conduction heat transfer between the coil outer surface and the undisturbed ground soil ($\text{m}^2^\circ\text{C}/\text{W}$). These three thermal resistance values can be calculated as:

$$R_c = \frac{1}{2\pi r_1 L h_c} \quad (3.42)$$

$$R_p = \frac{1}{2\pi L k_p} \ln \frac{r_2}{r_1} \quad (3.43)$$

$$R_s = \frac{1}{2\pi L k_s} \ln \frac{r_2 + r_3}{r_2} \quad (3.44)$$

Where r_1 is the inner pipe radius (m), r_2 is the outer pipe radius (m), and r_3 the distance between the pipe outer surface and the undisturbed soil (m), which can be assumed to be equal to the radius of the pipe; L is the coil length (m); and k_p and k_s are the thermal conductivity (W/m°C) of the pipe material and the soil respectively.

The convective heat transfer coefficient at the inner pipe surface in Equation (3.42), h_c (W/m²°C), is a function of Nusselt number, Nu , and thermal conductivity of the fluid k_s (W/m°C), which can be expressed as follows:

$$h_c = \frac{Nu k_s}{2 r_1} \quad (3.45)$$

The Nusselt number Nu , determined using fluid mechanics correlations for forced convection in pipes (the appropriate formula applies for each laminar or turbulent flow condition), is function of the fluid Prandtl Pr_s and Reynolds Re_s numbers calculated as follows:

$$Pr_s = \frac{Cp_s \mu_s}{k_s} \quad (3.46)$$

$$Re_s = \frac{\rho_s v_s L}{\mu_s} \quad (3.47)$$

Where Cp_s , ρ_s and μ_s are the specific heat (J/kg°C), the density (kg/m³) and the dynamic viscosity (Pa.s) respectively of the source side fluid, L is the pipe length (m) and v_s is the fluid velocity (m/s), which is function of its flow rate and the pipe section.

In order to evaluate the overall coefficient of performance of the GSHP system (COP_{sys}), the total electrical input power must take into account the pumping energy (W_{pump}) required for the circulation of the heat exchanging fluids in both the ground loop and the distribution system circuit. The overall coefficient of performance of the GSHP system (COP_{sys}) can be written as in Equation (3.48).

$$COP_{sys} = \frac{Q_{cond}}{W_{comp} + \sum W_{pumps}} \quad (3.48)$$

The energy input in the form of work provided by the pump, W_{pump} is calculated as:

$$W_{pump} = \frac{v \Delta P}{\eta_{pump}} \quad (3.49)$$

Where v is the volumetric flow rate of the pumped fluid (m^3/s), ΔP is the pressure loss through the pump circuit (Pa), which includes pressure loss through the heat exchanger, the ground coil collector, as well as linear and local pressure losses through circuit pipes, fittings and valves accordingly to the corresponding pump circuit, ρ is the fluid density, and η_{pump} is the pump efficiency.

In practice, the performance of a GSHP system is affected by installation conditions and depends on the continual changes in the surroundings environment, i.e. variable source and sink temperature and load. Indeed, heat source and sink temperatures have a direct impact on the pressure (and thus the temperature) at which the evaporation and condensation occur in the refrigeration cycle. Any change in evaporating or condensing temperature affects the density of the refrigerant, which alters the compression ratio between the low-pressure and high-pressure sides, and thus the performance of the compressor.

The type of refrigerant fluid flowing in the cycle also influences the performance of a heat pump. Fluid density, viscosity, thermal conductivity and specific heat are all factors affecting the compression efficiency and heat transfer capacities through the evaporator and condenser. Heat pump manufacturers usually make the decision for the choice of refrigerant based on system cost and application range requirements, considering fluid boiling and condensing temperatures.

3.2.3 Performance prediction

GSHP performance data are usually published by GSHP manufacturers in the form of tables for certain discrete values of the operating fluid temperatures and flow rates conditions. An example of a specification data table for the NDW100 WaterFurnace GSHP in heating mode is given in Table 3.3 [248]. The performance parameters available in manufacturer's tables in the GSHP heating mode are the heat extracted from the ground (HE), the compressor power input (P), the heat pump heating capacity (HC) and the COP (i.e. the dependent variables), as a function of the operating conditions, such as the source and load inlet temperatures (t_{is} and t_{il}) and

the source and load flow rates (v_s and v_l) (i.e. the independent variables). The different variable parameters in the GSHP heating mode are shown in Figure 3.13, where t stands for temperature, v is flow rate, subscripts i , l and s are short for the heat pump inlet conditions, load and source, respectively.

The capacity tables of the GSHP in cooling mode are arranged identically as in Table 3.3, but providing observations of cooling capacity (CC), heat rejected (HR) and cooling energy efficiency (EER) as a function of temperature and flow rate parameters, with the distribution and the ground circuits being respectively the source and the load side.

Manufacturer catalogue data are produced on the basis of the ISO Standard 13256-2 [249] for the testing of water-to-water GSHP units. The prescribed conditions to produce the ISO data include testing at steady flow conditions for a set temperature of source and sink and the measured inputs consist of compressor energy and the circulation pump requirements to overcome the frictional resistance of the evaporator and condenser. Therefore, manufacturer's COP/EER values are generally higher than those obtained in real installations, when taking into account the full energy input for circulation pumps and system fans plus all associated controls. Kim et al. [250] compared the manufacturer's data based on the ISO standard to the actual GSHP performance, and propose a verification method allowing the identification and correction of eventual gaps.

During preliminary studies of building design and GSHP sizing, engineers often have to deal with the selection of GSHP using such data tables. However, when the design conditions do not match those listed in the manufacturer's tables, the correct value of the GSHP performance may be difficult to estimate [251, 252]. This can have an adverse impact on the selection and sizing of the most suitable system device, which then can be crucial in designing the most appropriate GHE. Also, in dynamic simulation applications, such as in the modelling of GSHP systems integrated to buildings, there is a need to determine the GSHP performance under operating conditions other than those listed in the specification table.

Different methods can be used to predict GSHP performance from manufacturer's tables at design operating conditions other than those listed, namely the dimensional linear interpolation (DI) and the multiple regression (MR). This section introduces both methods, which can be employed for the performance prediction of any GSHP system, in heating or cooling mode using the corresponding specification table from the manufacturer catalogue.

3.2 Low-grade geothermal energy

Table 3.3. Heating Capacity Data NDW100 WaterFurnace GSHP [248]

| Source | | t_{il} (°C) | Load 0.95 | | | | | | Load 1.45 | | | | | | Load 1.89 | | | | | |
|------------------|----------------|------------------|------------------|------------|-----------|---------------------|-----|------------------|------------------|------------|-----------|---------------------|-----|------------------|------------------|------------|-----------|---------------------|-----|------------------|
| t_{is} (°C) | v_s (L/s) | | t_{ol} (°C) | HC (kW) | P (kW) | v_l HE (kW) | COP | t_{os} (°C) | t_{ol} (°C) | HC (kW) | P (kW) | v_l HE (kW) | COP | t_{os} (°C) | t_{ol} (°C) | HC (kW) | P (kW) | v_l HE (kW) | COP | t_{os} (°C) |
| -1.1 | 1.45 | 15.6 | 22.3 | 26.8 | 5.01 | 21.7 | 5.3 | -6.6 | 20.1 | 27.7 | 4.85 | 22.9 | 5.7 | -4.9 | 19.2 | 28.5 | 4.71 | 23.8 | 6.1 | -4.1 |
| | | 26.7 | 33.3 | 26.1 | 6.64 | 19.5 | 3.9 | -6.1 | 31.1 | 27.0 | 6.46 | 20.5 | 4.2 | -4.5 | 30.2 | 27.8 | 6.31 | 21.5 | 4.4 | -3.8 |
| | | 37.8 | 44.2 | 25.6 | 8.28 | 17.3 | 3.1 | -5.5 | 42.1 | 26.3 | 8.08 | 18.2 | 3.3 | -4.1 | 41.2 | 27.0 | 7.91 | 19.1 | 3.4 | -3.5 |
| | | 48.9 | 55.2 | 24.9 | 9.91 | 15.0 | 2.5 | -4.9 | 53.1 | 25.6 | 9.7 | 15.9 | 2.6 | -3.7 | 52.2 | 26.2 | 9.51 | 16.7 | 2.8 | -3.2 |
| | 1.89 | 15.6 | 22.4 | 27.0 | 5.1 | 21.9 | 5.3 | -6.6 | 20.2 | 28.2 | 4.94 | 23.3 | 5.7 | -4.9 | 19.3 | 29.3 | 4.8 | 24.5 | 6.1 | -4.2 |
| | | 26.7 | 33.3 | 26.3 | 6.77 | 19.6 | 3.9 | -6.1 | 31.2 | 27.5 | 6.59 | 20.9 | 4.2 | -4.6 | 30.3 | 28.5 | 6.43 | 22.1 | 4.4 | -3.9 |
| | | 37.8 | 44.3 | 25.8 | 8.43 | 17.3 | 3.1 | -5.5 | 42.2 | 26.8 | 8.24 | 18.6 | 3.3 | -4.2 | 41.3 | 27.8 | 8.07 | 19.7 | 3.4 | -3.6 |
| | | 48.9 | 55.2 | 25.1 | 10.1 | 15.0 | 2.5 | -4.9 | 53.2 | 26.1 | 9.89 | 16.3 | 2.6 | -3.8 | 52.3 | 27.0 | 9.7 | 17.3 | 2.8 | -3.3 |
| 10 | 0.95 | 15.6 | 23.1 | 30.0 | 5 | 24.9 | 6 | 3.7 | 20.7 | 30.9 | 4.84 | 26.1 | 6.4 | 5.7 | 19.6 | 31.7 | 4.7 | 27.1 | 6.8 | 6.6 |
| | | 26.7 | 34.1 | 29.3 | 6.62 | 22.7 | 4.4 | 4.3 | 31.7 | 30.2 | 6.44 | 23.8 | 4.7 | 6.1 | 30.6 | 31.0 | 6.29 | 24.7 | 4.9 | 6.9 |
| | | 37.8 | 45.1 | 28.8 | 8.2 | 20.5 | 3.5 | 3.0 | 42.7 | 29.5 | 8 | 21.5 | 3.7 | 6.4 | 41.6 | 30.2 | 7.88 | 22.3 | 3.8 | 7.2 |
| | | 48.9 | 56.0 | 28.1 | 9.87 | 18.3 | 2.9 | 5.4 | 53.7 | 28.8 | 9.65 | 19.2 | 3 | 6.8 | 52.6 | 29.5 | 9.47 | 20.0 | 3.1 | 7.5 |
| | 1.45 | 15.6 | 23.6 | 31.6 | 5.12 | 26.4 | 6.2 | 3.3 | 20.9 | 32.8 | 4.95 | 27.8 | 6.6 | 5.4 | 19.8 | 33.8 | 4.81 | 29.0 | 7 | 6.3 |
| | | 26.7 | 34.5 | 30.9 | 6.78 | 24.2 | 4.6 | 3.9 | 31.9 | 32.1 | 6.59 | 25.5 | 4.9 | 5.8 | 30.8 | 33.1 | 6.43 | 26.7 | 5.1 | 6.6 |
| | | 37.8 | 45.4 | 30.3 | 8.44 | 21.9 | 3.6 | 4.4 | 42.9 | 31.4 | 8.23 | 23.2 | 3.8 | 6.2 | 41.9 | 32.3 | 8.06 | 24.3 | 4 | 6.9 |
| | | 48.9 | 56.4 | 29.7 | 10.1 | 19.6 | 2.9 | 5.1 | 53.9 | 30.7 | 9.87 | 20.8 | 3.1 | 6.6 | 52.9 | 31.6 | 9.68 | 21.9 | 3.3 | 7.2 |
| | 1.89 | 15.6 | 23.9 | 32.9 | 5.23 | 27.7 | 6.3 | 3.0 | 21.2 | 34.4 | 5.06 | 29.4 | 6.8 | 5.2 | 20.1 | 35.7 | 4.9 | 30.8 | 7.3 | 6.1 |
| | | 26.7 | 34.8 | 32.4 | 6.92 | 25.4 | 4.7 | 3.6 | 32.2 | 33.7 | 6.73 | 27.0 | 5 | 5.6 | 31.1 | 35.0 | 6.56 | 28.4 | 5.3 | 6.4 |
| | | 37.8 | 45.8 | 31.7 | 8.61 | 23.1 | 3.7 | 4.2 | 43.2 | 33.1 | 8.4 | 24.6 | 3.9 | 5.9 | 42.1 | 34.2 | 8.21 | 26.0 | 4.2 | 6.7 |
| | | 48.9 | 56.8 | 31.2 | 10.3 | 20.8 | 3 | 4.7 | 54.2 | 32.4 | 10.07 | 22.3 | 3.2 | 6.3 | 53.1 | 33.4 | 9.87 | 23.6 | 3.4 | 7.0 |
| 21.1 | 0.95 | 15.6 | 24.0 | 33.4 | 5.1 | 28.3 | 6.5 | 13.9 | 21.3 | 34.7 | 4.94 | 29.8 | 7 | 16.2 | 20.1 | 35.9 | 4.8 | 31.1 | 7.5 | 17.2 |
| | | 26.7 | 34.9 | 32.8 | 6.74 | 26.0 | 4.9 | 14.6 | 32.3 | 34.0 | 6.57 | 27.5 | 5.2 | 16.6 | 31.1 | 35.1 | 6.41 | 28.7 | 5.5 | 17.5 |
| | | 37.8 | 45.9 | 32.2 | 8.39 | 23.8 | 3.8 | 15.1 | 43.3 | 33.3 | 8.19 | 25.1 | 4.1 | 16.9 | 42.1 | 34.3 | 8.02 | 26.3 | 4.3 | 17.8 |
| | | 48.9 | 56.9 | 31.6 | 10.03 | 21.5 | 3.1 | 15.7 | 54.3 | 32.6 | 9.82 | 22.8 | 3.3 | 17.3 | 53.1 | 33.6 | 9.63 | 23.9 | 3.5 | 18.1 |
| | 1.45 | 15.6 | 24.7 | 36.3 | 5.24 | 31.1 | 6.9 | 13.2 | 21.8 | 37.9 | 5.06 | 32.8 | 7.5 | 15.7 | 20.5 | 39.2 | 4.91 | 34.3 | 8 | 16.8 |
| | | 26.7 | 35.7 | 35.8 | 6.92 | 28.8 | 5.2 | 13.8 | 32.8 | 37.2 | 6.73 | 30.5 | 5.5 | 16.1 | 31.5 | 38.5 | 6.55 | 31.9 | 5.9 | 17.1 |
| | | 37.8 | 46.7 | 35.1 | 8.6 | 26.6 | 4.1 | 14.4 | 43.8 | 36.5 | 8.39 | 28.1 | 4.4 | 16.5 | 42.6 | 37.7 | 8.2 | 29.5 | 4.6 | 17.4 |
| | | 48.9 | 57.6 | 34.5 | 10.28 | 24.3 | 3.4 | 15.0 | 54.8 | 35.8 | 10.05 | 25.8 | 3.6 | 16.9 | 53.6 | 36.9 | 9.85 | 27.1 | 3.7 | 17.7 |
| | 1.89 | 15.6 | 25.4 | 38.9 | 5.37 | 33.6 | 7.3 | 12.6 | 22.3 | 40.6 | 5.17 | 35.5 | 7.9 | 15.3 | 20.9 | 42.1 | 5 | 37.1 | 8.4 | 16.4 |
| | | 26.7 | 36.3 | 38.3 | 7.08 | 31.3 | 5.4 | 13.2 | 33.3 | 39.9 | 6.86 | 33.1 | 5.8 | 15.7 | 31.9 | 41.4 | 6.68 | 34.7 | 6.2 | 16.7 |
| | | 37.8 | 47.3 | 37.7 | 8.79 | 29.0 | 4.3 | 13.8 | 44.3 | 39.3 | 8.56 | 30.7 | 4.6 | 16.1 | 42.9 | 40.6 | 8.36 | 32.2 | 4.9 | 17.1 |
| | | 48.9 | 58.3 | 37.1 | 10.5 | 26.6 | 3.5 | 14.4 | 55.2 | 38.6 | 10.25 | 28.3 | 3.8 | 16.4 | 53.9 | 39.8 | 10.03 | 29.8 | 4 | 17.3 |
| 32.2 | 0.95 | 15.6 | 24.8 | 36.8 | 5.2 | 31.6 | 7.1 | 24.2 | 21.9 | 38.5 | 5.04 | 33.5 | 7.6 | 26.7 | 20.6 | 40.0 | 4.9 | 35.1 | 8.2 | 27.8 |
| | | 26.7 | 35.8 | 36.2 | 6.87 | 29.3 | 5.3 | 24.8 | 32.9 | 37.8 | 6.69 | 31.1 | 5.7 | 27.1 | 31.6 | 39.2 | 6.53 | 32.7 | 6 | 28.1 |
| | 1.45 | 15.6 | 25.9 | 41.1 | 5.36 | 35.8 | 7.7 | 23.2 | 22.6 | 43.0 | 5.17 | 37.8 | 8.3 | 26.0 | 21.2 | 44.5 | 5.01 | 39.5 | 8.9 | 27.2 |
| | | 26.7 | 36.9 | 40.5 | 7.06 | 33.5 | 5.7 | 23.8 | 33.6 | 42.3 | 6.86 | 35.4 | 6.2 | 26.4 | 32.2 | 43.8 | 6.68 | 37.1 | 6.6 | 27.6 |
| | 1.89 | 15.6 | 26.9 | 44.9 | 5.5 | 39.4 | 8.2 | 22.3 | 23.3 | 46.9 | 5.29 | 41.6 | 8.9 | 25.4 | 21.7 | 48.5 | 5.1 | 43.4 | 9.5 | 26.7 |
| | | 26.7 | 37.9 | 44.3 | 7.23 | 37.1 | 6.1 | 22.8 | 34.3 | 46.2 | 7 | 39.2 | 6.6 | 25.8 | 32.7 | 47.8 | 6.8 | 41.0 | 7 | 27.1 |

3.2.3.1 Dimensional linear interpolation

During the design phase of GSHP, engineers often have to select from a number of performance data points, as obtained from the GSHP manufacturer, and construct a “curve fitting” function which closely fits those data points. The dimensional linear interpolation is a specific case of curve fitting, in which the function must go exactly through the data points.

In GSHP manufacturer catalogues, the dependent variables (i.e. *HC*, *HE* or *COP* in the heating mode) are generally a function of four key independent variables (i.e. the operating conditions, t_{is} , t_{il} , v_s and v_l). From such a five dimensions table, the method requires to go through the process of five successive triple interpolations, in order to find the exact value of a dependent variable at a particular point of operating conditions.

This section introduces the multiple dimensional interpolations considering the heat capacity (*HC*) variable as an example. Nevertheless, the methodology can also be applied to the other dependent variables (*P*, *HE* or *COP*). Table 3.4 presents the 114 observations of *HC* from the GSHP manufacturer’s data table as a function of the four independent variables.

Table 3.4. GSHP heating capacity (kW) data from manufacturer’s performance table

| | | v_l | 0.95 L/s | | | | 1.45 L/s | | | | 1.89 L/s | | | |
|-------------|------|---------------------------|----------|------|------|------|----------|------|------|------|----------|------|------|------|
| | | $t_{is} \setminus t_{il}$ | 15.6 | 26.7 | 37.8 | 48.9 | 15.6 | 26.7 | 37.8 | 48.9 | 15.6 | 26.7 | 37.8 | 48.9 |
| 0.95 L/s | 10.0 | 30.0 | 29.3 | 28.8 | 28.1 | 30.9 | 30.2 | 29.5 | 28.8 | 31.7 | 31.0 | 30.2 | 29.5 | |
| | 21.1 | 33.4 | 32.8 | 32.2 | 31.6 | 34.7 | 34.0 | 33.3 | 32.6 | 35.9 | 35.1 | 34.3 | 33.6 | |
| | 32.2 | 36.8 | 36.2 | - | - | 38.5 | 37.8 | - | - | 40.0 | 39.2 | - | - | |
| 1.45 L/s | -1.1 | 26.8 | 26.1 | 25.6 | 24.9 | 27.7 | 27.0 | 26.3 | 25.6 | 28.5 | 27.8 | 27.0 | 26.2 | |
| | 10.0 | 31.6 | 30.9 | 30.3 | 29.7 | 32.8 | 32.1 | 31.4 | 30.7 | 33.8 | 33.1 | 32.3 | 31.6 | |
| | 21.1 | 36.3 | 35.8 | 35.1 | 34.5 | 37.9 | 37.2 | 36.5 | 35.8 | 39.2 | 38.5 | 37.7 | 36.9 | |
| 1.89 L/s | 32.2 | 41.1 | 40.5 | - | - | 43.0 | 42.3 | - | - | 44.5 | 43.8 | - | - | |
| | -1.1 | 27.0 | 26.3 | 25.8 | 25.1 | 28.2 | 27.5 | 26.8 | 26.1 | 29.3 | 28.5 | 27.8 | 27.0 | |
| | 10.0 | 32.9 | 32.4 | 31.7 | 31.2 | 34.4 | 33.7 | 33.1 | 32.4 | 35.7 | 35.0 | 34.2 | 33.4 | |
| 1.89 L/s | 21.1 | 38.9 | 38.3 | 37.7 | 37.1 | 40.6 | 39.9 | 39.3 | 38.6 | 42.1 | 41.4 | 40.6 | 39.8 | |
| | 32.2 | 44.9 | 44.3 | - | - | 46.9 | 46.2 | - | - | 48.5 | 47.8 | - | - | |

3.2 Low-grade geothermal energy

The first triple interpolation occurs within a set of HC as a function of the two first independent variables. For example, one set of HC is represented in the red square in Table 3.4, where the two independent variables are inlet load and source temperatures (t_{il} and t_{is}). However, a triple interpolation could be done in any of the nine $t_{il} - t_{is}$ tables of Table 3.4, depending on the chosen v_s and v_l .

For any chosen t_{is} and t_{il} , the value of HC can be determined by three successive interpolations, as shown in Figure 3.19, where $t_{is,U}$, $t_{is,Lo}$, $t_{il,Le}$ and $t_{il,R}$ are the values of inlet source and load temperatures situated respectively at the proximity upper, lower, left and right of the chosen t_{is} and t_{il} . Similarly, HC_{ULe} , HC_{UR} , HC_{LoLe} and HC_{LoR} are the heating capacity data situated respectively at the proximity upper left, upper right, lower left and lower right of the HC value that is sought for the chosen t_{is} and t_{il} . It is important to note that $t_{is,U} < t_{is} < t_{is,Lo}$ and $t_{il,Le} < t_{il} < t_{il,R}$. The tabular interpolation method enables to find the response solution assuming linearity between the set of given manufacturer data.

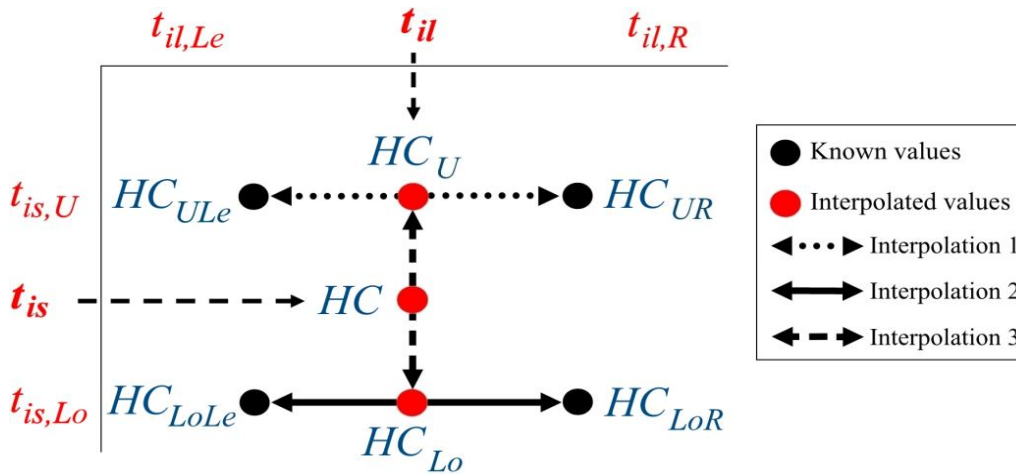


Figure 3.19. Three dimensional interpolations

The first interpolation, also described as first horizontal interpolation in Figure 3.19, enables to find HC_U between HC_{ULe} and HC_{UR} , at the table temperature $t_{is,U}$ and the specific chosen t_{il} , following Equation (3.50):

$$\frac{HC_U - HC_{ULe}}{HC_{UR} - HC_{ULe}} = \frac{t_{il} - t_{il,Le}}{t_{il,R} - t_{il,Le}} \quad (3.50)$$

The second interpolation described as second horizontal interpolation in Figure 3.19, which enables to find HC_{Lo} between HC_{LoLe} and HC_{LoR} , at the table temperature $t_{is,Lo}$ and the specific chosen t_{il} , can be transferred into Equation (3.51):

$$\frac{HC_{Lo} - HC_{LoLe}}{HC_{LoR} - HC_{LoLe}} = \frac{t_{il} - t_{il,Le}}{t_{il,R} - t_{il,Le}} \quad (3.51)$$

The third interpolation, described as vertical interpolation enables to find HC between HC_U and HC_{Lo} , found in the two previous equations at the specific chosen temperatures t_{is} and t_{il} , following Equation (3.52):

$$\frac{HC - HC_U}{HC_{Lo} - HC_U} = \frac{t_{is} - t_{is,U}}{t_{is,Lo} - t_{is,U}} \quad (3.52)$$

So, the final three dimensional interpolations can be written as one unique Equation (3.53).

$$HC = HC_{ULe} + (HC_{UR} - HC_{ULe}) \times \frac{t_{il} - t_{il,Le}}{t_{il,R} - t_{il,Le}} + \left(\begin{array}{l} \left[HC_{LoLe} + (HC_{LoR} - HC_{LoLe}) \times \frac{t_{il} - t_{il,Le}}{t_{il,R} - t_{il,Le}} \right] \\ - \left[HC_{ULe} + (HC_{UR} - HC_{ULe}) \times \frac{t_{il} - t_{il,Le}}{t_{il,R} - t_{il,Le}} \right] \end{array} \right) \times \frac{t_{is} - t_{is,U}}{t_{is,Lo} - t_{is,U}} \quad (3.53)$$

The five dimensional interpolations describes a number of interpolations to calculate the correct value between 16 points located in four different tables, as shown in the blue square of Table 3.4. The first triple interpolation, as described by Equation (3.53) must be repeated four times between the four $t_{il} - t_{is}$ data tables, and a final triple interpolation is required between the four interpolated values in order to find the solution value, which corresponds to the specific four independent variable data t_{is} , t_{il} , v_s and v_l .

3.2.3.2 Multiple regression modelling

The multiple regression method consists in developing an inverse model based on the specification data present in the manufacturer's capacity table. MR models are applicable over the entire solution space and representative of the global GSHP behaviour. Essentially, the whole set of observations available in the data table, or a just a sample of it may be used to find relationships between the response variables (*HC*, *HE* and *COP*) versus the four key predictor parameters (i.e. operating conditions): the source and load flow rates (v_s and v_l), the source and load inlet temperatures (t_{il} and t_{ls}). A linear multiple regression model may be represented by the following Equation (3.54) [253, 254, 255, 256]:

$$y_j = \beta_0 + \beta_1 x_{j1} + \beta_2 x_{j2} + \beta_n x_{jn} + \varepsilon_j \quad (3.54)$$

Where y_j is the j response to be predicted using the (predictor) variables, x_{j1} to x_{jn} given as input. n is the number of predictor variables and β the regression coefficients. ε is the j residual or error between the predicted response and the observation.

The MR models assume that a straight-line relationship exists between each independent variable (x_{j1} , x_{j2} , ... and x_{jn}), and the dependent variable (y). The dependent y -value is a function of the independent x -values. The method relies on the least squares principle to determine the regression coefficients. The least square principle determines the coefficients that produce the minimum sum of squared residual values, i.e. the best fitted regression line to the manufacturer's data. The accuracy of the regression line depends on the degree of scatter in the data. The more linear the data are, the more accurate the model will be. When there is only one independent x -variable, the calculations for β and ε are based on the following formulas:

$$\beta = \frac{\sum(x-\bar{x})(y-\bar{y})}{\sum(x-\bar{x})^2} \quad (3.55)$$

$$\varepsilon = \bar{y} - \beta\bar{x} \quad (3.56)$$

Where \bar{x} and \bar{y} are sample means, for example \bar{x} is the average of *known* x 's and \bar{y} the average of *known* y 's values. The formula can be adjusted to calculate other types of regression, but in some cases it requires the adjustment of the output values and other statistics.

The global behaviour of the GSHP can be represented in one multiple regression equation linking the various different variables. When building an inverse simulation model the regression model is more convenient since it is more transportable requiring fewer model parameters to retain. The MR models are more likely to be built in order to be integrated into dynamic simulation tools. However, the method consisting in developing such an inverse model can be time consuming for field engineers. If instead, an engineer wishes to predict the GSHP performance at a single operating point, the multiple dimensional interpolation model, being a straight forward and local model, may be more appropriate, easier and likely more accurate.

The most suitable method can be used depending on the situation during preliminary studies. Both methods can help in the selection and sizing of the most appropriate GSHP evaluating with precision its performance, and thus increase the potential of GSHP implementation in buildings.

3.3 Energy efficiency in buildings

Buildings represent the largest energy-consuming sector in the economy with approximately 40% of all energy and half of global electricity consumed there [73, 86, 87, 88, 89]. As a result, the building sector contributes to more than one-third of the global GHG emissions [257]. Moreover, with increasing urbanisation, the number and size of buildings will increase, resulting in an increased demand for electricity and other forms of energy commonly used in buildings. Thus, it is essential to reduce energy consumption in buildings in order to meet energy and environmental challenges. Opportunities for a more efficient use of the energy in buildings are enormous, and in recent years, energy efficiency in buildings and reducing environmental impacts from fossil fuel usage have become increasingly important in the construction industry [258]. While sustainable energy technologies are further developed, energy efficiency in buildings is seen as the most economically viable short-term solution to rapidly reduce residential energy usage and mitigate the repercussions of carbon emissions [259, 260]. Additionally, energy efficiency in homes is associated with improved health for individuals, further demonstrating its benefit and the necessity of its implementation [261].

Lighting and other home appliances are important energy consumers in buildings, and in each case there are opportunities for improving their performance (i.e. low-energy light bulbs, sensors that adjust light levels to occupancy and daylight, class-A electrical appliances, etc). For example, Jadraque Gago et al. [262] developed a calculation model which can be used to estimate energy use from lightings, based on daylight, building type and household profile. Such a model can be useful to predict scenarios of energy consumption from different types of lighting and investigate on the effectiveness of low-energy light bulbs to enhance energy efficiency. However, the investigation of the efficiency of the different energy system components is beyond the remit of this work, which focuses on the major area of energy consumption in buildings, i.e. the space heating, ventilation, and air-conditioning (HVAC).

3.3.1 Energy modelling

Since the energy consumption characteristics of buildings are complex and inter-related, comprehensive simulation models are needed to assess the economic impacts of adopting energy efficiency measures and renewable energy technologies suitable for building applications. The

concept is to build a physical model that appropriately relates the energy balance in buildings. The accurate modeling of a building can serve as an important tool for investigating and understanding the energy distribution throughout a building. Building energy simulation (BES) models may be used to predict energy consumption and compare the cost effectiveness of energy conservation measures (i.e. changes that can be made to a building to save energy), either in the design phase of a new building or in retrofitting existing buildings [263, 264]. Generally, BES models can be used in the area of: (1) energy consumption prediction, (2) energy savings calculation, and (3) baseline performance establishment, for instance in building regulation and certification standards [265].

BES models can be divided into two categories, the law-driven and the data-driven models [266]. Law-driven models of building systems link the known physical building, system, and environmental input variables in order to predict the building performance outputs. This approach presumes detailed knowledge not only of the various natural phenomena affecting system behaviour but also of the magnitude of various interactions (i.e. the algorithmic accuracy to the relevant physic based equations) [266]. The main advantage of this approach is that the system need not be physically built to predict its behaviour. This approach is ideal in the preliminary design and analysis stage and has consequently gained widespread acceptance by the design and professional community. Major simulation software tools, such as TRYNYSYS [267], ESP-r [268] and EnergyPlus [269], are based on law-driven simulation models. Law-driven BES modelling begins with a physical description of the building system and its components. For example, building geometry, geographical location, physical characteristics (e.g., wall material and thickness), type of heating and cooling equipments and operating schedules, etc., are specified. The peak and average energy use of such a building can then be predicted or simulated by the law-driven model using the relevant physic based equations. Examples of forward model approaches are degree-day methods [270, 271, 272], thermal networks [273, 274, 275], transfer functions [276, 277], response factors [278, 279, 280], Fourier series [281, 282, 283] and finite-difference methods [284, 285, 286].

In the case of data-driven models, input and output data are known and measured from long-term historical data training, and the objective is to determine a mathematical (e.g., statistical) description of the system and to estimate system parameters [287]. In contrast to the law-driven approach, the data-driven models are relevant when the building has already been built and actual

performance data are available for model development and/or identification. These models have high requirements for the quality and quantity of data, but lack physical meaning of the influential input parameters to measured outputs (e.g., with minus values) [288]. Examples of data-driven models include statistical linear regressions [289, 290, 291, 292], Auto Regressive Moving Average (ARMA) [293, 294, 295], Kalman filter [296, 297, 298], Monte Carlo [299, 300], artificial neural networks [301, 302, 303], and support vector machines [304, 305, 306].

The following section 3.3.2 introduces the physic based equations, which as a whole refers to a law-driven model for space heating and cooling energy use calculation. Such a model is based on the quasi steady-state calculation method proposed by the ISO 13790 standard [307], which takes into account the steady-state assumption that the building is heated or cooled for the thermal comfort of occupants (i.e. constant with respect to time), but also the dynamic effect of the building thermal inertia with utilization factors. Although this is a simplified method for estimating energy usage in buildings, various studies demonstrated its reliability with predictions in acceptable agreements as compared to results from fully dynamic simulation programs. For example, Josiako and Kumitski [308] studied the performance of the ISO 13790 model in predicting the annual energy demand in a residential building in Finland. They found that the monthly method ISO 13790 is reasonably applicable for residential buildings, as results were in acceptable agreement with the energy use calculated with a dynamic thermal simulation program (IDA- Indoor Climate and Energy). In Kalema et al. [309], the ISO 13790 model was validated with the EnergyPlus dynamic simulation software, with agreement below 9% deviation. Also, the standard's methodology has shown to give accurate results in calculating the residential annual energy in the context of energy certification [310, 311]. The ISO 13790 methodology is now widely used by practitioners, especially since it has been successfully included in several software packages approved by national certification bodies in Europe [312, 313], and thus, it can be recommended as a tool for building energy use assessment.

Unlike steady-state models, dynamic models are built on the assumption that the system behaviour is changing in time. In general, steady-state models are used for average estimations (yearly, monthly or daily), while dynamic models, which traditionally require solving a set of differential equations, are usually used for real time state estimation, as well as for hourly or sub-hourly estimation, and particularly in cases where the building's thermal mass is significant enough to delay heat gains or losses [314].

3.3.2 Fundamentals for energy use calculation

A building must be considered as an energy system designed to provide occupants with a comfortable environment. To maintain the required inside conditions, the building system must overcome the energy loads that are imposed by the climatic conditions outside the building and also, the energy loads that are imposed by factors inside the building itself.

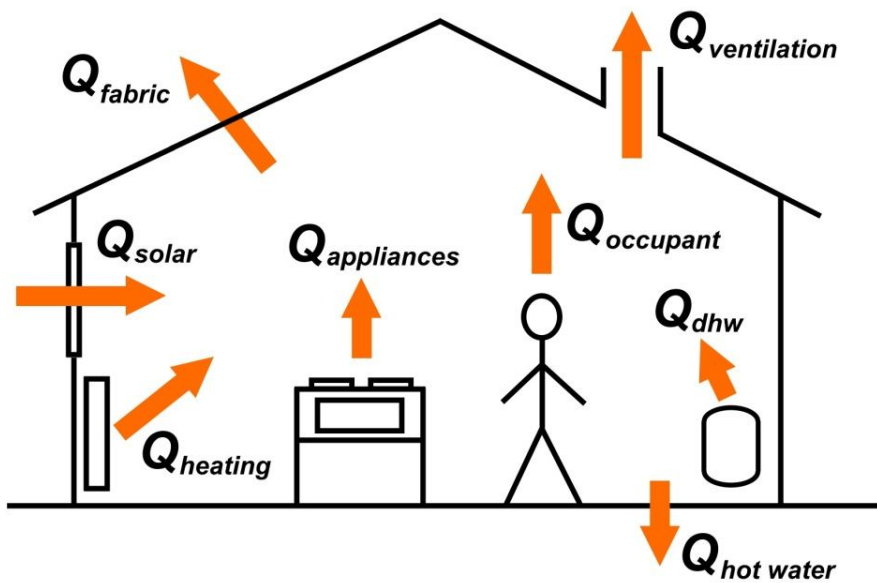


Figure 3.20. Energy balance of a building during winter [315]

Figure 3.20 shows these energy loads, where Q represents the rate of heat transfer or flow in Watts. The building envelope comprises walls, floors and roof, as well as windows and doors. It is the building envelope that separates the varying conditions outside the building from the conditions inside the building. The building systems must control the space temperature, relative humidity, air movement and air quality within acceptable limits. The building energy balance during the heating and cooling seasons can be written as in Equation (3.57) and (3.58) respectively, according to the ISO 13790 calculation method [307].

$$Q_h = (Q_f + Q_v) - \eta_{g,h} Q_{int} \quad (3.57)$$

$$Q_c = Q_{int} - \eta_{l,c} (Q_f + Q_v) \quad (3.58)$$

Where in Equation (3.57) and (3.58), Q_h and Q_c are the rate of heating and cooling energy required during winter and summer periods respectively; Q_{int} is the total internal heat gains; $\eta_{g,h}$ is the gain utilization factor for heating; $\eta_{l,c}$ is the loss utilization factor for cooling. The utilization factors correcting for the internal heat gains in the heating mode and the cooling needs in the cooling mode depend on the building thermal inertia. In this section, the steady-state calculation of the different types of heat transfer occurring buildings is described.

3.3.2.1 Heat transfer through fabric

Fabric heat transfer (Q_f) occurs through any building envelope components exposed to the outside air or to unheated areas such as the attic. Heat transfer is defined in physics as the transfer of thermal energy across a well-defined boundary around a thermodynamic system. It is a characteristic of a process and is never contained in matter. According to the Second Law of Thermodynamics, heat transfer is only possible in the direction from a higher temperature to a lower one. It becomes zero if temperatures are equal. The heat transfer through the building envelope is therefore proportional to the difference of inside and outside air temperatures (T_i and T_o), and can be calculated using Equation (3.59). It is based on the assumption that the inside air has a uniform temperature.

$$Q_f = \sum(UA) (T_i - T_o) \quad (3.59)$$

Where U is the heat transfer coefficient of the building element ($\text{W/m}^2\text{K}$); and A is the surface area of the building element (m^2).

Fundamental methods of heat transfer calculation in buildings include mainly conduction and convection, as shown in Figure 3.21. Conduction is the heat flow through a solid material from the warmer to the cooler side of the envelope. Convection is the heat transfer caused by the motion of heated air from a warmer to a cooler surface. Radiation is the transfer of heat by electromagnetic waves from a warmer to a cooler surface. It is transferred directly and is not affected by the temperature of the surrounding air. Heat transfer by radiation depends on the shape, temperature and emissivity of both the radiating surface and the receiving surface, or the environment to which it radiates. They are normally small and complex to estimate for buildings, so they are usually neglected in heat transfer calculations in buildings.

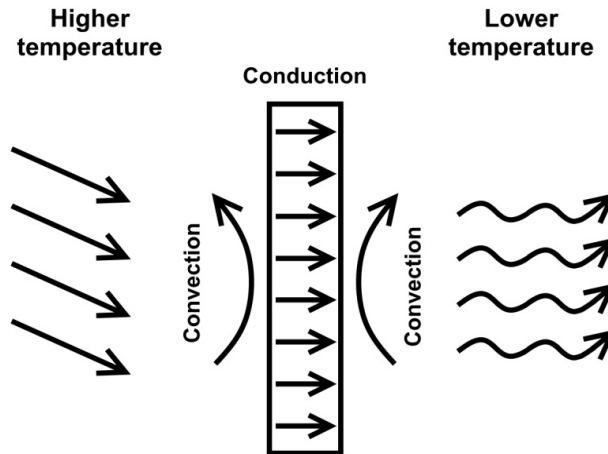


Figure 3.21. Conduction and convection heat transfer

The heat transfer coefficient U of a building material can be found using the material's R -value. The R -value is a measure of material's resistance to heat flow. For an element composed by different materials layers with different R -values measured in ($\text{m}^2\text{K}/\text{W}$), the overall heat transfer coefficient U of that element is the fraction of 1 over the sum of R -values, as shown in Equation (3.60).

$$U = 1 / \sum R \quad (3.60)$$

The heat flow resistance R of a material is determined by its thickness, t (m) and thermal conductivity, λ (W/mK), and is given by:

$$R = t / \lambda \quad (3.61)$$

Considering the heat transfer by convection, the outside and inside convective heat flow resistances are characterized by external and internal surface resistances, R_{se} and R_{si} , which must be taken into account in Equation (3.60). The external surface resistance R_{se} is function of the wind and depends on the building's exposure. The internal surface resistance R_{si} is function of the interior surface emissivity, radiative and convective heat transfer coefficients. For a simplification of the thermal processes that occur at surfaces, standardised values of R_{se} and R_{si} depending on the heat flow directions are given in the ISO 6946 standard [316]: the standard R_{se} value is 0.04 ($\text{m}^2\text{K}/\text{W}$) for all heat flow directions; the standard R_{si} is 0.13 ($\text{m}^2\text{K}/\text{W}$) for

horizontal heat flow through walls, $0.10 \text{ (m}^2\text{K/W)}$ for upward heat flow through ceilings, roofs or floors, and $0.17 \text{ (m}^2\text{K/W)}$ for downward heat flow through ceilings or floors.

In the case of a floor suspended over an under floor space, a ceiling exposed to the attic, or a wall exposed to a room situated outside the conditioned space, a correction factor $b = 0.9$ can be applied to Equation (3.59). Indeed, such unheated areas generally present a slightly warmer temperature in winter and cooler temperature in summer than the outside air. This method is widely used by professionals to evaluate the heat transfer through unheated areas.

The calculation of the heat transfer through the directly in contact with the ground is more complicated than that through above-ground components. The heat flow is three-dimensional and the thermal performance is affected by various factors including the size and shape of the floor, the thickness of the surrounding wall, the presence of all-over or edge insulation, and the ground temperature and thermal conductivity. According to the ISO 13370 standard [317], the heat transfer through the ground floor (Figure 3.22) can be calculated as follows.

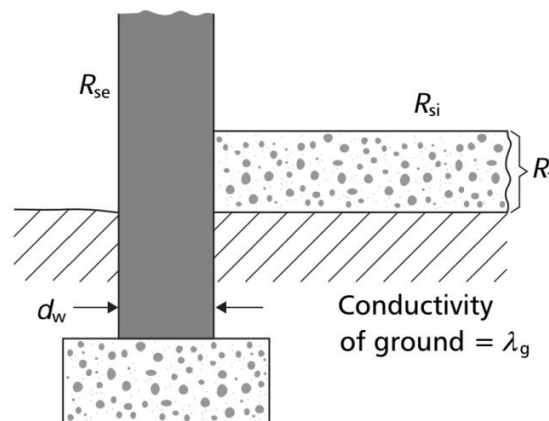


Figure 3.22. Characteristic dimension of solid ground floor [318]

The U -value of a solid floor in contact with the ground depends on the characteristic dimension of the floor (B'), the total equivalent thickness (d_{ef}), and the factors that restrict the heat flow (i.e. wall thickness, surface resistances, thermal insulation). The characteristic dimension B' is defined as follows, where A_f is the area of floor in contact with the ground (m^2), and p_f is the floor perimeter (m).

$$B' = A_f / 0.5 p_f \quad (3.62)$$

The total equivalent thickness (d_{ef}) is given by Equation (3.63), where d_w is the thickness of the wall surrounding the ground floor (m), λ_g is the ground thermal conductivity (W/mK), and R_f the floor thermal resistance (m^2K/W).

:

$$d_{ef} = d_w + \lambda_g (R_{si} + R_f + R_{se}) \quad (3.63)$$

The floor thermal resistance R_f includes the thermal resistance of any insulation layers above, below or within the floor slab, and that of any floor covering. Hardcore below the slab is assumed to have the same thermal conductivity as the ground and its thermal resistance is therefore not included. The thermal transmittance of the floor in contact with the ground is given by Equation (3.64) for $d_{ef} < B'$, and in Equation (3.65) for $d_{ef} \geq B'$.

$$U_f = \frac{2 \lambda_g}{\pi B' + d_{ef}} \log \left[\left(\frac{\pi B'}{d_{ef}} \right) + 1 \right] \quad (3.64)$$

$$U_f = \frac{\lambda_g}{(0.457 B' + d_{ef})} \quad (3.65)$$

In the case of ground floor insulated by means of edge insulation placed either horizontally or vertically around the perimeter of the floor (Figure 3.23), the following equations are valid taken into account that no significant thermal bridging is introduced. The U -value of an edge-insulated floor can be calculated by:

$$U_{fi} = U_f + 2 \psi_{fi} / B' \quad (3.66)$$

Where U_{fi} is the thermal transmittance of the edge-insulated floor (Wm^2/K), U_f is the thermal transmittance of the floor without insulation (Wm^2/K), ψ_{fi} is the factor related to the floor edge insulation (W/mK), which depends on the edge insulation thermal resistance, on whether the edge insulation is placed horizontally or vertically, and on its width W_i (if horizontal) or depth D_i (if vertical).

The calculation of ψ_{fi} depends upon the additional equivalent thickness resulting from the edge insulation, d_{ei}' (m), determined as follows.

$$d_{ei}' = R_i' \lambda_g \quad (3.67)$$

Where R_i' is the additional thermal resistance ($\text{m}^2\text{K}/\text{W}$) due to edge insulation. R_i' represents the difference between the thermal resistance of the edge insulation and that of the soil it replaces, and can be calculated as in Equation (3.68), where R_{fi} is the thermal resistance of the floor edge insulation ($\text{m}^2\text{K}/\text{W}$), and d_{fi} the thickness of the edge insulation (m).

$$R_i' = R_{fi} - (d_{fi} / \lambda_g) \quad (3.68)$$

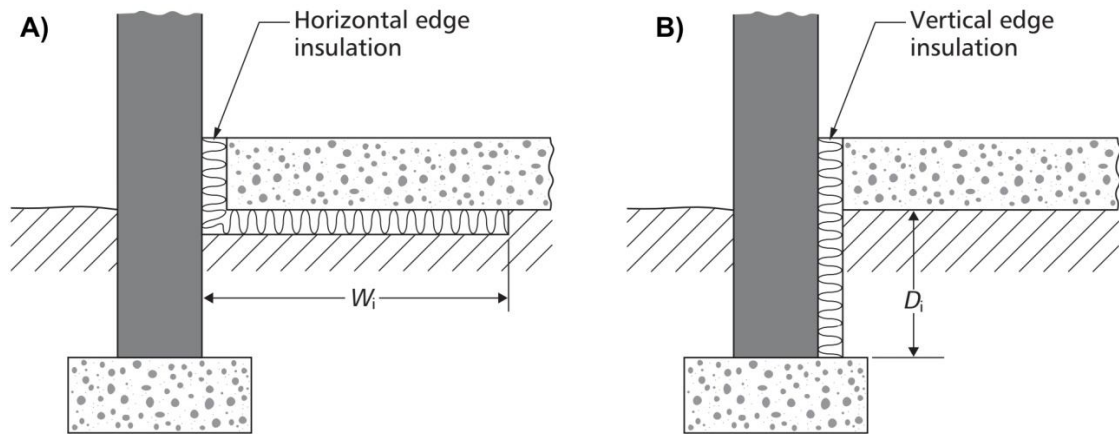


Figure 3.23. Solid ground floor with horizontal (A) and vertical (B) edge insulation [318]

The edge insulation factor ψ_{fi} can be calculated using the following Equation (3.69) or (3.70), in the case of edge insulation placed respectively horizontally (A) or vertically (B) around the perimeter of the floor.

$$\Psi_{fi} = - \frac{\lambda_g}{\pi} \left[\ln \left(\frac{W_i}{d_{ef}} + 1 \right) - \ln \left(\frac{W_i}{d_{ef} + d_{ei}'} + 1 \right) \right] \quad (3.69)$$

$$\Psi_{fi} = - \frac{\lambda_g}{\pi} \left[\ln \left(\frac{2 D_i}{d_{ef}} + 1 \right) - \ln \left(\frac{2 D_i}{d_{ef} + d_{ei}'} + 1 \right) \right] \quad (3.70)$$

An accurate estimation of the total heat transfer through fabric envelope needs to take account of the heat transfer through thermal bridges. Thermal bridging occurs where cavities or insulation are crossed by components or materials with high thermal conductivity. They are frequent around windows, doors and other wall openings through lintels, jambs and sills and can be particularly significant when a structural feature, such as a floor extending to a balcony, penetrates a wall. In buildings with relatively poor standards of thermal insulation, the transmission heat transfer is dominated by the heat transfer through the plain areas of the fabric.

Thermal bridging at junctions is usually a relatively small proportion of the total. For better insulated buildings, however, the effect of thermal bridging can be significant proportionally to the total, although it can be limited by good design of details. Linear and punctual thermal transmittance values are generally calculated by numerical analysis, or given by component manufacturers. A typical standard is that the additional effect of thermal bridging should not exceed 10 to 15% of the total transmission heat loss [319].

3.3.2.2 Heat transfer through ventilation

Ventilation in buildings is the process by which fresh air is provided to occupants and by which concentrations of potentially harmful pollutants are diluted and removed from a space. Ventilation is critical for minimizing the concentration of carbon dioxide, which is emitted as part of the metabolic process. From an energy perspective, losses resulting from ventilation and general air exchange can account for more than half of the primary energy used in a building. These losses comprise space heating and cooling losses.

Ventilation can be provided by natural or mechanical methods. Natural ventilation and air infiltration is driven by the climatic forces of wind and temperature, and thus the rate of ventilation is highly variable. Mechanical ventilation is applied by means of driving fans and a network of ducts. The rate of airflow through buildings depends on the areas and resistances of the various gaps and apertures (both intentionally provided and fortuitous) and the pressure difference between one end of the flow path and the other. This pressure difference may be due to the wind effect, the differences in density of the air due to the indoor–outdoor temperature differences (commonly referred to as “stack effect”), the pressure differences created by mechanical ventilation fans, or a combination of the three mechanisms [107].

The energy required to heat or cool the entering fresh air depends on the rate of the airflow, the specific heat of the fresh air, and the temperature through which it needs to be raised or cooled. The rate of air movement is typically measured in air-changes per hour (n). An air-change is when the full volume of air inside a house is replaced with a new volume of air. The steady-state heat transfer through ventilation can be determined from Equation (3.71), where ρ is the fresh air density (kg/m^3), V is the building volume (m^3), Cp_a is the fresh air specific heat (J/kg K).

$$Q_v = \rho V Cp_a n (T_i - T_o) \quad (3.71)$$

3.3.2.3 Internal heat gains

Internal heat gain, Q_{int} in Equation (3.57) and (3.58), is the sensible and latent heat emitted within the internal building space from any source which results in an increase in the temperature and humidity within the space. It includes the following sources:

- Solar radiation through windows;
- Bodies (human and animal);
- Lighting;
- Computers and other domestic equipment;
- Cooking appliances.

Internal heat gains differ depending on the building type and usage. The rate of internal heat gain can sometimes be estimated using benchmark values for the building type and intended use. Such benchmark values are generally based on surveys of measured internal heat gains from a number of buildings of particular types and usage, or empirical values considered good practice in the industry [320]. Though, when sufficient data is known about the use of the building and its equipments, internal heat gains can be modelled from mathematical relationships. The total internal heat gain Q_{int} is defined as the sum of the solar heat gains, Q_s , the sensible and latent heat rejection from occupants, Q_o , the heat gains from lightings and domestic appliances, Q_{app} , and 20% of the energy used for domestic hot water production, Q_{dhw} assumed to be lost by the hot water tank to the indoor environment [321]. Thus, the total internal heat gain Q_{dhw} , is written as:

$$Q_{int} = Q_s + Q_o + Q_{app} + 0.2 Q_{dhw} \quad (3.72)$$

According to Olofsson [321], 20% of the energy used for domestic hot water preparation is lost from the hot water piping and storage tank to its surroundings (i.e. the building indoor environment). The average consumption of hot water in homes can be considered to be in the range of 45 litres/person/day [322]. This figure includes the consumption of hot water for baths and showers, hand and face washing, and the cleaning of dishes at the sink. The heat required for domestic hot water (Q_{DHW}) can be calculated as follows, where m is the hot water consumption (m^3), ρ the water density (kg/m^3), Cp_w the water specific heat ($J/kg\ K$), T_{DHW} the temperature of the hot water ($^{\circ}C$), η_{wh} the overall efficiency of the water heater system.

$$Q_{DHW} = m \rho Cp_w (T_{DHW} - T_i) / \eta_{wh} \quad (3.73)$$

The contribution of solar heat gains Q_s through windows depends on the amount of direct and diffuse solar radiation incident upon each window area. The quantity of solar energy transmitted to the building indoor must take into account the solar radiation availability on inclined surface at a particular location, the surface area of the windows collecting the radiation and the energy transmittance (τ_w) of the glazing. For this purpose, the incident solar radiation can be estimated using the method introduced in the previous section 3.1.1, which is valid for surfaces of any orientation and inclination. The solar gain Q_s through the building windows can be determined as in Equation (3.74), where τ_w is the window transmittance, H_t is the solar radiation on a tilted surface (kW/m^2), A_w is the area of the window collecting the radiation (m^2), F is the window shading factor, and subscript n stands for the window number.

$$Q_s = \sum_n [\tau_{w,n} H_{t,n} A_{w,n} F_n] \quad (3.74)$$

All animal bodies including humans lose heat to their surroundings in the form of latent and sensible heat. The latent heat gain from a human body results in an instantaneous addition to the moisture content of the air, whereas the part of the sensible heat gain is radiant and convective, and depends on type of clothing, activity, mean radiant temperature and air velocity [320]. Lighting is also a non negligible source of internal heat, as all the electrical energy used by a lamp is ultimately released as heat by means of conduction, convection or radiation. The rate of

heat emission from a luminaire depends on its electrical input power, as well as its optical properties which can affect the radiant/convective proportion emitted by the lamp. As for heat gains from cooking and domestic appliances, estimates are subjective due to the variety of appliances, applications, time in use and types of installation. The energy input rating supplied by manufacturers should be used for such estimation, taking into account appropriate usage factors and efficiencies [320].

Overall, the contributions of occupants, lighting, and appliance gains (i.e. Q_o and Q_{app}) to peak sensible and latent loads can be estimated as in Equation (3.75) and (3.76) respectively where q_s is the sensible cooling load from occupants, lighting, and appliance internal gains (W), q_l is the latent cooling load from the same internal gains (W), A_{cf} is the floor area of the building conditioned space (m²), N_{oc} is the number of occupants [314, 323].

$$q_s = 136 + 2.2 A_{cf} + 22 N_{oc} \quad (3.75)$$

$$q_l = 20 + 0.22 A_{cf} + 12 N_{oc} \quad (3.76)$$

3.3.2.4 Thermal inertia

The dynamic effect of the building thermal inertia is taken into account in load calculations considering utilization factors correcting for the internal heat gains in the heating mode and the cooling needs in the cooling mode, according to the ISO 13790 calculation method [307]. The utilization factor is considered as a function of the ratio between the thermal losses and the thermal gains. It considers the mismatch between heat losses and gains leading to heating or cooling energy needs [324]. The gain utilization factor for heating, η_{Uh} , is determined as:

$$\eta_{Uh} = \frac{1 - \gamma_h^{a_h}}{1 - \gamma_h^{a_h + 1}} \quad \text{if } \gamma_h \neq 1 \quad (3.77)$$

$$\eta_{Uh} = \frac{a_h}{a_h + 1} \quad \text{if } \gamma_h = 1 \quad (3.78)$$

The loss utilization factor for cooling, η_{Uc} , is calculated as:

$$\eta_{Uc} = \frac{1-\gamma_c^{a_c}}{1-\gamma_c^{a_c+1}} \quad \text{if } \gamma_c > 0 \text{ and } \gamma_c \neq 1 \quad (3.79)$$

$$\eta_{Uc} = \frac{a_c}{a_c+1} \quad \text{if } \gamma_c = 1 \quad (3.80)$$

$$\eta_{Uc} = 1 \quad \text{if } \gamma_c < 0 \quad (3.81)$$

Where γ_h is the dimensionless gain/loss ratio for heating, $\gamma_h = Q_{int}/Q_h$; γ_c is the dimensionless gain/loss ratio for cooling, $\gamma_c = Q_c/Q_{int}$.

Coefficients a_h and a_c are linearly correlated with the time constant of the building τ , according to coefficients that depend on the building category, in terms of occupancy profile. The following correlation is valid for residential buildings, both for heating and for cooling:

$$a_h = a_c = 1 + \frac{\tau}{15} \quad (3.82)$$

The concept of time constant represents the time needed for the internal-external temperature difference to decrease in the absence of heat gains considering a constant external temperature. According to [307], the time constant of the building, expressed in hours, is determined as the ratio of the total internal heat capacity of the building, C expressed in (J/K), to the total load factor, TL in (W/K) caused by transmission and ventilation heat transfer.

$$\tau = C / TL \quad (3.83)$$

For instance, values of the loss utilization factor for cooling are plotted in Figure 3.24. This factor increases for high values of the building time constant of the building and for low values of the loss/gain ratio. In the case of a negative loss/gain ratio, which means that the average external temperature exceeds the internal temperature, the loss utilization factor is equal to 1 while $(Q_f + Q_v)$ in Equation (3.58) becomes negative.

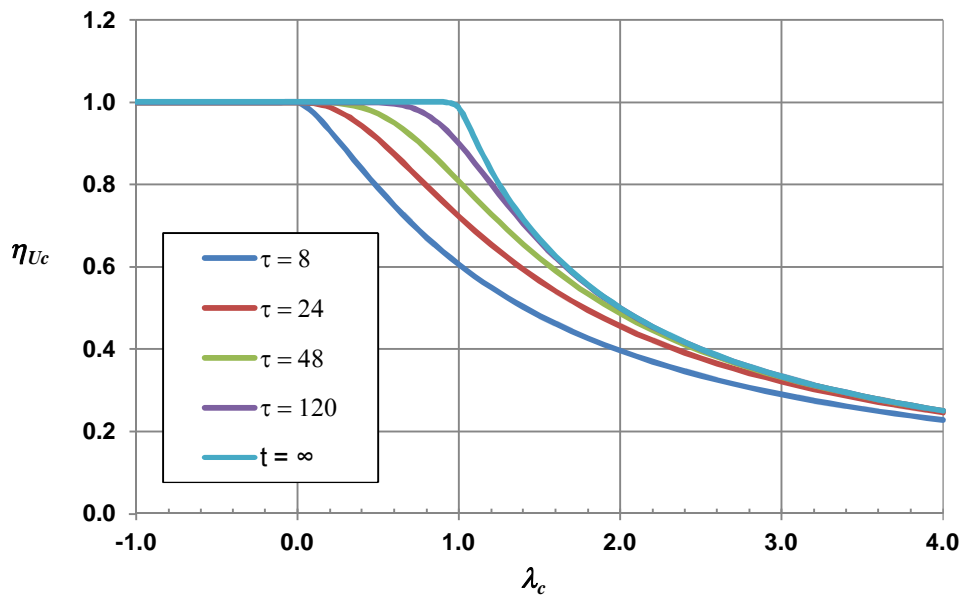


Figure 3.24. Cooling utilization factor vs. loss/gain ratio for different time constants, as in Equation (3.82)

3.3.3 Policy tools for enhancing building energy efficiency

An overall objective of energy policy in buildings is to save energy use without compromising comfort, health and productivity levels. In other words, consuming less energy while providing equal or improved building services, that is, being more energy efficient. Regulatory bodies (governments, energy agencies, local authorities, etc) have two basic instruments available for encouraging savings and maximising energy efficiency in buildings: regulation and certification [325].

3.3.3.1 Regulation requirements

Enforcing energy efficiency through mandatory requirements such as building energy regulations ensures that a certain minimum level of performance is achieved. The most effective regulation offer two options of compliance, called prescriptive and performance-based. Prescriptive standards set requirements for the building components, for example, the thermal conductivity of insulation or the efficiency of a heating or cooling system. They aim to maintain

consistency in term of thermal performance between the different components, in order to avoid having one particular component being responsible for the major part of the total energy use. On the other hand, performance-based standards set maximums on the energy consumption or annual predicted energy cost of a building taken as a whole. Unlike perspective standards, performance-based standards offer the designer the flexibility to vary from different options allowing specifications of less energy efficiency in some components in return for more efficiency in others. In that sense, performance-based standards are more economically efficient because they allow the designer or builder to optimize the selection of efficiency measures to minimize capital costs.

The major concern regarding building regulations is that the compliance criteria are usually set at levels that are relatively easy to achieve, so as not to incur heavy financial burdens on society. Otherwise, the building sector would strongly oppose the legislation, or numerous violations would render legislation difficult to enforce. Although such a regulatory instrument ensures a certain minimum level of performance to be achieved, studies have shown that when this instrument is the only one in place, it only leads to moderate results in terms of energy efficiency improvements [326, 327].

3.3.3.2 Building energy certification

While building energy regulations establish minimum requirements to achieve final energy or CO₂ emissions savings through more efficient building design, building energy certification consists of a rating or measurement procedure to assess the energy performance of a building. The level of energy performance under building certification schemes is assessed against a benchmark defined by the requirements of existing regulation standards. The energy certificate delivered as a result of the assessment provides a description of the building performance characteristics and information concerning the building energy efficiency. It also assigns an energy performance class or label to the building, based on a scale related to the labelling index, for comparison purposes between buildings assessed under the same scheme [328, 329].

Since BRE Environmental Assessment Method (BREEAM), the first building environmental assessment scheme, was launched in 1990 by the UK Building Research Establishment (BRE), there has been a significant rise in the number of building environmental assessment schemes that

promote sustainable building developments and energy certification [330]. The more widely known assessment schemes that are in use today include among others, the Leadership in Energy and Environmental Design (LEED) developed by the US Green Building Council (USGBC) [331], the Green Star developed by the Australian Green Building Council [332], the Building Environmental Performance Assessment Criteria (BEPAC) in Canada [333], the Evaluation Standard for Green Building (ESGB) in China [334], the Eco-Management and Auditing Scheme (EMAS) in the European Union [335], and the Building Environmental Assessment Method Plus (BEAM Plus) in Hong Kong [336]. Although they all use similar evaluation method, different criteria are assessed, among others, the energy use, ambient air quality, ecology, efficient use of water and materials used [337]. Among the large number of assessment schemes being used in different regimes, BREEAM from the United Kingdom and LEED from United States are the most widely recognized, i.e. not limited to their place of origin [338]. They represent the two main streams of methods currently in use across the world and have influenced enormously the development of more recently established schemes. As of 2017, more than 500,000 BREEAM certifications have been awarded and almost 2.3 million buildings are registered for assessment over 77 countries [339], while there are approximately 80,000 registered projects under LEED certifications and other 36,069 projects in LEED evaluation process in 155 countries [340, 341].

Although the use of energy certification instruments are based on voluntarism, it is often conceived as complementary to the regulatory instrument. In fact, in order to improve more effectively the levels of energy efficiency in buildings, studies tend to favour the adoption of a well-articulated mix of regulatory and voluntary instruments, which should also include incentive-based or rebate schemes to encourage the widespread use of new technologies and the selection of energy saving measures [342, 343]. Besides setting minimum regulation standards for all buildings, regulatory controls can also augment co-existing voluntary schemes. The voluntary certification schemes can benefit from the increased awareness and drive towards improvements triggered by the regulations. They can use the regulatory requirement as a baseline for defining enhanced performance, and provide indirect incentives for buildings to go beyond minimum regulatory requirements and common practices [329].

Chapter 4 – Methodology

In order to reach the specific objectives mentioned previously in Chapter 2, several methodologies have been carried out.

In relation to the specific objective 1), which consists in developing a mathematical model for the prediction of the levelised cost of electricity (LCOE) evolution for large scale solar electricity generation technologies, including PV, CSP, and hybrid PV-CSP with thermal storage, the methodology is developed in the section 4.1 below “*LCOE modelling for solar power in the PSDA*”.

In relation to the specific objective 2), which consists in developing a simplified method for multiple regression (MR) model identification from GSHP manufacturer performance data catalogues, the methodology is developed in the section 4.2 titled “*Developing MR models from GSHP catalogue data*”.

As for the specific objective 3), which consists in developing a building energy simulation (BES) tool for energy use and parametric sensitivity investigations, the methodology is detailed below in section 4.3 titled “*Modelling energy use in residential buildings*”.

4.1 LCOE modelling for solar power in the PSDA

Recent studies have proven that it is possible to make a continuous production of electricity implementing Solar-Solar plants [344, 345]. PV and CSP can be integrated for a reliable production of electricity.

The study presents an economic analysis of the feasibility of a combination of PV-CSP solar plants in northern Chile with the purpose of making a clean, secure and reliable Chilean energy matrix. The first approach calculates the LCOE for current PV and CSP technologies. The second approach evaluates economically the LCOE for a hybrid Solar-Solar plant, PV and CSP. Also, a projection of the LCOE for these plants was made in order to show the current and future scenario of the solar energy in the north of Chile.

The NREL model estimations of monthly average global horizontal solar radiation for four locations, representative of northern Chile are shown in Figure 4.1 [346]. As seen, the solar radiation peaks during summertime at values close to 8 kWh/m²/day, with winter minima nearing 3 kWh/m²/day.

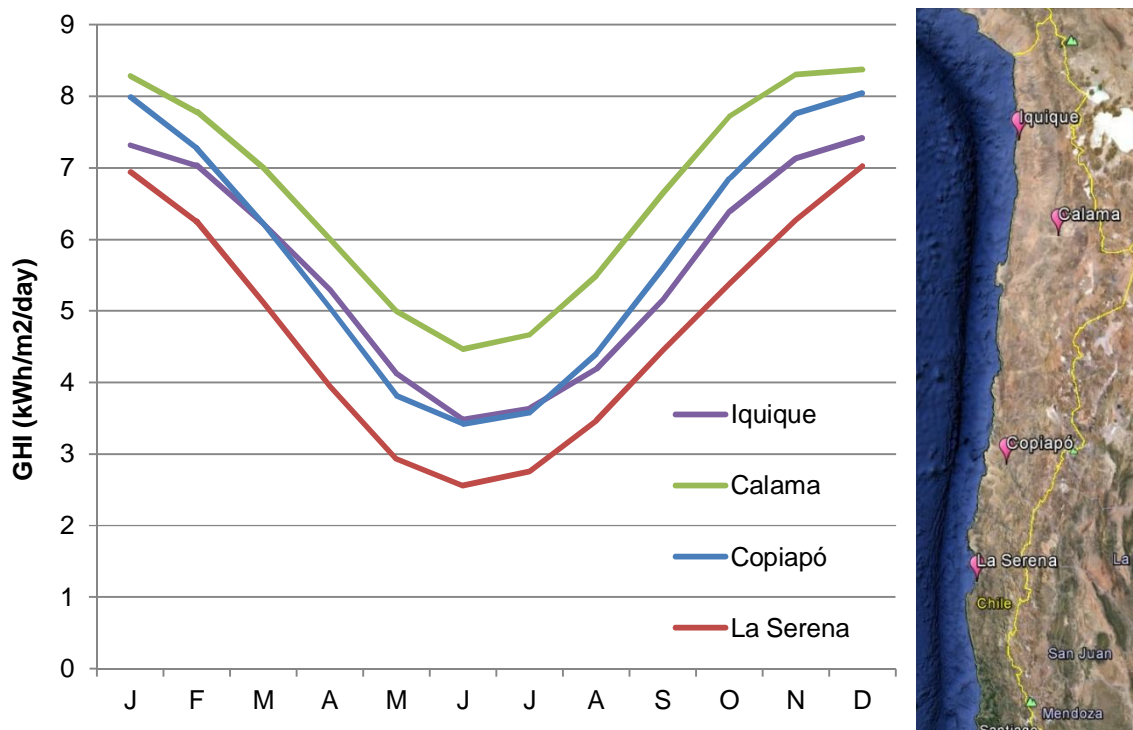


Figure 4.1. Daily average GHI on monthly mean at locations, representative of northern Chile

As electricity production is directly dependent on solar irradiation available, similar trends of annual electricity production would be observed as those of radiation in Figure 4.1. The solar electricity generation would be greater between the months of October and March and lower between the months of April and September, unless the solar plant is equipped with a fossil fuel back-up system able to compensate during winter months. For PV generation, a high inclination angle of the PV modules can be used to optimized generation in winter, and thus minimize seasonal differences at one particular location [344]. However, at equivalent plant specifications, the electricity generation would be greater in locations where the solar irradiation is higher, such as in Location 1 and 2 compared to Location 3 and 4.

CSP plants have the possibility to be hybridized with the fossil fuel to make the plant produce electricity for 24 h or/and can be integrated with a storage system to store a part of the heat during the day to generate electricity in the cloudy days or when the sun sets in order to improve its thermal efficiency and capacity factor and hence reduce the cost of the technology.

4.1.1 Configurations of the studied solar power plants

Solar energy is unattractive to some investors because of its lower capacity factor and higher electricity cost compared to conventional power plants. To make solar energy economically viable and supply secure, it is necessary to increase the efficiency of the plants. To do so, solar power requires storage (for load-balancing) to cope with its output intermittency resulting from weather/seasonal fluctuations.

Electrical energy storage (EES) such as batteries represents an effective solution to mitigate the imbalance associated to PV plants [347]. A background on the development of various energy storage options could be found in the Sandia National Laboratories handbook [348]. They are available at various sizes from a few kilowatts to hundreds of megawatts. Today, there are numerous commercial batteries including lead-acid, lithium-ion, sodium-sulphur, nickel-cadmium, or vanadium redox flow, each with different characteristics including energy capacity cost, round trip efficiency, depth of discharge, life, discharge duration, cycle frequency, energy/power density, environmental impact, etc. [348, 349, 350]. However, in spite of the recent developments on EES systems efficiency by the use of pulse width modulator inverters [351] or by ultracapacitors [352], batteries still require further work to improve their cycle life and thus

reduce the overall costs [353, 354]. According to Cervone et al. [355], only the lead-acid batteries can reach a suitable level of cost effectiveness in utility scale applications, while lithium-ion, sodium-sulphur or flow batteries still remain unsuitable until their costs decrease. However, lead-acid batteries have the disadvantages to be slow to charge, to have a limited depth of discharge and a limited amount of charge/discharge cycles [356]. EES are mainly used for off grid applications. For large-scale grid-connected PV power plants, EES is not an economically viable option. For these reasons, the integration of EES to the PV plant system is not considered in the cost projection analysis.

Regarding CSP technology, TES systems are an effective solution to increase the plant capacity factor allowing electricity generation for an extra 3 to 17 hours a day. TES systems use molten salt, typically a mixture of sodium and potassium nitrates ($\text{KNO}_3\text{-NaNO}_3$) which melts at about 220°C [357], as a heat carrier and storage medium. The capacity factor of a CSP plant is approximately 40% without storage and 60% with TES [155, 358]. The other option to increase the capacity factor of CSP plants is to incorporate a back-up system that can generate either electricity or the remaining thermal energy required in order to reach the nominal power output of the steam turbine in a continuous operation mode. The back-up system can make the use of other energy sources, such as the conventional fossil fuels, but also the wind, biomass, or the sun [175].

An accurate assessment of the energy resources available at the plant location is important to select the most appropriate energy mix that can provide continuous delivery. On the PSDA, the DNI and GHI values are some of the highest of the world, thus making hybrid PV-CSP plants an interesting option to investigate for this location.

Three types of solar plants of 50 MW capacity each are included in the analysis. It is assumed a fixed-angle PV power plant without storage systems. The second plant is a parabolic trough CSP system with 15 hours of TES and the third one is a hybrid PV-CSP plant enabling 24-hour electricity generation composed with 20 MWp fixed-angle PV and 30MW parabolic trough CSP with 15 hours of TES. In order to optimize the hybrid PV-CSP system output, the plant is set to prioritize the generation of electricity from the PV side when solar resource is available. During this time the CSP side is used to collect molten salt in order to produce electricity later at night. For both the PV and the hybrid PV-CSP plants, the PV collector area is constituted with south orientated monocrystalline silicon PV modules, inclined at the yearly optimum inclination angle.

4.1.2 LCOE model

According to Hernández-Moro et al. [359], an analytical model can be used for the projection of the LCOE of solar technology. The LCOE is equal to the sum of all the cost incurring during the lifetime of the project divided by the units of energy produced during its lifetime [184, 359]. For a precise LCOE projection for CSP and PV, the most convenient approach is to use the life-cycle cost method as given by Hernández-Moro et al. [186, 359]. The LCOE of the solar plant installed in a year t can be calculated using Equation (4.1) as follows:

$$LCOE(t) = \left(C(t) + L + \sum_{i=1}^T \frac{C(t)(O\&M+I)}{(1+d)^i} \right) / \left(\sum_{i=1}^T \frac{S \cdot TF \cdot \eta (1-DR)^i}{(1+d)^i} \right) \quad (4.1)$$

Where $C(t)$ is the total installation cost of the system (\$/W), L is the land cost (\$/W), $O\&M$ represent the operation and maintenance costs (%), I the insurance costs (%), S stands for the solar resource (kWh/m²/year), TF is the tracking factor (%), η is the performance factor (m²/W), DR the degradation rate (%), d the discount rate (%), and T the estimated lifetime of the system (years). This expression represents the LCOE for a one plant type per year of the projection. The computational simulation was made in Matlab. The most important variables used are $C(t)$, S and η because they depend on the plant location. The cost of the system at a certain time t , $C(t)$, depends of the cumulative installed capacity at that time, $q(t)$, and is defined as follows:

$$C(t_2) = C(t_1) \left(\frac{q(t_2)}{q(t_1)} \right)^{-b} \quad (4.2)$$

The learning coefficient (b) is related to the learning rate (LR) and the progress ratio (PR) that reflects the advance of technology [360]. The learning rate and progress ratio are given by:

$$PR = 2^{-b} \quad (4.3)$$

$$LR = (1 - PR) \quad (4.4)$$

Therefore, the learning coefficient can be calculated as follows:

$$b = - \frac{\log(LR-1)}{\log(2)} \quad (4.5)$$

4.1.3 Simulation

4.1.3.1 Calculating global parameters for PSDA

Several sources in the literature were consulted in order to obtain precise initial values for annual CSP electricity production and the cumulative installed capacity [16, 19, 52, 358]. Figure 4.2 shows the global cumulative installed capacity between 1990 and 2014. It can be observed that during the period between 2008 and 2014 the global cumulative installed capacity increased rapidly, due to the large number of technological improvements. This fact has helped many international companies to increase their capital investments in solar energy industry in different global locations [361]. Unlike CSP, Figure 4.3 shows that the cumulative installed capacity of PV has been increasing from the year 2000 to the present. This trend is produced because of the early adoption of PV technology by the energy industry and researchers.

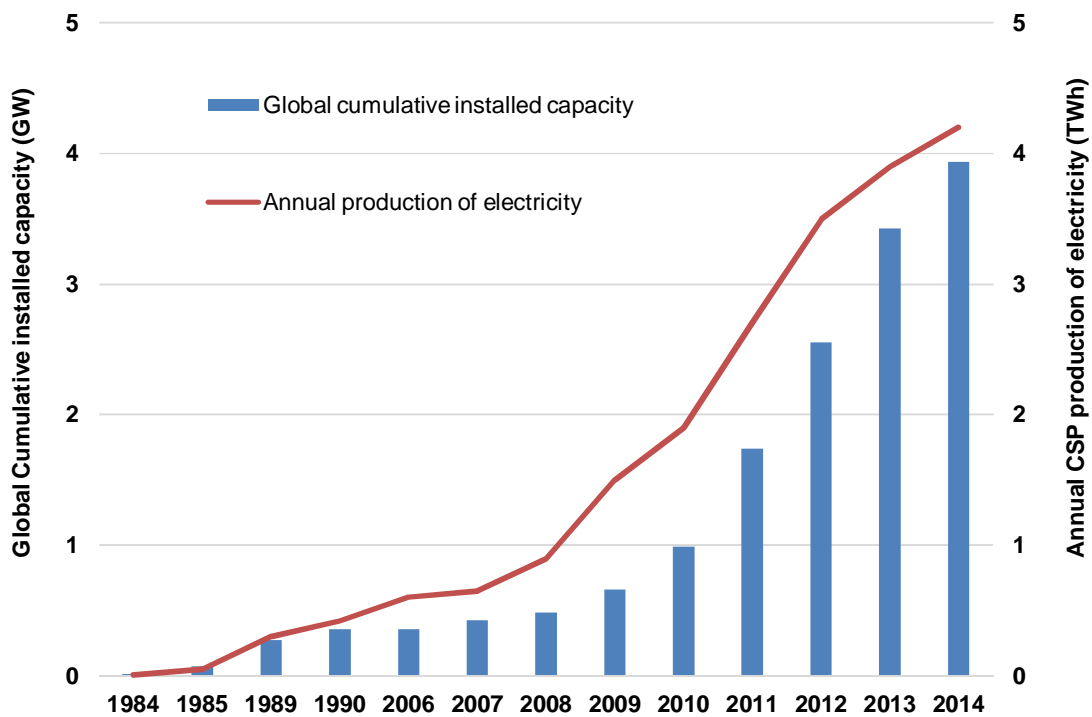


Figure 4.2. Global CSP cumulative installed capacity and annual CSP electricity production [16, 19, 358]

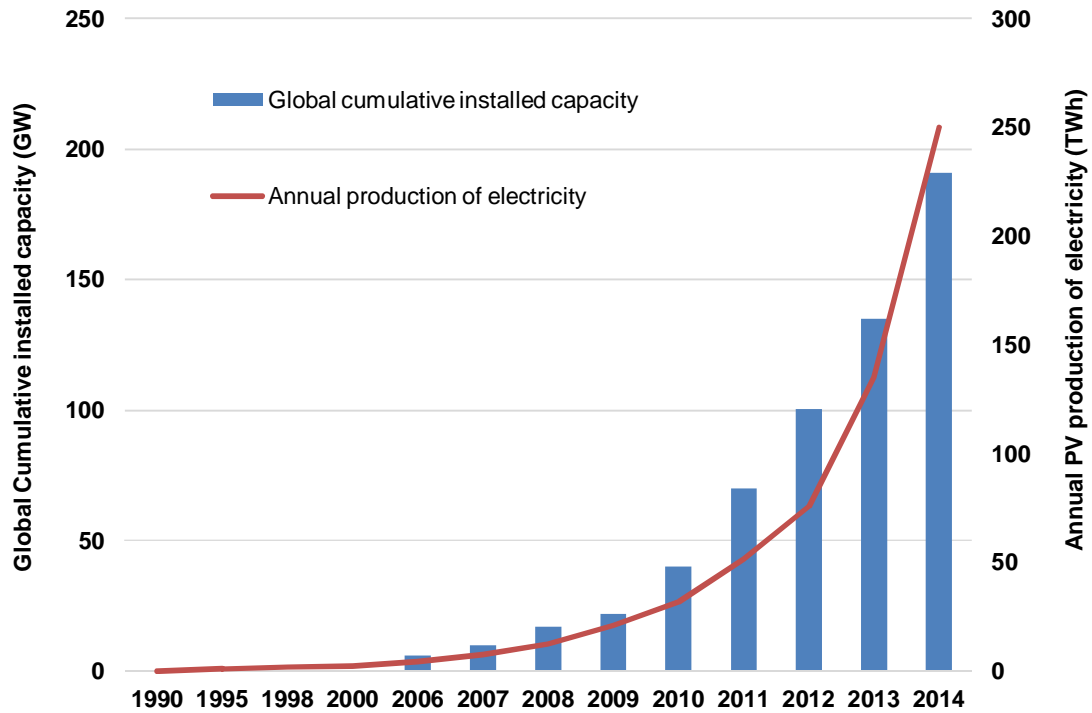


Figure 4.3. Global PV cumulative installed capacity and annual PV electricity production [16, 52, 358]

A projection for global cumulative installed capacity and annual production of electricity for the two technologies was made. At the beginning of 2014 the cumulative installed capacity, $q(0)$, was 191 GW for PV systems and 3.93 GW for CSP systems, and it was taken as a reference year for the projection to 2050. In order to obtain the correct projection to the $q(t)$, it was necessary to use the two different studies made by the International Energy Agency (IEA), Blue Map and Roadmap scenarios [19, 52]. Each scenario gives a projection of PV and CSP technologies up to 2050 with different market penetrations. According to the Blue Map and Roadmap scenario, PV and CSP systems would provide respectively 6% and 5% of the annual global electricity production in 2050 [16, 19, 52]. The Roadmap scenario has a high expectation for massive installation of future solar technologies worldwide; unlike the Blue Map scenario, which is more conservative with the evolution of the solar market.

For PV technology and for both projection scenarios, a logistic function called the S-shaped curve can be used because it best fits the data. For CSP technology in the Blue Map scenario the same logistic function is utilized, while for the Roadmap Scenario a second grade polynomial function is used [359]. The S-shaped curve and the second grade polynomial function used to

4.1 LCOE modelling for solar power in the PSDA

calculate the projections of cumulative installed capacity in the Blue Map and Roadmap scenarios are expressed by the following Equation (4.6) and (4.7).

$$q(t) = \frac{e^{r(t-2014)}}{\left(\frac{1}{q(0)}\right) - \left(\frac{1}{M}\right) + \left(\frac{e^{r(t-2014)}}{M}\right)} \quad (4.6)$$

$$q(t) = 0.459(t - 2014)^2 + 9.0725(t - 2014) + 3.9 \quad (4.7)$$

Where $q(0)$ and M are values of the initial and maximum cumulative installed capacity, respectively, and r is the growth parameter. According to Hernández-Moro et al [359], the specific values for PV according to the Blue Map and Roadmap scenario are respectively: $q(0)$ is 191 GW and 191 GW in 2014, M is 1150 GW and 3155 GW in 2050 and r is 0.102 and 0.185. For CSP technology according to the Blue Map $q(0)$ is 3.93 GW, M is 630 and r is 0.32. For the Roadmap Scenario to CSP only a $q(0)$ of 3.93 GW is necessary, given that the expression is a second grade polynomial [359].

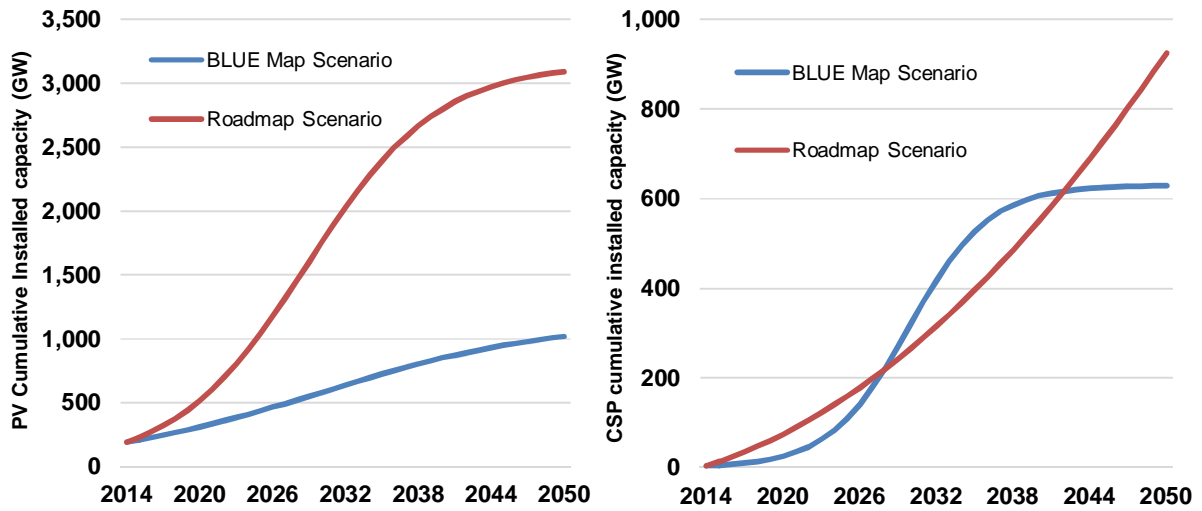


Figure 4.4. Projection of cumulative installed capacity for Blue Map and Roadmap scenario to PV and CSP technologies

Figure 4.4 demonstrates that the photovoltaic technology will lead solar generation in 2050 with approximate 3000 GW of cumulative installed capacity, while the CSP will reach almost 1000 GW. This situation could be produced because PV technology was investigated previous to

CSP [358]. Presently, several researchers have published new methods to boost the efficiency of solar panels, reaching higher values compared to current panels. Unlike PV, CSP does not reach the highest value of cumulative installed capacity, but in contrast with the present situation of the technology, the maximum at 2050 (1000 GW) is an excellent projection. Several researchers have investigated different options of CSP designs such as the parabolic trough, dish stirling, linear fresnel and solar tower [19, 362]. These technologies are helping to expand the solar energy across the world because each one has its own characteristics, making them feasible for different global scenarios.

4.1.3.2 Calculating specific parameters for PSDA

According to the model from Hernández-Moro et al. [186], there are three factors that are specific to the location of the plant: the cost of the system in each year, $C(t)$, the solar resource, S , and the performance factor, η .

The SAM software was used to obtain the costs of the system and the LCOE from the different studied technologies [189]. The cost obtained for the base year $C(0)$ is 1.24 US\$/W for PV and 6.12 US\$/W for CSP [363, 364, 365].

For the studied location in the PSDA region (Lat: -24.087° , Long: -69.913°), the values of DNI and GHI are $3421.9 \text{ kWh/m}^2/\text{year}$ and $2576 \text{ kWh/m}^2/\text{year}$ respectively [346]. The performance factors for the CSP technology, η_{CSP} , and for PV, η_{PV} can then be calculated using the following Equation (4.8) and (4.9).

$$\eta_{csp} = \frac{\text{Electricity produced per installed watt } \left(\frac{\text{kWh}}{\text{W}}\right)}{\text{Utilized solar resource (DNI)} \left(\frac{\text{kWh}}{\text{m}^2}\right)} \quad (4.8)$$

$$\eta_{pv} = \frac{\text{Electricity produced per installed watt peak } \left(\frac{\text{kWh}}{\text{Wp}}\right)}{\text{Utilized solar resource (GHI)} \left(\frac{\text{kWh}}{\text{m}^2}\right)} \quad (4.9)$$

The studied parabolic trough solar plant in the PSDA location has an electricity production per installed watt of 4715.2 kWh/W . This value was calculated dividing the electricity produced by the plant in one year, 235.75 GWh , by the plant capacity, 50 MW . The utilized solar resource

4.1 LCOE modelling for solar power in the PSDA

corresponding to DNI was 3421.9 kWh/m²/year. Therefore, the CSP performance factor for the chosen location is 1.377 m²/kWh. For the PV plant, the electricity production per unit of installed capacity is 1374.61 kWh/Wp. This value was obtained dividing the electricity produced by the PV plant in one year, 68.73 GWh, by the plant capacity, 50 MWp. With a GHI value of 2576 kWh/m²/year at the studied location, the PV performance factor is then 0.533 m²/kW. In summary, two performance factors were obtained, 1.377 m²/kW and 0.533 m²/kW for CSP and PV technology respectively. These values are very different, due to the fact that CSP technology uses only the direct radiation of the sun, while PV uses both direct and diffuse irradiation. The CSP electricity production value was obtained from the SAM software for two types of CSP plants, a parabolic trough and a flat plate of 50 MW each.

Table 4.1 gives the specific parameters for the location in the Atacama Desert. Values for hybrid PV-CSP plant was prorated according to the percentage of each technology in the mix, using the values in Table 4.1. The cost of PV technology is lower than CSP because the PV technology is more mature and its market penetration is stronger than CSP [52]. However, CSP technology cost tend to decrease and will become more affordable in the future, due to recent developments in TES systems introducing new materials for thermal storage [366].

Table 4.1. Values for the projection of LCOE for PV and CSP

| Factor | Symbol | Units | PV | CSP |
|---|---------------|--------------------------|------------|--------------|
| Cost of the system in 2014 | $C(0)$ | US\$/W | 1.24 | 6.12 |
| Cumulative installed capacity in 2014 | $q(0)$ | GW | 191 | 3.935 |
| Cumulative installed capacity in year t | $q(t)$ | GW | Figure 4.4 | Figure 4.4 |
| Learning rate | LR | % | 18 [186] | 10 [186] |
| Land cost | L | US\$/kW | 20 [367] | 20 [367] |
| Discount rate | d | % | 10 [186] | 10 [186] |
| O&M costs | $O\&M$ | % | 1.5 [186] | 2 [186] |
| Annual insurance rate | I | % | 0.25 [186] | 0.5 [186] |
| Solar resource | S | kWh/m ² /year | 2576 | 3421.9 |
| Tracking factor | TF | Dimensionless | 1 [186] | 0.9711 [186] |
| Performance factor | η | m ² /kW | 0.533 | 1.377 |
| Lifetime of the system | T | Years | 25 [186] | 30 [186] |
| Annual output degradation rate | DR | % | 0.6 [186] | 0.2 [186] |

4.2 Developing MR models from GSHP catalogue data

In dynamic simulation applications, such as in the modeling of heat pump systems integrated to buildings, it is required to evaluate the heat pump performance under particular operating conditions. However, it becomes difficult to estimate the correct performance value at operating conditions which do not exactly correspond to those listed in the manufacturer's data tables [251, 252].

The present investigation introduces a general methodology based on MR modeling able to determine the heat capacity (HC) and the coefficient of performance (COP) of GSHPs in heating mode from different working fluid temperatures and flow rates. Essentially, an optimal set of operating parameters from the manufacturer data tables would be to find relationships between the response variables (HC and COP) versus four operating parameters: the source flow rate (v_s), the load flow rate (v_l), inlet load temperature at the heat pump condenser (t_{il}) and inlet source temperature at the heat pump evaporator (t_{is}). The compressor power input (P) and heat extracted (HE) can then be deduced from HC and COP values. All these parameters are shown previously in Figure 3.13.

The operational method for the identification of MR models can be integrated in dynamic simulation tools such as EnergyPlus and TRNSYS in order to predict the performance of GSHP at particular operating conditions. The same approach can be employed for the development of MR models for the performance simulation of any GSHP system in heating or cooling mode using the corresponding capacity table from the manufacturer catalogue.

The method consists in selecting a sample of observations from the specification table, which can be used for the development of multiple regression models. The performance data of the remaining observations in the manufacturer table are then compared to the predictions calculated from the identified models. The statistical analysis further evaluates the models' robustness and prediction accuracy, determining the models' goodness-of-fit and the coefficients of variation (CV) of the prediction residual errors.

An important aspect of the selection of the observation sample is that it needs to provide a fair representation of the entire input space. In this concern, the observation sample is selected in a way that there are an equal number of low-range, mid-range and high-range values for each of the variables, and the combination selection is appropriately spread out so that the whole input space

is represented. Each combination of particular operating conditions corresponds to an observed value of HC and COP from the manufacturer catalogue. Since there are four independent variables (v_s , v_l , t_{il} and t_{is}), a complete factorial design as used in statistical experiments would require 81 observations. For the purpose of the study, three incomplete factorial designs are proposed using Latin squares, i.e. three samples containing 12, 24 and 36 observations respectively, in order to evaluate the influence of the sample size on model accuracy.

The approach involves using multiple linear regression of the first and second order to estimate the heat pump HC and COP values in heating mode under specified conditions of the four operating parameters (t_{is} , t_{il} , v_s and v_l). As seen in Figure 4.5 to 4.8 below, although some of the relationships are close to linear, others are distinctly non-linear, and thus the higher order terms are introduced to allow linear regression on non-linear relationships.

4.2.1 Description of studied manufacturer's data tables

In order to make it easier for engineers when it comes to GSHP selection and sizing for a particular building, GSHP manufacturers offer performance data tables from their catalogue. An example is shown in Table 3.3.

The analysis is based on three manufacturer performance tables of three commercially available GSHPs in heating mode. Table 4.2 provides the technical features of the three commercially available GSHPs considered in the study (called HP1, HP2 and HP3). The working operations in heating mode of the studied GSHPs range between the interval limits shown in Table 4.3. However there are some conditions for which operation is not recommended by the manufacturer. These extreme conditions for the three studied equipments are as following:

- HP1: When t_{is} varies between -1.1 and 10°C , v_s cannot vary between 0.95 and 1.45L/s ;
When t_{is} varies between 21.1 and 32.2°C , t_{il} cannot vary between 26.7 and 48.9°C .
- HP2: When t_{is} varies between 21.1 and 32.2°C , t_{il} cannot vary between 48.9 and 60.0°C .
- HP3: When t_{is} varies between -3.9 and -1.1°C , v_s cannot vary between 0.25 and 0.44L/s ;
When t_{is} varies between 21.1 and 32.2°C , t_{il} cannot vary between 26.7 and 48.9°C .

Therefore, the total number of observations in the data tables in heating mode is 114 for HP1, 171 for HP2 and 138 observations for HP3.

Table 4.2. Technical features of the considered GSHP

| | HP1 | HP2 | HP3 |
|----------------------------------|--|-------|----------------------|
| Compressor (number; type) | 2; scroll | | 1; scroll |
| Evaporator | Plate heat exchanger | | Coaxial tube-in-tube |
| Condenser | Plate heat exchanger | | Coaxial tube-in-tube |
| Refrigerant fluid | R410a | R134a | R410a |
| Ground loop fluid | 15% propylene glycol antifreeze solution | | |
| Distribution loop fluid | 15% propylene glycol antifreeze solution | | |

Table 4.3. Parameter variation in data tables in heating mode and operating limits

| | HP1 | HP2 | HP3 |
|---------------|------------------------|------------------------------|----------------------------|
| t_{is} (°C) | -1.1, 10, 21.1, 32.2 | -1.1, 10, 21.1, 32.2 | -3.9, -1.1, 10, 21.1, 32.2 |
| t_{il} (°C) | 15.6, 26.7, 37.8, 48.9 | 15.6, 26.7, 37.8, 48.9, 60.0 | 15.6, 26.7, 37.8, 48.9 |
| v_s (L/s) | 0.95, 1.45, 1.89 | 0.95, 1.26, 1.58 | 0.25, 0.35, 0.44 |
| v_l (L/s) | 0.95, 1.45, 1.89 | 0.95, 1.26, 1.58 | 0.25, 0.35, 0.44 |

In Figure 4.5 and 4.6 the heating capacity data of HP1 are reported into charts, as a function of the inlet source and load temperatures for the three different source and load flow rates. In Figure 4.7 and 4.8, the corresponding *COP* data given by the manufacturer for HP1 is shown¹. At higher inlet source temperature and/or source flow rate, Figure 4.5 shows that higher thermal output can be reached, because higher thermal energy is extracted. Higher inlet source temperature and/or source flow rate raises the evaporating pressure and temperature, and as the compression ratio remains the same, the condensing pressure and temperature also increases, resulting in higher thermal energy output. As the heating capacity is linear with inlet load temperature, Figure 4.6 shows the degradation of compressor efficiency at higher temperatures, because it is getting near the heat pump operational limits (condensing temperature about 55 to 60°C). Figure 4.7 shows that the heat pump *COP* increases when the inlet temperature and/or the

¹ Charts for the two other studied GSHPs (not reported here) indicate similar trends.

source flow rate increases. The interpretation of Figure 4.7 is similar to the one of Figure 4.5. However, the slopes of the curves in Figure 4.7 seem to decrease at higher temperature, showing the degradation of the compressor efficiency at higher refrigerant temperatures (higher compressor inputs required at higher temperature in order to reach the same compression ratio). The *COP* value always increases when the temperature difference between the heat source and the heat sink decreases. This is also shown in Figure 4.8 where the heat pump efficiency lowers when the inlet load temperature increases and/or the inlet source temperature decreases.

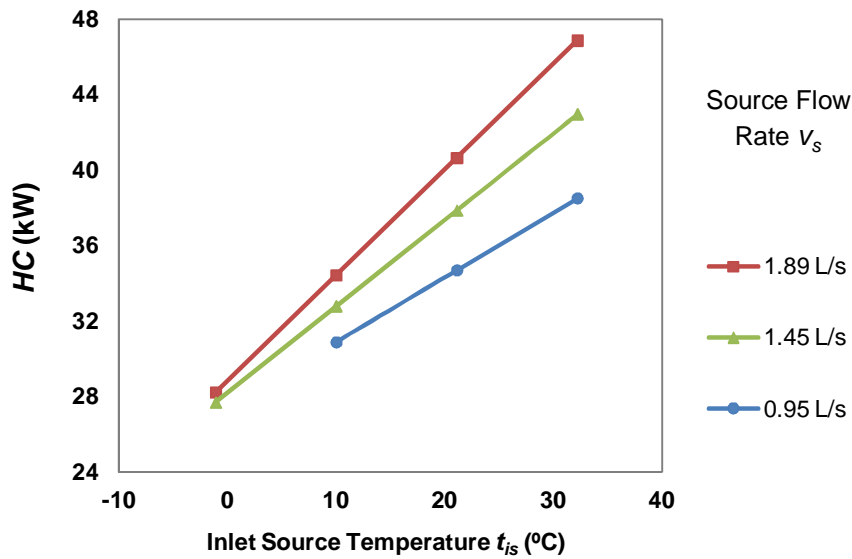


Figure 4.5. Heat capacity against inlet source temperature for $t_{il} = 15.6^\circ\text{C}$ and $v_l = 1.45\text{L/s}$

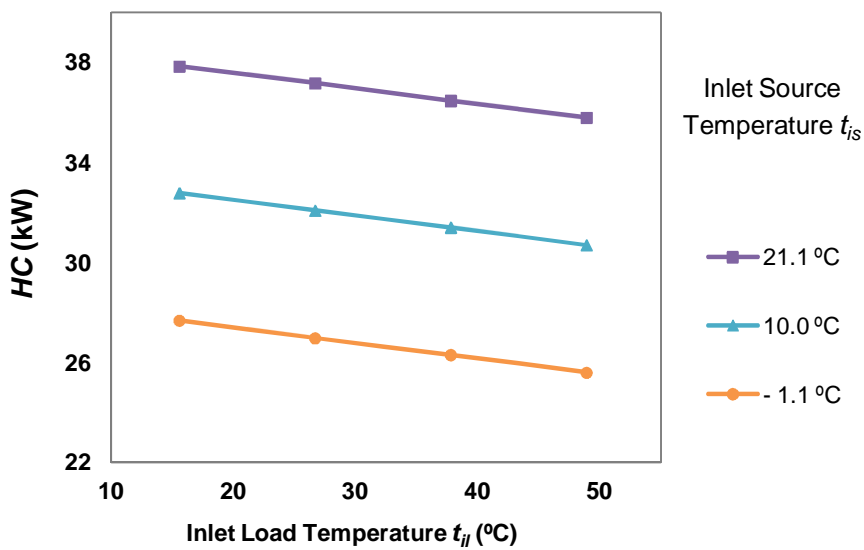


Figure 4.6. Heat capacity against inlet load temperature for $v_s = 1.45\text{L/s}$ and $v_l = 1.45\text{L/s}$

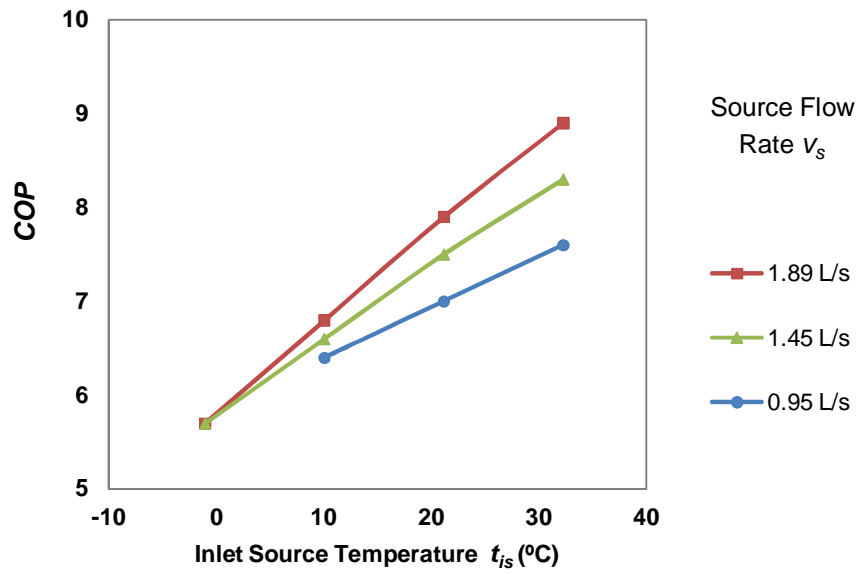


Figure 4.7. COP against inlet source temperature for $t_{il} = 15.6^\circ\text{C}$ and $v_l = 1.45\text{L/s}$

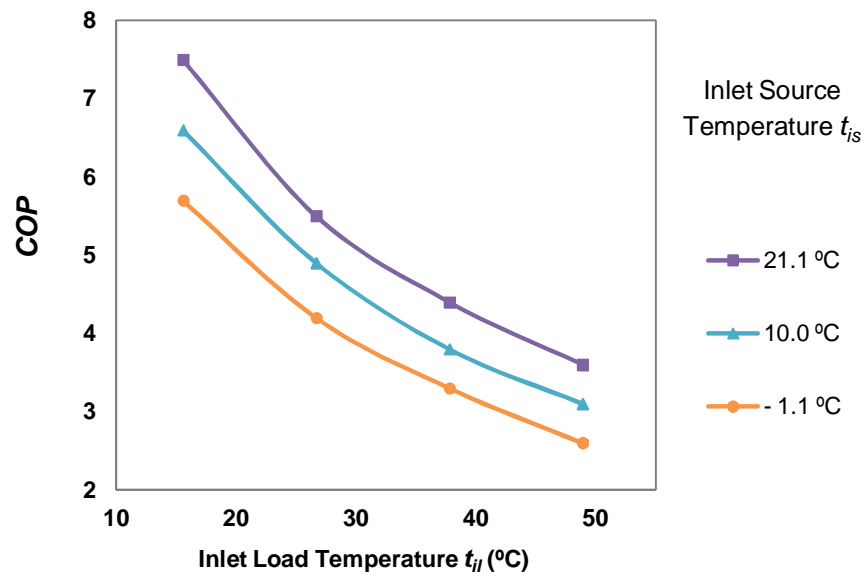


Figure 4.8. COP against inlet load temperature for $v_s = 1.45\text{L/s}$ and $v_l = 1.45\text{L/s}$

4.2.2 MR model identification

A linear MR model may be represented by the following Equation (4.10). Details of such method are given in standard textbooks on regressions such as in Draper et al. [253], Neter et al. [254], James et al. [255] or Johnson et al. [256].

$$y_j = \beta_0 + \beta_1 x_{j1} + \beta_2 x_{j2} + \beta_n x_{jn} + \varepsilon_j \quad (4.10)$$

Where y_j is the j response to be predicted using the (predictor) variables, x_{j1} to x_{jn} given as input. n is the number of predictor variables and β the regression coefficients. ε is the j residual or error between the predicted response and the observation.

The output shows the results of fitting a linear MR model to describe the relationship between a dependent variable *HC* or *COP* and 14 independent variables, which are as follows: t_{is} , v_s , t_{il} , v_b , t_{is}^2 , v_s^2 , t_{il}^2 , v_b^2 , $t_{is} \cdot v_s$, $t_{is} \cdot t_{il}$, $t_{is} \cdot v_b$, $v_s \cdot t_{il}$, $v_s \cdot v_b$ and $t_{il} \cdot v_b$. The models have been run with a stepwise forward multiple regression and so only the statistically significant model terms have been retained, i.e. those which indicate a significance level superior than 95% (p-value inferior to 0.05). This method allows a more robust model to be identified than including all variables as is done in standard regressions.

4.2.3 Statistical evaluation

The observations used for MR model fitting (for example, such as those shown in Table 3.3) are data which can include some error, due to measurement inaccuracies, instrument calibration failure, test conditions such as observations taken before the operation has reached steady-state, etc. Although the intent of regression modeling is to capture only the structural behavior of the system, depending on the veracity and quantity of observations, a certain amount of these errors may be captured in the model. This is called model over-fitting.

The coefficient of variation (CV) or relative variability aims to evaluate the relative sizes of the model squared residuals and outcome values from the regression model. The lower is the CV; the smaller are the residuals relative to the predicted value. For the purpose of the study, two

types of CV value are introduced in the statistical analysis, first the CV found during model fitting (also called internal prediction error or internal CV), applying to the observations used for model identification, and secondly the CV when applying the identified model to the remaining of the observations of the manufacturer table (called external prediction error or external CV). The comparison between internal and external CVs allows detecting the cases of model overfitting. The internal CV is a measure of model goodness-of-fit over the observation sample, while the external CV is a measure of how well the model is likely to predict future system behavior. The internal CV is expected to be smaller than the external CV, because the set of data points used for model identification is an incomplete sample of the full dataset, and so they are likely to contain fewer errors than in the remaining of observations in the table.

As suggested in statistics books [18, 21], in order to reduce the probability of model overfitting, the number of data points used to fit a MR model has to be at least three times the number of independent x -variables in the model, otherwise one variable starts fitting noise. Therefore, the maximum number of x -parameters which are used to fit a model from a set of 12, 24 and 36 observations is respectively four, eight and twelve.

4.3 Modelling energy use in residential buildings

In relation to the specific objective 3) of this investigation, the study proposes an example of a BES tool referred to as a forward model. This simulation program, called MEEDI, can be used to simulate energy use and carbon emissions in buildings. The model is based on the degree-days technique for the climatic parameter characteristics [266, 368] and the monthly calculation method of building heating and cooling energy use from the ISO 13790 Standard [307] with two additional procedures for the calculation of the heat transfer through the floor and the internal solar heat gain.

Using the MEEDI simulation program, the investigation focuses on the characterization of the residential energy consumption in Chilean homes and the analysis of the degree and impact of various building design factors affecting energy usage. Several researches in the literature have investigated on the influential parameters for improving energy efficiency in buildings. Al-ajmi and Hanby [369] investigated the effect of building envelope, window types, size and direction, infiltration and ventilation of domestic buildings in Kuwait. Bojic et al. [370] investigated the influence of applying advanced glazing types in a typical high-rise residential building in Hong Kong. Yang et al. [371] study the effect of different building envelope designs for five climate zones in China. Eskin and Turkmen [372] examined the effect of insulation and thermal mass, window area and glazing types on annual building energy requirements in office buildings in four climatic regions in Turkey with the use of EnergyPlus. Kaynakli [373] investigated the energy demand of a generic building in Turkey for design parameters, such as air infiltration rate, glazing type, and area, and determined optimum insulation thicknesses based on energy costs for various fuels types. Jaber and Ajib [374] discussed an assessment of best building orientation, windows size and thermal insulation thickness from an energetic, economic and environmental point of view for a typical residential building located in the Mediterranean region. Raji et al. [375] performed a sensitivity analysis to determine the influence of the glazing type, window-to-wall ratio, sun shading and roof strategies on the energy consumption for an office building in the Netherland. Ihm et al. [376] performed simulation analysis to determine the impact of window features on the total energy use of a typical residential building in two representative climates in South Korea. Kurekci [377] calculated values of optimum insulation thicknesses, energy gain savings and payback periods for several combination scenarios of fuels, energy systems and

insulation materials in five regions in Turkey. Mechri et al. [378] evaluated the impact of different design variables, including compactness ratio, envelope transparent surface ratio, orientation, shading factor and internal heat capacity on the energy performance for an office building in five climatic regions in Italy.

Dynamic simulation programs are widely used in the literature for convenience and their accuracy. However, these tools are difficult to be mastered due to their particular computerized procedures and thus, they are generally limited to trained professionals. This investigation proposes a simulation tool based on a simplified manual method with brief procedures, which is accurate and concise for hand computation, and can be used by architects and engineers during the preliminary design phase of new constructions or in building retrofits in order to evaluate the relative influence of the different input parameters to the annual energy usage.

The above-mentioned studies reported in the literature have only focused either on one particular envelope component or one particular climate condition in generic buildings, and they do not always provide evaluations in terms of economic aspects. There is a lack of comparative study of the relative efficiency and influence of design strategies in different climates in terms of both annual energy usage and economic viability. Besides, the literature survey does not show any indications of presence concerning studies covering building energy demand (cooling and heating) in Chilean climates. Therefore, the objective of this investigation is to verify and use the MEEDI simulation program to characterize the energy consumption in Chilean homes and demonstrate the degree and impact of several building design factors affecting energy usage.

The present study investigates the energy use in a reference household called “*base-case home*” (BCH) in various cities throughout Chile across different climate regions, considering the building’s layout, the materials used in its construction, and the climate conditions of the seven designated locations. The following presents the description of the selected typical single-family home in Chile, for which the load analysis will be conducted. The building description includes the building design data, construction material data, as well as its usage profile and air infiltration rate. The weather library includes temperature and solar radiation data, as well as the Heating Degree-Day (HDD) and Cooling Degree-Day (CDD) values for each location.

Then, the methodology employed for the building energy simulation is introduced. The energy use will be calculated monthly, according to the ISO13790 standard. Two additional procedures for the calculation of the heat transfer through the floor and the solar heat gain are used to

4.3 Modelling energy use in residential buildings

improve the ISO 13790. The solar gain consists of the solar radiation through the windows. The heat transfer through the floor is calculated using the procedure given in the international standard, ISO 13370 [307]. For the calculation purposes, the MEEDI numerical tool is constructed applying equations directly in an MS Excel spreadsheet.

An analysis of the type and performance of energy systems used for space heating and cooling will be conducted. For this purpose, the analysis includes two case scenarios. The scenario 1 (S1) takes into account that space heating is provided by a conventional gas boiler running on natural gas, while the scenario 2 (S2) assumes an electrical based heating system. Cooling is assumed to be provided by an electric air-conditioning unit in both scenarios. Household billing costs and carbon emissions for energy use are determined according to each scenario.

The methodology is presented below and summarized in Figure 4.9. The MEEDI modeling tool will be used to simulate the building energy consumption, evaluate the impact of envelope materials and the building orientation on annual space heating and cooling energy use, and finally to analyze the cost and carbon effectiveness of different envelope improvement measures.

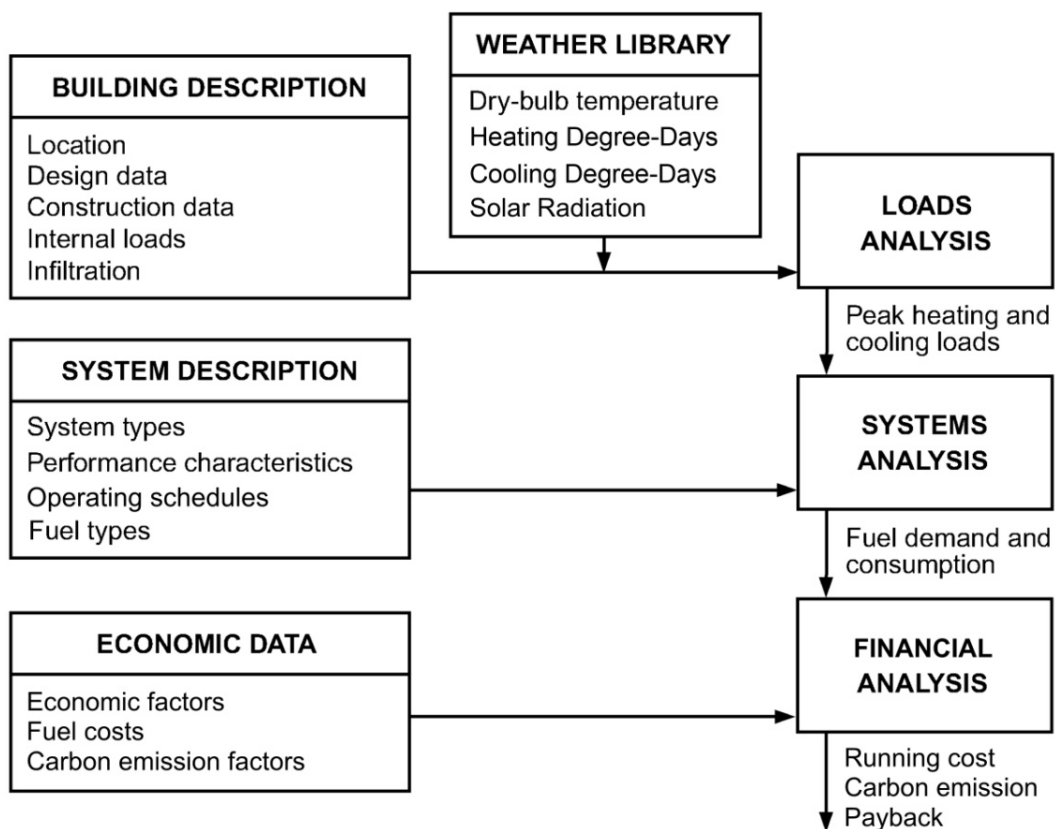


Figure 4.9. Structure of the MEEDI simulation tool

4.3.1 Input data gathering

4.3.1.1 Climate data

Among the climatic parameters, the HDD and CDD indicators can be used to quantify the heating and cooling energy demands, providing a quick method of figuring out the building's thermal energy consumption [379, 380]. Degree-day values are calculated as the sum of the difference in temperatures between a base temperature and the outside temperatures. Since the MEEDI include the numerical modeling of the internal heat, the base temperature is taken equal to the desired indoor air temperature, which is set to 20°C in winter ($T_{in,w}$) and 23°C in summer ($T_{in,s}$) in order to maintain an adequate level of comfort.

Table 4.4 shows the climate conditions in the seven locations considered in the study [381, 382], including the heating and cooling design conditions for the selected base temperatures (HDD₂₀ and CDD₂₃). The available solar radiation data given by the Chilean Ministry of Energy [383] are the total radiation on a horizontal surface, with its direct and diffuse parts. Such radiation data are relevant to evaluate the solar contribution to annual energy use of buildings, because they are based on the average data of many years. Seasonal heating and cooling periods shown in Table 4.5 are determined by assessing the available daily HDD₂₀ and CDD₂₃ data. Annual degree-day values shown in Table 4.4 are the sum of the daily values during the heating and cooling seasons respectively.

Table 4.4. Climate conditions of 7 Chilean locations [381, 382, 383]

| Location | Latitude | Altitude (m) | HDD ₂₀ (°C day) | CDD ₂₃ (°C day) | Annual average temperature (°C) | Annual GHI (kWh/m ²) | Climate zone |
|---------------------|----------|--------------|----------------------------|----------------------------|---------------------------------|----------------------------------|--------------|
| Antofagasta | 23.4S | 135 | 783 | 4 | 17.9 | 2212 | 1 |
| Copiapó | 27.3S | 204 | 1301 | 1 | 15.9 | 2019 | 1 |
| Valparaíso | 33.0S | 141 | 1738 | - | 14.8 | 1705 | 2 |
| Santiago | 33.4S | 475 | 1562 | 83 | 14.6 | 1828 | 3 |
| Concepción | 36.8S | 12 | 1992 | - | 13.0 | 1642 | 4 |
| Temuco | 38.8S | 114 | 1847 | - | 12.5 | 1467 | 5 |
| Puerto Montt | 41.4S | 85 | 2874 | - | 11.1 | 1219 | 6 |

Table 4.5. Heating and cooling seasons by location

| Location | Heating season | Cooling season |
|---------------------|-----------------------------|-----------------------------|
| Antofagasta | May – October (6 months) | December – March (4 months) |
| Copiapó | May – November (7 months) | February – March (2 months) |
| Valparaíso | April – November (8 months) | Not required |
| Santiago | May – October (6 months) | December – March (4 months) |
| Concepción | April – November (8 months) | Not required |
| Temuco | April – November (8 months) | Not required |
| Puerto Montt | March – November (9 months) | Not required |

This sample set of locations was selected as it represents the vast majority of the Chilean population and climate disparity. All climatic zones of the General Law of Urban Planning and Construction [102, 384] are represented except from the zone 7. Climate zone 1 is represented by two locations due to the wide range of HDD encountered within this climate zone. The coldest climate of zone 7 is not included because it represents a miniscule percentage of the Chilean population. Additionally, special subsidiary benefits are applied to this zone, making it incomparable to other regions for the purposes of this study.

The thermal conductivity of the ground, λ_g , depends on several factors including density, moisture content, and particle size, type of mineral constituting the particles and whether the ground is frozen. Consequently, the thermal properties vary from one location to another. However, for the purpose of the study, it will be assumed that the soil exhibits constant thermal conductivity λ_g of 2.4 (W/mK), and a ground solar reflectivity ρ_g of 0.2 for all locations.

4.3.1.2 Building geometry and occupancy

According to the National Statistics Institute [385], the majority (76%) of households built in 2014 had a surface area between 36 and 75m² and 63% of these buildings were individual households. For this study, a one story single-family house with 72m² surface area is utilized. Table 4.6 summarizes the dimensions of the reference case house. The window shading factor value is 0.5 for each location. The distribution of the window areas towards different directions is given in Table 4.7.

The studied home is assumed to be occupied by a four members family (two adults and two children), and equipped with conventional compact fluorescent lightings and all common appliances.

Table 4.6. Reference house dimensions

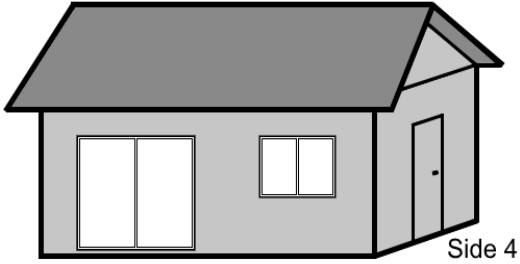
| | | |
|-------------------------|-----------------------|--|
| Conditioned area | 12 x 6 m ² |  |
| Ceiling height | 2.5 m | |
| Door area | 2.0 m ² | |
| Windows area | 10.5 m ² | |

Table 4.7. Reference house orientation and window distribution

| Windows | Orientation (Azimuth angle γ) | Area (m²) | Part of side envelope area | Part of total windows area |
|----------------|--|-----------------------------|---------------------------------------|---------------------------------------|
| Side 1 | North (0°) | 5.7 | 20% | 54% |
| Side 2 | East (-90°) | 1.2 | 11% | 11% |
| Side 3 | South (180°) | 3.6 | 13% | 34% |

4.3.1.3 Characteristics of building envelope materials

Most homes in Chile are built with heavy materials such as bricks (45%) and concrete (28%), and a smaller percentage are built with lightweight materials, such as wood (13%) [103]. In the study, one type of home featuring envelope materials of an average performance quality range is proposed. Such home is referred to as the “*Base-Case Home*” (BCH). The ground floor is made of a 15cm concrete slab, with a layer of sand gravel on top of the ground. Flooring consists of ceramic tiles. The walls are made of brick with insulation placed on the interior wall. The ceiling is a wooden frame, with flexible insulation. Table 4.8 summarizes the construction materials of the BCH. In the study, thermal bridges are assumed to represent 10% of the total building heat transmittance.

4.3 Modelling energy use in residential buildings

Table 4.8. Physical characteristics of the BCH envelope materials

| Component | Structure | Thermal Isolation |
|---|---|---|
| Exterior wall | - Brick, $t = 0.14$ m, $R = 0.75$ m ² K/W, $C_p = 840$ J/kgK, $\rho = 1900$ kg/m ³ - Plasterboard, $t = 0.012$ m, $R = 0.05$ m ² K/W, $C_p = 1090$ J/kgK, $\rho = 850$ kg/m ³ | Glass wool, $t = 0.1$ m, $\lambda = 0.04$ W/mK, $C_p = 840$ J/kgK, $\rho = 28$ kg/m ³ |
| Ceiling | - Pine wood, 10 cm x 10 cm, $C_p = 1300$ J/kgK, $\rho = 670$ kg/m ³ - Plasterboard, $t = 0.012$ m, $R = 0.05$ m ² K/W, $C_p = 1090$ J/kgK, $\rho = 850$ kg/m ³ | Glass wool, $t = 0.15$ m $\lambda = 0.04$ W/mK, $C_p = 840$ J/kgK, $\rho = 28$ kg/m ³ |
| Floor | - Concrete slab directly on ground soil, $t = 0.2$ m $R = 0.15$ m ² K/W, $C_p = 850$ J/kgK, $\rho = 2400$ kg/m ³ - Ceramic tiles, $t = 0.006$ m $R = 0.04$ m ² K/W, $C_p = 1000$ J/kgK, $\rho = 1700$ kg/m ³ | Polyurethane panel, $t = 0.05$ m $\lambda = 0.024$ W/mK, $C_p = 1400$ J/kgK, $\rho = 24$ kg/m ³ |
| Windows | PVC frame, Low emissivity double coated glazing 4/16(Argon)/4mm $U = 1.8$ W/m ² K, Solar radiation transmittance $\tau_w = 0.65$ | |
| Doors | PVC insulated door $U = 1.8$ W/m ² K | |
| Air infiltration/ventilation: $n = 1.1$ ach | | |

4.3.1.4 Heating/Cooling systems

In order to estimate the energy consumption, it is assumed that the space heating and cooling systems provide uniform air temperature distribution in the rooms. The overall efficiency of each system represents the ratio of energy output (heat or fresh air) over the energy input (gas combustion or electricity). Table 4.9 summarizes the efficiencies of the space heating systems and the coefficient of performance (COP) of the air-conditioning unit.

Table 4.9. Heating and cooling systems overall efficiencies

| System | Efficiency |
|---------------------------|------------|
| Conventional gas boiler | 85% |
| Electrical radiant heater | 97% |
| Air-conditioning unit | COP = 1.7 |

4.3.1.5 Fuel costs and CO₂ emissions factors

The analysis of the results is based on assessing the financial sustainability of different building envelope components. For the purpose of estimating annual energy billing costs, the price of electricity and natural gas of 0.19 and 0.11 (US\$/kWh) respectively is assumed. These are average prices in Chile in January 2017 [386, 387], and both include market price, standing charge and taxes. In order to estimate the building environmental impact, it is assumed carbon dioxide emission factors of 0.194 (kg_{CO2}/kWh) for natural gas consumption [388], and 0.42 (kg_{CO2}/kWh) for electricity consumption considering the actual share of fossil fuel sources in the Chilean electricity generation fuel mix [29, 389]. Table 4.10 shows fuel costs and carbon emission factors used throughout the study.

Table 4.10. Fuel costs and carbon emission factors

| Fuel Source | Cost (US\$/kWh) | CO₂ emission (kg_{CO2}/kWh) |
|--------------------|----------------------------|---|
| Natural gas | 0.11 | 0.194 |
| Electricity | 0.19 | 0.420 |

4.3.2 Data processing: energy use modelling

4.3.2.1 Heat transfer through envelope fabric

The heat loss/gain through the fabric envelope is proportional to the difference of inside and outside air temperatures. Steady-state heat loss in the heating season ($Q_{fabric,h}$), expressed in W, can be calculated using Equation (4.11a), when the outside air temperature (T_{out}) is inferior to the required inside air temperature in winter ($T_{in,w}$). Steady-state heat gain in the cooling season ($Q_{fabric,c}$) is given by Equation (4.11b), when T_{out} is superior to the required inside air temperature in summer ($T_{in,s}$). Fabric heat transfer occurs through building structure parts exposed to outside air or to non-air-conditioned areas such as the attic. The energy modeling in MEEDI assume the uniformity of inside air temperatures.

$$Q_{fabric,h} = \Sigma (UA) \cdot (T_{in,w} - T_{out}) \quad (4.11a)$$

$$Q_{fabric,c} = \Sigma (UA) \cdot (T_{out} - T_{in,s}) \quad (4.11b)$$

Where U is the heat transfer coefficient (W/m^2K); A is the surface area (m^2).

The U-value of structure parts can be found using the material's conduction R-value measured in (m^2K/W). For an element composed by different materials layers, the overall U-value of that element is the fraction of 1 over the sum of R-values. Convective heat flow resistance is characterized by external (R_{se}) and internal (R_{si}) surface resistances. The U-value for outside walls and ceilings can be calculated as follows:

$$U = \frac{1}{\Sigma R} = \frac{1}{R_{si} + \Sigma \frac{t}{\lambda} + R_{se}} \quad (4.12)$$

Heat flow through the ground floor is three-dimensional and thermal performance is affected by factors, including the size and shape of the floor, the thickness of the surrounding wall and type of insulation, ground temperature, and thermal conductivity. The calculation of the heat transfer through the floor directly in contact with the ground is based on the ISO 13370 standard [317], as shown previously in section 3.3.2.1.

4.3.2.2 Heat transfer through infiltration/ventilation

Ventilation/infiltration is defined as the intentional or unintentional leakage of air from the building. The amount of energy required depends on the rate at which fresh air enters and its temperature. The rate of air movement (n) is measured in air-changes per hour (ach). An air-change is when the full volume of air inside a house is replaced with a new volume of air. The heat lost/gained is equal to the energy stored in the warm/cool air relative to the external temperature in winter and summer respectively, which can be found using Equation (4.13a) and (4.13b) as follows:

$$Q_{ventilation,h} = \frac{\rho_w V}{3600} C_{p,w} n (T_{in,w} - T_{out}) \quad (4.13a)$$

$$Q_{ventilation,c} = \frac{\rho_s V}{3600} C_{p,s} n (T_{out} - T_{in,s}) \quad (4.13b)$$

Where ρ is the inside air density (kg/m^3); V is the volume of the building (m^3); C_p is the specific heat of the inside air (J/kg K) and n is the ventilation rate per hour ($1/\text{h}$). For a desired inside air temperature set to 20°C in winter ($T_{in,w}$) and 23°C in summer ($T_{in,s}$), according to the air density and specific heat properties table, the constants in Equation (4.13a) and (4.13b) are respectively 0.336 and 0.333 ($\text{J/m}^3\text{K}$).

4.3.2.3 Internal heat gains

The total internal heat gain (E_{int}) takes into account 20% of the energy used for domestic hot water production (E_{dhw}) assumed to be rejected from the hot water tank to the house internal environment, the internal gains from lightings and domestic appliances (E_{app}), and the gains due to sensible and latent heat rejection from occupants (E_o). The total internal heat gain is thus defined as follows:

$$E_{int} = 0.2E_{dhw} + E_{app} + E_o \quad (4.14)$$

4.3.2.4 Solar gains through windows

The solar energy on earth consists of three different parts. The direct beam solar radiation (H_b) reaches the earth's surface without being scattered or absorbed by the atmosphere. The diffuse solar radiation (H_d) is the scattered radiation reaching the earth's surface from all directions. The ground-reflected solar radiation (H_g) is a reflected part from the ground and surrounding. The incident global solar radiation (H) on an inclined surface is composed from the three radiation parts and is defined as:

$$H = H_b + H_d + H_g \quad (4.15)$$

The solar gain through a window depends on the solar radiation present at a certain location, the surface area of the window collecting the radiation (A_{window}) and the energy transmittance (τ_w) of the glazing. The daily solar gain into the building E_{sol} expressed in (kWh) is given by:

$$E_{sol} = \tau_w \times \bar{H}_\beta \times A_{window} \times F \quad (4.16)$$

Where \bar{H}_β is the monthly average daily radiation on a tilted surface (kWh/m²); F is the shading factor.

Since only the solar radiation data on a horizontal surface are available, there is a need to calculate the radiation on the vertically tilted windows. A method to estimate \bar{H}_β on a tilted surface oriented directly towards the equator has been developed by Liu and Jordan [128], as:

$$\bar{H}_\beta = \bar{R} \times \bar{H} \quad (4.17)$$

Where \bar{H} is the monthly average daily total radiation on a terrestrial horizontal surface; \bar{R} is the monthly average ratio of the global radiation on a tilted surface to that on a horizontal surface. The methods assumed that each the diffuse and ground-reflected radiations are isotropically distributed over the sky hemisphere. The overall tilt factor is defined as:

$$\bar{R} = \left(1 - \frac{\bar{H}_d}{\bar{H}}\right) \bar{R}_b + \frac{\bar{H}_d}{\bar{H}} \left(\frac{1+\cos\beta}{2}\right) + \rho_g \left(\frac{1-\cos\beta}{2}\right) \quad (4.18)$$

Where (\bar{H}_d/\bar{H}) is the monthly average diffuse-to-total radiation ratio for a horizontal surface; \bar{R}_b is the ratio of the average beam radiation on a tilted surface to that on a horizontal surface; β is the tilt angle of the surface from horizontal; ρ_g is the ground reflectivity.

The monthly average daily radiation on a tilted surface is then calculated by Equation (4.19):

$$\bar{H}_t = \bar{H} \left(1 - \frac{\bar{H}_d}{\bar{H}}\right) \bar{R}_b + \bar{H}_d \left(\frac{1+\cos\beta}{2}\right) + \bar{H} \rho_g \left(\frac{1-\cos\beta}{2}\right) \quad (4.19)$$

In order to calculate \bar{H}_β for surfaces facing different orientations, the MEEDI uses the development of the Klein method [130] (as shown in section 3.1.1.2), in which \bar{R}_b is dependent on the horizontal tilt angle, surface azimuth, declination angle and latitude.

4.3.2.5 Space heating/cooling energy use

The steady-state heat loss/gain through the building envelope materials needs to be added to the infiltration/ventilation heat loss/gain, in order to calculate the total Heating Load requirement (Q_{HL}) or the total Cooling Load (Q_{CL}) of the building, expressed in (W), as shown in Equation (4.20a) and (4.20b).

$$Q_{HL} = (\Sigma(UA) + 0.336 V n) (T_{in,w} - T_{out}) \quad (4.20a)$$

$$Q_{CL} = (\Sigma(UA) + 0.333 V n) (T_{out} - T_{in,s}) \quad (4.20b)$$

The expression of the Total Heating Load coefficient (THL) and Total Cooling Load coefficient (TCL) in (W/K) is given by:

$$THL = \Sigma(UA) + 0.336 V n \quad (4.21a)$$

$$TCL = \Sigma(UA) + 0.333 V n \quad (4.21b)$$

The total annual energy use E , expressed in (kWh), can be found using the following Equation (4.22). The space heating energy usage E_{SH} is the sum of all monthly heating requirements $E_{h,i}$ during the year taking into account the internal heat gains reduced by the heating utilization factor, $\eta_{Uh,i}$ (Equation 4.23a). The space cooling energy usage E_{SC} is the sum of all monthly internal heat gains during the year taking into account the monthly cooling energy use $E_{c,i}$ reduced by the cooling utilization factor, $\eta_{Uc,i}$ (Equation 4.23b).

$$E = E_{SH} + E_{SC} \quad (4.22)$$

$$E_{SH} = \sum_{i=1}^{12} [E_{h,i} - \eta_{Uh,i} (d_{h,i} E_{sol,i} + E_{int,i})] \quad (4.23a)$$

$$E_{SC} = \sum_{i=1}^{12} [(d_{c,i} E_{sol,i} + E_{int,i}) - \eta_{Uc,i} E_{c,i}] \quad (4.23b)$$

4.3 Modelling energy use in residential buildings

Where i is the month number; $d_{h,i}$ is the number of days during the month i when heating is required, $d_{c,i}$ is the number of days during the month i when cooling is required; $E_{sol,i}$ is the monthly average daily solar gain through the building windows; $E_{int,i}$ is the monthly internal heat gain due to occupants, lightings, domestic appliances and hot water production.

Assuming that the internal temperature is maintained by heating and cooling at a particular constant value throughout the whole 24 hours, the heating/cooling operating time in Equation (4.24a) and (4.24b) represents the number of hours in a day, 24 hrs. The monthly heating $E_{h,i}$ and cooling $E_{c,i}$ energy use due to heat transfer through fabric envelope and ventilation/infiltration can be calculated as follows.

$$E_{h,i} = \frac{24 \cdot HDD_i \cdot THL}{\eta_h} \quad (4.24a)$$

$$E_{c,i} = \frac{24 \cdot CDD_i \cdot TCL}{\eta_c} \quad (4.24b)$$

Where HDD_i and CDD_i are the monthly heating and cooling Degree Days; η_h is the overall efficiency of the space heating system; η_c is the overall efficiency of the air conditioning system (COP).

The time constant of the building in the heating τ_h and cooling τ_c season, expressed in hours (h), is calculated from:

$$\tau_h = C / THL \quad (4.25a)$$

$$\tau_c = C / TCL \quad (4.25b)$$

Where C is the total internal heat capacity of building (J/K), THL is the total heat load coefficient of the building (W/K) and TCL is the total cooling load coefficient (W/K) caused by transmission and ventilation heat losses.

For the month i in the heating season, the utilization factor $\eta_{Uh,i}$ is function of the dimensionless gain/loss ratio for heating, $\gamma_{h,i} = (E_{int,i} + E_{sol,i})/E_{h,i}$, and is calculated as follows:

$$\eta_{Uh,i} = \frac{1 - \gamma_{h,i}^{a_h}}{1 - \gamma_{h,i}^{a_h + 1}} \quad \text{if } \gamma_{h,i} \neq 1 \quad (4.26a)$$

$$\eta_{Uh,i} = \frac{a_h}{a_h + 1} \quad \text{if } \gamma_{h,i} = 1 \quad (4.26b)$$

The utilization factor for the cooling demand $\eta_{Uc,i}$ is a function of the monthly loss-gain ratio $\gamma_{c,i} = E_{c,i}/(E_{int,i} + E_{sol,i})$, and is calculated as:

$$\eta_{Uc,i} = \frac{1 - \gamma_{c,i}^{a_c}}{1 - \gamma_{c,i}^{a_c + 1}} \quad \text{if } \gamma_{c,i} > 0 \text{ and } \gamma_{c,i} \neq 1 \quad (4.27a)$$

$$\eta_{Uc,i} = \frac{a_c}{a_c + 1} \quad \text{if } \gamma_{c,i} = 1 \quad (4.27b)$$

$$\eta_{Uc,i} = 1 \quad \text{if } \gamma_{c,i} < 0 \quad (4.27c)$$

The coefficients a_h and a_c that depends on the time constant of the building (building inertia) are found using Equation (3.82).

Chapter 5 – Results

This chapter presents and discuss the results obtained following the three methodologies introduced previously in chapter 4.

Each section of this chapter is related to the corresponding investigation specific objective, as defined in chapter 2. Next section 5.1 introduces the LCOE projections of the three studied solar power plants until 2050. The following section 5.2 presents the regression analysis, including a statistical evaluation of the identified multiple regression models, and a validation of the proposed approach. Finally, the study of the influence of several factors (including climate conditions, envelope materials and building orientation) on annual energy use, as well as a financial analysis of a set of design improvement measures, are introduced in section 5.3

5.1 2050 LCOE projection for solar power in the PSDA

The main goal of the simulation is to compare the LCOE evolution until 2050 of the two most used solar technology plants (PV, CSP), as well as with the LCOE of a hybrid PV-CSP plant with 24 hours of electricity generation. The parameters for the LCOE projection were calculated according to the model developed by Hernandez et al. [359].

Applying the calculation method introduced in section 4.1, the LCOE was calculated for three types of solar plants: a fixed optimally-inclined south-oriented 50 MWp PV system; a 50 MW parabolic trough CSP plant with 15 hours of TES; and a PV-CSP hybrid plant able to operate 24 hours a day constituted with a fixed optimally-orientated and inclined 20 MWp PV system and a 30MW parabolic trough CSP system with 15 hours of TES.

5.1 2050 LCOE projection for solar power in the PSDA

Figure 5.1 and 5.2 shows the LCOE of PV and CSP for two scenarios: Blue Map (1) and Roadmap (2) scenarios. For the scenario (1), LCOE values obtained varied between 12.88 and 8.43 cUS\$/kWh for PV technology and between 15.29 and 9.02 cUS\$/kWh for CSP technology, between 2014 and 2050 respectively. For the scenario (2), LCOE values obtained varied between 10.74 and 7.79 cUS\$/kWh for PV technology and between 14.93 and 7.57 cUS\$/kWh for CSP technology. LCOE values obtained for both PV and CSP technology and both scenarios in 2014 are in the same range than those obtained by Kost et al. [365] in the PSDA location, showing that such LCOE values are from the lowest in the present market. In Kost et al. [365], the LCOE for solar technologies reaches values between 9.21 and 17.68 cUS\$/kWh for PV and between 17.27 and 24.36 cUS\$/kWh for CSP. The competitive costs obtained for the two technologies are explained by the high solar radiation available in the Atacama Desert and the low capital cost (\$/W) of the technology calculated for the current location. From 2014 to 2050, further reductions in capital costs are expected, which will allow solar technology to reach grid parity with than conventional fossil fuel technologies [358].

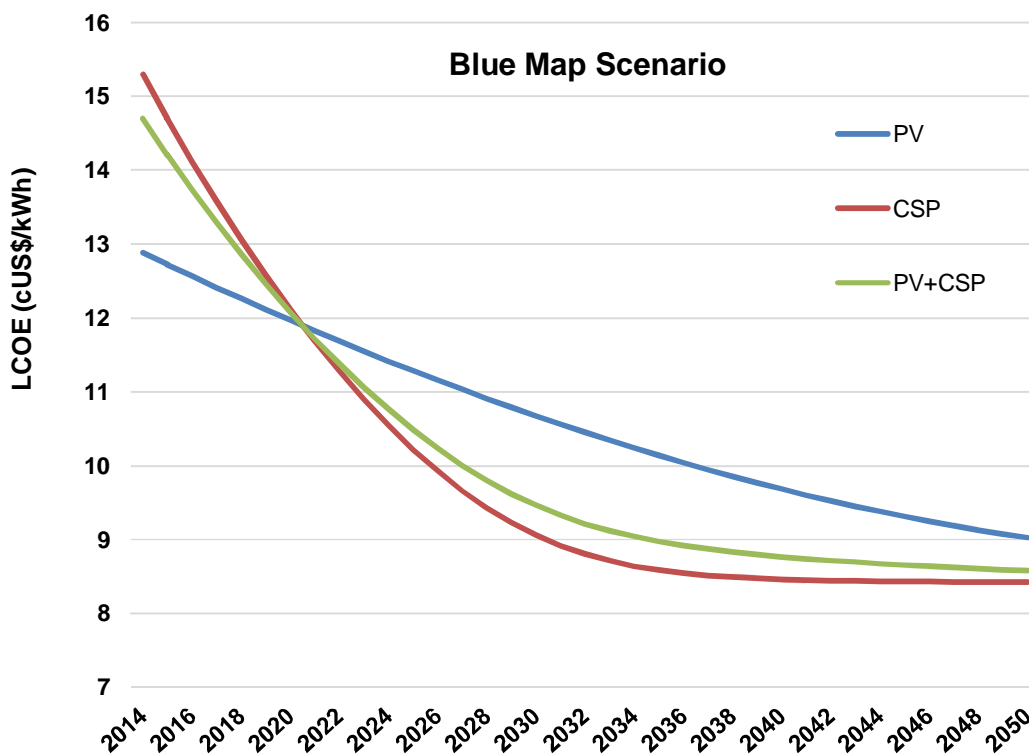


Figure 5.1. 2050 LCOE projection to PSDA between 2014 and 2050 for PV, CSP and PV-CSP in Blue Map scenario (1)

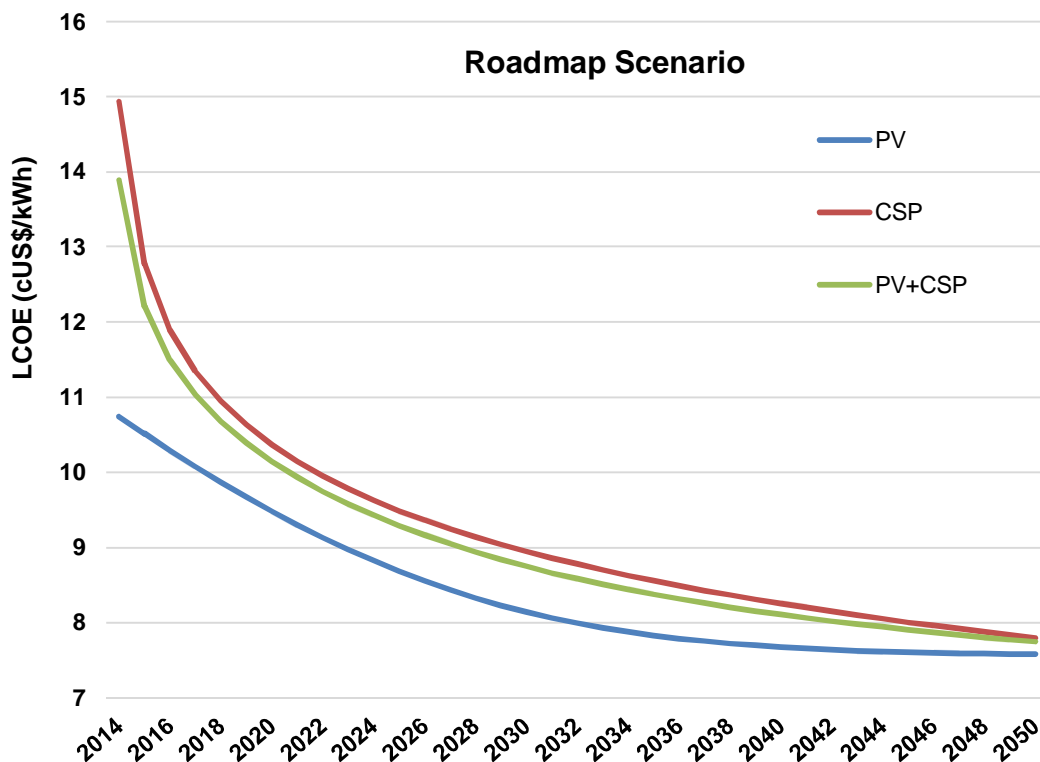


Figure 5.2. 2050 LCOE projection to PSDA between 2014 and 2050 for PV, CSP and PV-CSP in Roadmap scenario (2)

In addition, Figure 5.1 and 5.2 show the LCOE for the studied 50 MW hybrid PV-CSP plant according to the two mentioned scenarios. For the scenario (1), LCOE values obtained varied between 14.69 and 8.57 cUS\$/kWh between 2014 and 2050 respectively. For the scenario (2) LCOE values obtained varied between 13.88 and 7.74 cUS\$/kWh. In Figure 5.1, according to the Blue Map scenario, the three plants LCOE have tendency to decrease over time. The CSP plant will reach the lowest LCOE value compared to the other two, followed closely by the hybrid PV-CSP plant. According to the Roadmap scenario in Figure 5.2, the three plants have the same tendency, their LCOE decreases over time, but it is the PV plant which will reach the lowest LCOE value in 2050 followed by the hybrid PV-CSP plant. According to these calculations, in the Blue Map scenario, it is predicted that CSP market will increase faster and stronger than PV market, due to a greater growth of CSP global installed capacity. The Roadmap scenario, which is based on different projection criterias, is predicting a greater growth of global PV installed

capacity in the future, given that PV is a more mature technology than CSP, that it has lower cost and thus it is more accessible.

These two different situations are explained by the value of learning rate included in the model. The studies on learning rate factors are very useful for modeling technical change and informing policy decisions related to energy technology. Learning rate models have a variety of forms to describe the relationship between cumulative capacity and cost [360]. The learning rate of a technology is derived from the accumulation of experiences in production. Its value gives an indication on how fast the LCOE of the technology can be expected to decrease over the years. In the Blue Map scenario, according to the learning rate of CSP technology, it is expected that CSP will be further developed in the coming years, the global installed capacity is expected to significantly increase, thus reaching a lower LCOE than the other studied plants. In the Roadmap scenario, however, it is expected a higher growth in PV installed capacity in the future, thus leading to a lower LCOE for the PV technology compared to the other two types.

Although the PV and CSP plants separately reach a lower LCOE than the hybrid combination, either in the Blue Map and the Roadmap scenarios, the hybrid PV-CSP plant enable 24-hour electricity generation and reach higher capacity factors than the other two. Therefore, this type of hybrid PV-CSP plants can effectively provide power supply and match the 24-hour 7-day power demand of the mining industry in Chile. The mining industry is also the first sector of CO₂ emissions in Chile, so it is important to search clean and reliable options to supply its electricity demand. Hybrid PV-CSP plants are an option to ensure 24 hours continuous supply of electricity and reduce the country's dependence on fossil fuels. The similar LCOE for future years between Hybrid, PV and CSP can be an important factor to determinate new options to satisfy the mining sector power demand, allowing hybrid PV-CSP plants to be the most economically and environmentally viable option even if its LCOE is not the lowest. Also, the mitigation of CO₂ emissions from mining industries resulting from the use of solar resource instead of fossil fuel electricity would lead to non-negligible reductions in pollution taxes, and directly affecting business cash flows.

5.2 Regression analysis

The previous section 4.2 introduced the methodology employed in this particular study based on step forward multiple regression modeling. The regression analysis presented below includes a description of the studied manufacturer specification tables, an overview of regression models, the statistical evaluation of the identified MR models, the proposed approach validation and finally a discussion about the findings.

5.2.1 Statistical evaluation for HP1

The test results on the statistical evaluation of MR models for the studied HP1 are listed in Table 5.1 for HC_I and COP_I predictions. Subscript I is the notation referring to HP1. These results reveal the R-square values adjusted for degrees of freedom of the identified models, the internal CV, the external CV, as well as an indication about the pattern formed by external residuals when plotted against the predicted responses for the remaining of the data set, where C, SE and N stand for clear, some kind of evidence and no residual specific pattern respectively. The simple R-square statistic is not reported because its value is generally biased. The magnitude of the bias in simple R^2 values depends on how many observations are available to fit the model and how many variables are relative to the sample size. It is more appropriate to use the adjusted R^2 value (coefficient of determination) to compare models with different numbers of independent x -variables, as it takes into account the size of the data set and the number of predictor variables [255, 256]. For the models with the highest number of x -variables, the value of adjusted R-square is seen to approach unity. Results suggest that models with a lower number of x -variables are less robust, although they still indicate excellent goodness-of-fit within the observation sample. For instance, the evaluation of the models for HC_I and COP_I predictions as fitted from the 24 observations with 8 significant x -variables shows that the adjusted R^2 statistic explains 99.998% and 99.88% of the variability in HC_I and in COP_I respectively, while the evaluation of the models identified with only three variables indicates 97.85% and 97.18% respectively.

The input parameters for the modeled results were varied accordingly within the different independent x -variable combinations for the observations used for fitting the models, as well as

for the remaining observations in the manufacturer table, and for each case the predicted values of HC and COP were found. The coefficient of variation (CV) of the residual errors was calculated using the following Equation (5.1):

$$CV = \frac{RMSE}{\mu} \quad (5.1)$$

Where $RMSE$ is the root mean square of error, also called the standard error of the estimate and μ is the mean value of the observed data.

The internal CV values (Table 5.1) suggest of a good model fit for most of the HC_I models, the COP_I models describing a poorer fit in terms of relative closeness of the predictions to the actual values from the observation sample. Cases of model over-fitting are detected for second-order COP_I models with three and four x -variables identified from the 12 observation sample, where the external CV is much larger than the internal CV. First-order COP_I models, first-order HC_I model with one x -variable identified from the 12 observation set, as well as some second-order HC_I and COP_I models identified with a low number of x -variables, are all models for which the internal CV is found larger than the external CV, thus indicating of model over-fitting. For all the remaining models developed for HP1, the internal CV values are slightly smaller than external CVs, demonstrating that the observation sample used for model identification is a fair representation of the entire data table. In these cases, the identified models have successfully captured the structural behavior of the HP1 system.

In order to validate the proposed approach, it is assumed that the external CV value should be inferior to a 5% threshold limit, which is an acceptable level in statistical analysis. For the COP_I prediction, this level of prediction accuracy is only achieved when there are a minimum of five independent variables in the model.

Another condition required to validate the method is that no specific pattern should be formed by external residuals when plotted against the predicted responses. Indeed, no specific pattern in such a plot indicates that residual errors have constant variance and that they are independent, i.e. there is no correlation with regression coefficients or the response. Although the majority of the MR models identified are found robust and relatively accurate in predicting the remaining data listed in the manufacturer's catalogue, the only tests where model residuals are found to have constant variance is for second-order models with eight significant x -variables identified from the

36 observation sample. A clear pattern formed by residuals was found in most of the other model tests, particularly for models with fewer parameters and identified from a lower number of observations, i.e. when the degree of freedom is low.

Table 5.1. Test results of MR models for HP1

| Observation sample | Model order | Number of x -variables | HC_1 | | | | COP_1 | | | |
|--------------------|-------------|--------------------------|------------|---------|---------|--------------|------------|---------|---------|--------------|
| | | | Adj. R^2 | Int. CV | Ext. CV | Res. pattern | Adj. R^2 | Int. CV | Ext. CV | Res. pattern |
| 12 observations | First | 2 | 0.9730 | 3.8% | 4.9% | C | 0.9206 | 12.5% | 10.9% | C |
| | | 1 | 0.8793 | 8.1% | 7.4% | C | 0.8547 | 17.0% | 19.2% | C |
| | Second | 4 | 0.9987 | 0.8% | 1.1% | C | 0.9886 | 4.7% | 16.8% | C |
| | | 3 | 0.9931 | 1.9% | 2.6% | C | 0.9657 | 8.2% | 17.7% | C |
| | | 2 | 0.9851 | 2.8% | 3.4% | C | 0.8758 | 15.7% | 17.3% | SE |
| 24 observations | First | 4 | 0.9809 | 2.7% | 2.9% | C | 0.9446 | 9.5% | 8.1% | C |
| | | 3 | 0.9755 | 3.1% | 3.8% | SE | 0.9352 | 10.3% | 9.2% | C |
| | | 2 | 0.9570 | 4.1% | 4.7% | C | 0.9228 | 11.3% | 10.7% | C |
| | Second | 8 | 0.99998 | 0.1% | 0.2% | C | 0.9988 | 1.4% | 2.7% | SE |
| | | 7 | 0.99996 | 0.1% | 0.2% | C | 0.9984 | 1.6% | 3.0% | SE |
| | | 6 | 0.9995 | 0.4% | 0.7% | C | 0.9974 | 2.3% | 3.8% | C |
| | | 5 | 0.9990 | 0.6% | 0.7% | C | 0.9940 | 3.1% | 4.1% | C |
| | | 4 | 0.9997 | 0.3% | 0.4% | C | 0.9869 | 4.6% | 6.0% | C |
| | | 3 | 0.9785 | 2.9% | 3.0% | C | 0.9718 | 6.8% | 7.7% | C |
| | | 2 | 0.9730 | 3.2% | 3.2% | C | 0.8793 | 14.1% | 12.7% | C |
| 36 observations | First | 4 | 0.9798 | 2.8% | 3.0% | C | 0.9426 | 9.6% | 7.9% | SE |
| | | 3 | 0.9759 | 3.0% | 4.2% | C | 0.9263 | 10.9% | 8.4% | SE |
| | | 2 | 0.9583 | 4.0% | 5.4% | C | 0.9047 | 12.4% | 9.5% | C |
| | Second | 8 | 0.99996 | 0.1% | 0.2% | N | 0.9984 | 1.6% | 2.6% | N |
| | | 7 | 0.9999 | 0.2% | 0.2% | SE | 0.9979 | 1.8% | 2.8% | SE |
| | | 6 | 0.9998 | 0.3% | 0.3% | C | 0.9942 | 3.1% | 3.6% | C |
| | | 5 | 0.9998 | 0.3% | 0.3% | C | 0.9930 | 3.4% | 3.5% | C |
| | | 4 | 0.9995 | 0.4% | 0.6% | C | 0.9802 | 5.6% | 5.4% | C |
| | | 3 | 0.9844 | 2.4% | 2.1% | C | 0.9705 | 7.5% | 8.0% | C |
| | | 2 | 0.9765 | 3.0% | 3.6% | C | 0.9314 | 10.1% | 9.1% | C |
| 1 | 0.9601 | 3.9% | 4.0% | C | 0.7485 | 20.1% | 19.7% | C | | |

5.2.2 Modelling approach validation

The statistical analysis shows that a validated approach is to develop second-order MR models containing eight statistically significant x -variables from 36 observations. Using this operational approach, the fitted models fulfilled the two above mentioned conditions, i.e. CV inferior to 5% and no specific pattern formed by residuals, for both HC_I and COP_I predictions. Following this particular approach, Table 5.2 and 5.3 assemble the coefficients for each of the model independent variables along with their standard errors and their p-values for HC_I and COP_I models respectively. The MR models (shown in Table 5.2 and 5.3) yield predictions within the range of the HP1 working operations. Temperatures are in degrees Celsius, flow rates in Liters per second, the heat capacity in kilowatt and the COP is dimensionless.

Each of the coefficients indicates the influence of each predictor x -variable on the GSHP working data. For instance, the coefficient of the load inlet temperature (t_{il}) is lower for the HC_I model, indicating that the benefit of increasing t_{il} will have smaller impact on the HC_I compared to COP_I . On the other hand, increasing the load flow rate (v_l) will have higher impact on the HC_I compared to COP_I . The standard errors of each of the coefficients are the margins for the model output to remain within a 95% confidence interval of the predicted values. They are all seen to be minor compared to the coefficients.

Additionally, the p-values for each of the coefficients represent the probability of each of the predictor variables being insignificant for the model result. For most of the coefficients in the two models, the p-values are lower than 0.0001, i.e. it is certain that the corresponding variables are important for the predicted HC or COP . Two exceptions are the v_s^2 variable in the HC_I model and the $v_s t_{il}$ variable in the COP_I model which have p-values of 0.0007 and 0.0046 respectively. However, since these p-values remain quite low, the x -variables can be considered to be significant at the 95% level.

Table 5.2. Model coefficients and statistics (Model for HC_I)

| Parameter | Coefficient | Std. Error | P-value |
|------------------|--------------------|-------------------|----------------|
| Constant | 25.325 | 0.1701 | 7E-41 |
| v_s^2 | 0.1176 | 0.0309 | 0.0007 |
| $t_{is} v_s$ | 0.232 | 0.002 | 4E-38 |
| $t_{is} v_l$ | 0.0457 | 0.002 | 2E-19 |
| $v_s v_l$ | 0.6882 | 0.0691 | 2E-10 |
| $t_{il} v_l$ | -0.0212 | 0.0021 | 9E-11 |
| t_{is} | 0.0543 | 0.004 | 1E-13 |
| t_{il} | -0.0313 | 0.0029 | 3E-11 |
| v_l | 1.4856 | 0.1722 | 3E-09 |

Table 5.3. Model coefficients and statistics (Model for COP_I)

| Parameter | Coefficient | Std. Error | P-value |
|------------------|--------------------|-------------------|----------------|
| Constant | 7.8871 | 0.2042 | 4E-25 |
| t_{il}^2 | 0.0025 | 0.0001 | 3E-16 |
| $t_{is} v_s$ | 0.0432 | 0.0024 | 2E-16 |
| $t_{is} t_{il}$ | -0.0009 | 0.0001 | 2E-08 |
| $t_{is} v_l$ | 0.0153 | 0.0026 | 3E-06 |
| $v_s t_{il}$ | -0.007 | 0.0022 | 0.0046 |
| $t_{il} v_l$ | -0.018 | 0.0032 | 7E-06 |
| t_{il} | -0.222 | 0.0118 | 5E-17 |
| v_l | 1.0687 | 0.1215 | 2E-09 |

The mapping method for the identification of MR models was found valid for the prediction of the HP1 catalogue data. Therefore, the same operational approach is used to develop MR models for HP2 and HP3 data. Subscripts 2 and 3 are the response y-variables notations as representing the studied HP2 and HP3 respectively.

The results on the statistical evaluation of MR models for HP1, HP2 and HP3 are listed in Table 5.4. These results indicate the R-square values adjusted for degrees of freedom, the F-

5.2 Regression analysis

significance resulting from the analysis of variance table, the external CV, as well as the external the root mean square of error (RMSE) when applying the model to the remaining of the observations. The adjusted R-square value for all the models is seen to approach unity, except for the COP_2 model, where the adjusted R-square statistic explains only 97.888% of the variability in COP_2 . Overall, such high values indicate that the independent x -variables used in the models can jointly predict the variation in the outcome with a high accuracy. Moreover, all six models are statistically strong judging from the F-significances.

Table 5.4. Summary of statistical evaluation of MR models for HP1, HP2, and HP3

| Model | Adjusted R ² | F-significance | External RMSE | External CV |
|---------|-------------------------|----------------|---------------|-------------|
| HC_1 | 99.996% | 4E-43 | 0.0710 | 0.21% |
| COP_1 | 99.843% | 3E-38 | 0.1290 | 2.62% |
| HC_2 | 99.960% | 3E-45 | 0.2817 | 0.95% |
| COP_2 | 97.880% | 5E-22 | 0.2367 | 4.91% |
| HC_3 | 99.942% | 4E-43 | 0.0842 | 1.02% |
| COP_3 | 99.868% | 3E-38 | 0.1564 | 3.21% |

The external CV values suggest of a good model fit for each of the six models (i.e. CV inferior to the 5% threshold value), the COP models describing a slightly poorer fit in terms of relative closeness of the predictions to the actual values. The RMSE shows the standard deviation of the residuals. The standard error for all the models is relatively small compared to the ranges of HC and COP . This is illustrated in Figure 5.3, where the predicted values for the HC_1 and COP_1 model are plotted against the observed. It is evident that the predicted heat capacities are very close to the observed values. The prediction is seen to be slightly poorer with the COP_1 model, confirming graphically the difference of external CV values between these two models.

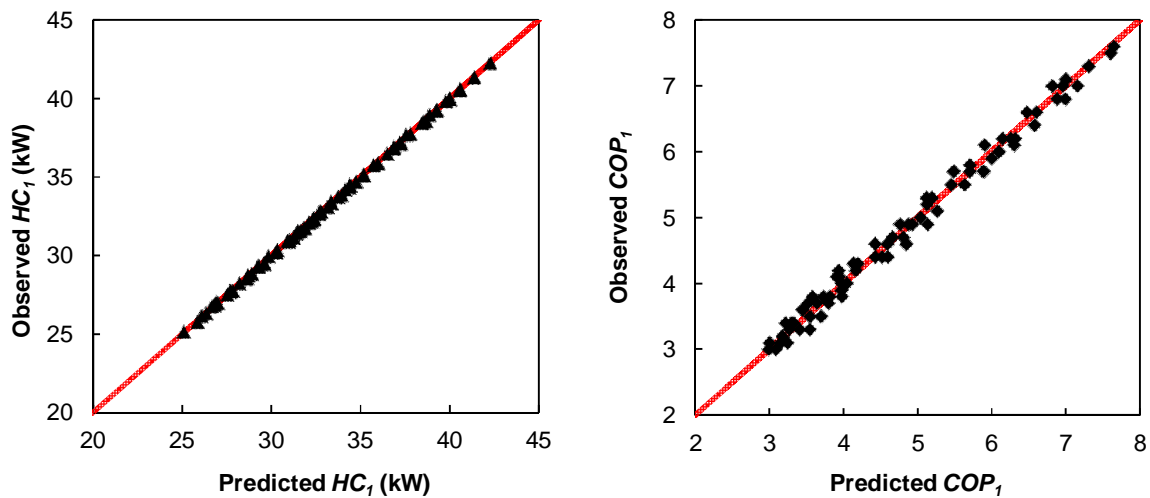


Figure 5.3. Plot of HC_1 (kW) and COP_1 observed versus predicted

The CV values in Table 5.4 reveal that the size of the residual relative to the predicted value is bigger for COP models compared to HC models. However, when considering the range value of HC compared to COP , the size of residuals is not so different in term of absolute value. For instance, the standard error is smaller for the COP_2 model than it is for the HC_2 model, although the range value of HC_2 is higher. This remark is illustrated in Figure 5.4, 5.5, and 5.6, which depict the external residuals plotted against the predicted y -variables. In the six charts, no specific pattern formed by the external residuals can be observed, thus verifying that residuals are independent and have constant variance.

There are only three data points which are outliers (greater than ± 2) in the model for HC_1 , and two outliers in the model for COP_1 . For these data points, the model prediction output is poorer. There are seven and five outliers respectively in the models for HC_2 and COP_2 , while there are one and three outliers in the model for HC_3 and COP_3 . However, the fit is overall excellent for each of the six models. The maximum difference of obtained predicted values as compared with the observed manufacturer data are less than 1% and 7% for COP_1 and HC_1 predictions, 3% and 16% for HC_2 and COP_2 , and 3% and 12% for HC_3 and COP_3 respectively. These errors concern only a few individual points, particularly these in the lower range values.

5.2 Regression analysis

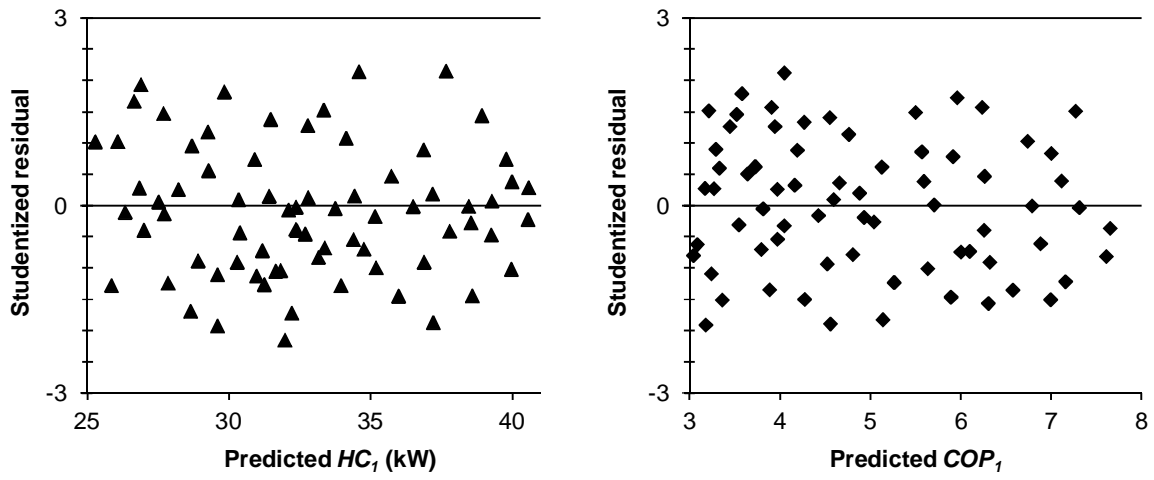


Figure 5.4. Plot of residuals versus predicted HC_1 (kW) and COP_1

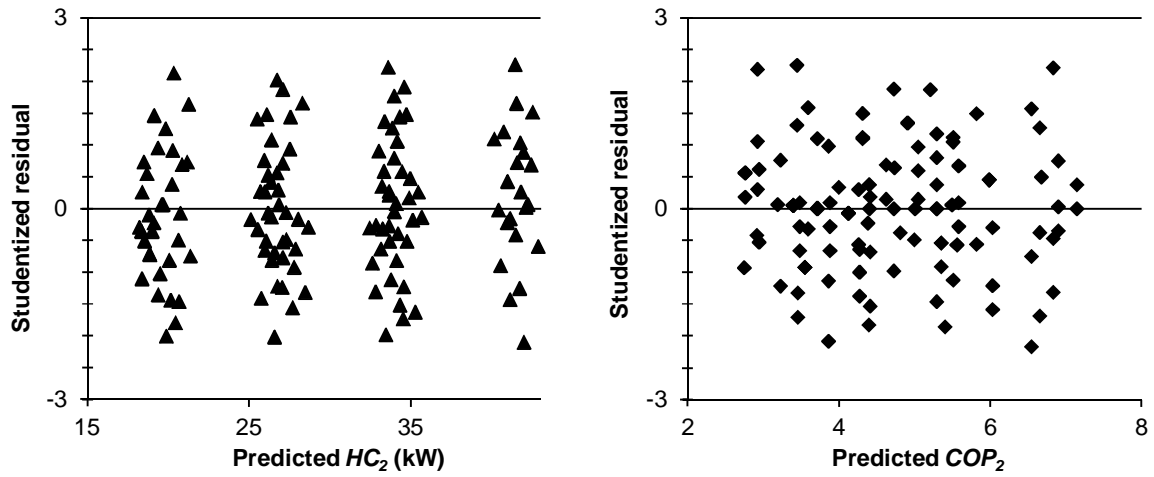


Figure 5.5. Plot of residuals versus predicted HC_2 (kW) and COP_2

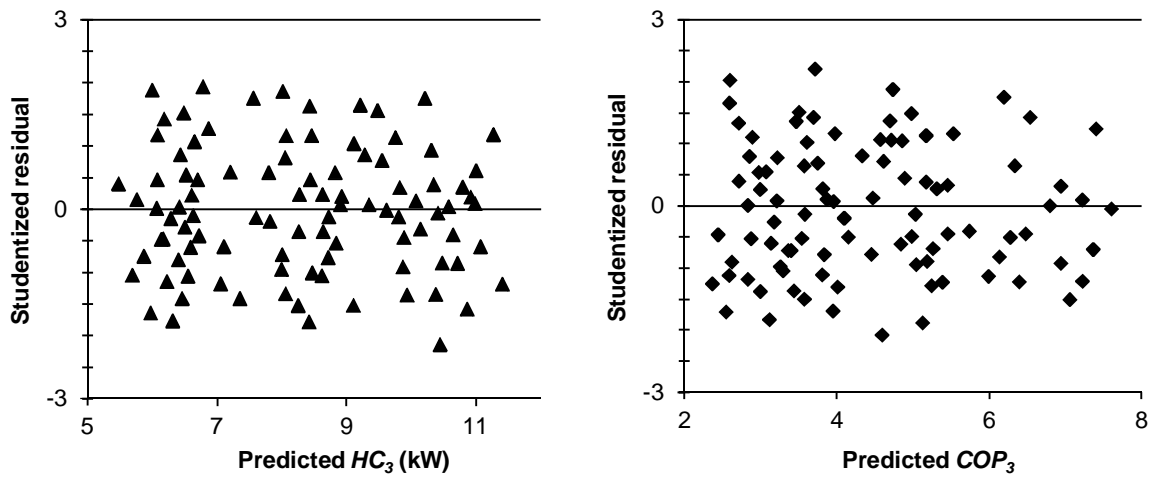


Figure 5.6. Plot of residuals versus predicted HC_3 (kW) and COP_3

5.2.3 Discussion

The statistical evaluation of the models identified for HP1 has demonstrated the influence of the number of significant x -variables and their order level on prediction accuracy. The meaning of the observation sample size on model robustness and prediction error was also investigated. It was found that the global GSHP behavior cannot be predicted accurately when fitting MR models from the 12 observations sample. When the degree of freedom is low, the models tend to capture the errors present in the observation data, thus leading to model over-fitting. The 24 observations are sufficient to achieve acceptable levels of accuracy for *HC*, even with a low number of x -variables, as well as for the *COP* with second-order models including at least five significant x -parameters. Model robustness increased and prediction error dropped for models fitted from the 36 observation set as compared to these identified from 24 observations. However, the only models which were statistically validated are second-order models identified from the 36 observations and containing eight x -variables, for which the residuals checking revealed no specific pattern formation.

Following the validated model identification method, the six models introduced in the study are found excellent with these of *COP* being slightly poorer. Such results indicate that the manufacturer data is certainly data generated from a controlled experiment and is not data collected from the field. The high R-squares, such as those over 99.9% are also an indication of model over-fitting. In that sense, our guess is that the observation data are actually based on a regression model developed by the heat pump manufacturers, and that the model used for *HC* data is in fact a second-order one. The proprietary regression models used by the manufacturer to generate the performance data tables were closely reproduced, particularly with the models for *HC*.

The operational approach consisting in the identification of MR models containing eight significant independent variables from a set of 36 observations can be employed to predict the performance of GSHPs with quite good precision. The proposed mathematical models appear to be reliable tools to be implemented into dynamic building-plant energy simulation codes or into building energy certification tools. Indeed, the proposed method can be applied to any GSHP, to

determine HC and COP in heating mode or CC and EER in cooling mode using their corresponding performance data tables.

Using multiple regression calculation demonstrates that it is possible to rapidly create equation linking different variables, such a model being representative of the GSHP global behavior with acceptable accuracy and applicable over the entire solution space. However, such a method can be time consuming for services designer. Besides, data of the equipment operating range and capacity are generally sufficient when it comes to heat-pump selection for a particular building. This is why suppliers provide performance data listed in tables instead of offering MR models in their catalogue. It is more practical for engineers to utilize these tables rather than mathematical models for their professional use.

5.3 Analysis of input parameter influence on residential energy use

Following the methodology introduced in section 4.3, this particular study investigates the energy use in a reference household (BCH) in various cities throughout Chile across different climate regions. The results from this reference Chilean household are compared to the energy use of hypothetical homes having different orientations or consisting of different performance envelope components, in order to show in which proportion energy savings can be achieved with appropriate building orientation or improved construction materials. The study demonstrates the degree and impact of several factors which affect residential energy usage. These include, among others; building envelope materials, solar radiation and local environments. A financial analysis presenting the economic viability (payback period) of a set of envelope improvements is included, which shows the effectiveness of such design measures for energy savings and carbon emissions reductions.

5.3.1 Simulated energy use and model validation

The thermal transmission U-values expressed in ($\text{W}/\text{m}^2\text{K}$) for each building component are shown in Table 5.5. Using the MEEDI model, the annual heating and cooling energy use for the BCH (E_{BCH}) was found for both scenarios at each location (Figure 5.7). The discrepancy between scenario 1 and 2 is due to the difference in overall efficiency of the selected heating systems. Results show that using radiant heaters compared to gas-fired heating system for equivalent thermal energy production is more expensive and produces more carbon emissions, even though gas heating system has lower overall energy efficiency. This clearly demonstrates the disadvantage of electrical heating versus gas heating system, which has significantly lower fuel cost and CO_2 emission factor.

Table 5.5. BCH envelope component U-values

| Component | U-value ($\text{W}/\text{m}^2\text{K}$) |
|---------------|---|
| Exterior Wall | 0.29 |
| Ceiling | 0.25 |
| Floor | 0.30 |
| Windows | 1.80 |
| Doors | 1.80 |

5.3 Analysis of input parameter influence on residential energy use

In order to test the predictive accuracy of the MEEDI model, a comparison with the EnergyPlus simulation software is proposed. The characteristic parameters of the BCH and the climate data of the studied locations were input in EnergyPlus during the verification process. The annual energy use E for each city and energy scenario as calculated by the EnergyPlus software is plotted in Figure 5.7. The prediction deviations can be explained by considering that MEEDI is derived from the quasi-steady-state approach, in which a monthly averaged radiation and temperature is assumed, neglecting all effects due to the hourly variation. Furthermore, the utilization factor may not be sufficient to reproduce the thermal inertia effect, especially for cooling energy consumptions, which appear to be underestimated by the MEEDI model.

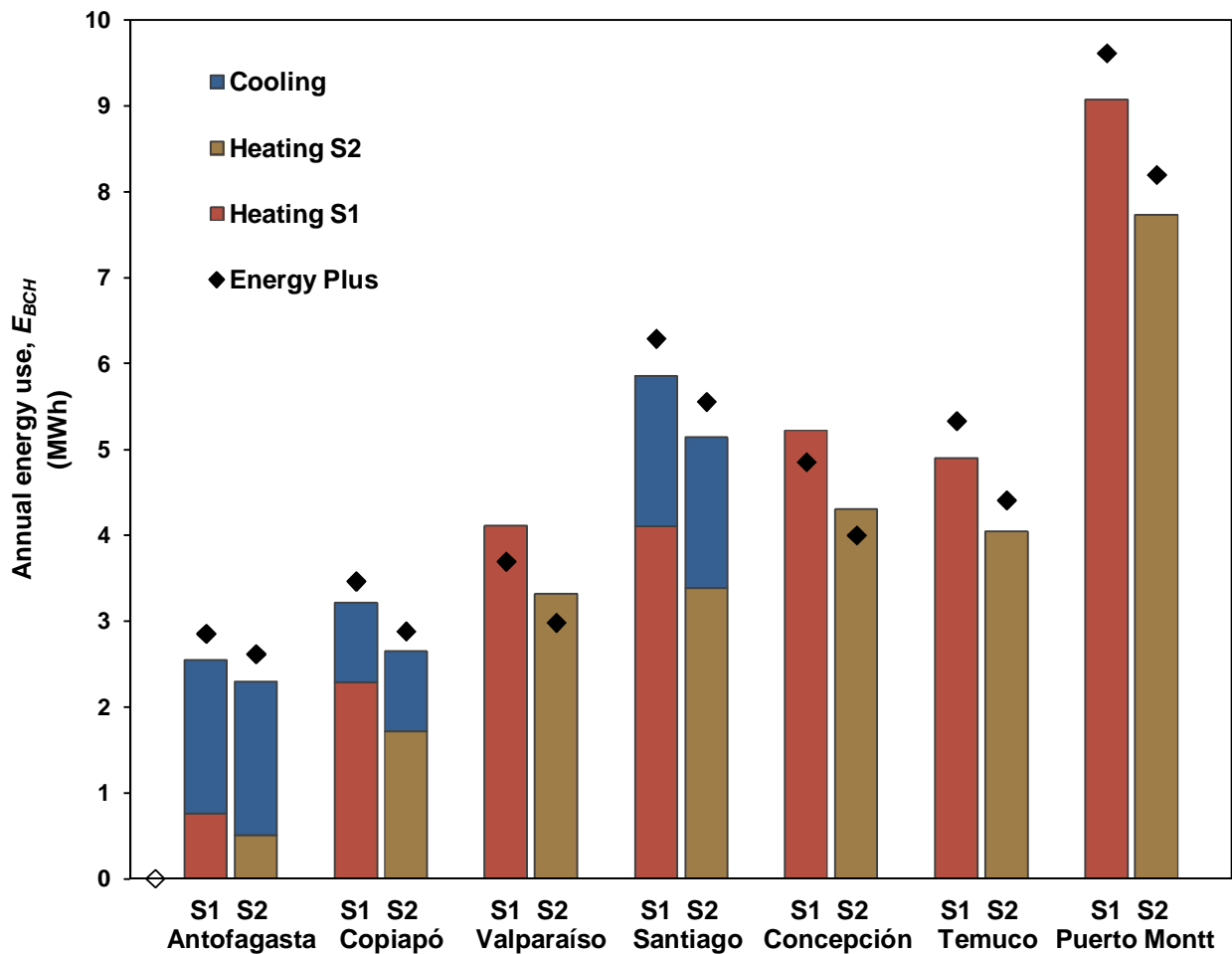


Figure 5.7. BCH annual energy use for scenario 1 and 2 (S1 and S2)

Nevertheless, the comparison shows that predictions are in acceptable agreement for all climate conditions and energy scenarios. Particularly, the average deviation between MEEDI and EnergyPlus simulators in calculating the annual energy use is 8%. Therefore, the MEEDI tool can be useful for energy investigations on the influence of the various input parameters to the calculated energy use.

5.3.2 Influence of envelope factors on energy use

This section investigates building envelope materials and their influence on annual energy use E . MEEDI has been used to investigate a set of refurbishment measures, referencing energy use from the BCH with the thermal management system of scenario 1. The results are shown in Figure 5.8, where E is plotted as a function of the following parameters, wall and ceiling insulation thicknesses, window and door U-values and infiltration/ventilation rate. For each parameter, the characteristics of the BCH are the reference points. Energy use from scenario 2 is not included here, but results would yield similar trends.

In order to reduce space heating and cooling energy consumption, a frequent measure is to add insulation. The influence of insulation on the energy use depends mainly on the surface dimensions and the insulation thickness. Figure 5.8(a) and Figure 5.8(b) illustrate the influence of additional insulation at the walls and ceiling, respectively. Figure 5.9 shows the ratio of the calculated energy usage (E) over that of the BCH (E_{BCH}) as a function of the additional thickness of wall/ceiling insulation in Santiago. The influence of the insulation thickness for each investigated region is clear for the first 0.05 m, particularly for walls. From an economic perspective, it is advantageous to find the optimal insulation thickness. The improvement of the wall U-value induced by thicker insulation does not necessarily have to be very significant to reduce the energy use. This is because of the larger area of the walls compared to the ceiling. For example, Figure 5.9 shows that the addition of 0.12 m wall insulation in Santiago climate reduces the annual energy consumption by almost 9%, while the same measure on the ceiling results in a reduction of just over 6%.

5.3 Analysis of input parameter influence on residential energy use

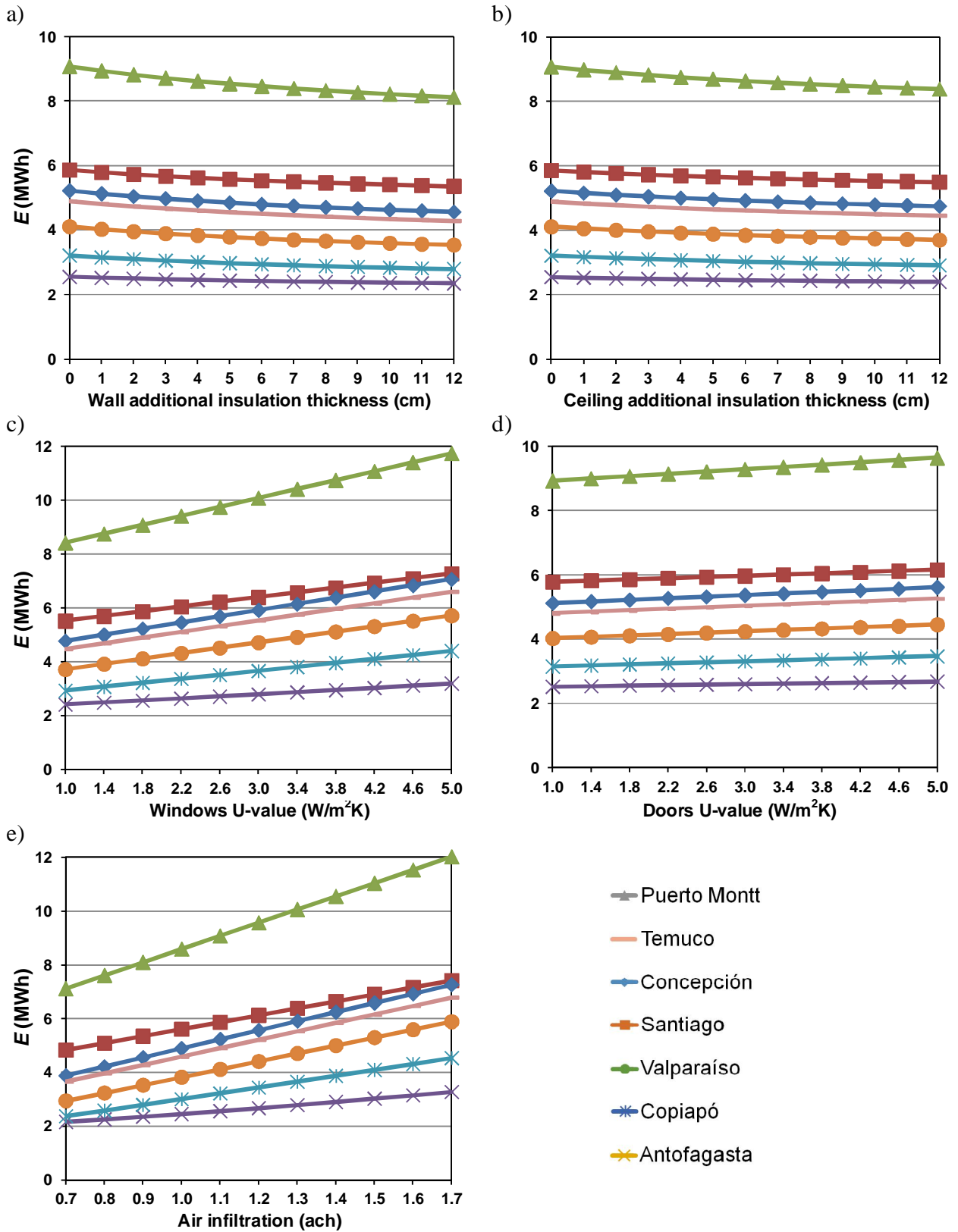


Figure 5.8. Influence of wall (a), ceiling (b) additional insulation thickness, windows (c), doors (d) U-values, and air infiltration rate (e) to the annual energy use E

Windows usually represents a small fraction of the total envelope area and doors even less. However, due to high heat transmittance characteristics compared to other envelope components, significant energy savings can be achieved by reducing their U-values, as shown in Figure 5.8(c) and Figure 5.8(d). Windows and doors should be able to provide reasonable resistance to thermal energy transfer. Although the U-value of openings varies due to the commercial availability of different types of windows and doors, its influence on the energy consumption is linear (Figure 5.10). The replacement of windows of U-values from 5.0 to 1.0 ($\text{W}/\text{m}^2\text{K}$) reduces the energy use by 30% to 48% depending on the location, which is considerable, especially in regions with high heating requirements. Replacing doors of U-values from 5.0 to 1.0 ($\text{W}/\text{m}^2\text{K}$) results in energy use reductions by 6% to 10% depending on the location. The reduction differences observed between locations are explained by considering the differences in local solar radiations.

Another important parameter that influences the energy usage is air infiltration/ventilation. The larger is the volume of air flowing through the building, the more energy is demanded to heat or cool the entering outside air. Thus, air infiltration/ventilation can represent a considerable loss of energy. Figure 5.8(e) shows that improving the rate of air infiltration/ventilation from 1.7 to 0.7 in the BCH means a reduction of annual energy use by 43% to 72% depending on the location.

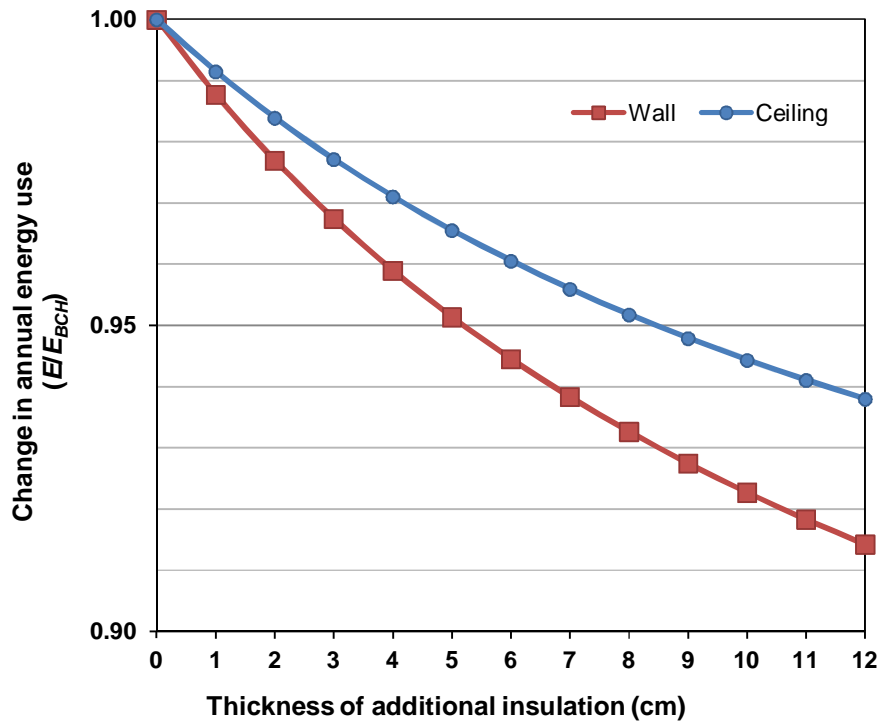


Figure 5.9. Influence comparison of wall/ceiling insulation thickness on annual energy use in Santiago

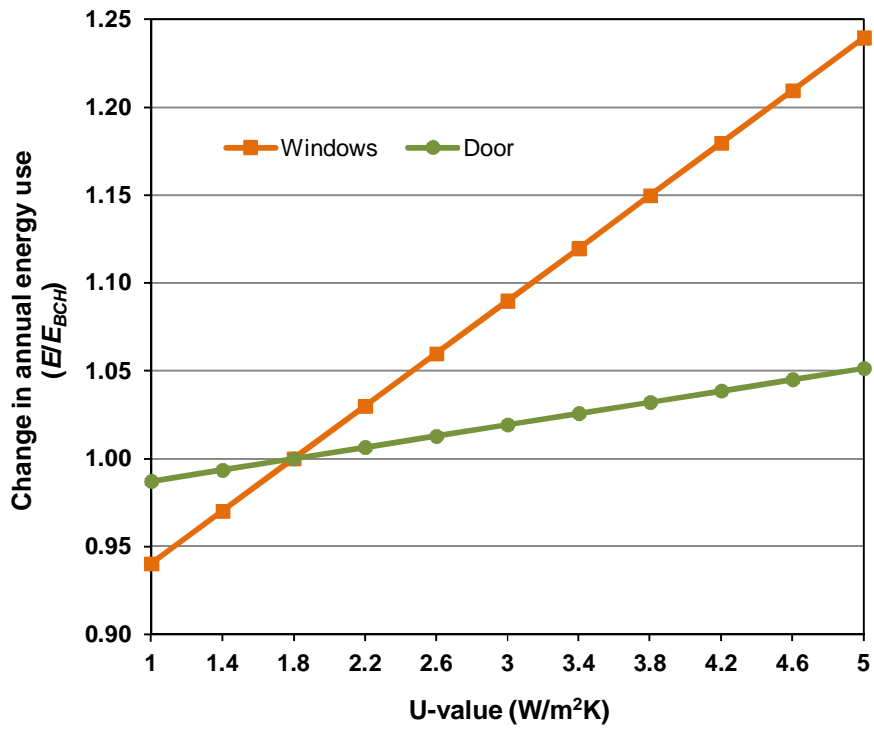


Figure 5.10. Influence comparison of window/door U-value on annual energy use in Santiago

5.3.3 Influence of building orientation on energy use

The thermal transmittance of windows is generally much higher than that of other envelope components. However, in regions with high solar radiation, the appropriate placement of windows can result in significant solar heat gains in winter, which can reduce energy use. This section investigates the potential savings on energy use based on the contribution of the solar heat gains related to the building orientation. Figure 5.11 shows the annual solar gain through windows of the BCH side 1 as a function of its direction. When the side 1 is directed towards the north (azimuth = 0°) solar gains will be 2.3 to 2.8 higher depending on the location than when directed towards the south. The difference between sites is due to local available solar radiation.

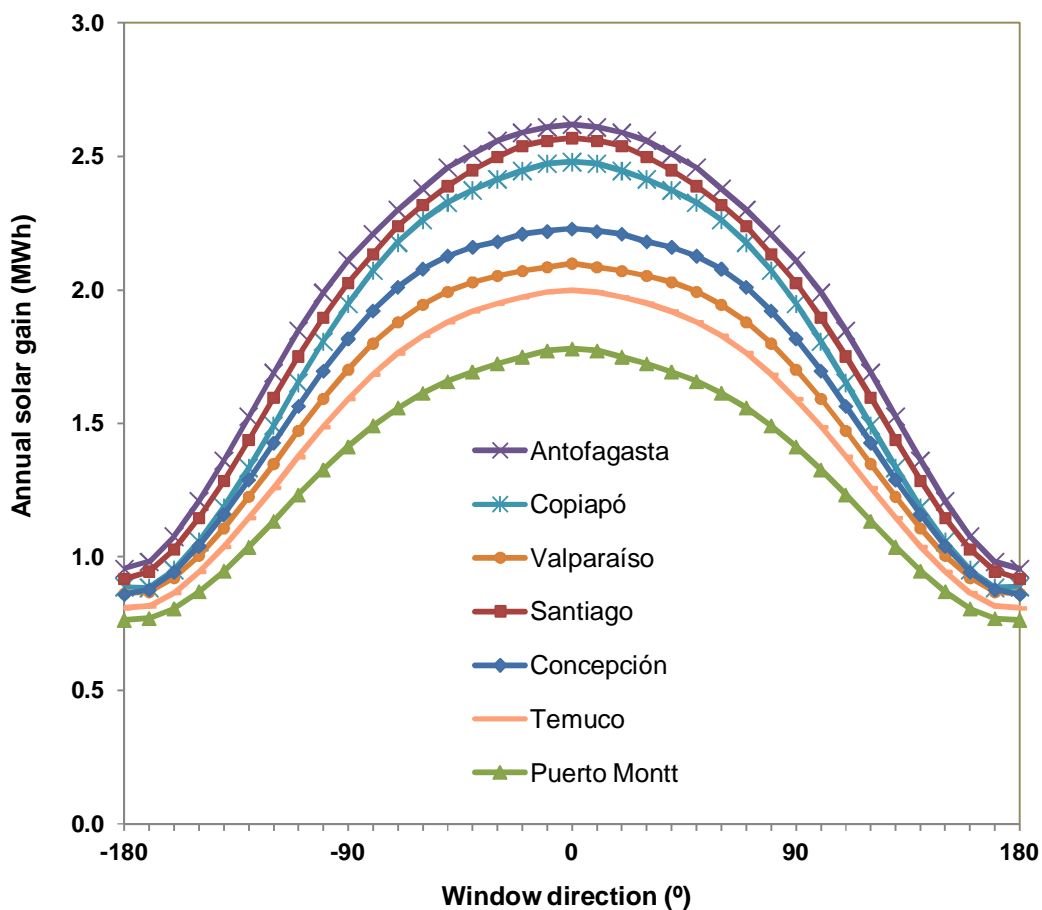


Figure 5.11. Annual solar gain through side 1 windows

The orientation of the building has not the same influence on the annual energy use at different locations. Figure 5.12 shows that the BCH rotation has the highest impact on the energy use in Antofagasta, where the energy demand is the lowest and the solar radiation the highest. The impact on the energy use is also slightly different between east and west orientations, due to the BCH window distribution. In that sense, the influence of the building orientation would be lower for buildings having a uniform window distribution at different directions.

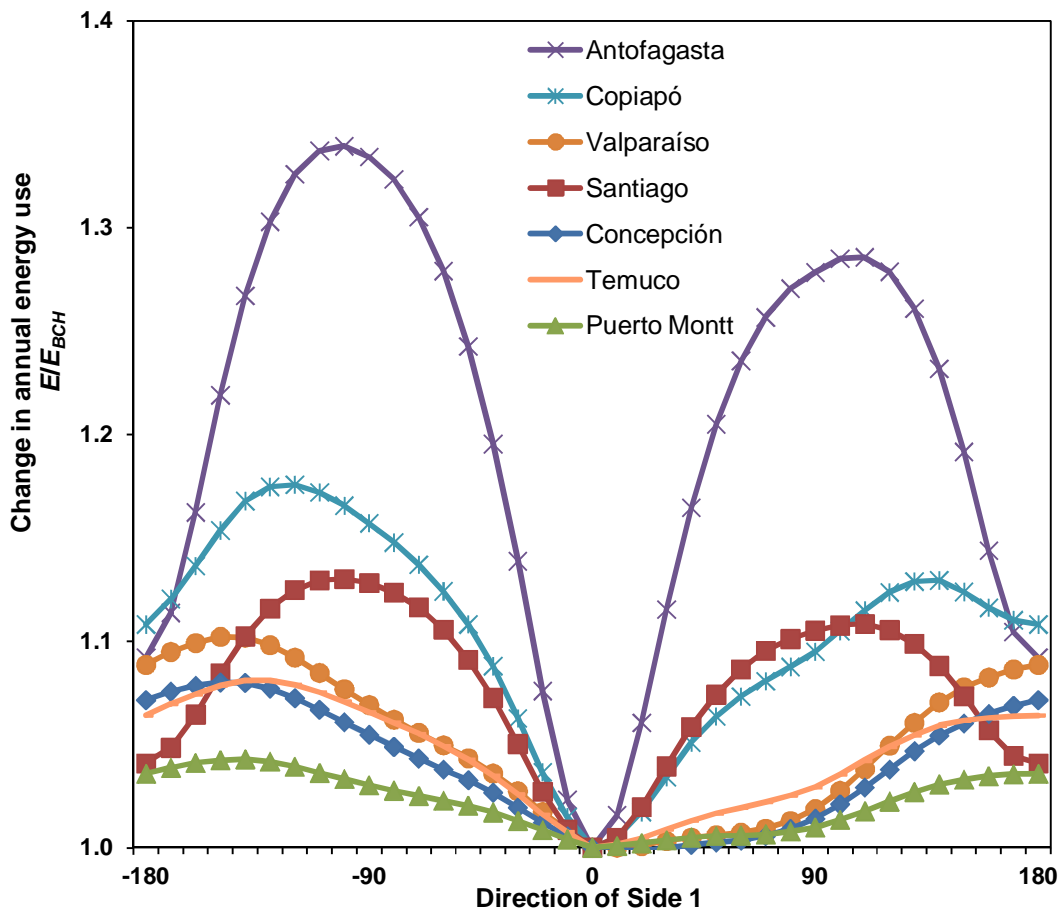


Figure 5.12. Influence of BCH orientation on annual energy use

Figure 5.13 shows a three-dimension result for the BCH with the thermal management system of scenario 1 in Santiago. It displays the relationship between the building orientation (solar gains), the ratio of window-to-total envelope area and the change in annual energy use. The BCH has the optimal orientation when side 1 is facing north, because the heating demand is superior to the cooling demand. An increase of the window area from 12% (as in the BCH) to 50% of the total envelope area results in an increase of the annual energy use of 31%, despite higher solar gains. This is due to the higher U-value of windows compared to that of walls, ceiling and floor.

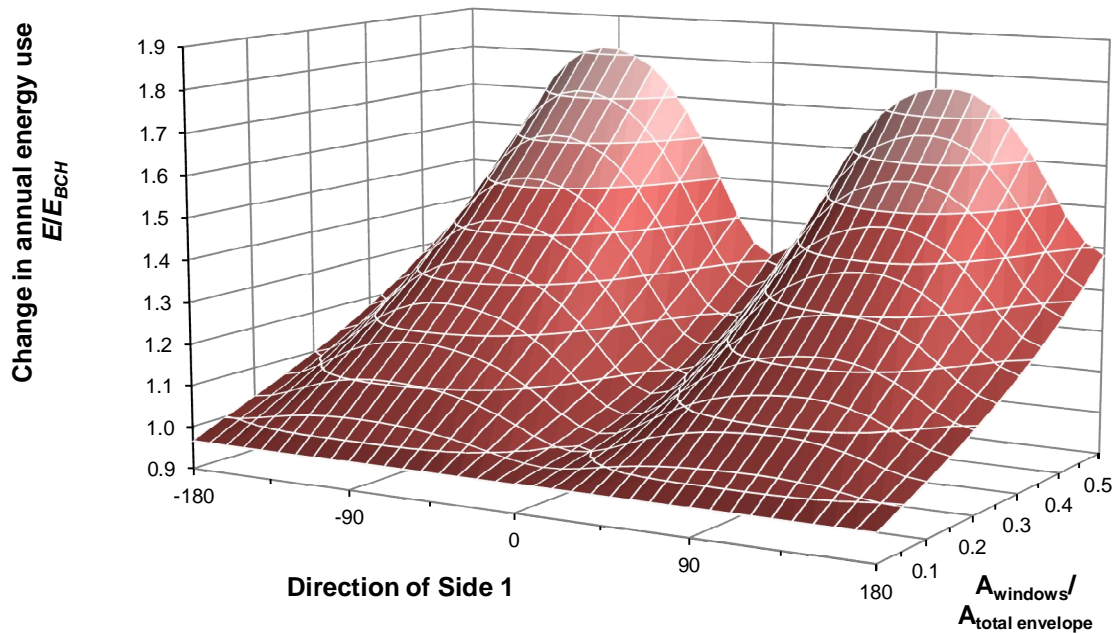


Figure 5.13. Influence of window area and building orientation on annual energy use in Santiago

5.3.4 Financial analysis

As seen in section 1.2.7.2, almost 80% of homes in Chile were built before 2000 and about half of these before 1976 [93]. Older homes are usually built with heavier structural materials and few of them have thermal insulation unless they have been refurbished or restored. In this section, a financial and environmental analysis is conducted. Such analysis compares the annual energy use between the BCH and a typical Chilean home featuring lower performance envelope materials referred to as “*Low-Efficiency Home*” (LEH). The framework and dimensions are identical for each home in question. The envelope characteristic differences of the LEH as compared to the BCH are given in Table 5.6.

For this purpose, it is considered the additional investment during the construction stage for the different envelope components of the BCH compared to those of the LEH, and their potential energy use savings. It is assumed that the installation of the higher performance coated windows ($U = 1.8 \text{ W/m}^2\text{K}$) instead of single glazed ones ($U = 5 \text{ W/m}^2\text{K}$), as well as a higher performance door at the construction stage for the BCH represents an additional investment of US\$ 3,000 considering six windows with a total area of 10.5 m^2 and one entrance door. The over-cost for the insulation fabric is estimated to be US\$ 5,000 for the entire envelope. These additional costs are due almost entirely to the differences in material costs, not installation. The additional cost for the building air tightening, which involve mainly draught-proofing, is estimated to be US\$ 1,000 to reduce the air infiltration/ventilation rate from 1.7 to 1.1 ach.

Table 5.6. Physical characteristics of the LEH

| Component | Difference with BCH | U-value ($\text{W/m}^2\text{K}$) |
|------------------------------|--|--|
| External wall | Insulation thickness $t = 0.04 \text{ m}$ | 0.51 |
| Ceiling | Insulation thickness $t = 0.08 \text{ m}$ | 0.44 |
| Floor | No insulation | 0.38 |
| Window | Wood frame, Single glazed 4mm, $\tau_w = 0.78$ | 5.0 |
| External door | Wood solid core | 5.0 |
| Air infiltration/ventilation | High draught, $n = 1.7 \text{ ach}$ | |

The energy performance characteristics of building envelope materials have a direct impact on space heating and cooling energy use. The annual savings on energy use achieved by the BCH as

compared to the LEH for both scenarios at each location are displayed in Table 5.7, along with payback periods for the set of higher performance materials present in the BCH. Savings vary for each location due to site climate conditions and for each scenario due to energy system efficiencies. As billing costs and carbon emission factors are directly linked with energy use, identical savings are found on both running costs and CO₂ emissions between LEH and BCH, except for three cities in scenario 1, where heating and cooling are provided by different energy sources. For Antofagasta, Copiapó and Santiago in scenario 1, savings are respectively 39%, 51% and 41% on running costs and 35%, 49% and 39% on carbon emissions. Although the heating energy system in scenario 1 is less efficient than that in scenario 2, savings in energy use and carbon emissions are more significant for scenario 2, principally due to the higher cost and emission factor for electricity compared to natural gas. Payback periods are shorter for scenario 2 for the same reason.

Payback periods for each location are found acceptable, well within the range of building lifetimes. Locations with higher heating and cooling demands have shorter payback periods for the proposed envelope improvement measures. For example in Puerto Montt, where energy demand is the highest among the studied cities, the payback period is the shortest. Insulation is much more effective in extreme climates, where the potential for absolute energy savings is greater. The same analysis applies for carbon emission reductions. For example, greatest carbon savings can be achieved between the LEH and BCH in regions where energy demand is the highest, such as in Puerto Montt, Temuco and Concepción.

Table 5.7. Annual energy savings from BCH to LEH and payback periods

| City | Scenario 1 | | Scenario 2 | |
|---------------------|---------------------------|------------------------|---------------------------|------------------------|
| | Annual energy use savings | Payback period (years) | Annual energy use savings | Payback period (years) |
| Antofagasta | 48% | 31.3 | 46% | 22.4 |
| Copiapó | 55% | 19.2 | 57% | 12.9 |
| Valparaíso | 56% | 14.5 | 59% | 9.5 |
| Santiago | 46% | 15.5 | 46% | 10.3 |
| Concepción | 54% | 12.6 | 56% | 8.2 |
| Temuco | 54% | 13.5 | 56% | 8.8 |
| Puerto Montt | 50% | 8.5 | 51% | 5.5 |

Chapter 6 – Conclusions

Driven by the introduction of energy agencies, programs and regulatory frameworks from Chilean authority bodies to reduce the country's dependence on energy imports and comply with targets to reduce carbon dioxide emissions, the energy sector is observing a boom in solar energy installations. On the other side, the construction industry is experiencing a strong push towards the improvement of the energy performance of new and refurbished buildings. Much work has been carried out in this area in Chile, including the approved building thermal regulations, which is inspired by regulation frameworks adopted by countries of the European Union. All this is occurring under the National Energy Strategy 2012-2030 plan, which lists energy efficiency and renewable energy generation as priorities number one and two.

The study introduces a simulation model to predict LCOE evolution of three different types of large scale solar power plants for clean electricity generation in the Atacama solar platform in Chile. Results indicate that from 2014 to 2050, LCOE decreases by 35% for the PV plant, by 42% for the CSP plant with TES, and by 41% for the hybrid PV-CSP power plant with TES. This particular investigation has important ramifications for the energy industry in Chile, especially for mining companies located in the studied area. Chile has a rich solar resource, which exploitation is still in its infancy. The main concern regarding solar energy is the discontinuity, intermittency of electricity production. However, the hybrid PV-CSP mix modeled in the study is a sound solution to this problem. The hybrid PV-CSP mix in the Atacama desert is a promising option for sustainable power generation. It represents a reliable and clean solution to the concern

of power supply in Chile, particularly because it could satisfy the continuous power demand of the large local industries that mostly rely on fossil fuel resources.

Additionally, it is important to note that the solar resource in the Atacama desert is greater than that of other sunny areas where huge solar energy projects have been developed, such as the two leading countries in solar investment, the US and Spain. This means that there is an untapped natural resource that can also be converted into a profitable endeavor for public and private companies. Foreign energy investors should pay special attention to this geographic area, given that the unused solar resource could be the future source of power for the mining industry in Chile, which is in the same time seeking solutions for reducing its environmental impact.

The investigation, in its second specific objective, suggests a methodology for predicting the performance of GSHPs at particular operating fluid temperatures and flow rates conditions using multiple regression models as applicable to manufacturer catalogue data. Indeed, for higher level system modeling and simulation purposes, GSHP performance data in the form of tables provided by equipment manufacturers are not convenient. The mathematical models developed in this study estimate the heat capacity and *COP* at particular operating secondary fluids temperature and flow rate conditions based on manufacturer data tables. The proposed operational procedure, which consists in the identification of second-order MR models containing eight statistically significant *x*-variables from a sample of 36 observations taken from the manufacturer table, was successfully validated in the statistical analysis. Predicted performance results are in good agreement with the remaining of observed data, the external prediction errors reaching 0.21%, 0.95% and 1.02% for *HC* predictions, and 2.62%, 4.91% and 3.21% for *COP* predictions for HP1, HP2 and HP3 respectively. The external residual errors as plotted against the model responses showed no correlation with the regression coefficients or the prediction response, thus validating the models. The operational approach appears to be a reliable tool to be incorporated in dynamic simulation codes developed by engineers, as the method is applicable to any GSHP catalogue data.

This particular study also shows that global GSHP behavior can be predicted when fitting MR models from a limited number of observation data. Nevertheless, the limitation to a smaller data set for model identification may remain questionable when the full data set is available in the manufacturer catalogue. Results indicate that manufacturers do not need to provide tables with

such a large amount of data points to specify the complete performance map of GSHP. On the other hand, the experimental design evaluations provide insights into how experiments in actual operating GSHP systems should be conducted.

Moreover, results from the proposed parsimonious MR models point out that manufacturer data may be generated from proprietary regression models. Since no goodness-of-fit of the latter is provided, some caution must be exercised in the use of such data and corresponding models identified.

In relation to the third specific objective, the study introduced a BES tool which can be used for parametric sensitivity investigations of energy efficiency in the home, and how envelope improvement measures and building orientation affect the energy consumption. The proposed MEEDI model is based on the ISO13790 monthly calculation method and two improved procedures for the calculation of the solar gain and the heat transfer through the floor. The model predictive accuracy was tested with the EnergyPlus simulation software and an average deviation of 8% was observed in calculating the annual energy use. Thus, the MEEDI program was found reliable for investigations on the influence of physical and meteorological input parameters to the calculated energy use.

Although the MEEDI model was used to evaluate the particular energy demand of a typical Chilean home, it has the flexibility to allow testing with a series of scenarios; it can calculate efficiency for different types of envelope materials, climate conditions, and energy systems, among others. The MEEDI permits such future investigations, which could utilize different parameters for the financial viability of small-scale renewable energy systems depending on the specific characteristics of the region to be analyzed.

Despite the inclusion of climate conditions, this work primarily emphasizes the influence of building envelope materials on energy efficiency in the home. The outcome of the introduced procedure is illustrated in graphical figures in sections 5.3.2 and 5.3.3. These figures can be used to identify the influential parameters to the energy use and validate effective retrofitting measures. The proposed MEEDI simulation tool can also be used in the design process of new buildings for investigations of how design measures can influence energy use and CO₂ emissions in particular.

The results show how reductions of energy use and CO₂ emissions can be achieved with higher performance envelope components compared to a typical poorly insulated home. The impact of enhanced envelope U-values in the BCH as compared to the LEH is a savings between 48% and 59% on energy use and between 35% and 59% on CO₂ emissions depending on the location and energy system scenario. The economic viability analysis of specific measures for building envelope materials reveals payback periods well within the range of building lifetime, from 6 to 31 years depending on location and energy scenario. The investigation proves that energy efficiency can be an effective strategy to address the issue of growing energy demand, and to develop a more sustainable home in Chile.

Conclusiones

Impulsado por las agencias de energía, los programas y los marcos regulatorios por parte de las autoridades chilenas, con el objetivo de reducir la dependencia de las importaciones de energía del país y cumplir con metas de reducción de emisiones de dióxido de carbono, el sector energético está observando un auge de las instalaciones de energía solar. Por otro lado, la industria de la construcción está experimentando un fuerte impulso hacia la mejora del rendimiento energético de los edificios nuevos y los reformados. Se ha trabajado mucho en esta área en Chile, incluyendo el reglamento térmico aprobado, que se inspira en los marcos de regulación adoptados por los países de la Unión Europea. Todo ello en el marco del Plan Nacional de Energía 2012-2030, que hace referencia a la eficiencia energética y la generación de energía de fuentes renovables como prioridades número uno y dos.

El estudio introduce un modelo de simulación para predecir la evolución del LCOE de tres tipos diferentes de plantas de energía solar de gran escala para la generación de electricidad limpia en la plataforma solar de Atacama en Chile. Los resultados indican que de 2014 a 2050, el LCOE disminuye en un 35% para la planta fotovoltaica, en un 42% para la planta CSP con TES y en un 41% para la planta híbrida PV-CSP con TES. Esta investigación tiene ramificaciones importantes para la industria energética en Chile, especialmente para la industria minera ubicada en el área estudiada. Chile tiene un rico recurso solar, cuya explotación aún está en su infancia. La principal preocupación con respecto a la energía solar es la discontinuidad e intermitencia de la producción de electricidad. Sin embargo, la mezcla híbrida de PV-CSP, modelada en el estudio, es una solución sólida a este problema. La mezcla híbrida de PV-CSP en el desierto de

Atacama es una opción prometedora para la generación de energía sostenible. Representa una solución fiable y limpia a la preocupación por el suministro de energía en Chile, sobre todo porque podría satisfacer la demanda continua de energía de las grandes industrias locales que dependen en su mayoría de los recursos de combustibles fósiles.

Además, es importante señalar que el recurso solar en el desierto de Atacama es mayor que el de otras áreas soleadas donde se han desarrollado enormes proyectos de energía solar, como los dos países líderes en inversión solar, Estados Unidos y España. Esto significa que hay un recurso natural sin explotar que también puede convertirse en un esfuerzo rentable para las empresas públicas y privadas. Los inversionistas extranjeros de energía deben prestar especial atención a esta área geográfica, dado que el recurso solar no utilizado podría ser la fuente futura de energía para la industria minera en Chile, que al mismo tiempo busca soluciones para reducir su impacto ambiental.

La investigación, en su segundo objetivo específico, sugiere una metodología para predecir el rendimiento de GSHPs a condiciones particulares de temperaturas y caudales de los fluidos de funcionamiento utilizando modelos de MR aplicables a los datos de catálogo de fabricantes. De hecho, para fines de modelación y simulación dinámica de sistemas, los datos de rendimiento de GSHP en forma de tablas proporcionadas por los fabricantes de equipos no son convenientes. Los modelos matemáticos desarrollados en este estudio estiman la capacidad calorífica (HC) y el COP para condiciones particulares de temperatura y caudal de los fluidos secundarios basadas en tablas de datos del fabricante. El procedimiento operativo propuesto, que consiste en la identificación de modelos de MR de segundo orden que contienen ocho x -variables estadísticamente significativas de una muestra de 36 observaciones, tomadas de la tabla del fabricante, se validó con éxito con el análisis estadístico. Los pronósticos de rendimiento son coherentes con el resto de los datos observados. Los errores de predicción externa alcanzan 0,21%, 0,95% y 1,02% para las predicciones de HC y 2,62%, 4,91% y 3,21% para las predicciones de COP para HP1, HP2 y HP3 respectivamente. Los errores residuales externos, tal como se trazaron en relación con las respuestas del modelo, no mostraron correlación con los coeficientes de regresión o la respuesta de predicción, validando así los modelos. El enfoque operacional parece ser una herramienta fiable que se puede incorporar en los códigos de

simulación dinámica desarrollados por los ingenieros, ya que el método es aplicable a cualquier dato del catálogo de GSHP.

Este estudio también muestra que el comportamiento global de GSHP puede predecirse cuando se ajustan los modelos de MR a partir de un número limitado de datos de observación. Sin embargo, la limitación a un conjunto de datos más pequeño para la identificación del modelo puede seguir siendo cuestionable cuando el conjunto de datos completo está disponible en el catálogo del fabricante. Los resultados indican que los fabricantes no necesitan proporcionar tablas con una cantidad tan grande de datos para especificar el mapa de rendimiento completo del sistema de GSHP. Por otro lado, las evaluaciones de diseño experimental proporcionan información sobre cómo deben llevarse a cabo los experimentos en los sistemas operativos actuales de GSHP.

Además, los resultados de los modelos MR propuestos indican que los datos del fabricante podrían ser generados en un principio a partir de modelos de regresión del mismo fabricante. Dado que no se proporciona bondad de ajuste de este último, debe tenerse cierta precaución en el uso de tales datos y modelos correspondientes identificados.

En relación con el tercer objetivo específico, el estudio introdujo una herramienta de simulación de energía en edificios que puede utilizarse para las investigaciones paramétricas de sensibilidad de la eficiencia energética en edificios, y cómo las medidas de mejora de la envoltura y la orientación del edificio afectan el consumo de energía. El modelo MEEDI propuesto se basa en el método de cálculo mensual ISO 13790 y dos procedimientos mejorados para el cálculo de la ganancia solar y la transferencia de calor a través del suelo. La exactitud predictiva del modelo se probó con el software de simulación EnergyPlus y se observó una desviación media del 8% en el cálculo del consumo anual de energía. Por lo tanto, el programa MEEDI se encontró confiable para las investigaciones sobre la influencia de los parámetros físicos y meteorológicos para el uso de energía.

Aunque el modelo MEEDI se utilizó para evaluar la demanda de energía de un hogar típico chileno, tiene la flexibilidad para permitir la realización de pruebas con una serie de escenarios. El modelo permite calcular la eficiencia del edificio para diferentes tipos de materiales de la envoltura, condiciones climáticas y sistemas energéticos, entre otros.

A pesar de la inclusión de las condiciones climáticas, este trabajo enfatiza principalmente la influencia de los materiales de la envoltura del edificio en la eficiencia energética. El resultado del procedimiento introducido se ilustra en figuras gráficas en las secciones 5.3.2 y 5.3.3. Estas figuras pueden utilizarse para identificar los parámetros que influyen en el uso de la energía y validar las medidas de reacondicionamiento eficaces. La herramienta de simulación MEEDI propuesta también puede utilizarse en el proceso de diseño de nuevos edificios para investigar cómo diferentes medidas de diseño pueden influir en el uso de la energía y las emisiones de carbono en particular.

Los resultados muestran cómo las reducciones del uso de energía y las emisiones de CO₂ pueden lograrse con componentes de envoltura de mayor rendimiento en comparación con un hogar típicamente mal aislado. El impacto de los valores de transmisión de calor de la envoltura mejorada en el BCH en comparación con el LEH es un ahorro entre el 48% y el 59% en el uso de energía y entre el 35% y el 59% en las emisiones de CO₂ dependiendo de la localización y del escenario de sistema energético. El análisis de viabilidad económica de medidas específicas para materiales de la envoltura de edificios revela períodos de retorno dentro del rango de vida útil de los edificios, de 6 a 31 años, dependiendo de la localización y del escenario de sistema energético. La investigación demuestra que la eficiencia energética puede ser una estrategia eficaz para abordar la creciente demanda de energía y desarrollar un hogar más sostenible en Chile.

References

- [1] IEA, “Key World Energy Statistics 2016,” Organisation for Economic Co-operation and Development / International Energy Agency (OECD/IEA), Paris, France, 2017.
- [2] FAO, “What woodfuels can do to mitigate climate change?,” in *Food and Agriculture Organization of the United Nations*, Rome, Food and Agriculture Organization (FAO), 2010, pp. 1-98.
- [3] Muneer T, Asif M, Munawwar S, “Sustainable production of solar electricity with particular reference to the Indian economy,” *Renewable and Sustainable Energy Reviews*, vol. 9, pp. 444-73, 2005.
- [4] Sokolski H, “Nuclear Power Goes Rogue,” *Newsweek*, 28 November 2011.
- [5] National Oceanic and Atmospheric Administration (NOAA), “Measuring & Analyzing Greenhouse Gases: Behind the Scenes,” Earth System Research Laboratory, Global Monitoring Division, US Department of Commerce, 2011.
- [6] Donohoe M, “Global warming: a public health crisis demanding immediate action,” *World Affairs*, vol. 11, no. 2, 2007.
- [7] IPCC, “IPCC 4th Assessment Report, Synthesis Report,” Intergovernmental Panel on Climate Change (IPCC), Geneva, Switzerland, 2007.
- [8] Guha-Sapir D, Vos F, Below R, Ponslerre S, “Annual Disaster Statistical Review 2011, The numbers and trends,” Catholic University of Louvain, Brussels, Belgium, 2011.
- [9] Muneer T, Asif M, Kubie J, “Generation and transmission prospects for solar electricity: UK and global markets,” *Energy Conversion Management*, vol. 44, no. 1, pp. 35-52, 2003.

References

- [10] IEA, “World Energy Outlook 2010,” Organisation for Economic Co-operation and Development / International Energy Agency (OECD/IEA), Paris, France, 2010.
- [11] IEA, “World Energy Outlook 2015 Factsheet,” Organisation for Economic Co-operation and Development / International Energy Agency (OECD/IEA), Paris, France, 2015.
- [12] McCrone A, Usher E, “Global Trends in Renewable Energy Investment 2012,” School of Finance & Management gGmbH, Frankfurt, 2012.
- [13] Burgos-Payán M, Roldán-Fernández JM, Trigo-García AL, Bermúdez-Ríos JM, Riquelme-Santos JM, “Costs and benefits of the renewable production of electricity in Spain,” *Energy Policy*, 2013.
- [14] BP p.l.c., “BP Statistical Review of World Energy,” BP Petrol, London, 2016.
- [15] Sims REH, Rogner H, Gregory K, “Carbon emission and mitigation cost comparisons between fossil fuel, nuclear and renewable energy resources for electricity generation,” *Energy Policy*, vol. 31, pp. 1315-26, 2003.
- [16] IEA, “Energy Technology Perspectives 2010: Scenarios and Strategies to 2050,” Organisation for Economic Co-operation and Development / International Energy Agency (OECD/IEA), Paris, France, 2010.
- [17] IEA, “World Energy Outlook 2012 Executive Summary,” Organisation for Economic Co-operation and Development / International Energy Agency (OECD/IEA), Paris, France, 2012.
- [18] Paridaa B, Iniyamb S, Goicc R, “A review of solar photovoltaic technologies,” *Renewable and Sustainable Energy Reviews*, vol. 15, pp. 1625-1636, 2011.
- [19] IEA, “Concentrating Solar Power Technology Roadmap,” Organisation for Economic Co-operation and Development / International Energy Agency (OECD/IEA), Paris, France, 2010.
- [20] Bernhardson W, Chile & Easter Island: A Lonely Planet Travel Atlas, Hawthorn, Victoria, Australia: Lonely Planet Publications, 1997.
- [21] INE, “Censo 2012,” Instituto Nacional de Estadísticas (INE), Santiago, 2013.
- [22] Ministry of Energy, “Importación y producción,” Ministry of Energy (Ministerio de Energía), Santiago, 2014.
- [23] IEA, “Chile: Indicators for 2014,” Organisation for Economic Co-operation and Development / International Energy Agency (OECD/IEA), Paris, France, 2017.
- [24] IEA, “CO2 Emissions From Fuel Combustion Highlights (2015 Edition),” Organisation

References

- for Economic Co-operation and Development / International Energy Agency (OECD/IEA), Paris, France, 2015.
- [25] IMF, “World Economic Outlook Database,” International Monetary Fund (IMF), 2016.
- [26] CIA, “World Factbook: GDP, Composition by sector of origin,” Central Intelligence Agency (CIA), 2016.
- [27] U.S. EIA, “International Energy Statistics,” U.S. Energy Information Administration, 2016.
- [28] Yanine FF, Sauna EE, “Review of grid-tie micro-generation systems without energy storage: Towards a new approach to sustainable hybrid energy systems linked to energy efficiency,” *Renewable and Sustainable Energy Reviews*, vol. 26, p. 60–95, 2013.
- [29] Ministry of Energy, “National Energy Balance 2014,” *Energía Abierta*, Comisión Nacional de Energía (Comisión Nacional de Energía, CNE), Ministry of Energy (Ministerio de Energía), Santiago, 2015.
- [30] CER, “CER Report September 2014,” Renewable Energy Center (Centro de Energías Renovables, CER), Santiago, 2014.
- [31] Färe R, Grosskopf S, Pasurka CA, “Toxic releases: an environmental performance index for coal-fired power plants,” *Energy Economy*, vol. 32, pp. 158-165, 2010.
- [32] Georgakellos D, “Impact of a possible environmental externalities internalization on energy prices: the case of the greenhouse gases from the Greek electricity sector,” *Energy Economy*, vol. 32, pp. 202-209, 2010.
- [33] Garreaud R, Falvey M, “Regional cooling in a warming world: Recent temperature trends in the SE Pacific and along the west coast of subtropical South America (1979-2006),” *Journal of Geophysical Research*, pp. Vol.114, D04102, doi:10.1029/2008JD010519, 2009.
- [34] MMA, “Official Environment Status Report 2011,” Minister of Environment (Ministerio del Medio Ambiente, MMA)), Santiago, Chile, 2012a.
- [35] OECD, “Maintaining momentum, OECD perspectives on policy challenges in Chile,” OECD, 2011.
- [36] Gobierno de Chile, “Decreto 466. Crea comite Nacional Asesor Sobre Cambio Global,” Biblioteca del Congreso Nacional de Chile, Santiago, 1996, Available online: <http://www.leychile.cl/Navegar/?idNorma=13618&idVersion=1996-05-29&idParte>.
- [37] Vega AR, “El Cambio Climático en el Sector Silvoagropecuario de Chile,” Fundación para la Innovación Agraria FIA, 2010.

References

- [38] Generadoras de Chile A.G., “Boletín del Mercado Eléctrico, Sector generación, Diciembre 2016,” Dirección de Estudios y Contenidos, Santiago, 2017.
- [39] Hanel M, Escobar R, “Influence of solar energy resource assessment uncertainty in the levelized electricity cost of concentrated solar power plants in Chile,” *Renewable Energy*, vol. 49, pp. 96-100, 2013.
- [40] Peltier R, "Plant of the year: AES Gener's Angamos power plant earns POWER's highest honor," *Power Mag*, 1st August 2012.
- [41] Lopez E, Ulmer A, “Chile top court rejects \$5 bln Castilla power project,” Reuters, 2012.
- [42] Business Monitor International, “Chile oil and gas report Q1 2013,” Market Research, 2013.
- [43] LNG World News, “Enagas Completes GNL Quintero Stake Acquisition, Chile,” LNG World News, 2012.
- [44] United Press International, “Chile thinking again of nuclear power use,” United Press International, 2012.
- [45] Reyes JR, “Technology assessment for embarking countries,” Chilean Nuclear Energy Commission (CCHEN), Vienna International Center, 2013.
- [46] Ulloa G, “Autoridades aprueban proyecto hidroeléctrico HidroAysén,,” Biobio Chile, 2011.
- [47] Celedón, S, Concha M, “CPC prepara segundo informe con propuestas para avanzar en proyectos energéticos al 2020,” *El Mercurio*, p. B2, 23 07 2013.
- [48] IEA, “Oil and gas security, Chile,” Organisation for Economic Co-operation and Development / International Energy Agency (OECD/IEA), Paris, France, 2012.
- [49] European Commission, “External Costs: Research Results on Socio-environmental Damages due to Electricity and Transport,” Directorate-General for Research, Directorate J-Energy, Brussels, 2003.
- [50] European Commission, “ExtemE—Externalities of Energy: Methodology 2005 Update,” Directorate-General for Research, Sustainable Energy Systems, Brussels, 2005.
- [51] Šúri M, Huld TA, Dunlop ED, Ossenbrink HA, “Potential of solar electricity generation in the European Union member states and candidate countries,” *Solar Energy*, vol. 81, pp. 1295-305, 2007.
- [52] IEA, “Technology Roadmap - Solar Photovoltaic Energy,” Organisation for Economic Co-operation and Development / International Energy Agency (OECD/IEA), Paris,

References

- France, 2010.
- [53] SolarGIS, “GHI Solar map - Chile,” © 2010-2015 GeoModel Solar.
- [54] Gonzalez B, “Profiting from PV in Chile,” PV Insider, 2013.
- [55] CIFES, “CIFES Report (December 2015),” Sustainable Energy Development and Innovation Center (Centro para la Innovación y Fomento de las Energías Sustentables, CIFES), Santiago, 2015.
- [56] CIFES, “CIFES Report (June 2016),” Sustainable Energy Development and Innovation Center (Centro para la Innovación y Fomento de las Energías Sustentables, CIFES), Santiago, 2016.
- [57] Photon International, “Solar policy, regulatory and market news across the Americas,” *Photon International - The Solar Power Magazine*, July 2016.
- [58] PV Insider, “Global solar installations to grow 48% in 2016; EDF commissions 146 MW Chile solar plant,” *New Energy Update: PV*, 05th December 2016.
- [59] Ayre J, “Chile 110 MW CSP Plant Moves Forward,” *Solar Love*, 13th May 2014.
- [60] Electricidad, “Planta termosolar de proyecto Cerro Dominador entraría en operaciones en 2019,” *Electricidad, La revista energética de Chile*; © 2013 editec S.A. ®, 14th March 2017.
- [61] CIFES, “CIFES Report (June 2015),” Sustainable Energy Development and Innovation Center (Centro para la Innovación y Fomento de las Energías Sustentables, CIFES), Santiago, 2015.
- [62] Galindez M, “New grid inter-connectivity in Chile to boost solar industry,” *Renewable Energy World*, 2014.
- [63] Diario de Atacama, “Avanzan obras en parque eólico San Juan en la región de Atacama,” *Diario de Atacama*, 17th March 2016.
- [64] REVE, “Eólica en Chile: Acciona construirá un parque eólico de 183 MW en La Araucanía,” *Revista Eólica y del Vehículo Eléctrico (REVE)*, 17th August 2016.
- [65] Fuentes Besoain V, “Aprueban construcción de Parque Eólico Malleco, proyecto que atraerá una inversión por US\$ 500 millones a La Araucanía,” *El Mercurio*, 20th Octubre 2016.
- [66] Centro de Energías Renovables (CER), “Reporte CER Febrero 2014,” CER, 24 02 2014. [Online]. Available: <http://cer.gob.cl/sobre-las-ernc/datos-y-estadisticas/>. [Accessed 25 02 2014].

References

- [67] CNE, “Monthly Report NCRE, Vol: 5, January 2017,” National Energy Commission (Comisión Nacional de Energía, CNE), Santiago, 2017.
- [68] Kenning T, “Chile expected to add 1.5GW of renewables in 2017,” *PVTech, Solar Media Ltd*, 06th January 2017.
- [69] Olivares A, Almarza D, Bauzá A, Barahona M, Poklepovic I, Delpino I, et al., “Guía de Gestión, Aspectos claves en el desarrollo de proyectos ERNC,” Renewable Energy Center (Centro de Energías Renovables, CER), Santiago, 2013.
- [70] CER, “Centro de Energías Renovables detalló plan de fomento ERNC 2014,” Renewable Energy Center (Centro de Energías Renovables, CER), Santiago, 2014.
- [71] Renewable Energy World, “Latin America Report: How Chile Is Shepherding Its Renewable Energy Expansion,” Renewable Energy World, 2014.
- [72] CORFO, “Con énfasis en la Industria Auxiliar se realizó el V Foro Internacional de Inversiones en ERNC,” CORFO, Santiago, 2010.
- [73] Yildiz A, Güngör A, “Energy and exergy analyses of space heating in buildings,” *Applied Energy*, vol. 86, p. 1939–48, 2009.
- [74] Norero J, Sauma E, “Ex-ante assessment of the implementation of an energy efficiency certificate scheme in Chile,” *Journal of Energy Engineering—ASCE*, vol. 138, pp. 63-72, 2012.
- [75] Ministry of Energy, “Factores de Emisión SIC – SING,” Energía Abierta, Commission National of Energy (Comisión Nacional de Energía, CNE), Ministry of Energy (Ministerio de Energía), Santiago, 2017.
- [76] IEA, “Chile - Energy Policy Review,” Organisation for Economic Co-operation and Development / International Energy Agency (OECD/IEA), Paris, France, 2009.
- [77] Ministry of Energy, “National Energy Strategy 2012-2030,” Ministry of Energy (Ministerio de Energía), Santiago, 2012.
- [78] CNE, “Las Energías Renovables No Convencionales en el Mercado Eléctrico Chileno,” National Energy Commission (Comisión Nacional de Energía, CNE), Santiago, 2009.
- [79] Ministry of Economy, Development and Reconstruction, “Ley 20.018,” Ministerio de Economía, Fomento y Reconstrucción (Ministry of Economy, Development and Reconstruction), Santiago, 2005.
- [80] CNE, “Chile crea Centro de Energías Renovables,” National Energy Commission (Comisión Nacional de Energía, CNE), Santiago, 2009.

References

- [81] CORFO, “Iniciativas de Fomento Integradas – IFI: Apoyo a Proyectos de Inversión Tecnológica,” CORFO, Santiago, 2015a.
- [82] CORFO, “Contratos Tecnológicos para la Innovación,” CORFO, Santiago, 2015b.
- [83] OLADE-UNIDO, “Chile - Fianl report - Component 3: Financial Mechanism,” Observatory of Renewable Energy in Latin America and The Caribbean, 2011.
- [84] IEA, “Invest Chile Project,” Organisation for Economic Co-operation and Development / International Energy Agency (OECD/IEA), Paris, France, 2014.
- [85] IEA, “Support for Non-Conventional Renewable Energy Development Programme,” Organisation for Economic Co-operation and Development / International Energy Agency (OECD/IEA), Paris, France, 2012.
- [86] Bolattürk A, “Determination of optimum insulation thickness for building walls with respect to various fuels and climate zones in Turkey,” *Applied Thermal Engineering*, vol. 26, no. 11, 12, pp. 1301-09, 2006.
- [87] Omer AM, “Ground-source heat pumps systems and applications,” *Renewable and Sustainable Energy Reviews*, vol. 12, pp. 344-371, 2008.
- [88] Juan YK, Gao P, Wang J, “A hybrid decision support system for sustainable office building renovation and energy performance improvement,” *Energy and Buildings*, vol. 42, p. 290–7, 2010.
- [89] Hepbasli A, “Low exergy (LowEx) heating and cooling systems for sustainable buildings and societies,” *Renewable and Sustainable Energy Reviews*, vol. 16, pp. 73-104, 2012.
- [90] Levermore GJ, “A review of the IPCC assessment report four, part 1: the IPCC process and greenhouse gas emission trends from buildings worldwide,” *Building Services Engineering Research & Technology*, vol. 29, pp. 349-61, 2008.
- [91] Papathanasopoulou E, “Household consumption: associated fossil fuel demand and carbon dioxide emissions: The case of Greece between 1990 and 2006,” *Energy Policy*, vol. 38, p. 4152–62, 2010.
- [92] Hevia A, “Energy Consumption and CO2 Emission Reduction for Space Heating using SAP in Chilean Dwellings,” in *46th Annual Conference of the Architectural Science Association (ANZAScA)*, Griffith University, 2011.
- [93] CDT, CChC, “Estudio de Usos Finales y Curva de Oferta de Conservación de la energía en el Sector Residencial de Chile,” Corporación de Desarrollo Tecnológico (CDT), Cámara Chilena de la Construcción (CChC), Santiago, 2010.
- [94] The World Bank, “World Development Indicators: Table 3.10. Carbon dioxide emissions

References

- by sector,” The World Bank Group, 2017.
- [95] INE, “Edificación: Informe Anual 2011,” Instituto Nacional de Estadísticas (INE), Santiago, Chile, 2012.
- [96] Romero Ramos NP, “Consumo de energía a nivel residencial en Chile y análisis de eficiencia energética en calefacción,” Universidad de Chile, Facultad de Ciencias Físicas y Matemáticas, Departamento de Ingeniería Civil, Santiago, Chile, 2011.
- [97] INE, “Edificación: Superficie Autorizada,” Instituto Nacional de Estadísticas (INE), Santiago, 2014.
- [98] CNE, “Política Energética. Nuevos Lineamientos. Transformando la crisis energética en una oportunidad,” National Energy Commission (Comisión Nacional de Energía, CNE), Santiago, Chile, 2008.
- [99] Minister of Energy, “Reglamento de la ley n° 20.365, que establece franquicia tributaria respecto de sistemas solares térmicos,” Government of Chile, Santiago, 2009.
- [100] CDT, CChC, *Revista SustentaBit, Technological Development Corporation (CDT), Chilean Construction Chamber (CChC)*, pp. números 1, 2 y 3, 2009.
- [101] CDT, CChC, “Calificación Energética de Viviendas,” in *SustentaBit N.15*, vol. 15, Santiago, Technological Development Corporation (Corporación de Desarrollo Tecnológico, CDT) and Chilean Construction Chamber (Cámara Chilena de la Construcción, CChC), 2012, pp. 24-26.
- [102] MINVU, “General Law of Urban Planning and Construction (OGUC),” Ministry of Housing and Urban Planning (Ministerio de Vivienda y Urbanismo, MINVU), Santiago, 2011.
- [103] Besser D, Rodrigues L, Bobadilla A, “New Chilean Building Regulations and Energy Efficient Housing in Disaster Zones, The thermal performance of prefabricated timber-frame dwellings,” in *PLEA2012 - 28th Conference, Opportunities, Limits & Needs Towards an environmentally responsible architecture*, Lima, Perú, 2012.
- [104] Fissore A, Colonelli P, “Sistema de certificación energética de viviendas para Ministerio de Vivienda y Urbanismo Chile. Informe final,” Instituto de Investigaciones Tecnológicas y Asistencia Técnica, Universidad de Concepción, Concepción, Chile, 2009.
- [105] Bustamante W, Encinas F, Rozas Y, Victorero F, “Desarrollo de la herramienta de certificación de comportamiento térmico de edificios en Chile: Manuales de Referencias Técnicas: fundamentos técnicos,” Pontificia Universidad Católica de Chile, Santiago, Chile, 2007.

References

- [106] Burgos D, “Thermal Regulations: Just the First Step,” 2011. [Online]. Available: <http://www.revistatc.com/?p=3898>.
- [107] CIBSE, “Guide A: Environmental Design, Section A4: Ventilation and air infiltration,” CIBSE, 2006.
- [108] World Commission on Environment and Development, “Our Common Future, Report of the World Commission on Environment and Development,” Oxford University Press, Published as Annex to UN General Assembly document A/42/427, Oxford, 1987.
- [109] Adams WM, “The Future of Sustainability: Re-thinking Environment and Development in the Twenty-first Century,” The World Conservacion Union, IUCN, Gland, Switzerland, 2006.
- [110] Ordóñez J, Gago EJ, Alegre Bayo J, Martínez Montes G, “The use of solar energy in the buildings construction sector in Spain,” *Renewable and Sustainable Energy Reviews*, vol. 11, pp. 2166-2178, 2007.
- [111] Boyle G, Renewable energy, Power for a sustainable future. 1st edition, Oxford: Oxford University Press, 1996.
- [112] Chevalier JM, Les grandes batailles de l’énergie, Paris, France: Edition Gallimard, 2004.
- [113] Chesné L, Duforestel T, Roux JJ, Rusaouën G, “Energy saving and environmental resources potentials: Toward new methods of building design,” *Building and Environment*, vol. 58, pp. 199-207, 2012.
- [114] Ayres JM, Stamper E, “Historical development of building energy calculations,” *ASHRAE Transactions*, vol. 101, pp. 841-8, 1995.
- [115] Hall K, Green Building Bible Third Edition, Volume 1, Green Building Press, 2005.
- [116] Hall K, Green Building Bible Third Edition, Volume 2, Green Building Press, 2005.
- [117] Williams DR, “Sun Fact Sheet,” NASA Goddard Space Flight Center, 2013.
- [118] Coddington O, Lean JL, Pilewskie AP, Snow M, Lindholm D, “Solar Irradiance Climate Data Record,” *Bulletin of the American Meteorological Society*, vol. 97, no. 7, 2015.
- [119] Bustos F, Toledo A, Contreras J, Fuentes A, “Sensitivity analysis of a photovoltaic solar plant in Chile,” *Renewable Energy*, vol. 87, pp. 145-153, 2016.
- [120] Duffie JA, Beckman WA, Solar engineering of thermal processes, 3rd edition, USA: John Wiley & Sons, 2006.
- [121] Iqbal M, An introduction to solar radiation, Canada: Academic Press, 1983, ISBN 0-12-

References

- 373752-4.
- [122] Muneer T, *Windows in Buildings: Thermal, Acoustic, Visual & Solar Performance*, Oxford: Architectural Press, 2000.
- [123] Muneer T, *Solar radiation and daylight models*, Oxford: Butterworth-Heinemann, 2004.
- [124] Girard A, Muneer T, Caceres G, “A validated design simulation tool for passive solar space heating: results from a monitored house in West Lothian, Scotland,” *Indoor and Built Environment*, DOI: 10.1177/1420326X13480057, 2013.
- [125] Kreider JF, Kreith F, *Solar energy handbook*, New York: Mcgraw-Hill Book Company, 1981.
- [126] Kondratyev KY, Manolova MP, “The radiation balance of slopes,” *Solar Energy*, vol. 4, p. 14, 1960.
- [127] Li DHW, Lam JC, Lau CCS, “A new approach for predicting vertical global solar irradiance,” *Renewable Energy*, vol. 25, pp. 591-606, 2002.
- [128] Liu BYH, Jordan RC, “Daily insolation on surfaces tilted toward the equator,” *Trans. ASHRAE*, vol. 67, pp. 526-541, 1962.
- [129] Klein SA, “Calculation of monthly average insolation on tilted surfaces,” *Solar Energy*, vol. 19, pp. 325-329, 1977.
- [130] Klein SA, Theilacker JC, “An algorithm for calculating monthly-average radiation on inclined surfaces,” *Journal of Solar Energy Engineering*, vol. 103, no. 1, pp. 29-33, 1981.
- [131] Erbs DG, Klein SA, Duffie JA, “Estimation of the diffuse radiation fraction for hourly, daily and monthly-average global radiation,” *Solar Energy*, vol. 28, no. 4, pp. 293-302, 1982.
- [132] Ordoñez J, Jdraque E, Alegre J, Martínez G, “Analysis of the photovoltaic solar energy capacity of residential rooftops in Andalusia (Spain),” *Renewable and Sustainable Energy Reviews*, vol. 14, pp. 2122-2130, 2010.
- [133] Kirkegaard JF, Hanemann T, Weischer L, Miller M, “Toward a sunny future? Global integration in the solar PV Industry,” Peterson Institute for International Economics, Washington, 2010.
- [134] Price S, Margolis R, “Solar technologies market report,” in *Energy Efficiency & Renewable Energy*, US Department of Energy, 2010, pp. 1-131.
- [135] Jogleka NR, Graber-Lopez ES, “A countdown towards solar power at grid parity: policy analysis based on the evolution of price-performance,” in *Proceedings of 2008 ISDSI*

References

- international conference*, 2008.
- [136] Klein J, "Comparative costs of California Central Station electricity generation: final staff report," Sacramento, CA: California Energy Commission, 2010, pp. 1-186.
- [137] Yang C, "Reconsidering solar grid parity," *Energy Policy*, vol. 38, pp. 3270-3, 2010.
- [138] Branker K, Pathaka MJM, Pearcea JM, "A review of solar photovoltaic levelized cost of electricity," *Renewable and Sustainable Energy Reviews*, vol. 15, pp. 4470-82, 2011.
- [139] Ito M, Kato K, Sugihara H, Kichimi T, Kichimi J, Kurokawa K, "A preliminary study on potential for very large scale photovoltaic power generation (VLSPV) system in the Gobi desert from economic and environmental viewpoints," *Solar Energy Materials & Solar Cells*, vol. 75, pp. 507-17, 2003.
- [140] Kobayashi H, Kurihara I, "Research and development of grid integration of distributed generation in Japan.," in *IEEE Power and Energy Society General Meeting*, Calgary, Canada, 26-30 July 2009.
- [141] Fraunhofer ISE, "Photovoltaics Report," Fraunhofer Institute for Solar Energy (ISE), Freiburg, Germany, 2016.
- [142] Philipps SP, Bett AW, Horowitz K, Kurtz S, "Current Status of Concentrator Photovoltaic (CPV) Technology," Fraunhofer Institute for Solar Energy Systems (ISE), National Renewable Energy Laboratory (NREL), Freiburg, Germany, 2016.
- [143] REN21, "Renewables 2010 global status report," REN21, Paris, 2010.
- [144] European Photovoltaic Industry Association (EPIA), "Global Market Outlook for Photovoltaics Until 2015," Brussels, EPIA, 2011.
- [145] REN21, "Renewables 2016: Global Status Report," REN21, Paris, 2016.
- [146] Teske S, Muth J, Sawyer S, "Energy revolution - A sustainable world energy outlook - 4th edition," Greenpeace International, European Renewable Energy Council (EREC) and Global Wind Energy Council (GWEC), isbn 978-90-73361-92-8, 2012.
- [147] Aldali YAA, "Solar thermal and photovoltaic electrical generation in Libya, PhD Thesis report," Edinburgh Napier University, Edinburgh, 2012.
- [148] Economist.com, "Pricing sunshine - The rise of solar energy," *The Economist Newspaper Limited*, 28th December 2012.
- [149] pvXchange, "Price index," *pvXchange*, 20th January 2017.
- [150] Fthenakis V, Kim HC, Frischknecht R, Raugei M, Sinha P, Stucki M, "Life Cycle Inventories and Life Cycle Assessment of Photovoltaic Systems," *International Energy*

References

- Agency (IEA), PVPS Task 12, Report T12-02:2011, 2011.
- [151] NREL, “Crystalline Silicon and Thin Film Photovoltaic Results -- Life Cycle Assessment Harmonization,” National Renewable Energy Laboratory (NREL), 2013.
- [152] Barlev D, Vidu R, Stroeve P, “Innovation in concentrated solar power,” *Solar Energy Materials & Solar Cells*, vol. 95, pp. 2703-25, 2011.
- [153] Steinmann WD, Eck M, “Buffer storage for direct steam generation,” *Solar Energy*, vol. 80, pp. 1277-1282, 2006.
- [154] Goswami DY, Vijayaraghavan S, Lu S, Tamm G, “New and emerging developments in solar energy,” *Solar Energy*, vol. 76, pp. 33-43, 2004.
- [155] IRENA, “Renewable Energy Technologies: Costs Analysis Series, Concentrating Solar Power, Volume 1, Issue 2/5,” International Renewable Energy Agency (IRENA), Bonn, Germany, 2012.
- [156] DeLaquil P, Kelly B, Lessley R, “Solar one conversion project,” *Solar Energy Materials*, vol. 24, pp. 151-161, 1991.
- [157] Herrmann U, Kearney DW, “Survey of thermal energy storage for parabolic trough power plants,” *Journal of Solar Energy Engineering*, vol. 124, pp. 145-152, 2002.
- [158] Py X, Azoumah Y, Olives R, “Concentrated solar power: Current technologies, major innovative issues and applicability to West African countries,” *Renewable and Sustainable Energy Reviews*, vol. 18, pp. 306-15, 2013.
- [159] Kurokawa K, “Energy from the Desert: Feasibility of Very Large Scale Power Generation (VLS-PV),” Routledge, 2003, pp. 1-256.
- [160] Tamme R, Laing D, Steinmann WD, “Advanced thermal energy storage technology for parabolic trough,” *Journal of Solar Energy Engineering*, vol. 126, pp. 794-800, 2004.
- [161] Watanabe T, Kikuchi H, Kanzawa A, “Enhancement of charging and discharging rates in a latent heat storage system by use of PCM with different melting temperatures,” *Heat Recovery Systems and CHP*, vol. 13, pp. 57-66, 1993.
- [162] Gil A, Medrano M, Martorell I, Lázaro A, Dolado P, Zalba B, Cabeza LF, “State of the art on high temperature thermal energy storage for power generation. Part 1-Concepts, materials and modellization,” *Renewable and Sustainable Energy Reviews*, vol. 14, pp. 31-55, 2010.
- [163] Lovegrove K, Luzzi A, Soldiani I, Kretz H, “Developing ammonia based thermochemical energy storage for dish power plants,” *Solar Energy*, vol. 76, pp. 331-337, 2004.

References

- [164] Medrano M, Gil A, Martorell I, Potau X, Cabeza LF, “State of the art on high-temperature thermal energy storage for power generation. Part 2 – Case studies,” *Renewable and Sustainable Energy Reviews*, vol. 14, pp. 56-72, 2010.
- [165] Jafarian M, Arjomandi M, Nathan GJ, “A hybrid solar and chemical looping combustion system for solar thermal energy storage,” *Applied Energy*, vol. 103, pp. 671-678, 2013.
- [166] Koca A, Oztop HF, Koyun T, Varol Y, “Energy and exergy analysis of a latent heat storage system with phase change material for a solar collector,” *Renewable Energy*, vol. 33, pp. 567-74, 2008.
- [167] Zanganeh G, Pedretti A, Zavattoni S, Barbato M, Steinfeld A, “Packed-bed thermal storage for concentrated solar power – Pilot-scale demonstration and industrial-scale design,” *Solar Energy*, vol. 86, pp. 3084-98, 2012.
- [168] Shinnar R, Citro F, “Solar thermal energy: The forgotten energy source,” *Technology in Society*, vol. 29, pp. 261-270, 2007.
- [169] Alexopoulos S, Hoffschmidt B, “Solar tower power plant in Germany and future perspectives of the development of the technology in Greece and Cyprus,” *Renewable Energy*, vol. 35, pp. 1352-56, 2010.
- [170] Fernandez-Garcia A, Zarza E, Valenzuela L, Perez M, “Parabolic-trough solar collectors and their applications,” *Renewable and Sustainable Energy Reviews*, vol. 14, pp. 1695-721, 2010.
- [171] Ummadisingu A, Soni MS, “Concentrating solar power – Technology, potential and policy in India,” *Renewable and Sustainable Energy Reviews*, vol. 15, pp. 5169-75, 2011.
- [172] Dersch J, Geyer M, Herrmann U, Jones SA, Kelly B, Kistner R, “Trough integration into power plants – a study on the performance and economy of integrated solar combined cycle systems,” *Energy*, vol. 29, no. 5-6, pp. 947-59, 2004.
- [173] Montes MJ, Rovira A, Muñoz M, Martínez-Val JM, “Performance analysis of an Integrated Solar Combined Cycle using Direct Steam Generation in parabolic trough collectors,” *Applied Energy*, vol. 88, pp. 3228-38, 2011.
- [174] Kearney AT, “Solar Thermal Electricity 2025,” Duesseldorf, Germany, GmbH, 2010.
- [175] REN21, “Renewables 2013 - Global Status Report,” REN21 Secretariat, Paris, 2013.
- [176] Rajgor G, “Renewable Power Generation - 2011 figures,” *Renewable Energy Focus*, Elsevier, 19th December 2012.
- [177] Aabakken J, “Power Technologies Energy Data Book, Fourth Edition,” National Renewable Energy Laboratory, 2006, pp. 1-231.

References

- [178] Chien J, Lior N, “Concentrating solar thermal power as a viable alternative in China’s electricity supply,” *Energy Policy*, vol. 39, pp. 7622-36, 2011.
- [179] IEA/NEA, “Projected Costs of Generating Electricity: Edition 2010,” Organisation for Economic Co-operation and Development / International Energy Agency / Nuclear Energy Agency(OECD/IEA/NEA), Paris, France, 2010.
- [180] Short W, Packey DJ, Holt T, A Manual for the Economic Evaluation of Energy Efficiency and Renewable Energy Technologies, Golden, USA: National Renewable Energy Laboratory (NREL), 1995, pp. 1-120.
- [181] Brown M, “Going for grid parity,” BP Global—reports and publications, 2005.
- [182] Singh PP, Singh S, “Realistic generation cost of solar photovoltaic electricity,” *Renewable Energy*, vol. 35, pp. 563-69, 2010.
- [183] Reichelstein S, Yorston M, “The prospects for cost competitive solar PV power,” *Energy Policy*, vol. 55, pp. 117-27, 2013.
- [184] Corral N, Anrique N, Fernandes D, Parrado C, Cáceres G, “Power, placement and LEC evaluation to install CSP plants in northern Chile,” *Renewable and Sustainable Energy Reviews*, vol. 16, pp. 6678-85, 2012.
- [185] Wang X, Kurdgelashvili L, Byrne J, Barnett A, “The value of module efficiency in lowering the levelized cost of energy of photovoltaic systems,” *Renewable and Sustainable Energy Reviews*, vol. 15, pp. 4248-54, 2011.
- [186] Hernández-Moro J, Martínez-Duart JM, “Analytical model for solar PV and CSP electricity costs: Present LCOE values and their future evolution,” *Renewable and Sustainable Energy Reviews*, vol. 20, pp. 119-132, 2013.
- [187] Hoffmann W, “PV solar electricity in EUMENA: head way in the world,” in *Mediterranean solar plan – introduction*, Valencia, 11th May 2010.
- [188] Campbell,M, “Charting the progress of PV power plant energy generating costs to unsubsidised levels, Introducing the PV-LCOE Framework,” in *Proceedings of the 26th European Photovoltaic Solar Energy Conference*, Hamburg, Germany, 2011.
- [189] NREL, “SAM Help, Levelized Cost of Energy (LCOE),” National Renewable Energy Laboratory (NREL), 2013.
- [190] Breyer C, Gerlach A, Müller J, Behacker H, Milner A, “Grid-parity analysis for EU and US regions and market segments—dynamics of grid-parity and dependence on solar irradiance, local electricity prices and PV progress ratio,” in *Proceedings of 24th European photovoltaic solar energy conference*, 2009.

References

- [191] Van der Zwaan B, Rabl A, “The learning potential of photovoltaics: implications for energy policy,” *Energy Policy*, vol. 32, no. 13, pp. 1545-54, 2004.
- [192] Hauff J, Verdonck M, Derveaux H, Dumarest L, Alberich J, Malherbe JC, El Gammal A, Llamas P, Masson G, Macías E, “Unlocking the Sunbelt Potential of Photovoltaics, Third edition,” EPIA (European Photovoltaic Industry Association), Brussels, Belgium, 2011.
- [193] Purohit I, Purohit P, “Techno-economic evaluation of concentrating solar power generation in India,” *Energy Policy*, vol. 38, no. 6, pp. 3015-29, 2010.
- [194] MIT, “The Future of Coal,” 2007. [Online]. Available: <http://web.mit.edu/coal/>. [Accessed 20 02 2013].
- [195] Dinica V, “Renewable electricity production costs - A framework to assist policy-makers’ decisions on price support,” *Energy Policy*, vol. 39, pp. 4153-67, 2011.
- [196] IRENA, “The Power To Change: Solar and wind cost reduction potential to 2025,” International Renewable Energy Agency (IRENA), Bonn, Germany, 2016.
- [197] IEA, “Renewable Energy, Medium-term market report 2015, Market trends and projections to 2020,” Organisation for Economic Co-operation and Development / International Energy Agency (OECD/IEA), Paris, France, 2015.
- [198] IEA, “Medium-Term Coal Market Report 2012, Market Trends and Projections to 2017,” Organisation for Economic Co-operation and Development / International Energy Agency (OECD/IEA), Paris, France, 2012.
- [199] Filippini M, Wild J, “Regional differences in electricity distribution costs and their consequences for yardstick regulation of access prices,” *Energy Economics*, vol. 23, pp. 477-88, 2001.
- [200] Hinkley, J, “Concentrating Solar Power-Drivers and Opportunities for Cost-competitive Electricity, CSIRO, Victoria,” Victoria, Commonwealth Scientific and Industrial Research Organisation (CSIRO), 2011.
- [201] Jablonski S, Tarhini M, Touati M, Gonzalez Garcia D, Alario J, “The Mediterranean Solar Plan: Project proposals for renewable energy in the Mediterranean Partner Countries region,” *Energy Policy*, vol. 44, pp. 291-300, 2012.
- [202] Pernick R, Wilder C, Winnie T, “Clean Energy Trends 2013,” Clean Edge, Inc. (www.cleaneedge.com), March 2013 , pp. 1-22.
- [203] Delucchi MA, Jacobson MZ, “Providing all global energy with wind, water, and solar power, PartII: Reliability, system and transmission costs, and policies,” *Energy Policy*, vol. 39, pp. 1170-90, 2011.

References

- [204] Nitsch J, “Leitstudie 2008 – Further development of the “Strategy to increase the use of renewable energies” within the context of the current climate protection goals of Germany and Europe,” German Federal Ministry for the Environment, Nature Conservation and Nuclear Safety (BMU), Stuttgart, 2008.
- [205] Swanson R, “The Silicon Photovoltaic Roadmap,” in *The Stanford Energy Seminar*, Stanford, USA, 14 November 2011.
- [206] Casey T, “Grid Parity In Sight For New Low-Cost Solar Cell,” *Clean Technica*, 08th December 2012.
- [207] Business Wire, “Global Photonic Energy Corporation Develops Potential Grid Parity Solar Cell,” *Business Wire*, 07th December 2012.
- [208] Fox W, “Breakthroughs in solar power,” *Futuretimeline*, 26th January 2013.
- [209] Hunt T, “True cost of solar energy and other renewables: California case study,” *Renewable Energy World*, 13th December 2010.
- [210] Hutchinson J, Inwood S, James R, Ramachandran G, Hamel J, Libby C, “Program on technology innovation: integrated generation technology options. 1019539.,” Electric Power Research Institute, Palo Alto, CA, 2009.
- [211] Schleicher-Tappeser R, “Photovoltaics – Turbulent Growth of a Disruptive Technology: Learning from the European Experience,” in *Seminar on German Solar Technologies*, Bangalore, India, 14th November 2011.
- [212] Schleicher-Tappeser R, “How renewables will change electricity markets in the next five years,” *Energy Policy*, vol. 48, pp. 64-75, 2012.
- [213] Girard A, Gago EJ, Ordoñez J, Muneer T, “Spain's energy outlook: A review of PV potential and energy export,” *Renewable Energy*, vol. 86, pp. 703-715, 2016.
- [214] Viebahn P, Kronshage S, Trieb F, Lechon Y, “D 12.2 Final report on technical data, costs, and life cycle inventories of solar thermal power plants,” NEEDS (New Energy Externalities Developments for Sustainability) Project no: 502687, 2008.
- [215] Tsikalakis A, Tomtsi T, Hatziaargyriou ND, Poullikkas A, Ch Malamatenios, Giakoumelos E, Cherkaoui Jaouadd O, Chenake A, Fayek A, Matar T, Yasin A, “Review of best practices of solar electricity resources applications in selected Middle East and North Africa (MENA) countries,” *Renewable and Sustainable Energy Reviews*, vol. 15, no. 6, pp. 2838-49, 2011.
- [216] Šúri M, Remund J, Cebecauer T, Hoyer-Klick C, Dumortier D, Huld T, Stackhouse PW Jr, Ineichen P, “Comparison of Direct Normal Irradiation Maps for Europe.,” in

References

- SolarPACES Conference "Concentrated Solar Power and Chemical Energy Systems"*, Berlin, Germany, 2009.
- [217] European Commission: Joint Research Center, "Photovoltaic Geographical Information System (PVGIS). Geographical Assessment of Solar Resource and Performance of Photovoltaic Technology," 2012. [Online]. Available: <http://re.jrc.ec.europa.eu/pvgis/>.
- [218] Breyer C, Gerlach A, "Global Overview on Grid Parity Event Dynamics," in *25th EUPVSEC / WCPEC-5*, Valencia, 2010.
- [219] Zelenika-Zovko I, Pearce JM, "Diverting indirect subsidies from the nuclear industry to the photovoltaic industry: energy and economic returns," *Energy Policy*, vol. 39, no. 5, pp. 2626-32, 2011.
- [220] De Weck J, "German Ministries Clashing Over Renewable Subsidies," *Renewable Energy World*, 11th February 2013.
- [221] Consentec, "Delaying grid maintenance and bringing wind back onshore could make Germany's energy reform cheaper," *PHOTON International*, March 2013.
- [222] Murphy T, "What's Driving, and Constraining, PV Demand in Greece," *Renewable Energy World*, 12th February 2013.
- [223] Omer AM, "Energy environment and sustainable development," *Renewable and Sustainable Energy Reviews*, vol. 12, pp. 2265-2300, 2008.
- [224] Zogou O, Stamatelos A, "Optimization of thermal performance of a building with ground source heat pump system," *Energy Conversion and Management*, vol. 48, pp. 2853-63, 2007.
- [225] Desideri U, Sorbi N, Arcioni L, Leonardi D, "Feasibility study and numerical simulation of a ground source heat pump plant, applied to a residential building," *Applied Thermal Engineering*, vol. 31, pp. 3500-11, 2011.
- [226] Girard A, Gago EJ, Muneer T, Caceres G, "Higher ground source heat pump COP in a residential building through the use of solar thermal collectors," *Renewable Energy*, vol. 80, pp. 26-39, 2015.
- [227] IEA, "Energy-efficient Buildings: Heating and Cooling Equipment, Technology Roadmap," Organisation for Economic Co-operation and Development / International Energy Agency (OECD/IEA), Paris, France, 2011.
- [228] Esen H, Inalli M, Esen M, "Technoeconomic appraisal of a ground source heat pump system for a heating season in eastern Turkey," *Energy Conversion and Management*, vol. 47, pp. 1281-97, 2006.

References

- [229] Pulat E, Coskun S, Unlu K, Yamankaradeniz N, “Experimental study of horizontal ground source heat pump performance for mild climate in Turkey,” *Energy*, vol. 34, pp. 1284-95, 2009.
- [230] Healy PF, Ugursal VI, “Performance and economic feasibility of ground source heat pumps in cold climate,” *International Journal of Energy Research*, vol. 21, pp. 857-70, 1997.
- [231] ASHRAE, *Applications Handbook - Chapter 32: Geothermal Energy*, Atlanta, USA: American Society for Heating Refrigerating and Air Conditioning Engineers (ASHRAE), 2003.
- [232] US DOE, “Geothermal Heat Pumps,” United States Department Of Energy (US DOE), 2015.
- [233] Zhai XQ, Qu M, Yu X, Yang Y, Wang RZ, “A review for the applications and integrated approaches of GCHP systems,” *Renewable and Sustainable Energy Review*, vol. 15, pp. 3133-3140, 2011.
- [234] Energy Saving Trust, “Energy Efficiency Best Practice in Housing. Domestic Ground Source Heat Pumps: Design and installation of closed-loop systems,” Energy Saving Trust, 2007.
- [235] Omer AM, “Soil Thermal Properties and the Effects of Groundwater on Closed Loops,” *International Journal of Sustainable Energy and Environmental Research*, vol. 3, no. 1, pp. 34-52, 2014.
- [236] Rawlings R, Parker J, Breembroek G, Cherruault JY, Curtis R, Freeborn R et al., “Domestic ground source heat pumps: Design and installation of closed-loop systems,” Energy Efficiency Best Practice in Housing. Energy Saving Trust. E&OE. CE82, March 2004.
- [237] BRE (Building Research Establishment), “The Government’s Standard Assessment Procedure for Energy Rating of Dwellings V9.90,” Department of Energy and Climate Change, Watford, March 2010.
- [238] Hayton J., “Calculation Procedure for the SAP Appendix Q Process for Electrically Driven Heat Pumps,” Building Research Establishment (BRE), Watford, 2010.
- [239] BSRIA, “Domestic Ground Source Heat Pumps: Design and Installation of Closed Loop Systems,” Energy Saving Trust, London, 2004.
- [240] Kusuda T, Achenbach PR, “Earth Temperature and Thermal Diffusivity at Selected Stations in the United States,” National Bureau of Standards – Building Research Division, Washington, 1965.

References

- [241] Gupta R, R Irving, “Development and application of a domestic heat pump model for estimating CO₂ emissions reductions from domestic space heating, hot water and potential cooling demand in the future,” *Energy and Buildings*, vol. 60, pp. 60-67, 2013.
- [242] Lund JW, Boyd TL, “Direct utilization of geothermal energy 2015 worldwide review,” *Geothermics*, vol. 60, pp. 66-93, 2016.
- [243] Lahsen A, Rojas J, Morata D, Aravena D, “Geothermal exploration in Chile: country update,” in *World Geothermal Congress 2015*, Melbourne, Australia, 2015.
- [244] Lund JW, Freeston DH, Boyd TL, “Direct utilization of geothermal energy 2010 worldwide review,” *Geothermics*, vol. 40, pp. 159-80, 2011.
- [245] Wu R, “Energy Efficiency Technologies – Air Source Heat Pump vs. Ground Source Heat Pump,” *Journal of Sustainable Development*, vol. 2, pp. 14-23, 2009.
- [246] Kwon O, Bae K, Park C, “Cooling characteristics of ground source heat pump with heat exchange methods,” *Renewable Energy*, vol. 71, pp. 651-657, 2014.
- [247] Sarbu I, Sebarchievici C, *Ground-Source Heat Pumps, Fundamentals, Experiments and Applications*, 1st edition, ISBN: 9780128042205: Academic Press, 2015.
- [248] WaterFurnace, “Envision Series - NDW Specification Catalog,” WaterFurnace, Fort Wayne, Indiana, USA, 2015.
- [249] ANSI/ARI/ASHRAE/ISO 13256-2, “Water-source heat pumps — Testing and Rating for Performance — Part 2: Water-to-Water and Brine-to-Water Heat Pumps,” ANSI/AHRI/ASHRAE/ISO, 1998.
- [250] Kim J, Jang JC, Kang EC, Chang KC, Lee EJ, Kim Y, “Verification study of a GSHP system Manufacturer data based modeling,” *Renewable Energy*, vol. 54, pp. 55-62, 2013.
- [251] Zhu N, Hu P, Xu L, Jiang L, Lei F, “Recent research and applications of ground source heat pump integrated with thermal energy storage systems: a review,” *Applied Thermal Engineering*, vol. 71, no. 1, pp. 142-151, 2014.
- [252] Zhang X, Huang G, Jiang Y, Zhang T, “Ground heat exchanger design subject to uncertainties arising from thermal response test parameter estimation,” *Energy and Buildings*, vol. 102, pp. 442-452, 2015.
- [253] Draper NR, Smith H, *Applied Regression Analysis*, Third Edition, New York: Wiley-Interscience, 1998.
- [254] Neter J, Kutner MH, Nachtsheim CJ, Wasserman W, *Applied Linear Statistical Models*, Fourth Edition, Chicago: Mc Graw-Hill/Irwin, 1996.

References

- [255] James G, Witten D, Hastie T, Tibshirani R, *An Introduction to Statistical Learning with Applications in R*, New York: Springer, 2013.
- [256] Johnson RA, Wichern DW, *Applied multivariate statistical analysis*, Upper Saddle River, New Jersey: Pearson; ISBN 9780135143506, 2007.
- [257] IEA, “Technology Roadmap - Energy Efficient Building Envelopes,” Organisation for Economic Co-operation and Development / International Energy Agency (OECD/IEA), Paris, France, 2013.
- [258] Sartori I, Napolitano A, Voss K, “Net zero energy buildings: A consistent definition framework,” *Building and environment*, vol. 48, pp. 220-232, 2012.
- [259] Radhi H, “Can envelope codes reduce electricity and CO₂ emissions in different types of buildings in the hot climate of Bahrain?,” *Energy*, vol. 34, pp. 205-215, 2009.
- [260] Ordóñez García J, Modi V, “Optimising CO₂ emissions from heating and cooling and from the materials used in residential buildings, depending on their geometric characteristics,” *Building and Environment*, vol. 46, pp. 2161-2169, 2011.
- [261] Wilkinson P, Smith KR, Beevers S, Tonne C, Oreszczyn T, “Energy, energy efficiency, and the built environment,” *Lancet*, vol. 307, pp. 1175-87, 2007.
- [262] Jadraque Gago E, Ordóñez García J, Espín Estrella A, “Development of an energy model for the residential sector: Electricity consumption in Andalusia, Spain,” *Energy and Buildings*, vol. 43, pp. 1315-1321, 2011.
- [263] Clarke JA, “Assessing building performance by simulation,” *Building and Environment*, vol. 28, no. 4, pp. 419-427, 1993.
- [264] Hien WN, Poh LK, Feriadi H, “The use of performance-based simulation tools for building design and evaluation — a Singapore perspective,” *Building and Environment*, vol. 35, no. 8, pp. 709-736, 2000.
- [265] Ji Y, Xu P, “A bottom-up and procedural calibration method for building energy simulation models based on hourly electricity submetering data,” *Energy*, vol. 93, pp. 2337-2350, 2015.
- [266] ASHRAE, *ASHRAE Handbook - Chapter 19 Fundamentals: Energy Estimating and Modeling Methods*, Atlanta, USA: American Society for Heating Refrigerating and Air Conditioning Engineers (ASHRAE), 2013.
- [267] Solar Energy Laboratory, “TRNSYS version 18 user manual and documentation,” University of Wisconsin-Madison, Madison, WI, 2017.
- [268] ESRU, “ESP-r,” Energy Systems Research Unit (ESRU), [Online]. Available:

References

- <http://www.esru.strath.ac.uk/Programs/ESP-r.htm>. [Accessed 16 03 2017].
- [269] USDE, “EnergyPlus Energy Simulation Software,” U.S. Department of Energy (USDE), 2015. [Online]. Available: <http://apps1.eere.energy.gov/buildings/energyplus>. [Accessed 16 03 2017].
- [270] Fels M, “Measuring energy savings: The scorekeeping approach,” *Energy and Buildings*, vol. 9, 1986.
- [271] Reddy TA, Saman NF, Claridge DE, Haberl JS, Turner WD, Chalifoux A, “Baselining methodology for facility level monthly energy use—Part 1: Theoretical aspects,” *ASHRAE Transactions*, vol. 103, no. 2, pp. 336-347, 1997.
- [272] Sonderegger RC, “Baseline equation for utility bill analysis using both weather and non-weather related variables,” *ASHRAE Transactions*, vol. 104, no. 2, pp. 859-870, 1998.
- [273] Rabl A, “Parameter estimation in buildings: Methods for dynamic analysis of measured energy use,” *Journal of Solar Energy Engineering*, vol. 110, pp. 52-66, 1988.
- [274] Yao R, Baker N, McEvoy M, “A simplified thermal resistance network model for building thermal simulation,” in *Sim2002, eSim*, Montreal, Canada, September 11–13, 2002.
- [275] Saelens D, Parys W, Baetens R, “Energy and comfort performance of thermally activated building systems including occupant behavior,” *Building and Environment*, vol. 46, pp. 835-848, 2011.
- [276] Westphal FS, Lamberts R, “The use of simplified weather data to estimate thermal loads of non-residential buildings,” *Energy and Buildings*, vol. 36, pp. 847-854, 2004.
- [277] AL-Rabghi Omar MA, AL-Johani Khalid M, “Utilizing transfer function method for hourly cooling load calculations,” *Energy Conversion and Management*, vol. 38, pp. 319-332, 1997.
- [278] Kusuda T, “Thermal response factors for multi-layer structures of various heat conduction systems,” *ASHRAE Transactions*, vol. 75, no. 1, pp. 246-271, 1969.
- [279] Mitalas GP, Stephenson DG, “Room thermal response factors,” *ASHRAE Transactions*, vol. 73, no. 1, pp. III.2.1-III.2.10, 1967.
- [280] Gough M, “Modelling heat flow in buildings: an eigenfunction approach,” PhD Thesis, University of Cambridge, 1982.
- [281] Shurcliff WA, Frequency method of analyzing a building’s dynamic thermal performance, Cambridge, MA, 1984.

References

- [282] Dhar A, Reddy TA, Claridge DE, "Modeling hourly energy use in commercial buildings with Fourier series functional form," *Journal of Solar Energy Engineering*, vol. 120, no. 3, pp. 217-223, 1998.
- [283] Dhar A, Reddy TA, Claridge DE, "Generalization of the fourier series approach to model hourly energy use in commercial buildings," *Journal of Solar Energy Engineering*, vol. 121, no. 1, pp. 54-62, 1999.
- [284] Clarke J, *Energy Simulation in Building Design*, Oxford: Butterworth-Heinemann, 2001.
- [285] Al-Anzi A, Krarti M, "Local/global analysis of transient heat transfer from building foundations," *Building and Environment*, vol. 39, pp. 495-504, 2004.
- [286] Tzivanidis C, Antonopoulos KA, Gioti F, "Numerical simulation of cooling energy consumption in connection with thermostat operation mode and comfort requirements for the Athens buildings," *Applied Energy*, vol. 88, no. 8, pp. 2871-84, 2011.
- [287] Zhang Y, O'Neill ZD, Dong B, Augenbroe G, "Comparisons of inverse modeling approaches for predicting building energy performance," *Building and Environment*, vol. 86, pp. 177-190, 2015.
- [288] Chaudhary G, New J, Sanyal J, Im P, O'Neill Z, Garg V, "Evaluation of "Autotune" calibration against manual calibration of building energy models," *Applied Energy*, vol. 182, pp. 115-134, 2016.
- [289] Ghiaus C, "Experimental estimation of building energy performance by robust regression," *Energy and Building*, vol. 38, no. 6, pp. 582-587, 2006.
- [290] Manfren M, Aste N, Moshksar R, "Calibration and uncertainty analysis for computer models—a meta-model based approach for integrated building energy simulation," *Applied Energy*, vol. 103, pp. 627-641, 2013.
- [291] Lam JC, Wan KKW, Wong SL, Lam TNT, "Principal component analysis and long-term building energy simulation correlation," *Energy Conversion and Management*, vol. 51, no. 1, pp. 135-139, 2010.
- [292] Korolija I, Zhang Y, Marjanovic-Halburd L, Hanby VI, "Regression models for predicting UK office building energy consumption from heating and cooling demands," *Energy and Buildings*, vol. 59, pp. 214-227, 2013.
- [293] Hittle DC, Pedersen CO, "Periodic and stochastic behavior of weather data," *ASHRAE Transactions*, vol. 87, pp. 173-194, 1981.
- [294] Subbarao K, "Thermal parameters for single and multi-zone buildings and their determination from performance data. SERI Report SERI/TR- 253-2617.," Solar Energy

References

- Research Institute, Golden, CO, 1986.
- [295] Reddy T, “Application of dynamic building inverse models to three occupied residences monitored non-intrusively,” in *ASHRAE/ DOE/BTECC/CIBSE conference on "Thermal Performance of Exterior Envelopes of Buildings IV"*, Orlando, FL, 1989.
- [296] Hokoi S, Matsumoto M, Ihara T, “Statistical time series models of solar radiation and outdoor temperature—identification of seasonal models by Kalman filter,” *Energy and Buildings*, vol. 15/16, pp. 373-383, 1990/1991.
- [297] Hu M, “A data-driven feed-forward decision framework for building clusters operation under uncertainty,” *Applied Energy*, vol. 141, pp. 229-237, 2015.
- [298] Baldi S, Yuan S, Endel P, Holub O, “Dual estimation: Constructing building energy models from data sampled at low rate,” *Applied Energy*, vol. 169, pp. 81-92, 2016.
- [299] Haarhoff J, Mathews EH, “A Monte Carlo method for thermal building simulation,” *Energy and Buildings*, vol. 38, pp. 1395-1399, 2006.
- [300] Mui KW, Wong LT, “Cooling load calculations in subtropical climate,” *Building and Environment*, vol. 42, no. 7, pp. 2498-2504, 2007.
- [301] Azadeh A, Ghaderi SF, Sohrabkhani S, “Annual electricity consumption forecasting by neural network in high energy consuming industrial sectors,” *Energy Conversion and Management*, vol. 49, no. 8, pp. 2272-2278, 2008.
- [302] Hou Z, Lian Z, Yao Y, Yuan X, “Cooling-load prediction by the combination of rough set theory and an artificial neural-network based on data-fusion technique,” *Applied Energy*, vol. 83, pp. 1033-1046, 2006.
- [303] Karatasou S, Santamouris M, Geros V, “Modeling and predicting building’s energy use with artificial neural networks: methods and results,” *Energy and Buildings*, vol. 38, no. 8, pp. 949-958, 2006.
- [304] Dong B, Cao C, Lee SE, “Applying support vector machines to predict building energy consumption in tropical region,” *Energy and Buildings*, vol. 37, no. 5, pp. 545-553, 2005.
- [305] Li Q, Meng Q, Cai J, Yoshino H, Mochida A, “Applying support vector machine to predict hourly cooling load in the building,” *Applied Energy*, vol. 86, no. 10, pp. 2249-2256, 2009.
- [306] Li Q, Ren P, Meng Q, “Prediction model of annual energy consumption of residential buildings,” in *Proceedings of 2010 international conference on advances in energy engineering*, p.223-226, 2010.
- [307] ISO 13790, “Energy performance of buildings - Calculation of energy use for space

References

- heating and cooling,” International Organization for Standardization (ISO), Geneva, 2008.
- [308] Jokisalo J, Kurnitski J, “Performance of EN ISO13790 utilisation factor heat demand calculation method in a cold climate,” *Energy and Buildings*, vol. 39, no. 2, pp. 236-247, 2007.
- [309] Kalema T, Johannesson G, Pylsy P, Hagengran P, “Accuracy of energy analysis of buildings: A comparison of a monthly energy balance method and simulation methods in calculating the energy consumption and the effect of thermal mass,” *Journal of Building Physics*, vol. 32, no. 2, pp. 101-130, 2008.
- [310] Van Dijk H, Spiekman M, De Wilde P, “A monthly method for calculating energy performance in the context of European building regulations,” in *Building Simulation 2005, 9th International IBPSA Conference*, pp.255-262, Montréal, Canada, August 15-18, 2005.
- [311] Kokogiannakis G, Strachan PA, Clarke JA, “Comparison of the simplified methods of the ISO13790 standard and detailed modelling programs in a regulatory context,” *Journal of Building Performance Simulation*, vol. 1, no. 4, pp. 209-219, 2008.
- [312] Haydock H, Arbon JA, “Study on Energy performance of buildings, Policy department - economic and Scientific Policy,” European Parliament (commissioned by ITRE), February 2009.
- [313] Maldonado E, “Implementing of the energy performance of buildings directive (EPBD), featuring Country Reports 2012,” Concerted Action (CA) EPBD, European Commission, Brussels, 2013.
- [314] ASHRAE, ASHRAE Handbook - Chapter 17 Fundamentals: Residential Cooling and Heating Load Calculations, Atlanta, USA: American Society for Heating Refrigerating and Air Conditioning Engineers (ASHRAE), 2013.
- [315] IEA, “Calculation Methods to Predict Energy Savings in Residential Buildings,” Swedish Council for Building Research, IEA Energy Conservation in Buildings and Community Systems Programme – Annex 3, Stockholm, Sweden, 1983.
- [316] ISO 6946, “Building components and building elements. Thermal resistance and thermal transmittance. Calculation method,” British Standards Institution, London, 1997.
- [317] ISO 13370, “Thermal performance of buildings. Heat transfer via the ground. Calculation methods,” International Organization for Standardization (ISO), Geneva, 1998.
- [318] CIBSE, “Guide A: Environmental design, Section A3: Thermal properties of building structures,” CIBSE, 2006.

References

- [319] Department for Environment, Food & Rural Affairs (DEFRA), “Limiting thermal bridging and air leakage : robust construction details for dwellings and similar buildings.,” Stationery Office, London, 2001.
- [320] CIBSE, “Guide A: Environmental Design, Section A6: Internal heat gains,” CIBSE, 2006.
- [321] Olofsson T, Mahlia TMI, “Modeling and simulation of the energy use in an occupied residential building in cold climate,” *Applied Energy*, vol. 91, pp. 432-438, 2012.
- [322] Building Research Establishment (BRE), “Estimates of hot water consumption from the 1998 EFUS. Implications for the modeling of fuel poverty in England. A summary report presenting data from the 1998 EFUS produced by the BRE Housing Centre on behalf of DTI and DEFRA,” BRE Housing Centre, Watford, England, 2005.
- [323] Barnaby CS, Spitler JD, “Development of the residential load factor method for heating and cooling load calculations,” *ASHRAE Transactions*, vol. 111, no. 1, 2005.
- [324] Corrado V, Fabrizio E, “Assessment of building cooling energy need through a quasi steady state model: Simplified correlation for gain-loss mismatch,” *Energy and Buildings*, vol. 39, pp. 569-579, 2007.
- [325] Pérez-Lombard L, Ortiz J, González R, Maestre IR, “A review of benchmarking, rating and labelling concepts within the framework of building energy certification schemes,” *Energy and Buildings*, vol. 41, no. 3, pp. 272-278, 2009.
- [326] Feijoó ML, Franco JF, Hernández JM, “Global warming and the energy efficiency of Spanish industry,” *Energy Economics*, vol. 24, no. 4, pp. 405-423, 2002.
- [327] Lyon TP, Maxwell JW, “Self-regulation, taxation and public voluntary environmental agreements,” *Journal of Public Economics*, vol. 87, no. 7, pp. 1453-1486, 2003.
- [328] UNIDO, “Sustainable Energy Regulation and Policy Making Training Manual - Module 18: Energy Efficiency in Buildings,” United Nations Industrial Development Organization (UNIDO), 2009.
- [329] Lee WL, Yik FWH, “Regulatory and voluntary approaches for enhancing energy efficiency of buildings in Hong Kong,” *Applied Energy*, vol. 71, pp. 251-274, 2002.
- [330] BREEAM, “BRE Environmental Assessment Method,” Building Research Establishment UK (BRE), [Online]. Available: <http://www.breeam.org/>.
- [331] LEED, “LEED, Leadership in Energy and Environmental Design Program,” US Green Building Council (USGBC), [Online]. Available: <http://www.usgbc.org/>.
- [332] Green Star, Green Building Council Australia, [Online]. Available:

References

- <http://new.gbca.org.au/green-star/>.
- [333] Cole RJ, Rousseau D, Theaker IT, “Building Environmental Performance Assessment Criteria: Version 1-Office Buildings,” The BEPAC Foundation, Vancouver, Canada, 1993.
- [334] ESGB, “Evaluation Standard for Green Building (ESGB) (GB/T 50378-2006),” Ministry of Construction of the People’s Republic of China, March 7, 2006.
- [335] EMAS, “The EU Eco-Management and Audit Scheme (EMAS), Europa,” [Online]. Available: http://ec.europa.eu/environment/emas/index_en.htm.
- [336] BEAM Plus, “Hong Kong Building Environmental Assessment Method, BEAM Society, Hong Kong,” [Online]. Available: <http://www.hk-beam.org.hk/general/home.php>.
- [337] Lee WL, Burnett J, “Benchmarking energy use assessment of HK-BEAM, BREEAM and LEED,” *Building and Environment*, vol. 43, no. 11, pp. 1882-91, 2008.
- [338] Lee WL, “Benchmarking energy use of building environmental assessment schemes,” *Energy and Buildings*, vol. 45, pp. 326-334, 2012.
- [339] BRE, “BREEAM,” Building Research Establishment (BRE), [Online]. Available: <http://www.breeam.com/>.
- [340] Girard A., “Certificaciones de sustentabilidad, herramientas para la evaluación del desarrollo de edificación sustentable en Chile,” *El Dínamo*, 05 12 2013. [Online]. Available: <http://www.eldinamo.cl/blog/certificaciones-de-sustentabilidad-herramientas-para-la-evaluacion-del-desarrollo-de-edificacion-sustentable-en-chile/>. [Accessed 04 03 2014].
- [341] Powers JT, “BREEAM Certification to Share Green Market with LEED in U.S.,” *Green Building News*, 15th June 2016.
- [342] Chidiak M, “Lessons from the French experience with voluntary agreements for greenhouse-gas reduction,” *Journal of Cleaner Production*, vol. 10, no. 2, pp. 121-128, 2002.
- [343] Rietbergen MG, Farla JCM, Blok K, “Do agreements enhance energy efficiency improvement? Analysing the actual outcome of long-term agreements on industrial energy efficiency improvement in The Netherlands,” *Journal of Cleaner Production*, vol. 10, no. 2, pp. 153-163, 2002.
- [344] Green A, Diep C, Dunn R, Dent J, “High capacity factor CSP-PV hybrid systems,” *Energy Procedia*, vol. 69, pp. 2049-2059, 2014.
- [345] Larchet K, “Solar PV-CSP hybridisation for baseload generation, a technoeconomic

References

- analysis for the Chilean market. Master of Science Thesis,” KTH School of Industrial Engineering and Management, Stockholm, 2015.
- [346] NREL, “Solar and Wind Energy Resource Assessment (SWERA),” NREL, 2015. [Online]. Available: <https://maps.nrel.gov/swera/#/>. [Accessed 22 09 2015].
- [347] Koohi-Kamali S, Tyagi VV, Rahim NA, Panwar NL, Mokhlis H, “Emergence of energy storage technologies as the solution for reliable operation of smart power systems: a review,” *Renewable and Sustainable Energy Review*, vol. 25, pp. 135-65, 2015.
- [348] Akhil AA, Huff G, Currier AB, Kaun BC, Rastler DM, Chen SB, et al., DOE/EPRI2013 Electricity storage handbook in collaboration with NRECA, Albuquerque (New Mexico) and Livermore (California): US Department of Energy and Electric Power Research Institute (EPRI), 2013.
- [349] Chen HS, Cong TN, Yang W, Tan CQ, Li YL, Ding YL, “Progress in electrical energy storage system: a critical review,” *Progress in Natural Science*, vol. 19, pp. 291-312, 2009.
- [350] Battke B, Schmidt TS, Grosspietsch D, Hoffmann VH, “A review and probabilistic model of lifecycle costs of stationary batteries in multiple applications,” *Renewable Sustainable Energy Review*, vol. 25, pp. 240-250, 2013.
- [351] Fathabadi H, “Two novel techniques for increasing energy efficiency of photovoltaic-battery systems,” *Energy Conversion and Management*, vol. 105, pp. 149-166, 2015.
- [352] Glavin ME, Hurley WG, “Optimisation of a photovoltaic battery ultracapacitor hybrid energy storage system,” *Solar Energy*, vol. 86, pp. 3009-3020, 2012.
- [353] Barnhart CJ, Benson SM, “On the importance of reducing the energetic and material demands of electrical energy storage,” *Energy and Environmental Science*, vol. 6, pp. 1083-1092, 2013.
- [354] Mulder G, Six D, Claessens B, Broes T, Omar N, Van Mierlo J, “The dimensioning of PV-battery systems depending on the incentive and selling price conditions,” *Applied Energy*, vol. 111, pp. 1126-1135, 2013.
- [355] Cervone A, Carbone G, Santini E, Teodori S, “Optimization of the battery size for PV systems under regulatory rules using a Markov-Chain’s approach,” *Renewable Energy*, vol. 85, pp. 657-665, 2016.
- [356] Poullikkas A, “A comparative overview of large-scale battery systems for electricity storage,” *Renewable and Sustainable Energy Reviews*, vol. 27, pp. 778-788, 2013.
- [357] Morisson V, Rady M, Palomo E, Arquís E, “Thermal energy storage systems for

References

- electricity production using solar energy direct steam generation technology,” *Chemical Engineering and Processing*, vol. 47, pp. 499-507, 2008.
- [358] IEA, “World Energy Outlook 2013: Renewable Energy Outlook,” Organisation for Economic Co-operation and Development / International Energy Agency (OECD/IEA), Paris, France, 2013.
- [359] Hernández-Moro J, Martínez-Duart JM, “CSP electricity cost evolution and grid parities based on the IEA roadmaps,” *Energy Policy*, vol. 41, pp. 184-192, 2012.
- [360] Nemet GF, “Beyond the learning curve: factors influencing cost reductions in photovoltaics,” *Energy Policy*, vol. 34, pp. 3218-3232, 2006.
- [361] Ministry of Energy, “Energy 2050,” Ministry of Energy, Antofagasta, 2014.
- [362] CSP World, “CSP 2012 a review,” January 2013. [Online]. Available: www.csp-world.com.
- [363] Kolb GJ, Ho CK, Mancini TR, Gary JA, “Power Tower Technology Roadmap and Cost Reduction Plan. SAND2011-2419,” Sandia National Laboratories , Albuquerque, USA, 2011.
- [364] Turchi CS, “Parabolic Trough Reference Plant for Cost Modeling with the Solar Advisor Model (SAM),” NREL/TP-550-47605, 2010.
- [365] Kost C et al., “Levelized Cost of Electricity – Renewable Energy Technologies,” Fraunhofer Institute for Solar Energy Systems ISE, Freiburg, Germany, 2013.
- [366] Dinter F, Gonzalez DM, “Operability, Reliability and Economic Benefits of CSP with Thermal Energy Storage: First Year of Operation of ANDASOL 3,” *Energy Procedia*, vol. 49, pp. 2472-2481, 2014.
- [367] Ministry of National Goods (MBN), “Cuentas Públicas Nacionales,” MBN, 2014.
- [368] Letherman KM, Al-Azawi MMJ, “Predictions of the heating and cooling energy requirements in buildings using the degree hours method,” *Building and Environment*, vol. 21, no. 3, pp. 171-176, 1986.
- [369] Al-ajmi FF, Hanby VI, “Simulation of energy consumption for Kuwaiti domestic buildings,” *Energy and Buildings*, vol. 40, no. 6, pp. 1101-1109, 2008.
- [370] Bojic M, Yik F, “Application of advanced glazing to high-rise residential buildings in Hong Kong,” *Building and Environment*, vol. 42, no. 2, pp. 820-828, 2007.
- [371] Yang L, Lam JC, Tsang CL, “Energy performance of building envelopes in different climate zones in China,” *Applied Energy*, vol. 85, pp. 800-817, 2008.

References

- [372] Eskin N, Turkmen H, “Analysis of annual heating and cooling energy requirements for office buildings in different climates in Turkey,” *Energy and Buildings*, vol. 40, pp. 763-773, 2008.
- [373] Kaynakli O, “A study on residential heating energy requirement and optimum insulation thickness,” *Renewable Energy*, vol. 33, no. 6, pp. 1164-1172, 2008.
- [374] Jaber S, Ajib S, “Optimum, technical and energy efficiency design of residential building in Mediterranean region,” *Energy and Buildings*, vol. 43, pp. 1829-1834, 2011.
- [375] Raji B, Tenpierik MJ, van den Dobbelsteen A, “An assessment of energy-saving solutions for the envelope design of high-rise buildings in temperate climates: A case study in the Netherlands,” *Energy and Buildings*, vol. 124, pp. 210-221, 2016.
- [376] Ihm P, Park L, Krarti M, Seo D, “Impact of window selection on the energy performance of residential buildings in South Korea,” *Energy Policy*, vol. 44, pp. 1-9, 2012.
- [377] Kurekci NA, “Determination of optimum insulation thickness for building walls by using heating and cooling degree-day values of all Turkey’s provincial centers,” *Energy and Buildings*, vol. 118, pp. 197-213, 2016.
- [378] Mechri HE, Capozzoli A, Corrado V, “Use of the ANOVA approach for sensitive building energy design,” *Applied Energy*, vol. 87, pp. 3073-3083, 2010.
- [379] Al-Homoud MS, “Computer-aided building energy analysis techniques,” *Building and Environment*, vol. 36, no. 4, pp. 421-433, 2001.
- [380] Büyükalaca O, Bulut H, Yilmaz T, “Analysis of variable-base heating and cooling degree-days for Turkey,” *Applied Energy*, vol. 69, pp. 269-283, 2001.
- [381] ASHRAE, “ASHRAE Handbook – Chapter 14 Fundamentals - Climatic Design Information,” The American Society of Heating, Refrigeration, Air Conditioning (ASHRAE), Atlanta, 2013.
- [382] Navarro Schlotterbeck G, Anuario Climatológico 2012, Santiago: Dirección de Aeronáutica Civil, Dirección Meteorológica de Chile, ISSN 0716.3274, 2013.
- [383] Ministry of Energy, “Solar Energy Explorer (Explorador de Energía Solar),” Ministry of Energy - Chile University Geophysics Department, 2016. [Online]. Available: <http://walker.dgf.uchile.cl/Explorador/Solar3/>. [Accessed 16th October 2016].
- [384] MINVU, “Thermal Regulation Application Manual,” Ministry of Housing and Urban Planning (Ministerio de Vivienda y Urbanismo, MINVU), Santiago, 2006.
- [385] INE, “Edificación: Informe Annual 2014,” Energy National Institute (Instituto Nacional de Estadística, INE), Santiago, 2014.

References

- [386] Chilectra, “Listado de tarifas: Tarifas de Suministros Clientes Regulados - Tarifa Actual,” 2017.
- [387] CNE, “Hydrocarbons / Prices (Tarificación Hydrocarburos),” National Energy Commission (Comisión Nacional de Energía, CNE), Santiago, 2017.
- [388] DECC, “Guidelines to Defra/ DECC’s GHG conversion factors for company reporting,” UK Department of Energy and Climate Change (DECC), London, 2013.
- [389] Muñoz C, Zaror C, Saelzer G, Cuchí A, “Estudio del flujo energético en el ciclo de vida de una vivienda y su implicancia en las emisiones de gases de efecto invernadero, durante la fase de construcción. Caso Estudio: Vivienda Tipología Social. Región del Biobío, Chile,” *Revista de la Construcción*, vol. 11, no. 3, pp. 125-45, 2012.